THE "DIRECT METHOD AS APPLIED TO LIQUID ROCKET ENGINE COMBUSTION AND EXPLOSION PROBLEMS

Frediano V. Bracco

PRINCETON UNIVERSITY

DEPARTMENT OF
AEROSPACE AND MECHANICAL SCIENCES

THE "DIRECT METHOD AS APPLIED TO LIQUID ROCKET ENGINE COMBUSTION AND EXPLOSION PROBLEMS

Frediano V. Bracco

A DISSERTATION

PRESENTED TO THE

FACULTY OF PRINCETON UNIVERSITY

IN CANDIDACY FOR THE DEGREE

OF DOCTOR OF PHILOSOPHY

RECOMMENDED FOR ACCEPTANCE BY THE

DEPARTMENT OF

AEROSPACE AND MECHANICAL SCIENCES

June 1970

ABSTRACT

In this report, attention is focused on a method of investigating physical problems, which is referred to as the "direct" method. The method is then applied to the problems of liquid rocket engine combustion and detonations.

The "direct" method of analyzing a physical problem consists of i) measuring some specific variables ii) solving basic equations using the measured quantities to determine more of the unknown variables and, in the process, learning more about the nature of the physical problem and then iii) formulating the proper, complete physical model. This method contrasts with the more conventional approach where the complete model is proposed first. Occasionally the "direct" method has been used in the past (and called the "inverse" approach), but more as a clever trick to solve a specific problem than as a general method. To prove the generality of the "direct" method, this author has formalized the steps for its application. Advantages are shown in that the "direct" method: makes optimal use of the experimental data; provides a check on their accuracy; leads to mathematical simplifications and to the possibility of checking assumptions; allows one to gain insight into an unresolved physical problem and helps to define a correct model for it. The author is not aware of any previous generalization of the "direct" method and believes that such a generalization should encourage other applications.

By applying the "direct" method to the problem of steady liquid rocket combustion, it is shown that static pressure measurements along the engine are sufficient to determine all the gas variables

and the amount of vaporized propellant if only one propellant is in liquid form. No use is made of any drop drag, vaporization or distribution models; this can simplify development-stage engine studies. Useful to analytical instability studies are the conclusions (for the LOX/ethanol system) that: the steady-state is not axially uniform; the combustion is axially more distributed than current drop drag and vaporization models predict; the use of a distribution function is not essential; drag and vaporization effects on the momentum equation of the gas are of the same order; the energy source is not proportional to the mass source; and the initial momenta of the liquids should not be neglected in steady-state computations. A non axially uniform steady-state contrasts with the uniformity assumption usually made in theoretical studies and it confirms the findings of other investigators (e.g., Rocketdyne group).

The "direct" method has previously been applied to various aspects of the detonation problem. Here it leads to the derivation of a new functional form for the equation of state of the products of solid explosives. However, most of the study is concentrated on a method which allows one to compute the detonation variables without knowing the equation of state of the products if the detonation velocity versus the loading density is known. Its relationship to the Chapman-Jouguet theory is investigated. The two methods, although apparently different, are shown to yield very similar results. It is shown that a rough form of this method was previously used by Zel'dovich, although he thought he was applying the Chapman-Jouguet condition.

ACKNOWLEDGEMENTS

This research, under NASA Grant NGL 31-001-155, was sponsored by the Chemical Rocket Division of NASA Lewis Research Center, M. F. Heidmann, Project Manager.

The author is indebted to Professor Luigi Crocco for his guidance throughout the course of this investigation and for his many specific suggestions. The author gratefully acknowledge the special help of Mr. David T. Harrje, Senior Research Engineer and Lecturer, not only for his direction of the experimental work reported in this thesis, but also for his continuous, valuable encouragement during the entire course of this study. The author thanks also Professor William A. Sirignano for having been always available for fruitful discussions.

The author wishes to acknowledge the help of Mr. Lanny Hoffman in the first efforts to solve numerically some of the equations found in this work, of Mr. V. Warshaw for his design of the experimental hardware, of Mr. K. Gadsby for his able execution of the experiments and the reduction of some of the data, of Mr. C. L. Griffith for running the computer programs related to the parametric study of the LOX/ethanol system and for reducing some of the experimental data, of Miss D. Morris for having met the challenge of typing the draft of this thesis, and of Miss C. Hartmann for typing the final copy.

This thesis carries AMS No. 902T in the records of the Department of Aerospace and Mechanical Sciences.

TABLE OF CONTENTS

TABLE OF CONTENTS

TABLES

FIGURES

FIGURES

NOMENCLATURE

a = Atoms of carbon in the fuel molecule

A = Engine corss sectional area (cm^2)

b = Atoms of hydrogen in the fuel molecule

c = Atoms of oxygen in the fuel molecule

$c_{f,\phi}$ = Specific heat of the liquid fuel, oxidizer (erg/g ^oK)

$c_{p_{f,\phi}}$ = Specific heat of gaseous fuel, oxidizer (erg/g ^oK)

C_{p_i} = Specific heat of individual combustion products (erg/mole ^oK)

e = Specific internal energy of products (erg/g)

EQR = Vaporized propellant equivalence ratio (1 for fuel rich mixtures)

EQR_o = Injection vlaue of EQR also equal to complete combustion value of EQR (EQR_f)

$h = e + \frac{p}{\rho} + h^o$ = Specific enthalpy of products (erg/g)

$h^o = 4.186\ 10^{10} \sum_{i=1}^{8} X_i\ (H^o_{298})_i / m_{em}$ = Specific enthalpy of formation of products (erg/g)

$h^o_{f,\phi} = 4.186\ 10^{10}\ (H^o_{298})_{f,\phi} / m_{f,\phi}$ = Specific enthalpy of formation of the fuel, oxidizer (erg/g)

$H^o_{T^o}$ = Standard enthalpy of formation (Kcal/mole) at T^o = 298 ^oK

$m_{f,\phi}$ = Molecular weight of fuel, oxidizer

$m_{em} = m_p + 2 m_\phi$ Molecular weight of the equivalent mole = weight of the products per mole of vaporized fuel

$m = m_{em} / y$ Average molecular weight of the products

p = Static pressure (dym/cm^2)

p_o = Static pressure at injector end (dym/cm^2)

r = Drop radius (cm)

t = Time (sec)

T = Temperature of the products (^oK)

$T_{F,\phi}$ = Temperature of the liquid fuel, oxidizer (^{o}K)

$T_{v\,F,\phi}$ = Wet bulb temperature of the liquid fuel, oxidizer (^{o}K)

T° = Reference temperature = 298^{o}K

u = Velocity of the products (cm/sec)

$u_{F,\phi,\ell}$ = Velocity of the liquid fuel, liquid oxidizer, or liquid propellant (cm/sec)

$u_{o_{F,\phi,\ell}}$ = Liquid fuel, liquid oxidizer, or liquid propellant injection velocity (cm/sec)

$u_{x\,F,\phi,\ell}$ = Component of $u_{o_{F,\phi,\ell}}$ in the axial direction (cm/sec)

$w_{F,\phi}$ = Liquid fuel, oxidizer flux (g/sec cm^{2})

$w_{o\,F,\phi}$ = Injection fuel, oxidizer flux (g/sec cm^{2})

x = Distance from injector (cm)

X_i = Number of moles of product i per equivalent mole

Y = Total number of moles of products per equivalent mole

Z = $m_F(w_{o\phi} - w_\phi)/m_\phi(w_{oF} - w_F)$ = Moles of vaporized oxidizer per mole of vaporized fuel

$\lambda_{F,\phi}$ = Specific latent heat of vaporization of the liquid fuel, oxidizer (erg/g)

$\lambda^{\circ}_{F,\phi}$ = $\left[c\,(T_v - T^{\circ}) + \lambda + c_p\,(T^{\circ} - T_v)\right]_{F,\phi}$ = Specific latent heat of vaporization of the liquid fuel, oxidizer at T° = 298^{o}K, (erg/g)

$\Lambda_{F,\phi}$ = $-\left[c\,(T_v - T) + \lambda + c_p\,(T^{\circ} - T_v)\right]_{F,\phi} = -\left[\lambda^{\circ} + c\,(T^{\circ} - T)\right]_{F,\phi}$ = Specific vaporization energy of the liquid fuel, oxidizer referred to T° = 298^{o}K

ρ = Density of products (g/cm^{3})

ρ_L = Specific gravity of liquid propellant (g/cm^{3})

$\rho_{F,\phi,\ell}$ = Mass of liquid fuel, oxidizer, propellant per unit volume of the combustion chamber (g/cm^{3})

φ° = Specific chemical heat released (difference between the enthalpy of formation of the products and that of the reactants) (erg/g)

INTRODUCTION

In the Abstract, the content of this report was briefly summarized. This section is now used to introduce the reader to the subjects treated in this report. Three main subjects, rather than just one, are discussed so that some preliminary considerations on their inter-relationship might be of help to the reader.

The three subjects are i) the "direct" method (Section 1), ii) one-dimensional, laminar detonation problems (Section 2), and iii) the steady rocket combustion of the LOX/ethanol system (Section 3).

Interest is centered on the "direct" method; however, the two specific problems have been treated as thoroughly as possible so as to constitute two relatively complete studies. The studies are used as examples of applications of the "direct" method. Accordingly, there is no concluding section to the over-all report, but rather two concluding sections, one for the detonation problem (Section 2.6) and the other for the steady combustion of the LOX/ethanol system (Section 3.7). There was no need for a concluding section on the "direct" method, since the method and related properties are explained in Section 1 and applications are given in the other sections. The section on steady combustion of the LOX/ethanol system is the longest of all the sections because this was the topic of principal concern and effort at Princeton.

In Section 1, the "direct" method of solving a physical problem is defined, and its properties are listed. Here it might be useful to introduce this method in a less rigorous, more

discoursive way. A researcher who has to solve a new problem can often make some assumptions and write equations that, from his previous experience, he is rather confident will be valid. To complete his model, however, other assumptions and equations will be necessary whose validity is more uncertain and will be finally proved or disproved by experiments. Making these more uncertain assumptions, solving the complete set of equations and comparing the results with experimental data is what is here called the "conventional" way of solving a problem. The "direct" way consists of avoiding the use of the more uncertain assumptions and using instead experimental data. One looks at the equations which are believed to be reliable and decides which variables should be measured to avoid making the more uncertain assumptions. After having measured these variables, the more reliable equations are solved, and only then are the more uncertain assumptions studied. Both methods require experimental data sooner or later. The "direct" method uses this data more efficiently and offers other specific advantages which are listed in this report. This method is here called "direct" since it makes direct use of the experimental data to gain maximum information about a given problem rather than using them only to verify already obtained solutions. The "direct" method seems to the author to be the more natural one, particularly for complicated physical problems, since, if for no other reasons, it squeezes maximum information out of a set of experimental data. This method has previously been applied by other researchers (and called the "inverse" approach) but this author is not aware of any previous formalization of it and believes that some of the properties, listed in this report,

either were not known or were overlooked. Formalizing the method should aid in its application.

In Section 2.0, where laminar one-dimensional steady detonations are considered, a method is introduced which allows one to compute the detonation parameters without knowing the equation of state of the products but using "directly" measured detonation velocities versus loading density. This method is here called the envelope method and gives results which are close to those given by the various Chapman-Jouguet models. The physical reasons why this method leads to reasonably good results for both gaseous and solid explosives are not known. The relationship of the envelope method to the various Chapman-Jouguet models is illustrated and, in the process, the state of the art of laminar one-dimensional steady detonation studies is reviewed. A functional form for the equation of state of the products of solid explosives is then given.

In Section 3.0, the "direct" method is applied to the problem of steady liquid rocket combustion. It is then shown that the gas variables (pressure, velocity, density, temperature, composition, etc.) and the amount of vaporized propellant can be calculated if any one of the gas variables is first measured along the engine (generally static pressure or gas velocity) and if only one propellant is in liquid form at the station at which the gas variable is measured (if two propellants are present in liquid form, then two gas variables should be measured). No use is made of any droplet drag, vaporization, breakup or distribution models and the detailed knowledge of the processes occurring in the injector region is not necessary. Those models are necessary, on the contrary, if one follows the "conventional" approach. The

validity of the results obtained by conventional approaches are then subject to the validity of those models, whereas the results obtained by the direct method are not. By the direct method it was thus possible to show that the assumption of instantaneous chemical equilibrium of the reaction products leads to good results for the LOX/ethanol system. It was also shown that the steady state of the LOX/ethanol system is likely to exhibit marked axial nonuniformaties. Similar nonuniformities were previously calculated by conventional approaches by other researchers (at Rocketdyne, for example) and had been previously indicated by c* measurements (at Princeton, for example). However conventional studies include so many uncertain and sensitive assumptions that conclusions about the validity of any one of them must be considered only indicative (see for example the sensitivity of steady-state computations to the vaporization rate equation, to the initial drop radius and to the drag equation in Section 3.6). Similarly c* measurements yield only indicative results. Possibly for these reasons the steady state has always been assumed to be axially uniform in theoretical instability studies. It is then shown that axial nonuniformity can lower the frequency of a perturbation wave by some 20% with respect to its value calculated under the uniformity assumptions (Section 3.5). Other results of interest to theoretical instability studies have already been pointed out in the abstract and are summarized in Section 3.7. It should also be pointed out that this study was undertaken with the purpose of better relating instability studies to the actual steady combustion. Thus the effort was not toward considering the most complete of the available steady-state models but rather toward finding the simplest schematization that would contain the main physical elements and lead to a reasonably accurate description.

SECTION 1.0 THE "DIRECT" METHOD

The "conventional" way of investigating a physical problem consists of the following three steps:

i) Formulation of a model

ii) Solution of corresponding equations

iii) Comparison of theoretical results with experimental data.

The "direct" way of investigating the same physical problem consists of the following steps:

i) Collection of experimental data

ii) Solution of basic equations using direct experimental data

iii) Search of the model.

To illustrate the meaning of the above definitions, a hypothetical example is given first. Next, the two specific applications treated in this report are introduced from the view point of the direct approach. These are, the problem of detonation, and that of steady liquid propellants rocket combustion. Finally the properties of the direct method are listed. The properties will again be pointed out during the development of the two specific applications.

1.1 The General Idea and an Illustrative Example

For simplicity, consider a one-dimensional, steady flow in a duct of slowly varying cross sectional area. Assume that both the thermal and the caloric equations of state of the fluid are not known. Assume also that latent energy is added to the flow by some chemical reaction of unknown nature or rate. The fol-

lowing equations can then be written between any two sections of the duct:

$$\rho_1 u_1 A_1 = \rho_2 u_2 A_2$$

$$\rho_1 u_1^2 A_1 + p_1 A_1 + \int_{A_1}^{A_2} p\, dA = \rho_2 u_2^2 A_2 + p_2 A_2$$

$$e_1 + \frac{p_1}{\rho_1} + \frac{u_1^2}{2} + \varphi = e_2 + \frac{p_2}{\rho_2} + \frac{u_2^2}{2}$$

$$p = p(\rho, T, X_i)$$

$$e = e(\rho, T, X_i)$$

where the first three equations represent the conservation of mass, momentum and energy (with the energy source, φ, unknown) and the last two represent the missing thermal and caloric equations of state.

The conventional way of attacking the problem would be that of formulating a model which would lead to expressions for the energy source and for the equations of state. The above five equations would then be solved. Finally a quantity would be measured, say, the pressure along the duct and compared with the predicted one. The model would be modified until theoretical and experimental results match. Notice the following points:

1) The experimental data were used only to check the theoretical results and helped little or not at all in the process of formulating the model.

2) There is no way of knowing how accurate the experimental data are. The experimental data could be in error and the model might be adjusted to predict the wrong data.

3) In the theoretical study a system of five coupled equations had to be solved. To reach the solution certain approximations might be necessary.

4) In the formulation of the model many assumptions are usually made. If the model yields results not quite in agreement with the experimental ones, some difficulty may arise in deciding which of the assumptions should be modified.

The direct way of attacking the problem is to use the measured experimental pressure to solve the first two conservation equations without any assumption concerning the energy source and the equations of state. One notices that the first two equations contain three unknowns, p, ρ, u. Thus, if p is measured and ρ and u are given at some initial section, they can be computed at any other section by the first two equations.

Setting $\rho = \rho_2/\rho_1$, $u = u_2/u_1$, $p = p_2/p_1$, $A = A_2/A_1$ one gets:

$$u = 1 - [pA - 1 - \int_1^A p\,dA]/[\rho_1 u_1^2/p_1]$$

$$\rho = 1/uA$$

Now the investigator not only knows p but also knows ρ and u and he has more information on which to base his search for a model. Notice the following points:

1) Experimental data are needed in both approaches sooner or later. In the direct approach one squeezes more out of the experimental data since the knowledge of p led to the knowledge of ρ

and u without any more assumptions than were already imbedded in the equations (Experimental Data Information Optimization).

2) After having determined ρ and u one can make a few measurements of u and see if it agrees with that calculated by the first two equations. If it does, the first two equations are correct and pressure measurements are reliable. If it does not, either there is an error in the measurements or in the first two equations (for example, friction should not have been neglected). (Experimental Data Check).

3) The system of five equations has been split into two systems. A system of two equations (already solved) and a system containing the remaining three equations still to be solved. In the direct approach the mathematics is then simpler. (Mathematical Simplification and Set Splitting).

4) When the equations were split so were the assumptions. The assumptions going into the first two equations can be checked independently of the assumptions going into the remaining three equations (Assumptions Splitting).

The direct method offers other advantages which will be listed in the next section. They fundamentally stem from the fact that one can solve for some of the unknowns even if he does not know many aspects of his problem. The unknown aspects can then more

easily be investigated, since more information is then available and some features or properties of the problem have already been determined (Parameterization and Maximum Information). The first two steps of the "direct" method have thus been illustrated:

i) gathering of the experimental data, ii) solution of basic equations directly using experimental data. The third step, i.e., search of the model, can then be carried out by either studying that part of the solution which has become available and try to infer from it the complete solution or by trying several possible models and seeing how they fit the reduced set of equations (the last three equations, in the above example). The latter approach is expected to be the one more commonly used. It should be stated that the above considerations are not just conjectures. They are strictly facts that this author has established in specific applications of the direct method. Two of such applications will be discussed at length in this report.

The first application is to the problem of the detonation of solid explosives. The missing equation is the equation of state of the explosion products. The measured quantity is the detonation velocity versus the density of the explosive. Researchers using the "conventional" approach assumed several types of equation of state, solved their equations and compared their calculated velocities with the measured one. By the proper choice of a few constants appearing in their equation of state, they all were able to correlate well with the measured parameter. Their calculated energies and temperatures, however, varied conspicuously. By the "direct" approach (using as known quantity

the measured detonation velocity versus the density of the explosive) it was possible to show that detonation pressure, density and particle velocity can be calculated without using any equation of state while the detonation energy and temperatures are functions of the assumed equation of state. The general form of the equation of state was also derived. The problem of the actual equation of state is still unsolved yet one can now calculate many parameters without knowing the equation of state, and the class of functions, to which this equation of state belongs is now known. This much was not known previous to the application of the "direct" method, yet no extra information was used in the application of the "direct" method than has always been used in the application of the "conventional" method. Finally, the calculations by the "direct" method were considerably simpler than those required by the "conventional" method. The second application is to the problem of the steady state in liquid propellant rocket engines. The missing relations are those governing the production of gaseous products. The measured quantity is the static pressure or the particle velocity along the engine. Researchers using the "conventional" approach assumed certain droplet distribution, drag, and vaporization models, solved the equations and compared their calculated static pressure (or any other parameter) with the measured one. By the "direct" approach the measured static pressure (or particle velocity) was used. Then without any droplet distribution, drag, and vaporization model, all the combustion variables were calculated, namely: temperature, density, particle velocity, chem-

ical composition, flux of unvaporized fuel, etc. During this process much was learned about steady liquid propellant rocket combustion. Then some droplet distribution, drag, and vaporization models were studied with the purpose of selecting that one which gives all the calculated parameters. A third application of the "direct" method is briefly reviewed in Section 4.0. It is not due to this author but to Ya. B. Zel'dovich. It is in connection with the problem of unsteady solid propellant combustion where Zel'dovich suggested the direct use of experimental data thus avoiding the problem of formulating a model for the gaseous flame. Zel'dovich used directly experimental data also in connection with the problem of solid explosives (Section 2.2). Thus it seems as if Zel'dovich found it natural and rewarding to think "directly." A fourth application of the "direct" method is not discussed in this thesis but will be discussed in a separate report. It is in connection with unsteady liquid propellant combustion. It has been a very difficult application on which this author has actually spent most of his time as a graduate student. Professor Crocco suggested that a step shock be generated at the nozzle end of a liquid propellant rocket motor and its changes, as it moves toward the injector into the active combustion zone, be measured with the intent of studying the unsteady processes by which energy is fed into the shock. By measuring the pressure after the shock front at several locations along the motor, one experimentally determines $p = p(x,t)$. The one-dimensional, unsteady mass, momentum and energy conservation equations can

then be used to compute $\rho = \rho(x,t)$, $u = u(x,t)$ and $Q = Q(x,t)$ where Q is the unsteady mass-energy source. It is not necessary to postulate any droplet distribution, drag and vaporization models. On the contrary, such models can be studied a posteriori after having determined the unsteady pressure, density, particle velocity and mass-energy source. However, in order to obtain meaningful results from this unsteady liquid propellant combustion study, it was found necessary to achieve first a more accurate and specific understanding of the steady liquid propellant combustion. This originated the investigation of the steady combustion of the LOX/ethanol system reported in Section 3.0.

1.2 Properties Of The "Direct" Method

The above examples illustrate the usefulness of the "direct" method in cases when the model of a certain process is expected to be complex and when many models would seem to be just as reasonable. The properties of "direct" method are:

1) Experimental Data Information Optimization:

   The use of some experimental data directly in the basic equations allows the evaluation of all (or most of) the unknowns of a given problem. One has thus extracted maximum information from the experimental knowledge of a few parameters since by that he has calculated all (or most of) the unknowns.

2) Experimental Data Check:

   It would appear that the "direct" approach required more accurate experimental measurements.

To be used in the "direct" approach, the data must consistently fall on identifiable lines. Can one honestly use data which do not consistently fall on identifiable lines to verify the predictions of the "conventional" method? Researchers using the "conventional" approach often do not bother checking too closely the validity of the experimental data. On the other hand, experimentalists may not select the proper parameters to measure or may honestly be unaware of their experimental errors. Practice has shown that in using the "direct" method, seemingly consistent data were actually found to be in error and, subsequently, the source of error was identified. The reason is that when the experimental data are used in the basic equations and the equations are solved, the newly determined parameters often take on unrealistic values if the data used are in error.

3) Mathematical Simplification:

Both methods require the same amount of experimental data and the solution of the same basic equations but for different unknowns. The achieving of the solution of the same basic equations is then a problem of different difficulty in the two methods. In the "direct" method one always has to solve fewer equations than in the "conventional" one. In the "conventional" approach, a primary

source of error may be hidden in the approximations which are made to reach the more difficult solution.

4) Set Splitting:

An important aspect of the "direct" method is its splitting of the equations into uncoupled groups. This in turn, simplifies further the task of solving the equations and occasionally might reduce the number of parameters to be measured. In the previous example, the researcher investigating the pipe flow could have postulated a model in which all the five unknowns entered, and his five equations would then have been coupled. On the other hand, by measuring p and using it directly, his first two equations become uncoupled (containing only ρ and u as unknowns) and this is quite independent of what the actual model would then turn out to be. Similarly, in the solid explosion study, the system was split into two systems: the first one containing velocities, pressure and density, could be solved completely; the second one containing temperature and energies, and including the unknown equation of state, led only to the derivation of functional relationships between its unknowns. The unknowns also split

- those belonging to one group will be completely determined, those belonging to the other group will be bound by functional relationships.

5) Parametrization:

In the "direct" method, one looks at his basic equations and determines how many unknowns need to be measured to solve them without formulating a complex model. Usually one or more variables of the form $z = z(x)$ or $z = z(x, y)$ would need to be measured. If he measures as many unknowns as he needs he can then solve completely his equations for all the remaining unknowns. On the other hand, if one measures less unknowns than he would need he can still expect to be able to calculate completely some of the variables and to establish functional relationships between the remaining ones! This is due primarily to the splitting property of the "direct" approach. In the case of the solid explosive, the unknown equation of state is of the form $z = z(x, y)$ whereas the measured quantity (detonation velocity versus density of the explosive) is of the form $z = z(x)$. Still many variables were completely determined because the knowledge of the detonation velocity uncoupled the system of equations. However, in the liquid propellant steady-state study, it turned out that instead of needing the full measurement of two unknowns, as it appeared to be necessary to split the system of equations, the measurement of one unknown was actually sufficient. This was achieved by finding solutions for specific values of the second unknown. Thus a parametric set of solu-

tions were obtained rather than an unique solution. The family of solutions, however, turned out to be narrow enough to be used as an unique solution. The parametrization property is not really a property of the "direct" approach but rather a property of the physical process under consideration. However, it is when one starts thinking in terms of restricted solutions that the possibility of useful parametric solutions unfolds.

6) Assumption Splitting:

Associated with the property of splitting the equations into uncoupled groups, is the property of splitting the assumptions into groups as well. This property is important and therefore is given separate headings. In writing equations for a certain physical phenomenon several assumptions are made whose validity may be equally uncertain. If the "conventional" method yields a solution which doesn't quite agree with experimental data, the problem remains of determining which of the leading assumptions is to be corrected. The "direct" method yields the solution of only some of the equations which incorporate only some of the leading assumptions. If the results of "direct" method don't agree with further experimental data, one has then to review only a fraction of the leading assumptions. Thus, in the example given in this section, after having solved the direct problem,

one might want to verify the validity of his solution by measuring, say the gas velocity. Should the gas velocity disagree with the calculated one, the assumption of frictionless flow (the only significant assumption going into the mass and momentum equation as they are written), would be the only one which could be wrong. But had the researcher introduced a model through some assumptions and followed the "conventional" method, it would have been more difficult to decide whether the assumption of frictionless flow or those leading to his model were the wrong ones. Similarily in the liquid propellant steady-state study the only leading assumptions entering into the reduced set of equations, used in the "direct" method, was that of chemical equilibrium of the reaction products. This assumption could then be checked separately. Had one used the complete set of equations and followed the "conventional" approach further uncertain assumptions would have been needed about droplet distribution, motion and vaporization and separation of the effects might have been impossible.

7) Maximum Information:

This last property is possibly the most important yet the most difficult to define specifically. Having a complex problem, there is always some

variable which can be readily measured (like pressure in fluid dynamics problems). The basic equations can then be studied using directly the measured variable. During this study a wealth of information about the nature of the problem, the properties of its solution, the ordering of the terms in the various equations and the mathematical techniques to be used in the study of the complete set of equations become available. This is best illustrated by the discussion of the results obtained by the "direct" approach for the problem of steady-state liquid propellant combustion. It can be stated that, in general, these results can be expected to be of practical and theoretical values and can be obtained within the first two steps of the "direct" approach: i) measurement of some unknowns ii) solution of some of the equations using the measured unknowns, i.e., even before getting through the third and last step (determination of the proper model) which would complete the application of the "direct" method.

Both "direct" and "conventional" methods are equally effective when the problem under consideration is physically simple and related to some problem whose secret is already known. It is not difficult then to guess a reasonably good model for the new problem, neither should it be difficult to uncover the new law by studying the results of the "direct" method. If the problem is a complicated one, requiring one or more uncertain, yet far-

reaching, assumptions then the "direct" method should be seriously considered as the first one to be applied for its seven properties given above.

2.0 DETONATION PROBLEMS

2.1 Introduction

In recent years "it has been indisputably established experimentally that the wave front of all self sustaining detonations is three dimensional."[1] The wave front of what used to be the Chapman-Jouguet (C-J), steady, one-dimensional, laminar detonation front, with the Zel'dovich-von Neumann-Doring (ZND) structure, of tube confined explosions has now been proved to be actually made up of unsteady three dimensional shock patterns which include Mach stems, curved shocks and transverse waves. Most significantly the thickness of this unsteady three-dimensional front is of the order of 10 times the thickness of the old reaction zone. Within this new, nonuniform front, sharp variations in the values of the various detonation variables are found to exist so that concepts of average values become hard to justify. The practical success of the various versions of the C-J model in predicting detonation velocities is still unquestionably recognized. Why they work so well will, sooner or later, be explained. Presently, however, one must avoid drawing too many conclusions based on theoretical considerations of the C-J models.

The original suggestion of Chapman, that the actual detonation velocity is the smallest of all velocities compatible with the one-dimensional conservation equation, was not justified and was accepted because it was successful in predicting the detonation velocity of many explosives. In this section another unjustified suggestion is made by which detonation pressure (P),

density (ρ) and particle velocity (u) can be calculated if the detonation velocity (U) versus the loading density (ρ_0) is given. This suggestion turned out being a reinterpretation, an extension and an improvement of the procedure used by Zel'dovich and Kompaneets[2] to show that, for solid explosives, the detonation density is approximately 4/3 times the loading density. What follows is again a one-dimensional treatment of the detonation problem. In view of the complexity of the actual detonation structure, the quantities herein called detonation variables will have to be interpreted as average values at some distance after the front roughly coinciding with the old C-J plane quantities.

This section is organized as follows: First the envelope method is introduced. Next its relationship to the Zel'dovich-Kompaneets method of calculating the detonation parameters of solid explosives is illustrated. Application of the method to gaseous and solid explosives and comparison with experimental results are then made. The relationship between this method and the various versions of the C-J model is then discussed. For the purpose of this discussion, a brief review of the various C-J models is necessary and it is then given even though it is recognized that they are now largely superceded. In this context it might be interesting to notice that the conclusion of the review is that the C-J model never quite achieved self completeness. Finally, the problem of the equation of state of the reaction products of solid explosives is re-examined in the light of the results obtained with the current method.

For the one-dimensional case, the conservation equations through the shock can be written as follows:

(Mass Conservation) $$\frac{U}{v_0} = \frac{(U-u)}{v} \tag{1}$$

(Momentum Conservation) $$p_0 + \frac{U^2}{v_0} = p + \frac{(U-u)^2}{v} \tag{2}$$

(Energy Conservation) $$e - e_0 - \varphi^\circ = \frac{p+p_0}{2}(v_0 - v) \tag{3}$$

Where subscripted variables refer to conditions ahead of the shock and the others to conditions at any distance (x) behind the shock where conditions are stationary with respect to it. At x, e is the internal energy of the products and is related to p, v by the caloric equation of state, and φ° is the chemical heat released (difference between the enthalpy of formation of the products and that of the reactants) and in general is also a function of p, v. Mass and momentum conservation equations also give:

$$\frac{U^2}{v_0^2} = \frac{p-p_0}{v_0 - v} \tag{4}$$

$$u = U\left(1 - \frac{v}{v_0}\right) \tag{5}$$

Even assuming that $e = e(p, v)$ and $\varphi^\circ = \varphi^\circ(p, v)$ are known, Equations 1, 2 and 3 contain four unknowns: p, v, u and U. Thus the one-dimensional model is underspecified and some additional assumption needs to be made.

2.2 The Envelope Method

Equation 4 defines straight lines (Rayleigh lines) in the p, v plane if U, p_0, v_0 are given. For given U, p_0, v_0 the

actual solution of the one-dimensional problem will be represented by one point of the corresponding Rayleigh line (Point A). Keeping the same initial pressure, but increasing slightly the initial density of the explosive, the detonation pressure is known to increase, so that the new solution is represented by Point B.

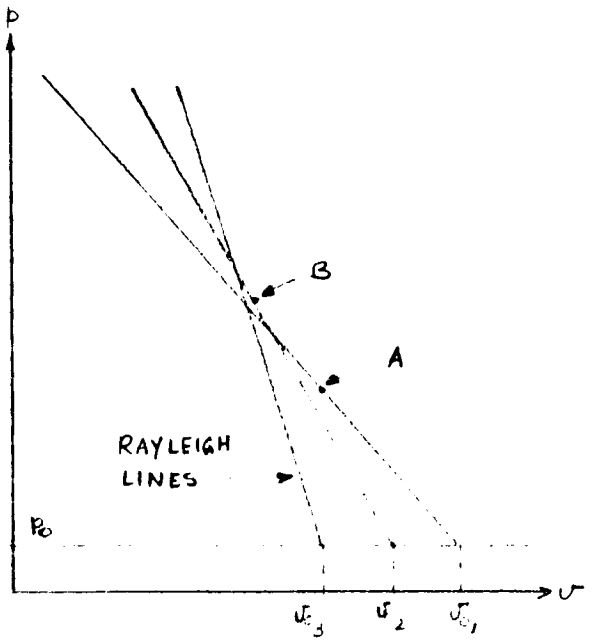

It is assumed that, as v_0 varies, the point representing the solution of the one dimensional problem moves along the envelope generated by the corresponding Rayleigh lines (envelope assumption). This assumption and the conservation equations constitute a complete system of equations for the solution of the one dimensional problem. (In essence this envelope assumption replaces the C-J assumption). Solving the complete set of equations with the use of the envelope assumption would be the "conventional" way of approaching the problem. However, detonation velocities have been measured for many explosives for various loading densities. It is thus known[3] that the detonation velocity of common gaseous mixtures is approximately constant for a given p_0 and for v_0 varying within a wide range ($D = a$), while the detonation velocity of common solid explosives increases with ρ_0. This increase is linear ($D = a + b\rho_0$) over a relatively narrow range of ρ_0's. In keeping then with the "direct" way of looking at physical

problems, the knowledge of $U=U(\rho_0)$ will be used directly together with the conservation equations and the envelope assumption to gain as much information about the various detonation variables as possible.

It is then assumed that $U=U(v_0)$ is known from experiments and the envelope of the Rayleigh lines is determined eliminating v_0 (the parameter of the envelope) between Equation 4 and its derivative with respect to v_0 (neglecting p_0)

$$f(p, v, v_0) = p - U^2 \frac{v_0 - v}{v_0^2} = 0 \tag{6}$$

$$\frac{\partial f}{\partial v_0} = 0 \quad \Rightarrow \quad 2(v_0 - v)\left(\frac{U'}{U} v_0 - 1\right) + v_0 = 0 \tag{7}$$

Equation 7, for any given $U=U(v_0)$, determines $v=v(v_0)$. Thus, for $U=a+b/v_0$ one finds

$$v = \frac{1}{2}\left[\frac{v_0 + 3b/a}{v_0 + 2b/a}\right] v_0 = K v_0 \tag{8}$$

Having $v=v(v_0)$, Equation 6 can be used to give $p=p(v_0)$ and mass conservation will give $u=u(v_0)$

$$u = U\left(1 - \frac{v}{v_0}\right) = U(1-K) \tag{9}$$

Where K is a weak function of v_0 for most solid explosives and only its average value ($\bar{K}$) may usually, be considered (see Table II Column 10). Eliminating v_0 between Equation 8 and Equation 6 one finds the equation of the envelope of the Rayleigh lines and, by assumption, the locus of the detonation states

$$p = \frac{U^2}{v_0^2}(v_0 - v) = \frac{(av + b\bar{K})^2}{v^3}\bar{K}(1-\bar{K}) \tag{10}$$

For a given v_0 , the tangent to the above envelope from p_0 , v_0 gives the detonation variables.

Further specializing to the case in which $U = a$ (gaseous explosives) one finds

$$K = 1/2 \tag{11}$$

$$v = v_0/2 \tag{12}$$

$$p = a^2/4v = U^2/4v = U^2/2v_0 \quad \& \quad pv = \text{const.} \tag{13}$$

$$u = U/2 \tag{14}$$

And for the case in which $U = \ell/v_0$ (roughly valid for solid explosives) one finds

$$K = 3/4 \tag{15}$$

$$v = 3v_0/4 \tag{16}$$

$$p = 3U^2/16v = U^2/4v_0 \quad \& \quad pv^3 = \text{const.} \tag{17}$$

$$u = U/4 \tag{18}$$

However, for solid explosives, one usually should use $U = a + \ell/v_0$ and the following relationships

$$K = \frac{1}{2}\left[\frac{v_0 + 3\ell/a}{v_0 + 2\ell/a}\right] \simeq \bar{K} \qquad (\bar{K} = .7 \text{ FOR TNT}) \tag{19}$$

$$v = K v_0 \tag{20}$$

$$p = \frac{U^2}{v} K(1-K) = \frac{U^2}{v_0}(1-K) \quad \& \quad pv^3 = (av + \ell K)^2 K(1-K) \tag{21}$$

$$u = U(1-K) \tag{22}$$

For solid explosives, Zel'dovich and Kompaneets[2] obtained, Equations 15 through 18 by a method which, in appearance, is different from the previous one, but which will be shown to be actually identical. First they set

$$U = D/v_0 \tag{23}$$

Next they assumed that $U = v_0/K$, with K a constant to be determined, and substituted U and v into Equation 4 (notice the equation of the Rayleigh lines) thus obtaining

$$p = \frac{U^2}{v_0^2}(v_0 - v) = \frac{D^2}{U^3}\left(\frac{K-1}{K^4}\right) \quad \text{OR} \quad p = B\rho^3 \quad \text{if} \quad B = D^2\frac{K-1}{K^4} \tag{24}$$

Next they stated: "We can then determine the constant K from the condition that the smallest possible detonation velocity must be achieved in experiment. We now specify the law $p = B\rho^3$ and write (using again Equation 4)

$$U^2 = \frac{p\rho}{\rho_0(\rho-\rho_0)} = \frac{B\rho^4}{\rho_0(\rho-\rho_0)} \tag{25}$$

We now determine the value of ρ for which U is minimum given B and ρ_0. In order to do this we calculate

$$\frac{dU^2}{d\rho} = \frac{B\rho^3(3\rho-4\rho_0)}{\rho_0(\rho-\rho_0)^2} = 0 \tag{26}$$

From which it follows that

$$\rho = \frac{4}{3}\rho_0 \qquad K = \frac{4}{3}$$

$$p = \frac{\rho_0 U^2}{4} \qquad u = \frac{U}{4} \quad ." \tag{27}$$

So they derived Equations 15 through 18. It would appear that

Zel'dovich and Kompaneets satisfied the C-J condition of minimum detonation velocity, but their calculation involves only momentum and mass conservation (from which Equation 4 is derived) whereas the C-J condition requires the selection of the minimum detonation velocity compatible with the complete system of equations (including the energy equation). They actually found the minimum detonation velocity compatible with Equation 4, i.e., the detonation velocity which is obtained by drawing the tangent to the envelope of the Rayleigh lines from p_0, v_0. Actually they overspecified their problem by assuming $v = v_0/k$ and found a solution because the overspecification happened to be compatible. To show this and to prove that Zel'dovich and Kompaneets method leads exactly to Equation 7, one proceeds as follows: Given $U = U(v_0)$, assume that $v_0 = J(v)$ (where $J(v)$ is an arbitrary function of v and setting $v_0 = J(v)$ is equivalent to assuming that ρ is an arbitrary function of ρ_0). Substitute $U = U(v_0)$ and $v_0 = J(v)$ into Equation 24 to obtain p as a function of v

$$p = U^2\left(J(v)\right)\frac{J-v}{J^2}$$

Substitute p back in Equation 4 to obtain U as a function of v and v_0

$$U^2 = \frac{v_0^2}{v_0 - v}\,U^2\left(J(v)\right)\frac{J-v}{J^2}$$

Set the derivative of U^2 with respect to v equal to zero (which is equivalent to setting the derivative of U^2 with respect to ρ equal to zero) and recall that $v_0 = J(v)$ thus obtaining

$$J J'\left[(J-v)(2U'J-U)+Uv\right] = 0$$

Excluding the trivial solutions $J = 0$ ($v_0 = 0$) and $J' = 0$ ($v_0 =$ const.), one finds the condition by which $v_0 = J(v)$ is determined if $U(v_0)$ is given

$$(v_0 - v)(2U' v_0 - U) + U v = 0$$

Which shows that, in general, one cannot start with selecting a particular form of $J(v)$ and still satisfy the above equation. The function $v_0 = J(v)$ is uniquely determined by the above equation when $U = U(v_0)$ is given. Thus, for $U = b/v_0$ one finds $v_0 = 4v/3$. Had Sel'dovich and Kompaneets started with, say, $p = K^{1/n} \rho_0^{1/n}$ with K and n constants to be determined and proceeded as they indicated they would have found $K = 4\rho^{n-1}/3$ which shows that, for K to be constant as assumed, n must be equal to 1. Thus finding again $\rho = 4\rho_0/3$. In conclusion, the functional dependence $v = v_0/K$ is not an assumption, as Zel'dovich and Kompaneets state, but is the unique solution of the problem. Re-arranging the terms of the above equations, one finds again Equation 7, thus proving the equivalence of the two approaches and explaining the real meaning of the Zel'dovich and Kompaneets method.

2.3 Comparison with Experimental Results

Before proceeding to some comparisons with experimental results it should be reminded that detonation velocity measurements can, it general, be considered accurate whereas detonation pressure measurements are, in general, less precise. This is so mostly because of the difficulty of defining which pressure has actually been measured in a situation in which the pressure varies sharply within a very narrow region. Thus data interpretation and extrapolation are often associated with pressure measurements.

This uncertainty must be remembered whether the agreement between theoretical and experimental pressures is good or not good.

Gaseous Explosives:

The first seven columns of Table I are from Lewis and von Elbe[3] and give theoretical and experimental data for various gaseous mixtures. The theoretical data of Lewis and von Elbe (Columns 2, 3, 4, 6 and 7) were calculated with the frozen Hugoniot (equilibrium composition) C-J model which will be reconsidered later. Taking the experimental detonation velocities of Column 5 and assuming that the detonation velocity does not change if v_o is changed and p_o is kept constant, one can calculate the detonation pressure, density and partical velocity by Equations 11 through 14. The detonation pressures thus calculated are given in Column 8. The detonation pressures measured by Gordon[4] (mixtures number 1, 3, 4) and by Campbell, Littler, Whitworth[5] (mixture number 1) are given in Column 9. It can be seen that the envelope method seems to give results at least as good as the C-J method used by Lewis and von Elbe.

Solid Explosives:

The first 6 columns of Table II are from Dremin[6] et al and give the measured values of the detonation variables for TNT and RDX and for various loading density. The detonation velocity was measured by the ionization method (Column 3). The detonation pressure was deduced by studying the transmission of the detonation shock into various metals (Column 5). The detonation particle velocity was then calculated (Column 4). The detona-

	1	2	3	4	5	6	7	8	9	
Mixture Number	Explosive mixture	Calculated p atm.	Calculated T_o °K	Detonation velocity, m./sec. Calculated	Detonation velocity, m./sec. Experimental	Concentrations, Per cent burned gas OH	Concentrations, Per cent burned gas H	Envelope Method p atm.	Experimental p atm	
1	$(2H_2+O_2)$	18.05	3583	2806	2819	25.3	6.9	20.1	18.3	20.4
2	$(2H_2+O_2)+1O_2$	17.4	3390	2302	2314	28.5	1.8	19.2		
3	$(2H_2+O_2)+3O_2$	15.3	2970	1925	1922	13.5	0.2	17.2	18	
4	$(2H_2+O_2)+5O_2$	14.13	2620	1732	1700	6.3	0.07	15.	16	
5	$(2H_2+O_2)+1N_2$	17.37	3367	2378	2407	14.7	3.3	19.6		
6	$(2H_2+O_2)+3N_2$	15.63	3003	2033	2055	5.5	0.9	17.8		
7	$(2H_2+O_2)+5N_2$	14.39	2685	1850	1822	2.1	0.2	15.4		
8	$(2H_2+O_2)+2H_2$	17.25	3314	3354	3273	5.9	6.5	18.		
9	$(2H_2+O_2)+4H_2$	15.97	2976	3627	3527	1.2	3.0	16.5		
10	$(2H_2+O_2)+6H_2$	14.18	2650	3749	3532	0.3	1.1	14.		

p_o = 1 atmosphere; T_o = 291°K

TABLE I COMPARISON OF CALCULATED AND EXPERIMENTAL DETONATION VELOCITIES OF MIXTURES OF HYDROGEN, OXYGEN, AND NITROGEN

1	2	3	4	5	6	7	8	9	10	11	12
Substance	ρ_o	U	u	p	u	U	p	u	κ	U	p
	g/cm^3	Km/sec		10^3At.	Km/sec	Curve-Fitted	Envelope	Envelope	Envelope	Curve-Fitted	Envelope
RDX	1.755	8.66	2.41	366		8.659	390.0	2.566	.7036		
RDX	1.59	8.10	2.23	287		8.100	313.2	2.432	.6998		
RDX	1.40	7.44	2.05	213		7.456	237.8	2.278	.6945		
RDX	1.20	6.75	1.87	152		6.778	172.3	2.118	.6875		
TNT	1.59	6.94	1.83	202	1.80	6.938	222.2	2.017	.7092	6.913	218.1
TNT	1.45	6.50	1.72	162	1.68	6.498	180.0	1.910	.7060	6.461	175.6
TNT	1.30	6.00	1.58	123	1.56	6.027	140.8	1.797	.7019	5.977	136.5
TNT	1.14	5.57	1.45	92	1.42	5.525	105.6	1.676	.6966	5.461	101.6
TNT	1.00	5.10	1.30	64	1.29	5.085	79.9	1.572	.6909	5.010	76.35

TABLE II DETONATION VARIABLE FOR RDX AND TNT

tion particle velocity was also deduced by a second method in which the reaction products displace a thin aluminum or copper U-shaped obstacle, and the motion of the obstacle in turn produces an induced electromotive force that is monitored and studied (Column 6). By this electromagnetic method the sound speed in the reaction products was also deduced. Linear curve fits of the measured detonation velocities (Column 3) were obtained (see Fig. 1 and Column 7), and using Equations 19 through 22 the detonation variables were computed and are given in Columns 8, 9, and 10. In Column 11 the detonation velocities of TNT measured by MacDougall[7] et al, are also given (see also Fig. 1) and the corresponding detonation pressures calculated by the envelope method are given in Column 12. The detonation pressure calculated by the envelope method is somewhat higher than the one measured by Dremin, et al. However, the difference is not too large particularly in view of the fact that the experimental pressure data cannot be taken as absolutely correct. Also, the linear curve fitting of the velocity data might be a bit arbitrary and the derivative of the curve fit appears in Equation 7. Thus the difference between the detonation velocity measured by Dremin, et al and by MacDougall, et al (Columns 7 and 11) is small, yet it has its bearing on the computation of the detonation pressure by the envelope method (Columns 8 and 12).

It might be worth noting that Dremin, et al, state that "the Hugoniot curve in the vicinity of the C-J point may be approximated, independently of the equation of state of the ex-

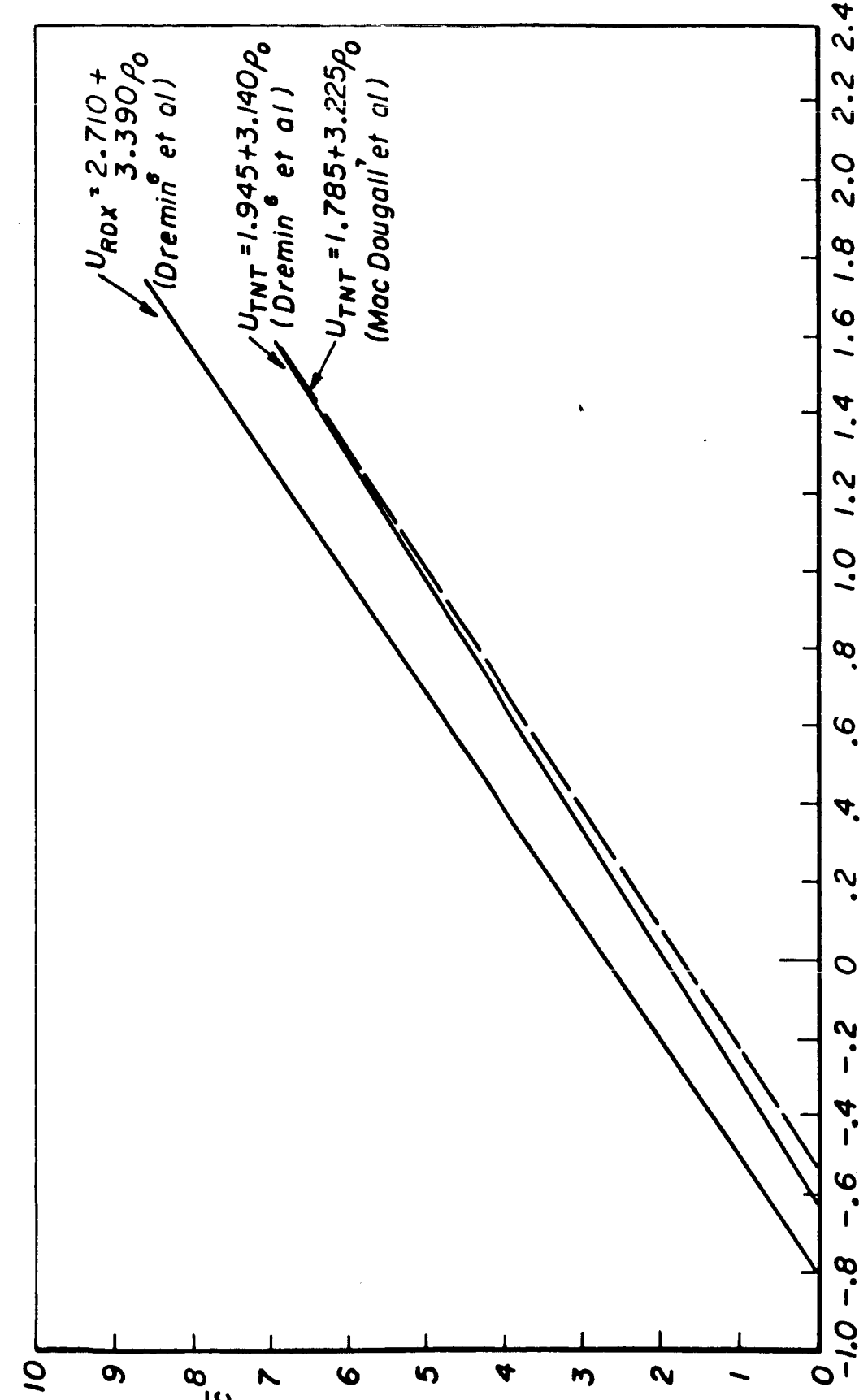

Detonation velocity vs loading density for RDX and TNT

Fig. 1

plosion products, by the power function $p v^{n} = A$ in which A and n are constants. For TNT $n \simeq 2.8$; for RDX it is $n \simeq 2.6$." Thus they must have made the same mistake that Zel'dovich and Kompaneets had made and that this author had made as well in an earlier version of this section. The mistake in the earlier version of this section was caught by Dr. L. Rudlin and Mr. M. Lurzky of the U. S. Naval Ordnance Laboratory (White Oak, Md.) who kindly advised this author of its presence. The accompanying skecth serves to clarify the point. For a given p_0 and v_0 (or ρ_0 = loading density) the energy equation (Eq. 3) defines a curve in the p, v plane which is called the Hugoniot curve. For the same p_0, v_0 there is one Rayleigh line which is tangent to the Hugoniot curve and the point of tangency is the C-J point. As v_0 varies a family of Hugoniot curves is obtained. The corresponding C-J points will define a new curve which can be called the locus of the C-J points. At the same time the Rayleigh lines will generate by envelope a third curve which has already been called the envelope. In general there is no reason to expect that for a given explosive and p_0 these three curves coincide. They would coincide if the Hugoniot curves collapsed into one single curve for all v_0's. However,

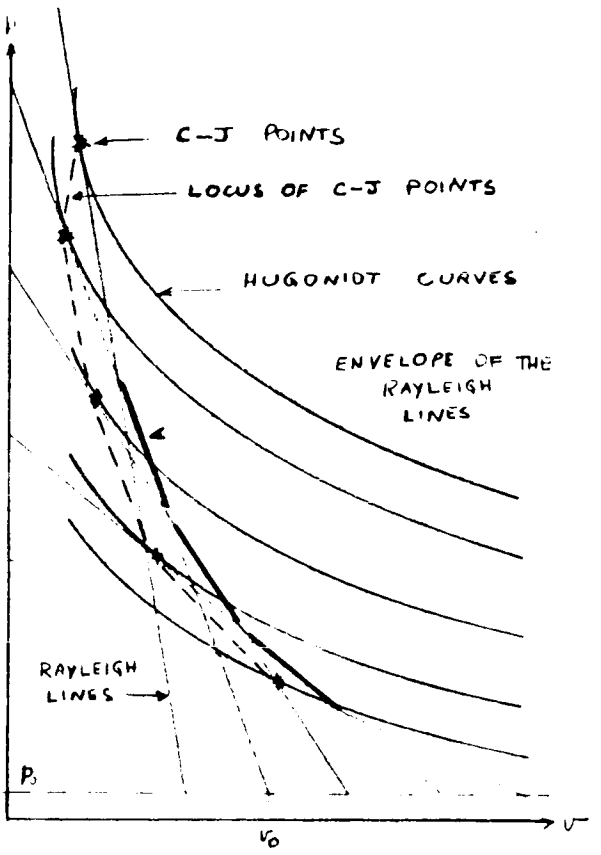

there is no way of using Dremin's measurements or any measurements to conclude that the Hugoniot curves indeed collapse into a single one without explicit consideration of the energy equation and in particular of the terms $e = e(p, v)$ and $\varphi^0 = \varphi^0(p, v)$ which in turn require the knowledge of the caloric equation of state of the products and of the chemistry of the process. The measurements of Dremin, et al, are sufficient to determine the locus of the C-J points (if one assumes that the pressure they measured is the C-J pressure). Indeed, having $p = p(v_0)$ and $U = U(v_0)$, Equation 4 defines $U = U(v_0)$ so that a $p = p(U)$ relation can be obtained. Also Dremin's $U = U(v_0)$ is sufficient to determine the envelope of the Rayleigh lines as it has already been seen (these two curves would have coincided if $p = p(v_0)$ calculated by the envelope approach had coincided exactly with the one measured by Dremin, et al). However, the data of Dremin cannot be used in the Hugoniot tangency condition

$$\left(\frac{\partial p}{\partial v}\right)_{s, p_0, v_0} = - \frac{p - p_0}{v_0 - v} \tag{28}$$

to obtain some Hugoniot curve as they seem to have done. Indeed they state that their measurements show that U/u is approximately constant and equal to 3.8 for TNT for all v_0's (actually it is between 3.79 and 3.95). Then they define the "Hugoniot" index n

$$n = \frac{U}{u} - 1 \tag{29}$$

From mass conservation it then follows that

$$\frac{v_0}{v} = \frac{n+1}{n} \tag{30}$$

At this point they must have eliminated v_0 from Equation 28 thus obtaining

$$\frac{dp}{dv} = -\frac{np}{v} \tag{31}$$

Upon integration, this yields the equation of what they call the "Hugoniot line"

$$p = A v^n \tag{32}$$

The error here is in having used Equation 28 for varying v_0 in the attempt to find some Hugoniot curve. This equation expresses the original Chapmann condition of tangency to the Hugoniot curve <u>for a given</u> p_0, v_0. Actually what Dremin, et al, have done is to find another envelope (different from the envelope of the Rayleigh lines). This envelope satisfies the condition that the tangent to each of its points goes through the point p_0, v_0 and is such that at the tangency point $v = nv_0/(n+1)$. However, the detonation velocity associated with this envelope is no longer of the form $U = a + b/v_0$. Now the detonation velocity is (from Equation 4 using Equations 30 and 32)

$$U = \left[\frac{A(n+1)^{(n+1)}}{n^n v_0^{(n-1)}}\right]^{1/2} \tag{33}$$

which further shows that if $n = 3$ then Equation 30 gives $v = 3v_0/4$ and Equation 33 gives $U \propto 1/v_0$ and one finds again the Zel'dovich-Kompaneets case.

It is by now clear that the various methods to calculate the detonation variables which have been discussed so far, are not equivalent to the C-J method and cannot be related to it in any obvious manner. It is nevertheless interesting to see how they compare with the various C-J models. In the next section a quick review of the C-J models is given with the purpose of comparing the models when possible, to the Rayleigh lines envelope method.

2.4 Review of C-J Models

Chapman (1889, sketch 1) suggested that the actual detonation velocity is the smallest of the velocities satisfying Equations 1, 2 and 3. For a given $e=e(p,v)$, $\varphi^0=\varphi^0(p,v)$ the energy equation defines a curve in the p, v plane called the Hugoniot curve. For a given p_0, v_0 and for various U, Equation 4 defines a family of straight lines, in the same plane, called Rayleigh lines. The minimum U satisfying the conservation equations is that for which the corresponding Rayleigh line is tangent to the Hugoniot curve. The point of tangency is called the Chapman-Jouget (C - J) point. Jouguet calculated the detonation velocity of several gaseous mixtures,

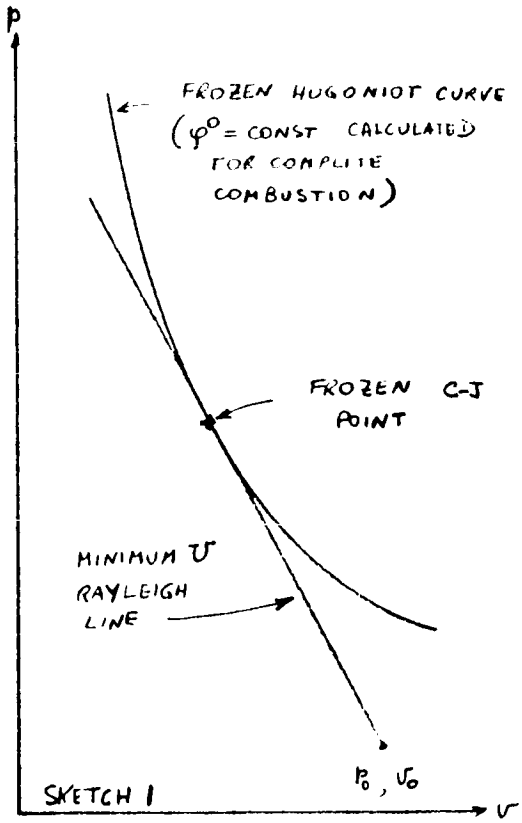

using the minimum detonation velocity condition (C-J condition) and computing φ° for the case of complete combustion of the reactants (no dissociation). The Hugoniot curve is then for φ° = constant and it is called a frozen Hugoniot curve since it corresponds to different solutions of the energy equation for the fixed complete composition for which φ° is evaluated. The detonation velocities calculated by Jouguet were in good agreement with the experimentally measured ones. Since dissociation is known to occur and to influence appreciably the calculation of detonation velocities, the explanation for the good results obtained by Jouguet is due to the fact that he used "specific heats calculated from measurements made by exploding gases in closed vessels. In such experiments dissociation certainly occurred, but in analyzing the results of such experiments no dissociation was allowed for".[8] Thus dissociation was included without realizing it. It can be shown[9] that in this model, the tangency condition is equivalent to setting $v = u + a_f$ which means that at the distance from the shock front at which the C-J condition is verified, the velocity is sonic with respect to the front and the speed of sound to be considered is the frozen speed of sound (a_f). It is instructive to apply this C-J approach to a specific problem. Thus consider the case of the gaseous mixture $(2H_2 + O_2) + 4H_2$. The products of complete combustion are $2H_2O + 4H_2$. The heat released by the complete combustion is $\varphi^\circ = 10.82\ 10^{10}$ erg/g. The equations to be used are

$$\frac{pv}{(\bar{\gamma}-1)} - \frac{p_0 v_0}{(\gamma_0-1)} - \varphi^\circ = \frac{p+p_0}{2}(v_0 - v) \qquad (34)$$

$$\frac{U^2}{v_0^2} = \frac{p - p_0}{v_0 - v} \tag{35}$$

$$\frac{\gamma p}{v} = \frac{p - p_0}{v_0 - v} \tag{36}$$

The first of the above equations is the energy equation (where the reference temperature is $0^{\circ}K$). The products are assumed to be thermally perfect. If the products are assumed to be also calorically perfect then $\bar{\gamma} = \gamma$. Otherwise $\gamma_0 = 1.4$, $\gamma = 1.24$ (expecting the products to be at approximately $3000^{\circ}K$) and $\bar{\gamma} = 1.3$ where an average γ is taken for the computation of the internal energy of the reaction product to avoid the integration, from the reference to the final temperature, which otherwise would be necessary. The second equation is again Equation 4 and the third equation is the C-J tangency condition written in its form $U = u + a_f$ and after having made use of mass and momentum conservation equations. For a given p_0, v_0 the above three equations contain three unknowns p, v, U so that, in general the detonation velocity thus calculated will be a function of v_0 (for a fixed p_0). The dependence $U = U(v_0)$ can be estimated from the following considerations. If one neglects p_0 with respect to p (p_0 can be expected to be about 6% of p) one finds

$$v = \gamma v_0 / (\gamma + 1) \tag{37}$$

$$p = \frac{U^2}{v_0(\gamma+1)} = \left[\frac{p_0 v_0}{\gamma_0 - 1} + q^0\right] / v_0 \left[\frac{2\gamma - (\bar{\gamma} - 1)}{2(\gamma+1)(\bar{\gamma} - 1)}\right] \tag{38}$$

$$U = \left\{\left[\frac{p_0 v_0}{\gamma_0 - 1} + q^0\right](\gamma+1) / \left[\frac{2\gamma - (\bar{\gamma} - 1)}{2(\gamma+1)(\bar{\gamma} - 1)}\right]\right\}^{1/2} \tag{39}$$

If one further neglects $p_0 v_0/(\gamma_0 - 1)$ with respect to φ^0 one finds that U is independent of p_0 and v_0. For the mixture under consideration (and assuming p_0 = 1 At. $T_0 = 293^0$K), $p_0 v_0/(\gamma_0 - 1) = .94\ 10^{10}$erg/g which is about 8.6% of φ^0 (Typically $p_0 v_0/(\gamma_0 - 1)$ is about 10% of φ^0 thus neglecting it brings about approximately a 10% error in p and a 5% in U). For practical calculations γ is often used instead of $\bar{\gamma}$ thus finding [2]

$$v = \gamma v_0/(\gamma+1) \tag{40}$$

$$p = U^2/v_0(\gamma+1) = 2\varphi^0(\gamma-1)/v_0 \tag{41}$$

$$U = [2\varphi^0(\gamma^2-1)]^{1/2} \tag{42}$$

And in so doing the term $(2\gamma - (\bar{\gamma}-1))/2(\gamma+1)(\bar{\gamma}-1) = 1.62$ is replaced by $1/2(\gamma-1) = 2.08$ and another 22% error is introduced. Both the detonation variables calculated by Equations 37, 38, 39 and those calculated by Equations 40, 41 and 42 are given in Table III and the differences cannot be considered negligible. The same variables calculated by other versions of the C-J models will presently be considered.

The above equations are simple enough so that one can illustrate the difference between the detonation pressure and specific volume calculated by this first C-J model and those calculated by the envelope method for the case in which the same detonation velocity is used in both cases ($U = a$ = constant). Thus comparing Equation 12 with Equation 37 one sees that the detonation specific volume calculated by the envelope method is

	v	p	U	OH	H	φ°_{298}
	cm^3/g	At.	m/sec	% of Burnt Gas		10^{10} erg/g
Frozen Hugoniot Curve (Complete Combustion: Eqs. 37, 38, 39)	2080	19.5	4060	0.0	0.0	11.00
Frozen Hugoniot Curve (Complete Combustion: Eqs. 40, 41, 42)	2080	14.0	3430	0.0	0.0	11.00
Frozen Hugoniot Curve (Equilibrium Composition: Lewis and Friauf[3])	2155	15.97	3627	1.2	3.0	---
Frozen Hugoniot Curve (Equilibrium Compos-tion: This author)	2210	16	3699	.6544	3.644	9.628
Equilibrium Hugoniot Curve (This author)	2100	17	3680	---	---	---
Experimental (see Lewis and von Elbe[3])	----	---	3527	---	---	---
Envelope of Rayleigh lines using U = 3527 m/sec	1880	16.5	3527	---	---	---

TABLE III DETONATION VARIABLES OF $(2H_2+O_2)+4H_2$ CALCULATED BY VARIOUS METHODS (p_0 = 1 At, T_0 = 293°K, v_0 = 3760 cm^3/g)

$(\gamma+1)/2\gamma$ times smaller than that given by this C-J model while comparing Equation 13 with Equation 38 one sees that the detonation pressure is $(\gamma+1)/2$ times larger. Since for gaseous explosives $\gamma \sim 1.25$, the envelope method will give a 10% smaller v and a 12.5% larger p than this C-J model. A more elaborate C-J model, which will be examined shortly, will tend to give lower v and higher p thus further reducing the difference between the two methods.

Lewis (1930, sketch 2) recalculated detonation velocities of gaseous mixtures using φ^0 = const but corresponding to its equilibrium value. Since the composition is still constant along the Hugoniot line (even though now it is the equilibrium composition rather than the complete combustion composition), the tangency condition is still exactly equivalent to setting $U = u + a_f$. In fact, this is the way Lewis applied the C-J condition when he set $a^2 = \gamma p/\rho$ which shows that a is the frozen speed of sound in the detonation products. Lewis used correct specific heats and his detonation velocities again agreed well with the measured ones[3] (except for highly diluted mixtures).

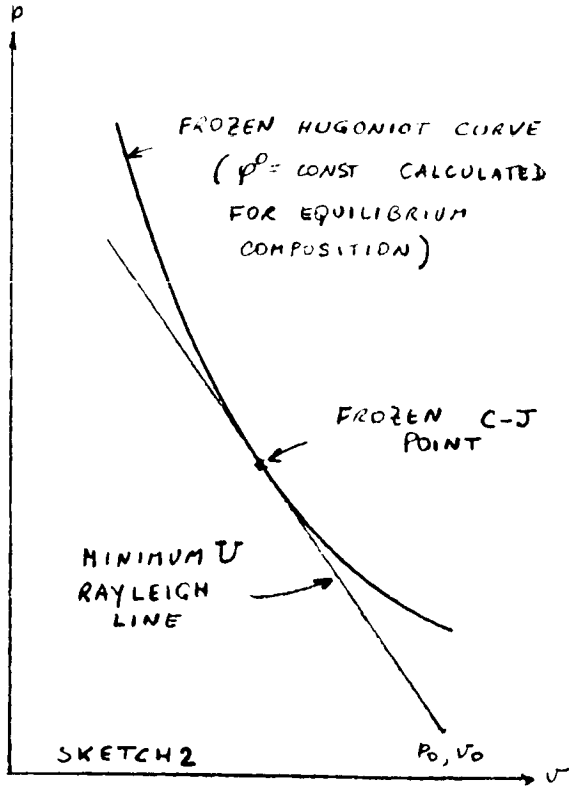

A model for the structure of the detonation wave was then suggested by Zel'dovich, von Neumann and Doring (ZND Model 1940, Sketch 3). According to this model a detonation wave is actually made up of an adiabatic shock, followed by a deflagration then followed by a rarefaction. The deflagration is stationary with respect to the adiabatic shock front. Within the deflagration zone the reaction proceeds controlled by chemical kinetics and various states of completion are identified by the quantity η which takes the value of 1 at that distance from the front at which the reaction is complete (C-J plane). In the formulation of von Neumann[10], within the deflagration zone, "a unit mass contains η parts of burnt gas, η-1 part of intact explosive." One is still free to choose that the η parts of burnt gas have reached a complete combustion state and have given out the complete combustion heat of reaction (no dissociation) or that they have reached their equilibrium state and given out the corresponding equilibrium heat of reaction. Gordon[4] calculated the intermediate and the final frozen Hugoniot curve for H_2-Air and using (probably) a succession of equilibrium states for the η parts of burnt gas. The important thing is that this study of the structure of the detonation wave did not alter the computation of the quantites at the C-J point. In this study, the presence of the

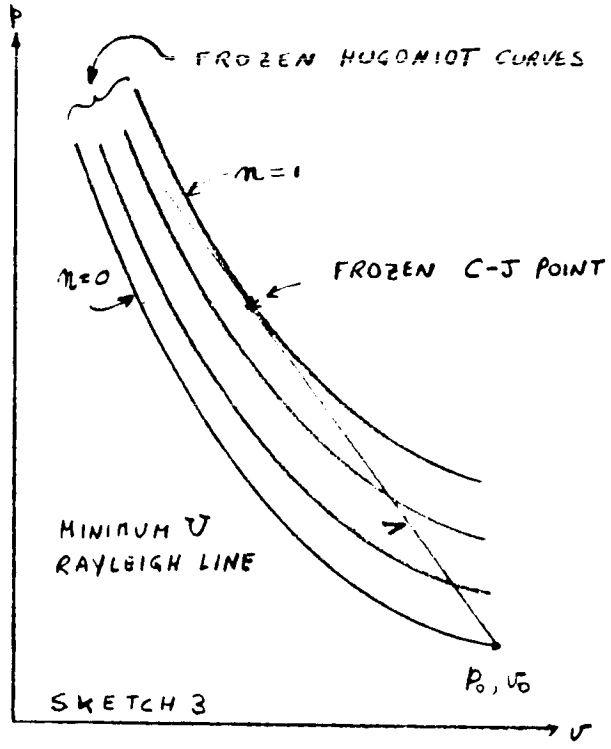

SKETCH 3

rarefaction wave is not considered. Instead it is stated that the combustion goes to completion at some distance behind the front.

The question of whether combustion goes to completion and what it is meant by it was investigated by Brinkley[11], Kirkwood and Wood[12], (1953, Sketch 4) by studying the interaction between the deflagration and the rarefaction waves. By imposing the condition that the characteristics from the two regions should join smoothly, Kirkwood and Wood concluded that there must exist a plane on which chemical equilibrium is reached and that on this plane the proper condition to apply is $U = u + a_f$ (forzen C-J point), thus confirming the consistancy of Lewis calculations. However, Wood[13] subsequently changed his previous conclusion and stated that on the plane on which chemical equilibrium is reached the proper condition to apply is $U = u + a_e$ (equilibrium C-J point). Indeed it would appear[9] that if one uses the equilibrium Hugoniot curve, the original tangency condition is equibalent to setting $U = u + a_e$ where a_e is the equilibrium speed of sound. If this model is correct, the calculations of Lewis are not accurate. From the examination of Sketch 4, it would appear that the various definitions of the C-J condition should lead to practically identical shock velocities but may lead to quite different detonation pressures and densities. This is due to the fact that the slope of the Rayleigh line should

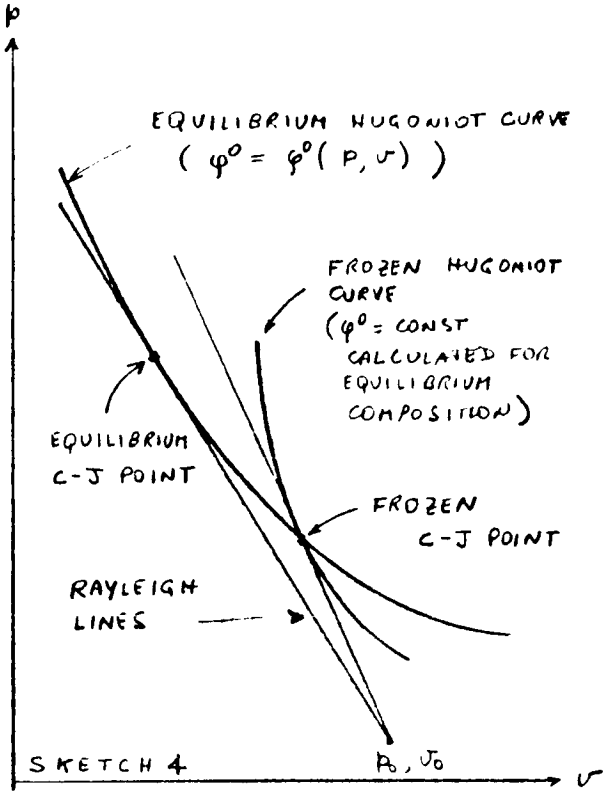

not be modified appreciably (and the detonation velocity is proportional to its square root), but the tangency point may shift considerably (see Sketch 4). This author then decided to evaluate the difference between the various approaches for the gaseous mixture: $(2H_2 + O_2) + 4H_2$ (p_o = 1 At.; $T_o = 293^oK$). This is one of the mixtures studied by Lewis and Friauf (see Table I) and the detonation velocity calculated by them (U = 3627 m/sec; p = 15.97 At.) was somewhat higher than the measured one (3527 m/sec). Lewis and Friauf, as previously stated (Sketch 2), used, as C-J condition, the tangency condition to the frozen, equilibrium Hugoniot curve. Since the condition of tangency to the equilibrium Hugoniot curve should yield a somewhat lower detonation velocity (Sketch 4), it was hoped that the detonation velocity thus calculated might have been in better agreement with the experimental one. The products considered were the same as those considered by Lewis and Friauf (H_2O , H_2, O_2, OH, H). The computation proceeds as follows. The equilibrium composition equations (see Sec. 3.2) are solved together with the energy conservation equation (Equation 3) and the equation of state of the products (perfect gases) for a specific value of p. This determines v , e , φ^o, T and the equilibrium composition, and obtains one point of the Hugoniot equilibrium curve (see Fig. 2). The process is repeated for several values of p thus defining the Hugoniot equilibrium curve. For a given point of this curve the composition is frozen (φ^o = const) and corresponding frozen, equilibrium Hugoniot curves are calculated. Two tangents can then be drawn: 1) to the equilibrium Hugoniot curve, thus obtaining p = 17 At., v = 2100 cm^3/g, U = 3680 m/sec; 2) to that frozen Hugoniot line whose tangency point is on the

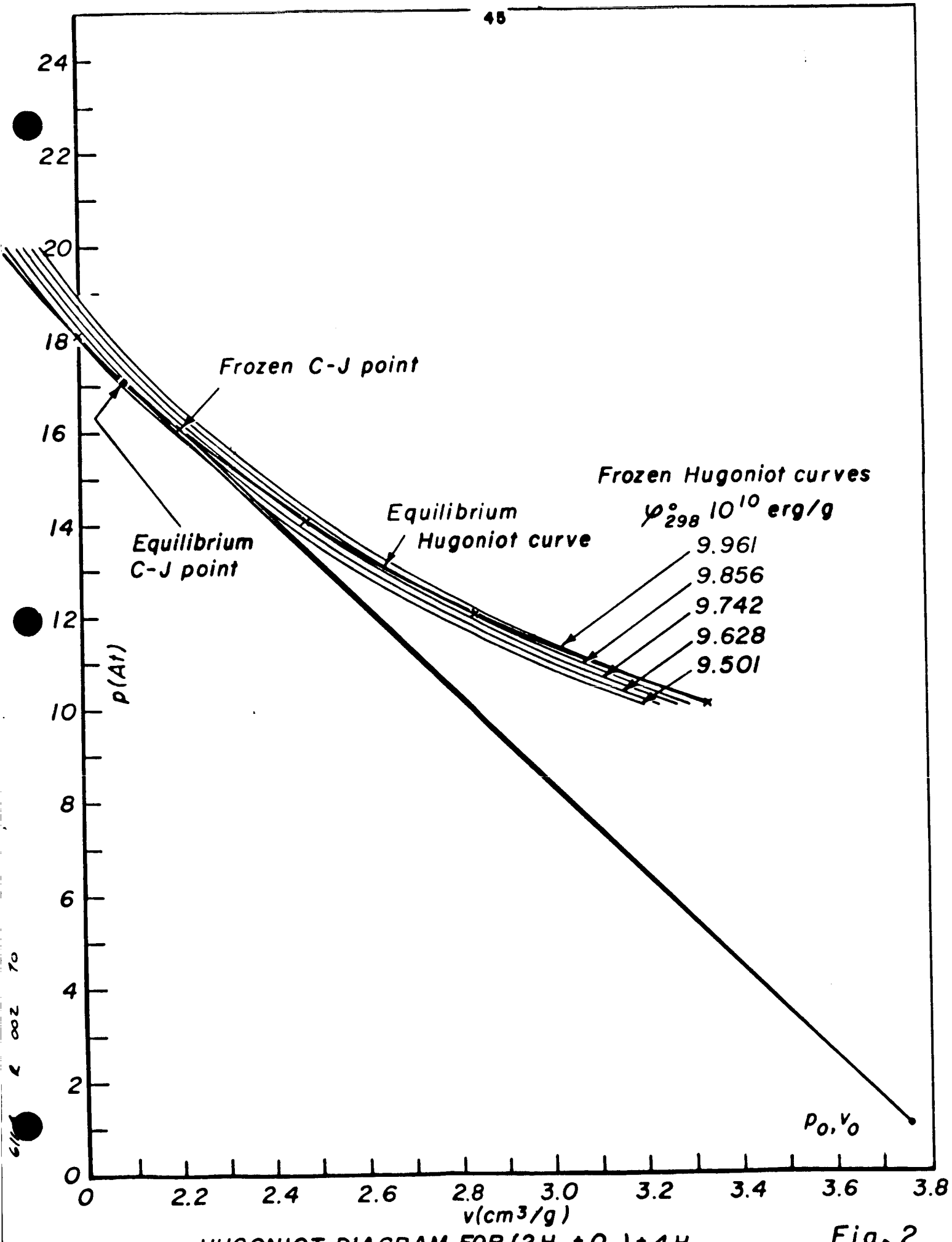

HUGONIOT DIAGRAM FOR $(2H_2 + O_2) + 4H_2$

Fig. 2

equilibrium Hugoniot line thus obtaining p = 16 At., v = 2210 cm^3/g, U = 3699 m/sec (Lewis and Friauf reported p = 15.97 At., v = 2155 cm^3/g, U = 3627 m/sec). These results are summarized in Table III.

On the basis of this computation one can make the following observations:

a) The tangency to the frozen Hugoniot curve (for equilibrium composition) should have yielded exactly the results of Lewis and Friauf but did not do so. In the present calculation, JANAF (1960) values for the specific heats of the various substances and for the equilibrium constants were used and computations made on a digital computer. Experience shows that this kind of equilibrium computations are sensitive to the above quantities which in turn have been somewhat improved over the years. Thus the difference could be accounted for by just the differences in the thermodynamic data used. Hence, the percent concentrations of OH and H reported by Lewis and Friauf are 1.2 and 3.0 while, with their p and T, this author obtains 0.5 and 2.94 respectively, thus indicating some difference in the equilibrium constants. Notice that the amount of dissociation is very small.

b) The two definitions of the C-J point yielded detonation velocities differences of only .516% but detonation pressure differences of

5.8% and detonation specific volume differences of 5.2%. Notice that these differences are for a case in which dissociation is very small. Had the dissociation been higher, greater differences would have been found. The influence of the dissociation is shown by its influence on φ^0 (see Fig. 3). In spite of the small dissociation the changes of φ^0 are not negligible.

c) Measurements of shock velocities will not resolve the problem of which of the two definitions is more accurate.

d) The fact that neither of the two approaches has yielded the measured detonation velocity suggests that something is still missing in the C-J model for the detonation process even for the simpler case of gaseous mixtures.

Wanting to look at the detonation process within the framework of the C-J model, one could formulate the following thoughts. For the mixture under consideration, one must assume that equilibrium was not reached and that some of the mixture had not reacted, thus casting some doubts on the assertion that an equilibrium composition is reached before the starting of the rarefraction wave. It could be a case of what are called "pathological" detonations whereby the Hugoniot curves representing the intermediate stages of the deflagration (see Sketch 3) intersect each other. In this case, according to von Neumann[10], they should form an envelope and the proper C-J condition is

not that of tangency to the $n = 1$ Hugoniot curve, but rather that of tangency to this envelope. But then, still according to von Neumann, the "pathological" detonation velocity should be higher than the normal one while the measured one is actually lower. It could also be that the current model of the normal detonation process is too strict. In summary this model calls for an adiabatic shock front followed by a deflagration which is stationary with respect to the shock front. The deflagration merges with the rarefaction wave and at the merging point (C-J point) chemical equilibrium is reached and $V = u + a_e$ is satisfied (the condition $V = u + a_e$ is here equivalent to the condition of tangency to the Hugoniot equilibrium curve[9]). It would seem that, for the C-J point to be stable, the condition should be $V = u + a$, where a is the actual speed of sound which is greater than a_e and smaller than a_f (the difference between a_e and a_f being as high as 10%). It would seem that, if at the C-J point $V = u + a_f$, then a rarefaction wave would overtake the front since it would move after it at the speed $u + a$ which is greater than $u + a_e$. One would then notice that the condition $V = u + a$ is sufficient to determine the detonation problem. It does not require any other restraint like that of chemical equilibrium. There seems to be no need of distinguishing between deflagration and rarefaction waves. There would be a stationary reactive region (up to the point at which $V = u + a$) followed by a nonstationary one. For a given mixture, the existence of a stable detonation velocity would simply imply that at some distance after the front

the condition $U = u+a$ is met. In principle, starting from a point after the adiabatic shock front one would integrate a set of 1st order O.D.E. representing the reaction kinetics together with the Rankine-Hugoniot equations (Equations 1, 2, 3) and the equation of state to calculate composition and all other variables as functions of the distance from the shock front. One would have to start with guessing U (so that the initial conditions for the O.D. equations became known) and calculate u and a at each distance from the front. If the condition $U = u+a$ is nowhere satisfied one would change U and repeat the process (for the H_2, O_2 system such calculations might be possible since some information is available about the corresponding reaction mechanism and reaction rate constants). This C-J model does not lead to a meaningful graphical description in the p, v plant since the C-J point would not in general coincide with any tangency condition. It would be that point of the Rayleigh line which satisfied the energy equation but at which the Rayleigh line is not necessarily tangent to either frozen of equilibrium Hugoniot curves. This model could be tested by studying the effects of additives on the detonation velocity of a mixture whose products do not seem to reach equilibrium composition (such as $(2H_2+O_2)+4H_2$). The additives would change the relative concentration of the products, thus altering the conditions under which $U = u+a$ and consequently the value of the detonation velocity (in general the detonation velocity of TNT, with inert additives, is found to be equal to the detonation velocity of TNT without additives but at a correspondingly lower loading density). However, Dremin re-

ports that the addition of SiO_2 (15% by weight) increases the detonation velocity quite strongly at high loading density).

The above computations would be complex and in light of the more recent knowledge of the structure of the detonation front perhaps not justifiable.

One can thus conclude this section by simply noticing that there are various modifications of the basic C-J model and that they lead to appreciably different results. None of them can be defined consistent with recent knowledge of the detonation front structure and all of them give reasonable estimates of the detonation variables. The Rayleigh line envelope method seems to give just as good an estimate of these variables and for its simplicity might be of practical use. The results of Table III support this conclusion.

2.5 On the Equation of State of the Products of Solid Explosives

The problem of the equation of state of the products of solid explosives is still largely unresolved. In "conventional" studies of the detonation of solid explosives, one assumes some equation of state (the ones this author is aware of can all be related to the Van Der Waal's equation) for the products which contains some arbitrary constants. The complete set of equations with some version of the C-J model (φ^0 is taken to be constant almost universally, i,e., frozen C-J models) is then solved for various loading densities. The detonation velocity $U = U(v_0)$ thus calculated is compared with the measured one and the arbitrary constants are so adjusted as to bring about agreement between the calculated and the measured $U = U(v_0)$. In the "direct"

approach on the contrary, one uses all the information that is available and tries to learn as much as possible about the equation of state with a minimum number of assumptions. Thus, the envelope method shows that $v/v_0 = K$ where K is very close to being constant over the range of interest of v_0's ($K = .7 \pm .01$ for TNT and $.695 \pm .0075$ for RDX, see Table II). One might prefer to take $v/v_0 = K$ as an experimental result obtained by Dremin, et al, (in this case $K = .736$ for TNT and .723 for RDX). Either way, one can write the energy equation as follows

$$e - e_0 - \varphi^0 = \frac{p}{2}(v_0 - v) = pv\left(\frac{1-\bar{K}}{2\bar{K}}\right) \tag{43}$$

Next two major assumptions are made. The first one is that the reaction products are in chemical equilibrium in which case

$$\left(\frac{\partial e}{\partial v}\right)_T = T\left(\frac{\partial p}{\partial T}\right)_v - p \tag{44}$$

The second one is that $e_0 + \varphi^0 = \text{const}$ as v_0 varies. Both assumptions are continuously made in the trade, but it is anything but evident that they are justified. Furthermore, in the conventional approach these assumptions are made on top of other assumptions which are here not necessary. The constancy of φ^0 will briefly be discussed later. With these two assumptions, one can eliminate e between Equations 43 and 44 (where e and p are seen as functions of v and T) thus obtaining

$$T\frac{\partial p}{\partial T} - \left(\frac{1-\bar{K}}{2\bar{K}}\right)v\frac{\partial p}{\partial v} = \left(\frac{1+\bar{K}}{2\bar{K}}\right)p \tag{45}$$

Notice that no restriction has been imposed on $e = e(v, T)$. The general solution of this first order linear P.D.E. for $p = p(v, T)$

can be written in several equivalent forms among which

$$F\left[T^{\frac{1-\bar{K}}{2\bar{K}}} v \; ; \; v^{\frac{1+\bar{K}}{1-\bar{K}}} p \right] = 0 \qquad (46)$$

Where F is any arbitrary function of its arguments. The equation of state of the products must satisfy the condition $F = 0$ which was derived from experimental data and the above two assumptions. Here one has a good example of the advantages that the direct method offers in some problems. Using the experimental fact that v/v_0 = constant, an expression was derived that the equation of state must satisfy thus getting the most out of the experimental data (Maximum Information). It was necessary to solve a simple P.D.E. versus the complications of conventional calculations (Mathematical Simplification). This was possible since only two of the five equations describing the problems were solved (Set Splitting). It was not necessary to require the validity of the C-J model and other assumptions which usually are made in the conventional approach (Assumption Splitting). Still two basic assumptions were made, but their validity could not be checked separately by additional experimental data. One could now study Equation 46 for various $T = T(v_0)$ or for the various equations of state which have been proposed and experience shows that such a study would be fruitful (Maximum Information). A similar study was performed for the problem of steady combustion of the LOX/ethanol system and the results are given in Section 3.6. Going back to Equation 46, the function F (and therefore the equation of state) cannot be determined without further experimental data or assumptions. The only condition available

is that F be such as to give the $v = v(\sigma_0)$ and the $p = p(\sigma_0)$, determined using $U = U(\sigma_0)$ and given by Equations 20 and 21 respectively, or the experimentally determined $v = v(\sigma_0)$ and $p = p(\sigma_0)$ given in Table II. Thus, choosing a particular form for F, one could set

$$v^{\frac{1+\bar{K}}{1-\bar{K}}} p = f\left(v\, T^{\frac{1-\bar{K}}{2\bar{R}}} \right) \tag{47}$$

where f is an arbitrary function of its argument. The left hand side of Equation 47 is a known function of σ_0 (through Equations 20 and 21). If $T = T(\sigma_0)$ is measured, one can determine f, and therefore the missing equation of state. Similarly for <u>any</u> selected $T = T(\sigma_0)$, a function f can be found which satisfies Equation 47. Which ultimately shows that the experimental knowledge of $U = U(\sigma_0)$; $p = p(\sigma_0)$; $v = v(\sigma_0)$; $u = u(\sigma_0)$ give no information at all about $T = T(\sigma_0)$. This is because U, p, v, u are essentially dynamic parameters related to the energy equation (Equation 43) only through the product pv. As far as this energy equation is concerned, the knowledge of U, p, v, u is used only in as far as it determines $p = p(v)$ and the function $p = p(v, T)$ cannot be completely determined using only one function of the form $p = p(v)$. One can reach the same conclusion also by the following reasoning. Detonation pressure, density and particle velocity can be calculated immediately without using any equation of state for the explosion products is the envelope method is assumed to be correct and if the detonation velocity versus the loading density is given. Conversely, this implies that the same detonation

pressure, density and particle velocity are calculated with any form of the equation of state when the same detonation veolcity versus loading density is used. The envelope method gives results which are very close to those obtained by the various C-J models to the point that many authors have taken the two methods to be equivalent. Thus, if the validity of some C-J models were assumed (instead of the validity of the envelope method) the conclusion would be reached that slightly different detonation pressure, density and particle velocity are calculated by completely different equations of state when the same detonation velocity is used. This explains why similar $p = p(v_0)$, $\rho = \rho(v_0)$, and $u = u(v_0)$ and completely different $T = T(v_0)$ have been calculated by various authors using similar $U = U(v_0)$ and different equations of state (the calculated temperature is a function of the assumed equation of state). Thus, according to some authors[15,16] T increases with ρ_0 (p, v and u increase) while according to others[14,17,18] T decreases with ρ_0. The problem of whether T increases or decreases is related to the problem of whether φ^0 can be taken to be constant with ρ_0. If the reaction products behave qualitatively as equilibrium perfect gases and if both p and T increase with ρ_0 then chances are that the assumption φ^0 = constant is not a bad one. This is so because φ^0 would increase with p and decrease with T due to the fact that dissociation decreases with p and increases with T.

2.6 Conclusions

The concept of using experimental data to solve basic equations with a minimum number of assumptions in order to get maximum information out of the experimental data has been applied

to the detonation problem within the frame work of steady, one dimensional, laminar detonation front. It has been shown that the knowledge of the detonation velocity versus loading density is sufficient to determine detonation pressure, density and particle velocity using only mass and momentum conservation equations and the envelope assumption. The envelope assumption has been shown to lead to slighly different results than those yielded by the various versions of the C-J model. The envelope method gives detonation pressures some 10% higher, and detonation specific volumes some 10% lower than the simplest of the C-J models. The difference tends to decrease for more complicated C-J models and, in any case, the envelope method is simpler than the C-J models and leads to predictions of the detonation variables which are in reasonably good agreement with experimental results for both gaseous and solid explosives. In the process of comparing the envelope method with the various C-J models, the conclusion has been reached that the C-J theory seems to have never achieved a state of self consistancy. After having solved mass and momentum conservation equations, with the envelope assumption, for detonation pressure, density and particle velocity, the energy conservation equation was considered with the purpose of gaining some information about the equation of state of the products of solid explosives. An expression was derived which would give the equation of state if the detonation temperature were measured. For that it was found necessary to assume that the energy released is independent of the loading density and that the products are in chemical equilibrium. The reason for which the de-

tonation temperature predicted by the various equations of state is so different while all the other detonation variables are very similar, was then explained.

3.0 STEADY COMBUSTION OF THE LOX/ETHANOL SYSTEM

3.1 Introduction to the "Direct" Method of Studying Liquid Propellants Steady Combustion

In this section, a simple model of steady-state combustion is first considered for the purpose of pointing out the basic differences between the "conventional" and the "direct" approaches. Only generalities are given in this section while specifics will be discussed in following sections. Thus, the oxidizer is assumed to vaporize much faster than the fuel and that part of the engine is considered where only liquid fuel drops exist. It is further assumed that all drops have initially the same velocity and radius and that there are no collisions, break-ups or nucleations. The following equations can then be written

$$\rho u = -(W_F - W_{OF}) + W_{O\beta} \tag{51}$$

$$\rho u^2 + p - p_o = -(W_F u_F - W_{OF} u_{xF}) + W_{O\beta} u_{x\beta} \tag{52}$$

$$\rho u\left(h + \frac{u^2}{2}\right) = -\left[W_F\left(\Lambda_F + \frac{u_F^2}{2} + h_F^o\right) - W_{OF}\left(\Lambda_{OF} + \frac{u_{OF}^2}{2} + h_F^o\right) - W_{O\beta}\left(\Lambda_{O\beta} + \frac{u_{O\beta}^2}{2} + h_{\beta}^o\right)\right] \tag{53}$$

$$T = T(p, \rho, X_i) \tag{54}$$

$$h = h(p, \rho, X_i) \tag{55}$$

$$\mathcal{F}_i(p, T, X_{1,2\ldots I}, W_{OF}, W_{O\beta}, W_F) = 0 \qquad i = 1, 2, \ldots I$$

$$\frac{W_F}{\frac{4}{3}\pi r^3} = \frac{W_{OF}}{\frac{4}{3}\pi r_o^3} \tag{56}$$

$$u_F \frac{du_F}{dx} = \frac{3}{8}\frac{C_D}{r}\frac{\rho}{\rho_L}|u - u_F|(u - u_F) \tag{57}$$

$$u_F \frac{dr}{dx} = -\frac{\kappa}{8r}\left[1 + g\,Re^{\delta}\right] \tag{58}$$

Where ρ, u, p, T, h are the combustion gas density, velocity, pressure, temperature, and latent enthalpy respectively (p_o is the value of p at the injector end). w_F (w_σ) is the local liquid fuel (oxidizer) flux and w_{oF} ($w_{o\sigma}$) is its value at $x=0$ (injector end). u_F (u_σ) is the liquid fuel (oxidizer) drop velocity, u_{oF} ($u_{o\sigma}$) is the injection velocity and u_{xF} ($u_{x\sigma}$) is its component in the $x$direction. Λ_F (Λ_σ) and h°_F (h°_σ) are the vaporization energy and the enthalpy of formation respectively. X_i are the number of moles of product i per mole of burned fuel. r is the local drop radius. ρ_L is the specific gravity of the liquid fuel. C_D and Re are the drag coefficient and the Reynold's number respectively and K, s, g, φ are coefficients to be defined later. Equations 51, 52, and 53 express mass, momentum and energy conservation, respectively. Equation 54 is the thermal equation of state of the combustion products, and Equation 55 is the caloric equation of state. $\mathcal{F}_i$ stands for a set of, say, I equations which are necessary to relate the amount of vaporized propellants to the variables of the gas (they are as many as the products of which the gas is assumed to be made up). Equation 56 states the conservation of the drop number. Equations 57 and 58 are possible forms of the drag and vaporization equations for individual drops. If the conditions at the injector end and basic thermodynamic data are known, these 8 + I equations contain the following 8 + I unknowns:

$$\rho, u, p, T, h, w_F, u_F, r, X_{1,2\ldots I} .$$

In the "conventional" approach one would solve numerically the above system of algebraic-differential equations. This task in itself would not be easy due to the fact that the above equations are strongly and sensitively coupled. The equations $\mathcal{F}_i$ which relate some of the gas properties to the amount of propellant vaporized are highly nonlinear algebraic equations even for the simplest of all possible assumptions, i.e., the assumption of instantaneous chemical equilibrium of the reaction products. After having solved the equations, the results would be compared with some experimental data by comparing, for example, the calculated loss of static pressure versus z with the measured one. If the comparison is not completely satisfactory, one would have to decide which of the main assumptions that went into this model need to be improved. The main assumptions are:

a) Assumption of chemical equilibrium (or equivalent assumption) going into the definition of the actual $\mathcal{F}_i$.
b) Assumption of uniform initial drop radius and velocity.
c) The droplet drag equation.
d) The droplet vaporization equation.

It is seen that, having several important assumptions, it might be difficult to select the weakest (there are other assumptions implied by Equations 51 through 58, but they are not as consequential as those above and they will be listed and discussed in Section 3.2 and 3.3.2).

In the "direct" approach one would observe that the first 5 + I equations could be solved if any two of the 7 + I unknowns appearing in them were given, in which case the last three equations could be dropped. Notice that the knowledge of <u>two parameters</u> allows the elimination of <u>three equations</u> (set splitting) since Equation 56 contains the drop radius which is used in the last two equations but not in the first 5 + I. Thus, one could specify u_p/u which is contained within known limits in most of the engine and use directly measurements of static pressure loss in some experimental engine (Parametrization). He can then solve only the first 5 + I equations (less equations to solve than in the "conventional" approach Mathematical Specification). After having solved his equations he would know all the gas parameters (Experimental Data Information Optimization) and could check the validity of his solution by further measurements, say, of the gas velocity. Should the calculated and measured particle velocity be in disagreement, one would have to decide which of the main assumptions, which went into the <u>first 5 + I equations</u>, need to be improved. But only two of the four main assumptions of the complete set of equations are necessary for the first five equations (assumptions (a) and (b)). Thus one can verify the validity of these first two assumptions even before considering the remaining two (Assumption Splitting).

Actually one can go one step further and argue that the solution of the first 5 + I equations does not change appreciably if the assumption of uniform initial drop radius and velocity is removed to allow for a distribution of initial drop radii. Then the validity of the first 5 + I equations is primarily related to the validity of the assumption of chemical equilibrium of combustion products. Thus, if a distribution function for the drop radii is introduced ($f = f(x, r)$) the following steady-state equations can be written[9]

$$\rho u = -\int_0^x \int_0^{r_{MAX}} \rho_L 4\pi r^2 R f \, dr \, dx + W_{0\phi}$$

$$\rho u^2 + p - p_0 = -\int_0^x \left[\int_0^{r_{MAX}} \rho_L \tfrac{4}{3}\pi r^3 F f \, dr + \int_0^{r_{MAX}} \rho_L 4\pi r^2 R (u_F - u) f \, dr \right] dx + W_{0\phi} u_{x\phi}$$

$$\rho u \left(h + \frac{u^2}{2} \right) = -\int_0^x \left[\int_0^{r_{MAX}} \rho_L \tfrac{4}{3}\pi r^3 F u_F f \, dr + \int_0^{r_{MAX}} \rho_L 4\pi r^2 R \left(\Lambda_F + \frac{u_F^2}{2} + h_F^0 \right) f \, dr \right] dx +$$

$$+ W_{0\phi} \left(\Lambda_{0\phi} + \frac{u_{0\phi}^2}{2} + h_\phi^0 \right)$$

$$T = T(p, \rho, X_i)$$

$$h = h(p, \rho, X_i)$$

$$\mathcal{F}_i \left(p, T, X_{1,2 \cdots I}, W_{0F}, W_{0\phi}, W_F \right) = 0 \qquad i = 1, 2 \cdots I$$

$$\frac{\partial}{\partial r}(Rf) + \frac{\partial}{\partial x}(u_F f) = 0$$

$$u_F \left(\frac{\partial u_F}{\partial x}\right)_{r_0, u_{0F}} = \frac{3}{8} \frac{C_D}{r} \frac{\rho}{\rho_L} |u - u_F| (u - u_F)$$

$$u_F \left(\frac{\partial r}{\partial x}\right)_{r_0, u_{0F}} = - \frac{K}{8r} \left[1 + q \cdot Re^{g}\right]$$

The first 5 + I of these equations can be written as the previous ones if one sets

$$W_F = W_{0F} + \int_0^x \int_0^{r_{max}^{(x)}} \rho_L 4\pi r^2 R f \, dr \, dx$$

$$\bar{u}_{F_1} = \left\{ W_{0F} u_{x_F} + \int_0^x \int_0^{r_{max}^{(x)}} \rho_L 4\pi r^2 \left[R (u_F - u) + \frac{qF}{3} \right] f \, dr \, dx \right\} / W_F$$

$$\Lambda_F + \frac{\bar{u}_{F_2}^2}{2} + h_F^0 = \left\{ W_{0F} \left(\Lambda_{0F} + \frac{u_{0F}^2}{2} + h_F^0 \right) + \right.$$

$$\left. + \int_0^x \int_0^{r_{max}^{(x)}} \rho_L 4\pi r^2 \left[R \left(\Lambda_F + \frac{u_F^2}{2} + h_F^0 \right) + \frac{qF u_F}{3} \right] f \, dr \, dx \right\} / W_F$$

Where $\bar{u}_{F_1}$ and $\bar{u}_{F_2}$ are then average liquid drop velocities so defined as to give the same local momentum and energy contributions to the gas that the actual drop do. In general $\bar{u}_{F_1}$ will be different from $\bar{u}_{F_2}$. One can expect $\bar{u}_{F_1}$, $\bar{u}_{F_2}$ to be equal to the actual velocities of some drop groups at any given distance from the injector. Thus, the ratios $\bar{u}_{F_1}/u$ and $\bar{u}_{F_2}/u$ will fall within the limit of zero to one in most of the engine, since in most of the engine the velocity of all drop groups will be less than or equal to the gas velocity. Thus, if the solution of the first 5 + I

equations does not change appreciably for $0 \leq \bar{u}_{F_1}/u \leq 1$ and $0 \leq \bar{u}_{F_2}/u \leq 1$ one can say that the gas variables calculated by those equations are valid independently of the actual drop distribution function. Indeed it turns out that the solution is completely insensitive to the value of $\bar{u}_{F_2}/u$ and not too sensitive to that of $\bar{u}_{F_1}/u$. In conclusion then, the "direct" method will give a solution for the gas variables which is independent of the actual drop drag and vaporization models and distribution function and dependent primarily on the assumption of chemical equilibrium of the reaction products. Thus this assumption can be verified separately. After having verified this assumption and calculated the gas variables (Sec. 3.2), one can then proceed to studying drop drag and vaporization models and distribution functions (Sec. 3.6) knowing the solution that they must be able to explain and fit.

There is at least one more advantage that the "direct" method offers. Many mathematical and physical properties of the steady-state liquid propellant combustion surface while studying the solution of the incomplete set of equations (the first 5 + I equations). This will be evidenced by the discussions appearing in Sections 3.3, 3.4 and 3.5 (Maximum Information). Indeed having an accurate solution of the incomplete set of equations is often more valuable than having an inaccurate one of the complete set. With the incomplete solution available more realistic assumptions can be made for the study of the complete set than would have been possible when no information at all was available.

3.2 Steady State Equations and Their Solution

In this section, the actual steady-state equations which

were solved are given together with their assumptions. The method by which they were solved is then briefly explained and the results of three specific applications are presented. Discussion of the assumptions, equations and results will be undertaken in the next section.

The following assumptions are made:

1) The oxidizer is oxygen and the fuel is made up of carbon, oxygen and hydrogen.
2) The combustion is steady.
3) At the station of interest the flow is one-dimensional (uniform through the cross-section) and with no recirculation.
4) The liquid propellants are at their wet bulb temperatures (but their boiling temperatures are actually used) and their vaporization is distributed (actually only the region in which liquid fuel is present is studied in all but one section).
5) Gaseous fuel and oxidizer react instantaneously to give equilibrium reaction products.
6) A single average velocity for the liquid phases ($\bar{u}_\ell$) is used.
7) Heat transfer (to the chamber walls and within the gas) and friction effects (to the chamber walls and within the gas) are neglected.

Under the above assumptions the following equations can be written (See Appendix A):

$$\rho u = W_{o_F} - W_F + W_{o_\phi} - W_\phi \tag{61}$$

$$\rho u^2 = p_o - p + w_{o_F} u_{x_F} - W_F \bar{u}_\ell + w_{o_\phi} u_{x_\phi} - W_\phi \bar{u}_\ell \tag{62}$$

$$\rho u \left[h + \frac{u^2}{2} \right] = W_{o_F} \left[c_F (T_{o_F} - T_{v_F}) - \lambda_F + c_{p_F} (T_{v_F} - T^\circ) + (H^\circ_{T^\circ})_F / m_F + \frac{u^2_{o_F}}{2} \right] - \tag{63}$$

$$- W_F \left[\quad - \lambda_F + c_{p_F} (T_{v_F} - T^\circ) + (H^\circ_{T^\circ})_F / m_F + \frac{\bar{u}^2_\ell}{2} \right] +$$

$$+ w_{o_\phi} \left[c_\phi (T_{o_\phi} - T_{v_\phi}) - \lambda_\phi + c_{p_\phi} (T_{v_\phi} - T^\circ) + (H^\circ_{T^\circ})_\phi / m_\phi + \frac{u^2_{o_\phi}}{2} \right] -$$

$$- W_\phi \left[\quad - \lambda_\phi + c_{p_\phi} (T_{v_\phi} - T^\circ) + (H^\circ_{T^\circ})_\phi / m_\phi + \frac{\bar{u}^2_\ell}{2} \right]$$

$$p = \rho Y \mathcal{R} T / m_{\ell m} = \rho \mathcal{R} T / m \tag{64}$$

$$C_a H_b O_c + z O_2 \rightarrow X_1 OH + X_2 CO + X_3 CO_2 + X_4 O + X_5 O_2 + X_6 H_2 + X_7 H_2O + X_8 H \tag{64a}$$

$$z = m_F (w_{o_\phi} - W_\phi) / m_\phi (w_{o_F} - W_F) \tag{65}$$

$$m_{\ell m} = m_F + z m_\phi = 12a + b + 16(c + 2z) \tag{66}$$

$$Y = \sum_{i=1}^{8} X_i \tag{67}$$

$$X_2 + X_3 = a \tag{68}$$

$$X_1 + 2X_6 + 2X_7 + X_8 = b \tag{69}$$

$$X_1 + X_2 + 2X_3 + X_4 + 2X_5 + X_7 = c + 2z \tag{70}$$

$$\log_{10} \left[\frac{X_4}{X_5^{1/2}} \left(\frac{p\, 10^{-6}}{Y} \right)^{1/2} \right] + \frac{1.3425\, 10^4}{T} - 3.528 = 0 \qquad \tfrac{1}{2} O_2 \rightleftharpoons O \tag{71}$$

$$\log_{10} \left[\frac{X_8}{X_6^{1/2}} \left(\frac{p\, 10^{-6}}{Y} \right)^{1/2} \right] + \frac{1.2009\, 10^4}{T} - 3.201 = 0 \qquad \tfrac{1}{2} H_2 \rightleftharpoons H \tag{72}$$

$$\log_{10} \left[\frac{X_1}{X_5^{1/2}\, X_6^{1/2}} \right] + \frac{0.1825\, 10^4}{T} - 0.686 = 0 \qquad \tfrac{1}{2} O_2 + \tfrac{1}{2} H_2 \rightleftharpoons OH \tag{73}$$

$$\log_{10} \left[\frac{X_7}{X_6 X_5^{1/2}} \left(\frac{p\, 10^{-6}}{Y} \right)^{-1/2} \right] - \frac{1.3241\, 10^4}{T} + 3.072 = 0 \qquad H_2 + \tfrac{1}{2} O_2 \rightleftharpoons H_2O \tag{74}$$

$$\log_{10} \left[\frac{X_3}{X_5^{1/2} X_2} \left(\frac{p\, 10^{-6}}{Y} \right)^{-1/2} \right] - \frac{1.446\, 10^4}{T} + 4.348 = 0 \qquad CO + \tfrac{1}{2} O_2 \rightleftharpoons CO_2 \tag{75}$$

$$h = 4.186\, 10^{10} \left\{ \sum_{i=1}^{8} X_i \left[\int_{T^\circ}^{T} c_{p_i}(T)\, dT + (H^\circ_{T^\circ})_i \right] \right\} / m_{\ell m} \tag{76}$$

As in the previous section, Equation 61 expresses the mass conservation between the injector (where $W_{o_{F,\emptyset}}$ are the injection flow rates, of fuel and oxidizer respectively, divided by the engine cross-section, i.e., injection fluxes) and any station at which the fluxes of liquid fuel and oxidizer are $W_{F,\emptyset}$ respectively.

Equation 62 expresses the momentum conservation between the injector and any station. The velocities $u_{x_{F,\emptyset}}$ are the axial components of the corresponding injection velocities.

Equation 63 expresses the energy conservation between the injector and any station. The reference temperature is $T^{o}=298^{o}K$. Notice that the heat of vaporization of the propellants which are usually included in their heats of formation, when at ambient pressure and temperature they are in their liquid states, are in Equation 63 considered explicitly.

Equation 64 is the perfect gas equation of state.

Equation 64a simply defines which product are being considered.

Equation 65 through 75 express the assumption of chemical equilibrium of the products. Equation 65 takes into account that not all the injected propellants are available for the chemical reaction since part of them are still in their liquid phases. Thus Z defines the local mixture ratio of the gases and changes with the distance from the injector.

Equation 66 defines $m_{\ell m}$ which is the weight of the products per mole of vaporized fuel (often called the "molecular weight" of the "equivalent mole" $C_a H_b O_{c+2Z}$).

Equation 67 defines the total number of moles of products

per mole of vaporized fuel.

Equations 68, 69, and 70 express the conservation of carbon, hydrogen and oxygen respectively.

Equations 71 through 75 express the chemical equilibrium between the indicated products.

Equation 76 defines the total enthalpy of the products. All the constants appearing in Equations 71 through 76 either come directly from "JANAF" tables or are curve fits of data available there.

Before briefly discussing how the solution of the previous system was reached, it should be noticed that the previous 16 equations contains 19 unknowns ($\rho, u, W_F, W_\phi, p, \bar{u}_e, \gamma, T, m_{2m}, z, X_{1\ldots8}, h$) if the parameters at the injector end are given ($W_{0_F}, W_{0_\phi}, p_0, u_{x_F}, u_{x_\phi}$) and the fuel is specified (a, b, c). This system, in which gas dynamics and chemical equilibrium equations are coupled, is not easy to solve, even numerically. Small variations in the local mixture ratio (z) bring about large variations in the composition of the reaction products (X_i). Similarly small variations in the static pressure (p) bring about large variations in the gas velocity (u) (since large variations of loss of static pressure, $p_0 - p$, generally correspond even to small variations of static pressure). Thus the chances of an iteration scheme to yield the desired solution from rough guesses for the controlling parameters, z and p, are very small. In such cases it is better to solve the system for fixed values of these controlling parameters. The first difficulty, however, is in spotting them out. Having recognized that z and p are the controlling pa-

rameters, the solution was obtained in two steps; the first step gives an approximate solution and the second refines it. In the first step $\bar{u}_e^2/2$ is neglected in the energy equation and ρ and u are eliminated from it using the mass conservation equation and the equation of state. The resulting energy equation is equal to the "adiabatic flame temperature" energy equation except for the kinetic energy term. This equation is then solved, together with Equation 66 through 76, for fixed values of W_F, W_ϕ, and p. Thus one determines y, T, m_{2m}, z, $X_{1\ldots8}$ and h. These quantities are rather insensitive to small changes in p as in the "adiabatic flame temperature" problem. The known pressure at the injector end (p_0) can then be used. Next the equation of state, and of mass and momentum conservations are reconsidered and written as follows:

$$\rho = p\,m/RT$$

$$u = \left(W_{OF} - W_F + W_{O\phi} - W_\phi \right)/\rho$$

$$\bar{u}_e/u = -\left(\rho u^2 - p_0 + p - W_{O_F} u_{x_F} - W_{O\phi}\, u_{x\phi} \right)/u\left(W_F + W_\phi \right)$$

The values of ρ, u and $\bar{u}_e/u$ are then calculated for selected values of p (to which they are very sensitive) using m and T previously calculated with p_0. A set of tables are now available from which an approximate solution of the given system of equations can be closely estimated for the specified values of W_F, W_ϕ, and p. In the second step the entire system of 16 equations in 19 unknowns is solved simultaneously by the Newton-Raphson method, using quite accurate guesses from the pre-

vious tables and for selected values of any three unknowns (generally W_ϕ , p , $\bar{u}_e/u$). In general, then, for a given engine, any three of the 19 unknowns should be measured to know the values of all of them. In practice, however, for LOX/hydrocarbon propellants the region where liquid oxygen is still present is small in comparison to the entire combustion length and highly non-uniform so that the previous equations wouldn't be accurate anyhow. The measurement of two parameters are then enough to study the region where no liquid oxygen exists ($W_\phi = 0$). Actually it will presently be seen that the solution of the given equations is not too sensitive to the value of $\bar{u}_e/u$ so that the measurement of only one parameter (generally the static pressure p) is sufficient to determine the solution. Indeed much can be learned without measuring anything but rather by simply studying the parametric solution of the previous equations (Section 3.3).

The results of three specific applications of this method are now shown. The basic engine parameters of the three configurations are given in Table IV. First the complete combustion, or final, values of the engine parameters were calculated by setting $W_\phi = W_F = 0$. They are also given in Table IV. These values were used as reference values (subscript f for "final value"). Next the static pressure along the combustion chamber was measured (Figs. 3, 8, 13). Finally the equations were solved for the region with no liquid oxygen ($W_\phi = 0$) and for several values of $\bar{u}_e/u$. The values of u/u_f , ρ/ρ_f , T/T_f and W_F/W_{OF} for the three engine configurations are given in Figs. 4, 5, 6 and 7 (first engine configuration), Figs. 9, 10, 11 and 12 (second

TABLE IV BASIC ENGINE PARAMETERS OF THE THREE ENGINE CONFIGURATIONS TESTED

	I	II	III
Oxidizer	LOX	LOX	LOX
Fuel	Ethanol	Ethanol	Ethanol
Injector Design	4X4 Impinging Like-on-Like Doublets	4X4 Impinging Like-on-Like Doublets	6X6 Impinging Like-on-Like Doublets
Injector Diameter (inches)	.059	.059	.040
Injection Angle	$27^{o}45'$	$27^{o}45'$	$27^{o}45'$
Static Pressure at Injector End (psia)	296	299	63.8
Engine Diameter (Inches)	3	3	3
Injection Oxidizer Flux (W_{o_ϕ} g/sec cm^2)	21.9	18.7	7.85
Injection Fuel Flux (W_{o_F} g/sec cm^2)	9.41	12.9	4.88
Injection Mixture Ratio(O/F)	2.33	1.44	1.6
Injection Equivalence Ratio (F/O)	.895	1.44	1.3
Injection Oxidizer Temperature (^{o}K)	98	98	98
Injection Fuel Temperature (^{o}K)	293	293	293
Injection Oxidizer Velocity (cm/sec)	2935	2511	1020
Injection Fuel Velocity (cm/sec)	1916	2637	966
Nozzle Entrance Mach Number	.15	.158	.314
Complete Combustion (Reference) Values of Some Parameters:			
Gas Velocity u_f (cm/sec)	17,080	19,100	36,980
" Density ρ_f (g/cm^3)	$1.832\ 10^{-3}$	$1.658\ 10^{-3}$	$3.448\ 10^{-4}$
" Temperature T_f (^{o}K)	3290	3174	3068
" Molecular Weight m_f (g/mole)	25.2	21.8	22.3
" Ratio of Specific Heats γ_f	1.201	1.210	1.211

Loss of static pressure vs distance from injector (configuration I)

Figure 3

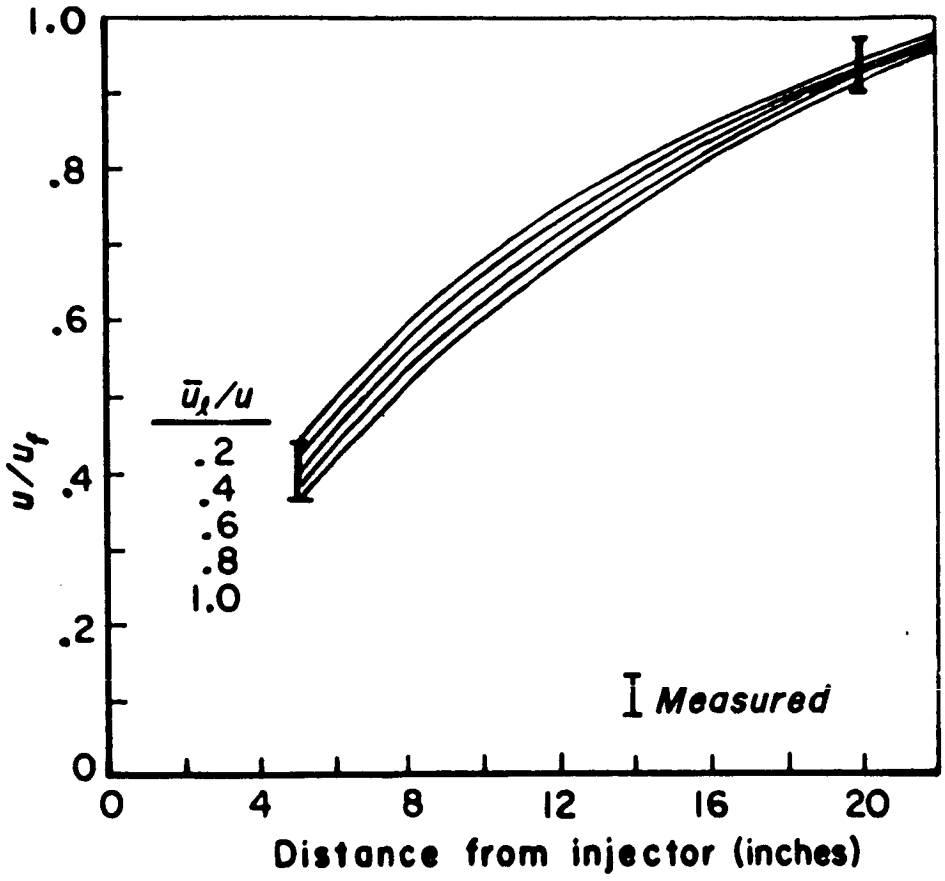

Dimensionless gas velocity vs distance from injector (configuration I)

Figure 4

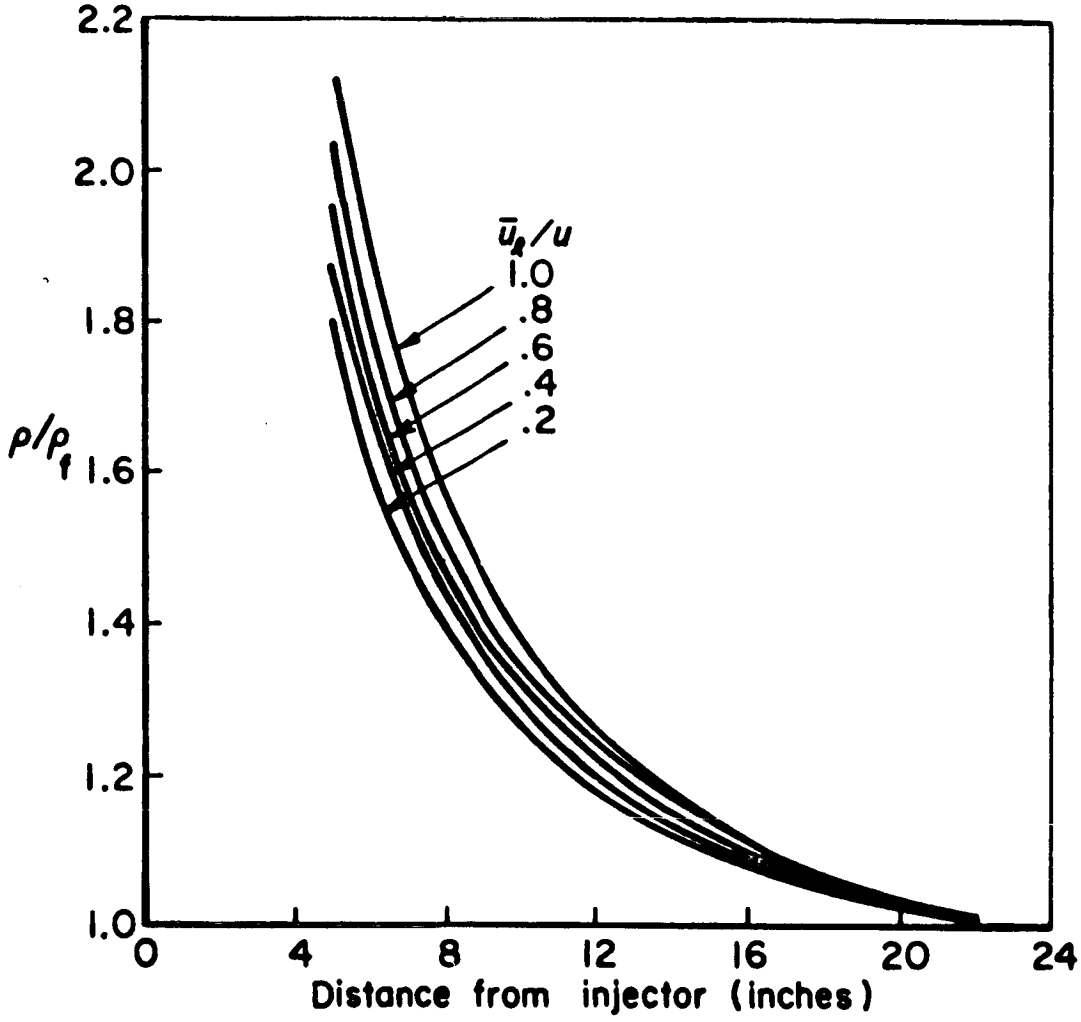

Dimensionless gas density vs distance from injector (configuration I)

Figure 5

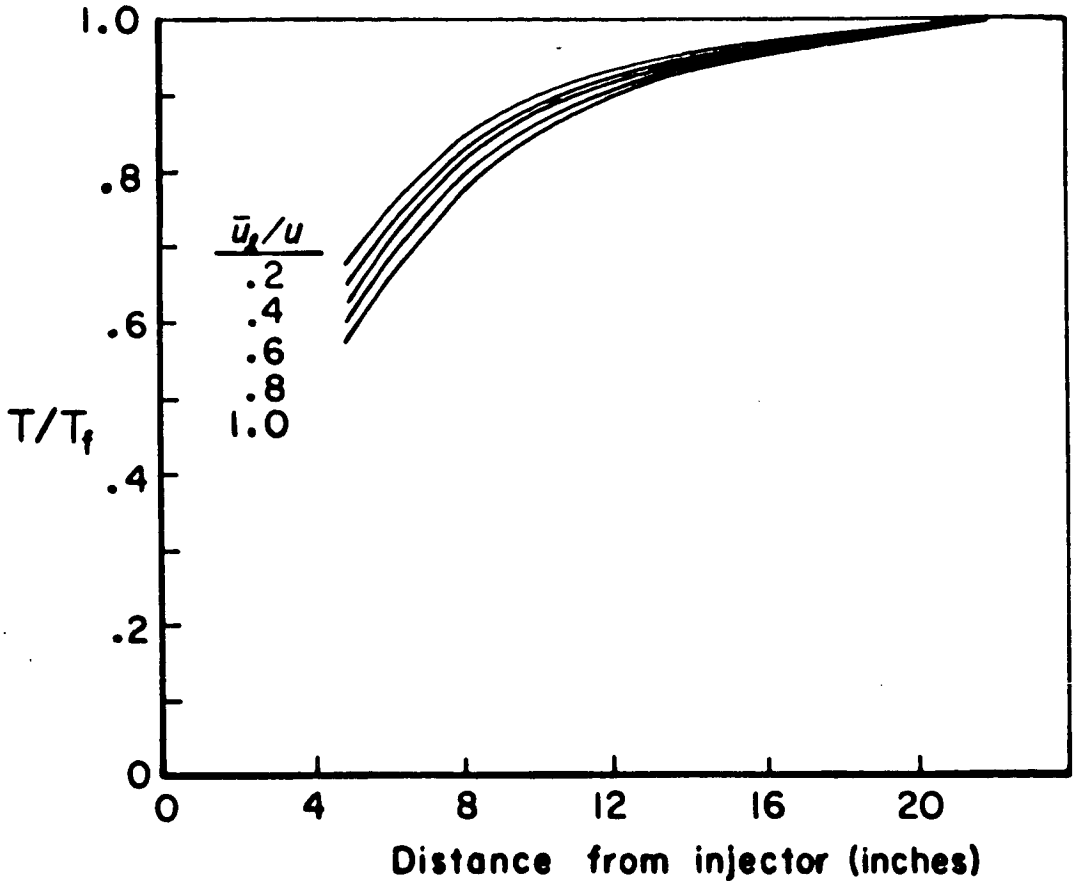

Dimensionless gas temperature vs distance from injector (configuration I)

Figure 6

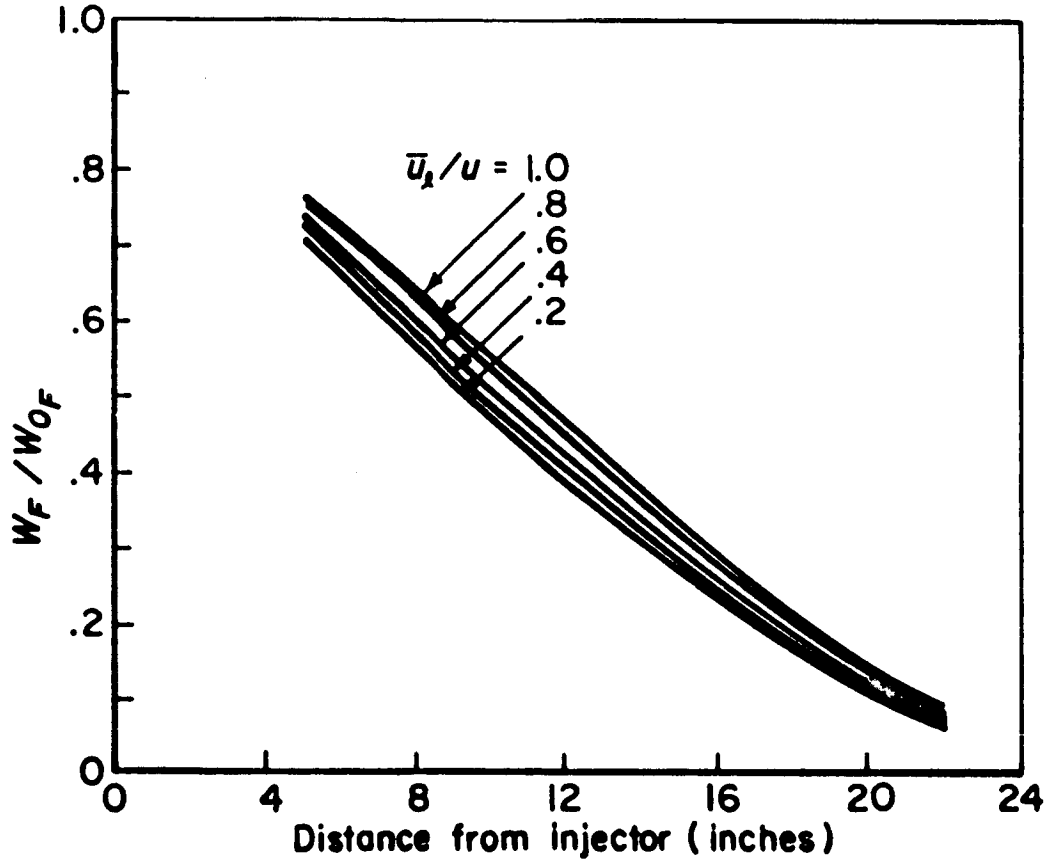

Dimensionless liquid fuel flux vs distance from injector(configuration I)

Figure 7

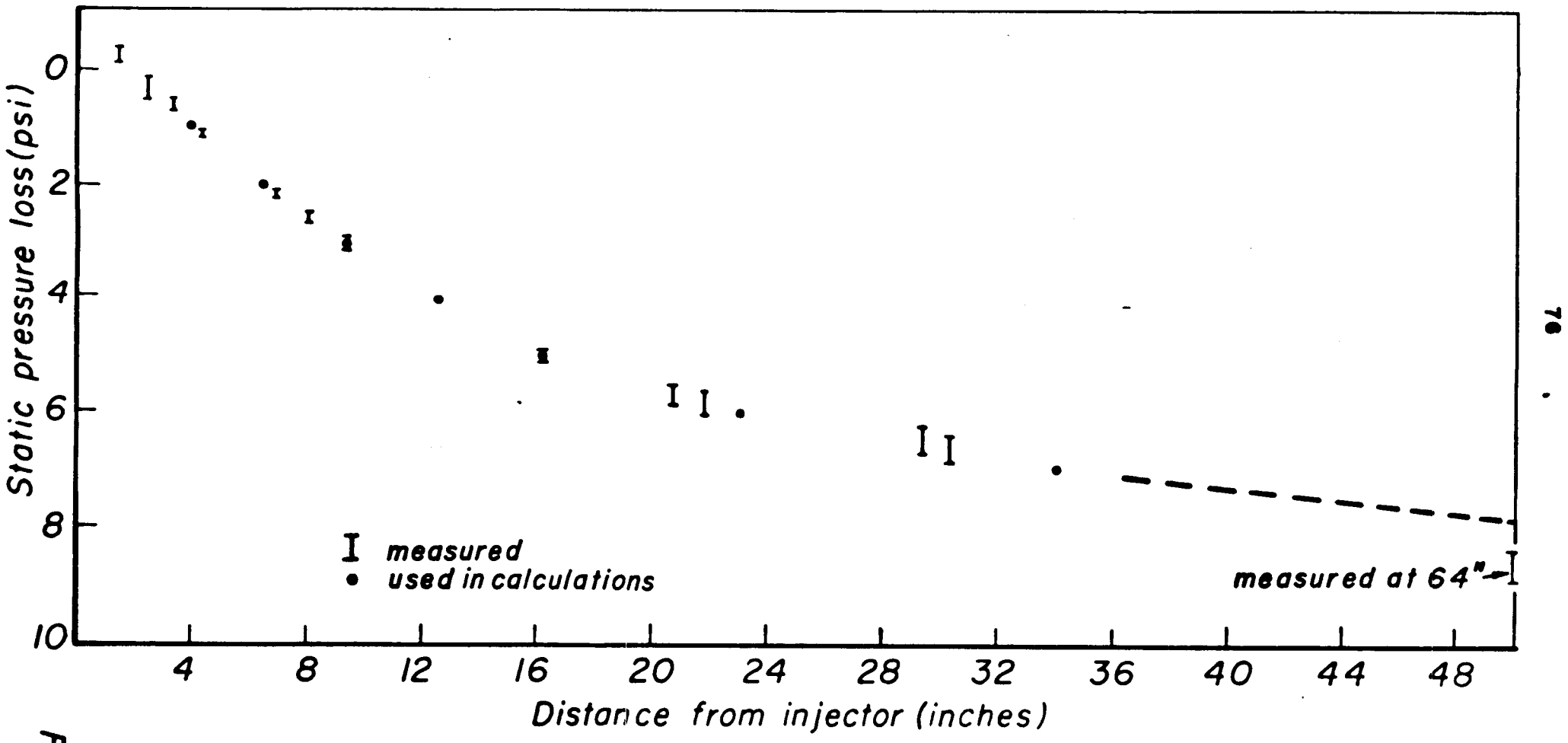

Figure 8

Loss of static pressure vs distance from injector (configuration II)

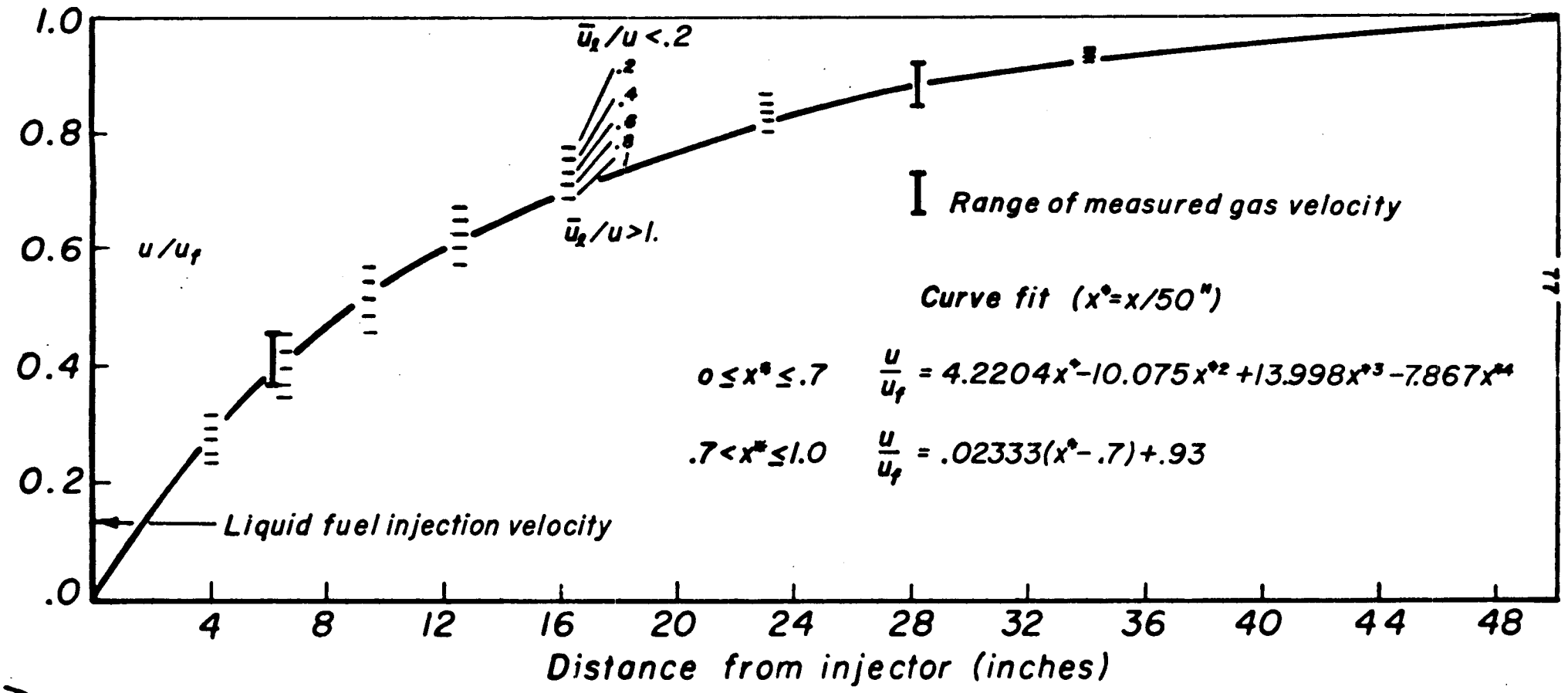

Figure 9

Dimensionless gas velocity vs distance from injector (configuration II)

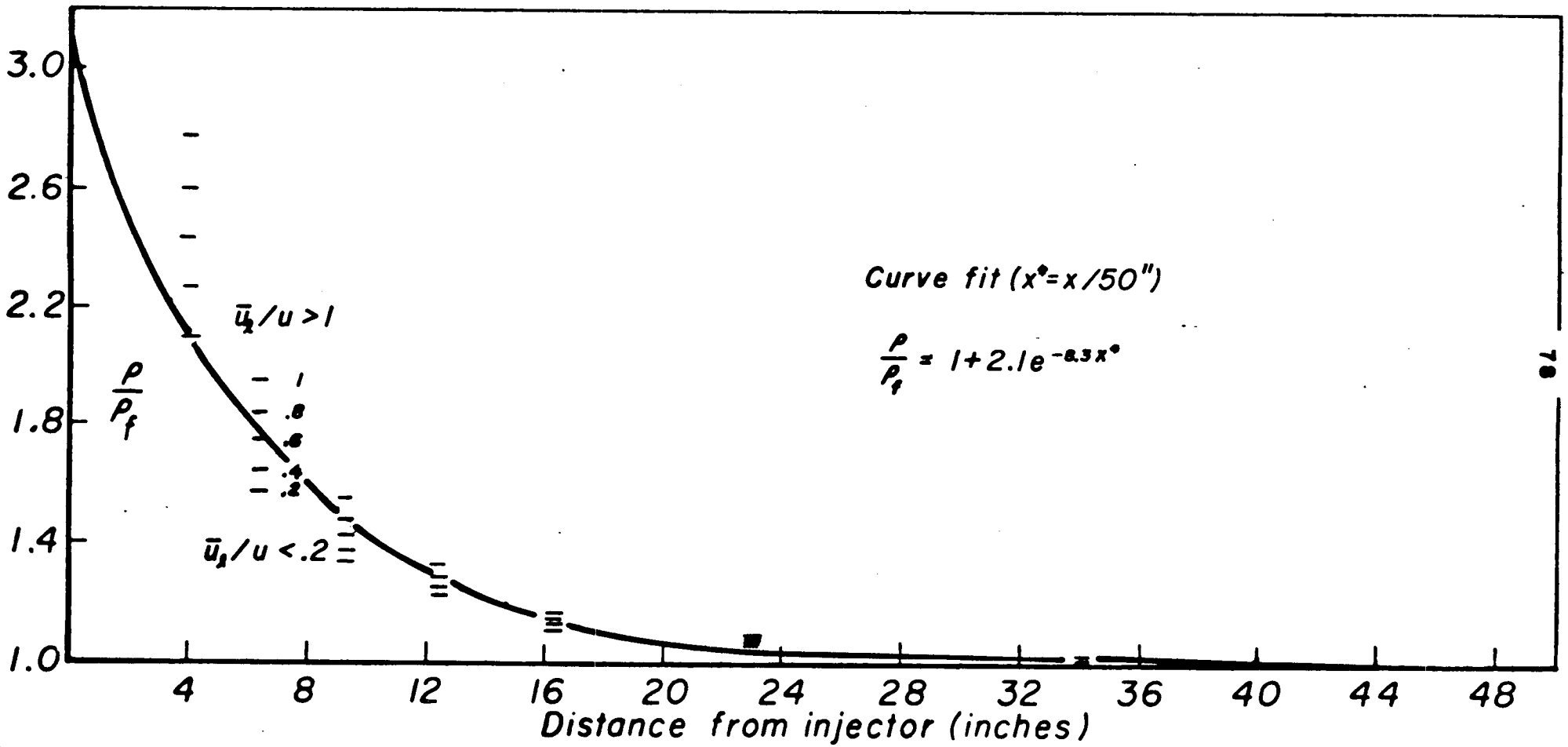

Figure 10

Dimensionless gas density vs distance from injector (configuration II)

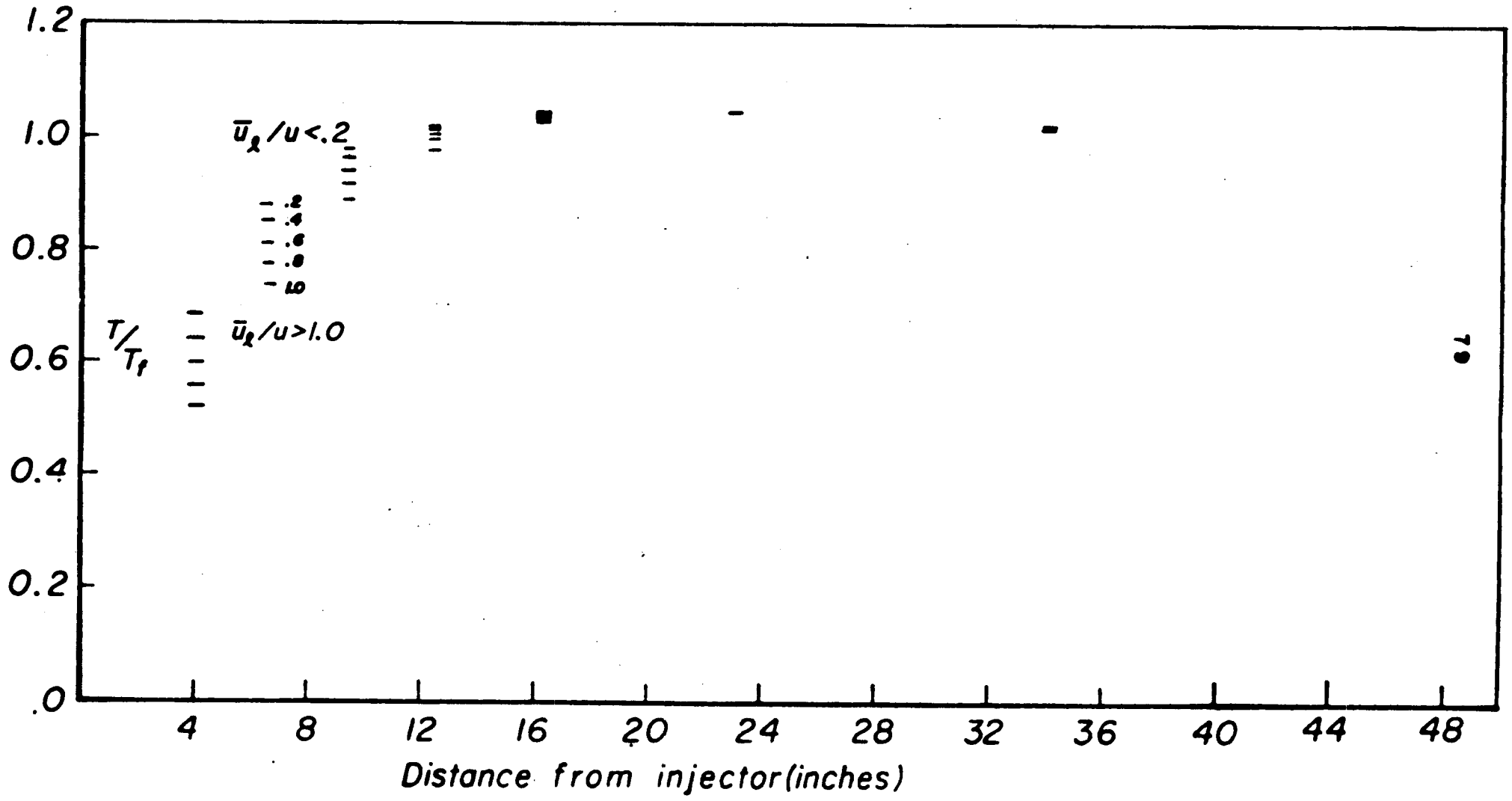

Figure 11

Dimensionless gas temperature vs distance from injector (configuration II)

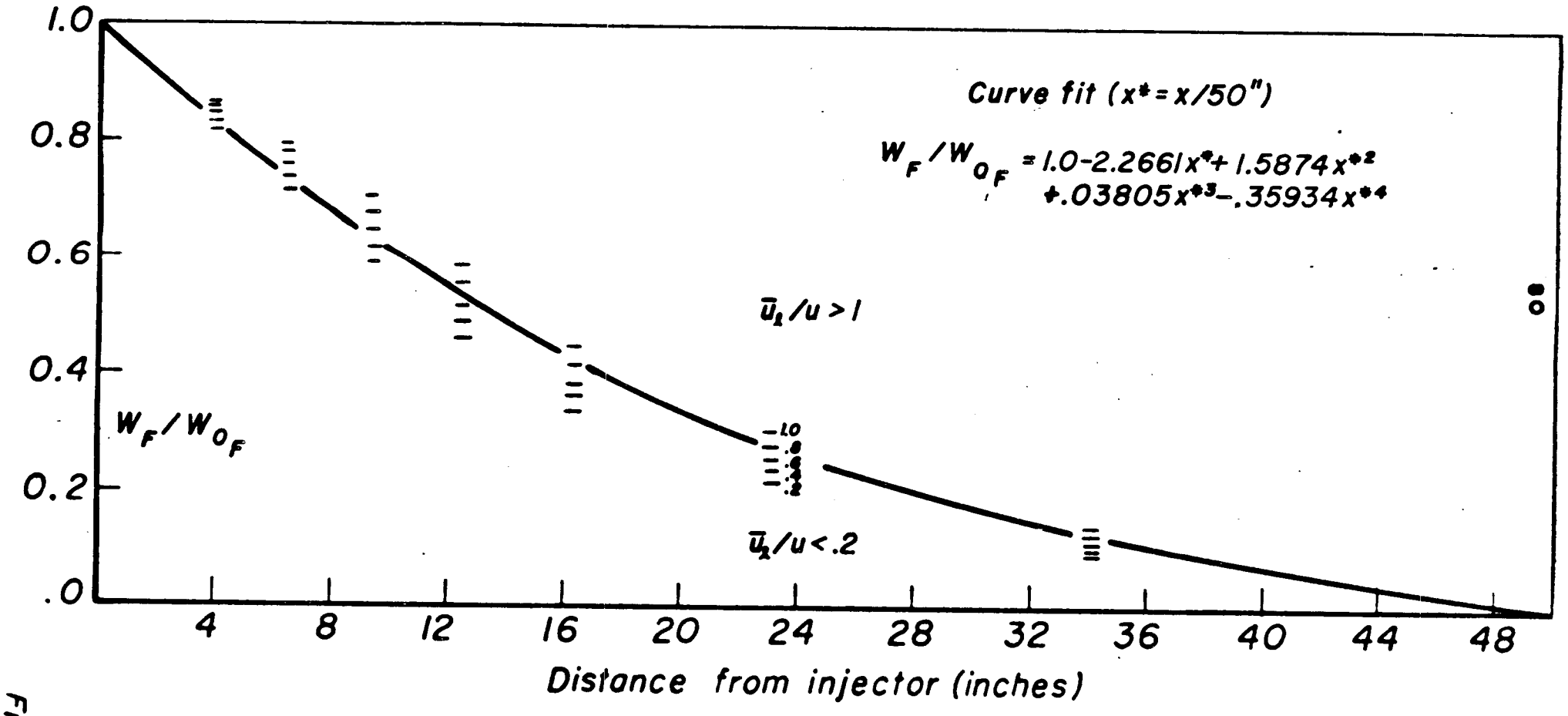

Figure 12

Dimensionless liquid fuel flux vs distance from injector (configuration II)

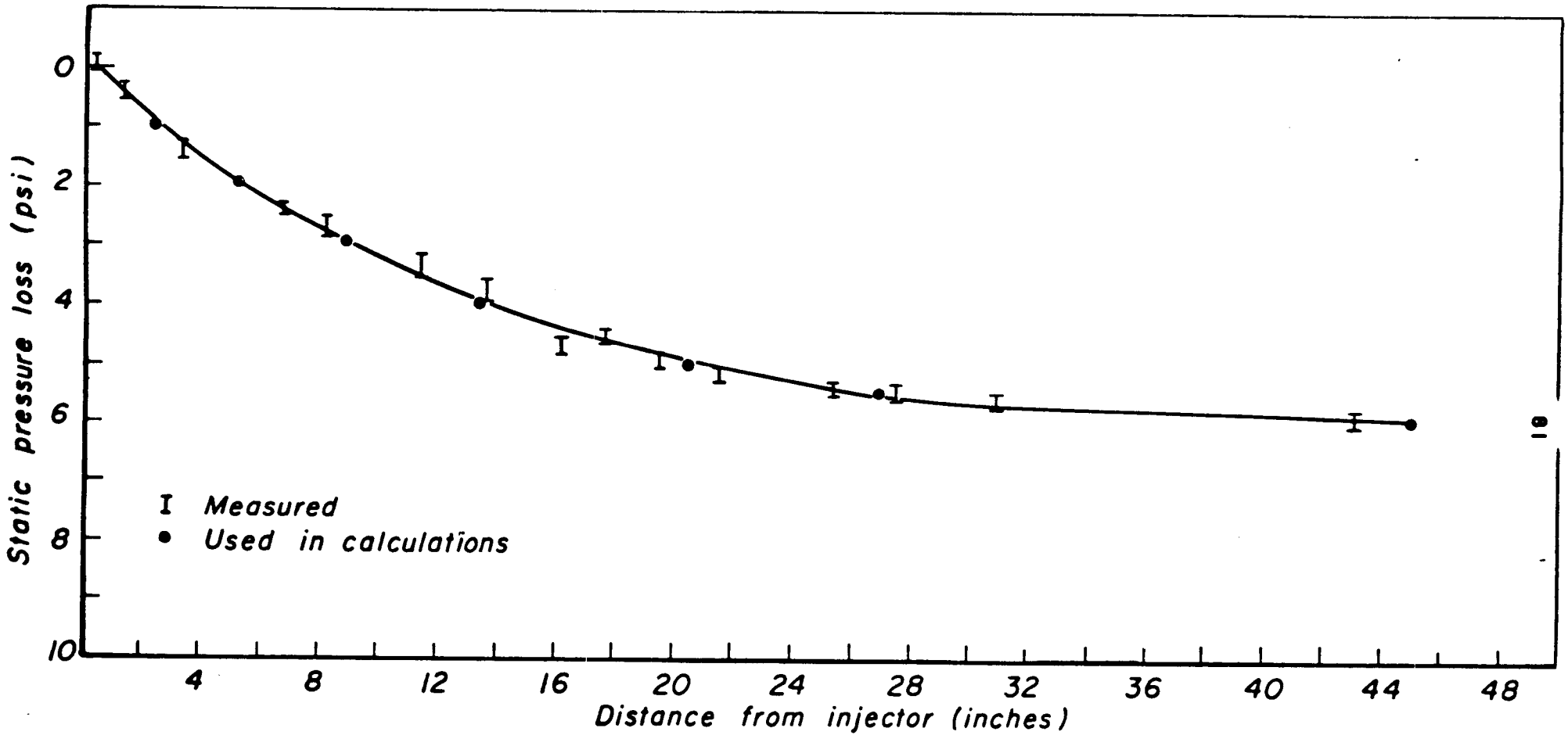

Loss of static pressure vs distance from injector (configuration III)

Fig. 13

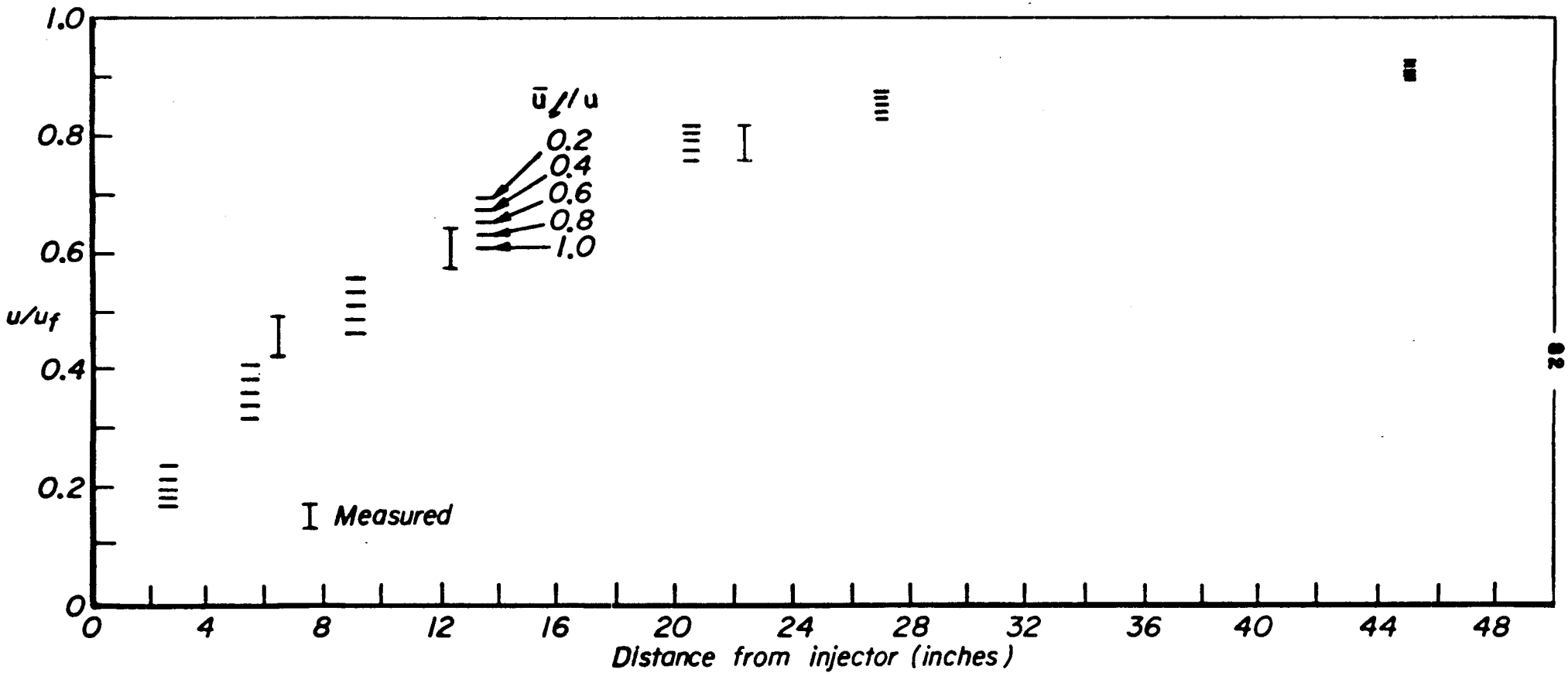

Dimentionless gas velocity vs distance from injector (configuration III)

Fig. 14

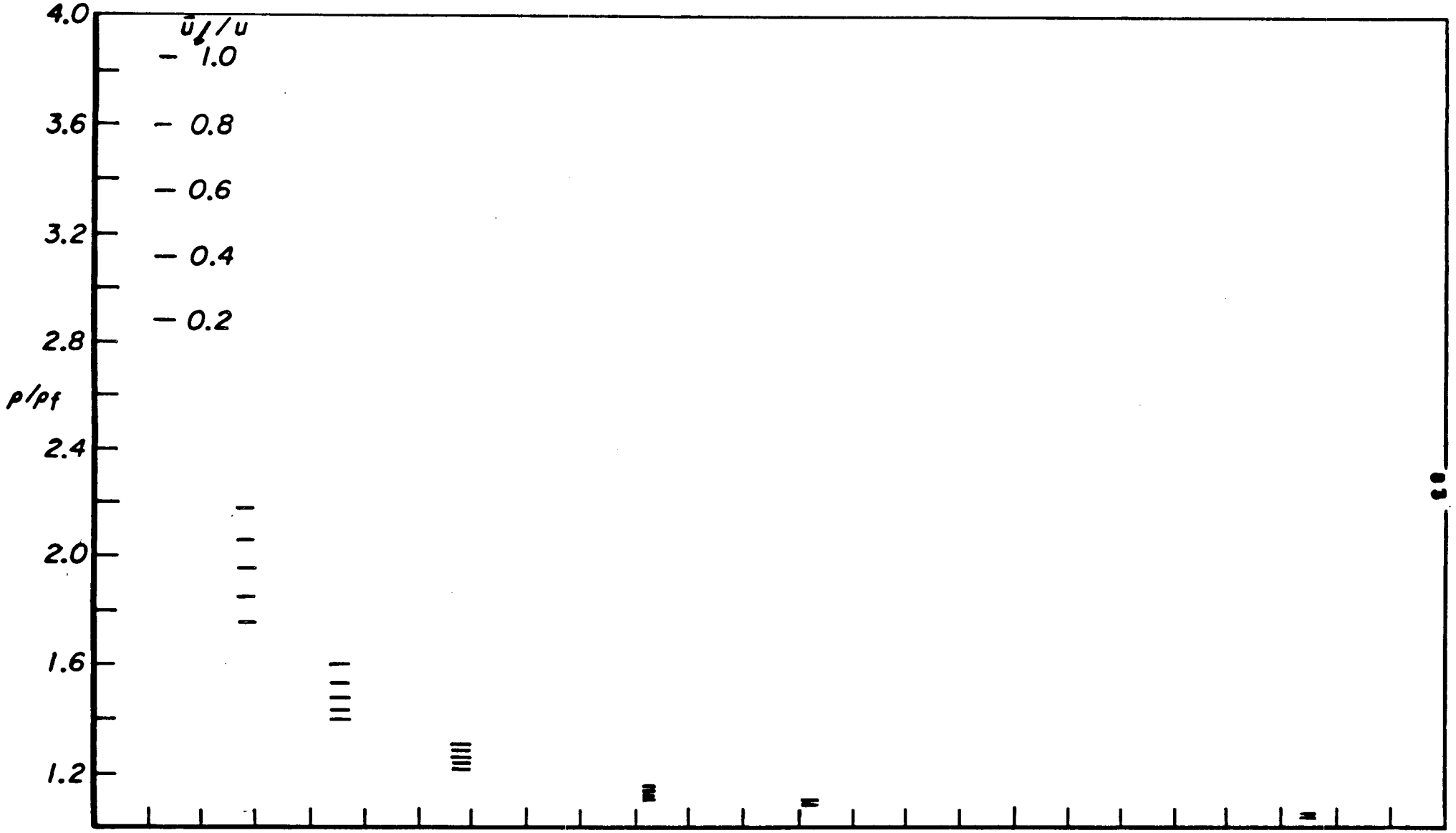

Fig. 15

Dimentionless gas density vs distance from injector (configuration III)

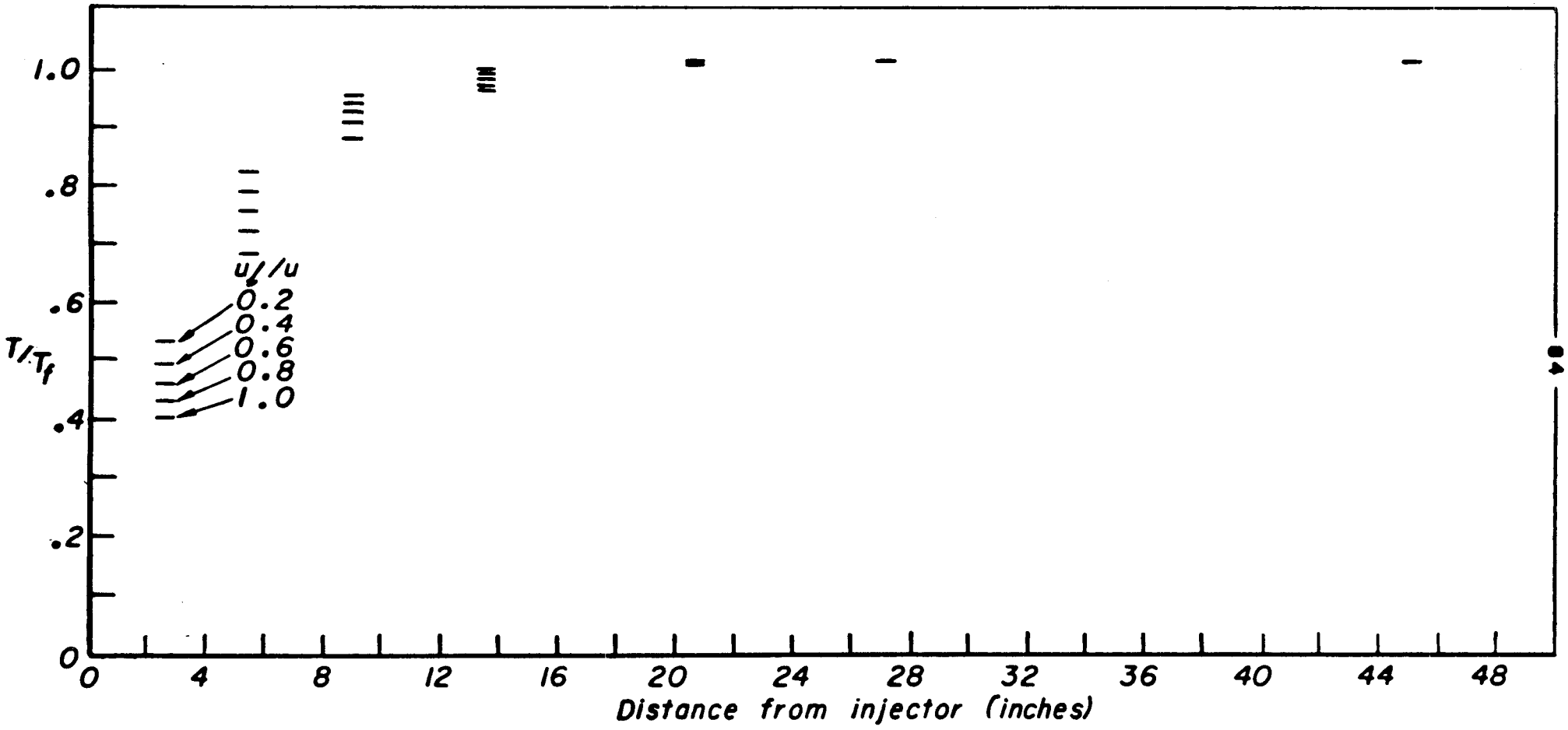

Fig. 16

Dimensionless gas temperature vs distance from injector (configuration III)

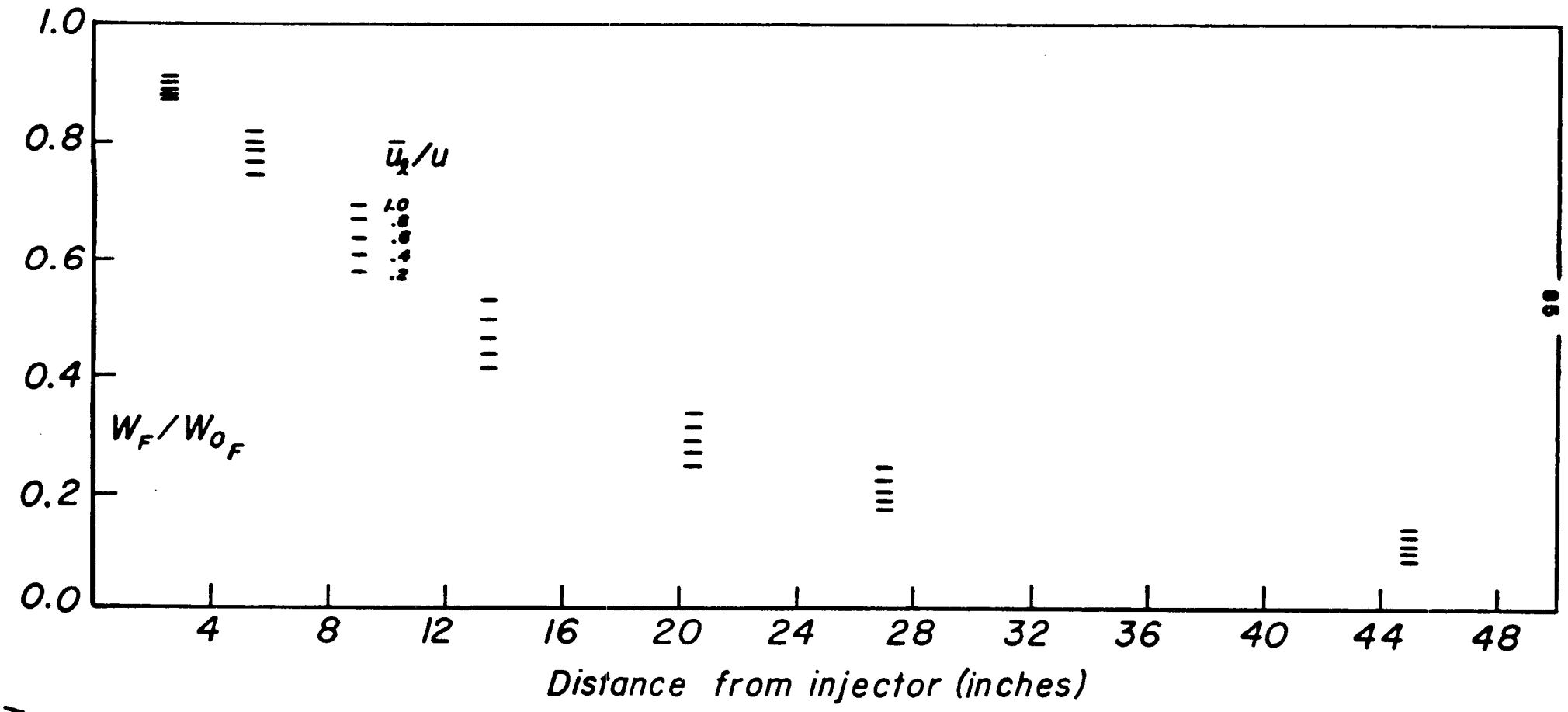

Figure 17

Dimensionless liquid fuel flux vs distance from injector (configuration III)

engine configuration) and Figs. 14, 15, 16 and 17 (third engine configuration). Similar curves could have been drawn for the other engine variables. In all cases it can be seen that a relatively narrow family of curves is obtained for all realistic values of $\bar{u}_\ell / u$. Thus the measurement of the static pressure and its direct use have been sufficient to determine most of the engine variables without having assumed anything about the way the fuel actually vaporizes and burns (no droplet drag and vaporization model was used). In order to verify the validity of the method, the particle velocity was also measured by streak photography at specific distances from the injector in all three configurations. The measured particle velocities are given in Figs. 4, 9 and 14, with their range of scattering (vertical bars). The agreement is satisfactory. Notice that further resolution, within the $\bar{u}_\ell / u$ families, could have not been achieved by streak photography.

3.3 Results And Discussion

In this section, the solution of the steady-state equations (Equations 61 through 76), for the case in which LOX/ethanol are the propellants, is discussed. A parametric study of the system was performed for the region where no liquid oxidizer exists and some conclusions were reached without any need of experimental data and of drop drag, vaporization, and distribution models. Thus the parameters of the study will first be defined, then the leading assumption of this study will be discussed. Next, the energy and chemical equilibrium equations will be considered to conclude that they could have been solved a priori

to yield something like an equation of state for the combustion products. Than the momentum equation will be considered and the influence of the initial momenta of the liquids and of the drag and vaporization of the drops will be discussed. Finally the problem of steady-state axial uniformity of the gas properties will be examined.

3.3.1 Definition Of The Parametric Study

The following parametric study of Equations 61 through 76 was performed. The equations were solved for the LOX and ethanol propellants. The injector design was kept constant. The only injector parameters entering into the equations are the number of orifices their diameters and their injection angles (16, .059" and 27^{o} 45' respectively for both propellants). The pressure at the injector end (p_o) was set equal to 150, 300, 600 psia. The injector fluxes of propellants were varied as to give injector equivalence ratios* (EQR_o) of .9, 1.44, 1.9 (where 1.44 cor-

---

* Several parameters are often used to identify the mixture ratio. It might be helpful to list those which have been used in this study:

$$z = \frac{\dot{m}_F (w_{o\phi} - w_\phi)}{\dot{m}_\phi (w_{oF} - w_F)}$$ = moles of vaporized oxidizer per mole of vaporized fuel

$z_s = 3$ = stoichiometric value of z since: $C_2H_5OH + 3O_2 \rightarrow 2CO_2 + 3H_2O$

$EQR \equiv EQR(F/\phi) \equiv \frac{z_s}{z}$ = equivalence ratio. NOTE: EQR > 1 for fuel rich mixtures

$\left(\frac{\%}{F}\right)$ = mixture ratio by weight $= z \frac{\dot{m}_\phi}{\dot{m}_F} = \frac{z_s}{EQR} \frac{\dot{m}_\phi}{\dot{m}_F} = 2.09/EQR$

In general there are injection values of z and EQR (called z_o, EQR_o and equal also to their complete combustion, or final values) and local values corresponding to the local gas mixture ratio.

responds to maximum c* while .9 (lean mixture) and 1.9 (rich mixture) give roughly the same c*) and complete combustion Mach numbers of approximately .15 and .55. The solutions were obtained for $\bar{u}_e/u$ = .2 and 1.0. Thus the system of equations was solved for 3x3x2x2=36 different input parameters. For each of these 36 cases, 5 computations were made for $(p_o - p)/(p_o - p_f)$ approximately equal to .2, .4, .6, .8 and 1.0. This parameter gives the loss of static pressure at some distance from the injector $(p_o - p)$ divided by the loss of static pressure corresponding to complete combustion $(p_o - p_f)$. It simply fixes the local static pressure since the pressure at the injector end (p_o) is part of the input and the complete combustion pressure (p_f) is uniquely determined by the overall input.

3.3.2 Discussion Of The Assumptions

Equations 61 through 76 are based on the seven assumptions given in the previous section. The computations clearly show that the solution is insensitive to the assumed temperature of the liquids (assumption 4) and to their kinetic energies (assumption 6). In the conventional approach, the local temperature of the liquids affects considerably the results of steady-state computations since it influences the droplet vaporization rate which, in turn, controls the results of the computations (see Section 3.6). In the direct approach,however,the drop vaporization rate does not appear, having been substituted with measured or fixed gas quantities such as $(p_o - p)/(p_o - p_f)$. The droplet temperature, then, enters only through the energy equation for the gases where it modifies the amount of heat necessary to

vaporize the liquid. This is a small fraction of the heat released by the chemical reaction, and therefore does not influence appreciably the solution of the equations. Checks on heat transfer and friction effects were made and found to be small (assumption 7). The assumption of no recirculation (assumption 3) is important. Recirculation can be expected to be active near the injector, within distances of the order of the distance between injector units. This region is also non-uniform and probably contains also liquid oxidizer. A qualitative investigation of this region is briefly carried out in (Section 3.4). In this section, however the combustion length is assumed to be considerably longer than the distance between injector units as is the case for most practical engines as well as for the experimental engine used in this research. Thus, the assumption of no recirculation is likely to be a good one as far as this study is concerned. On the other hand, the assumption that gaseous fuel and oxidizer react instantaneously to give equilibrium reaction products (assumption 5) is so important that the validity of the results of this study depends on it. It can be seen as the leading assumption of this study. One of the immediate consequences of this assumption is the calculated axial non-uniformity of the gas properties which will be discussed in the following pages. To support the validity of this assumption the following three evidences can be cited:

1) The current approach has led to the calculation of gas velocities which were then verified by streak photography in the three engine configurations tested (Figs. 4, 9, 14).

2) The amplitude of a shock moving toward the injector increases markedly while its velocity does not change appreciably indicating a lower speed of sound of the gases as the injector is approached (axial non-uniformity of the gas properties).

3) c* measurements yield temperature estimates close to those calculated in the present study.

In spite of the quoted evidences, the assumption of instantaneous chemical equilibrium must still be regarded as a working assumption and its validity evaluated case-by-case. One can say that it seems to be verified for the LOX/ethanol system when the combustion length is considerably longer than the distance between injector units (Combustion length >> Recirculation length).

3.3.3 The Energy And Chemical Equilibrium Equations

The energy and chemical equilibrium equations can approximately be solved independently of the other equations of the system. These equations are rewritten below in a form which is convenient for the present discussion. Gas velocity and density have been eliminated from the energy equation using mass conservation and the equation of state while the kinetic energy of the liquids has been neglected

$$Z = \frac{\dot{m}_F (w_{o\phi} - w_\phi)}{\dot{m}_\phi (w_{oF} - w_F)} \qquad EQR = 3/Z$$

$$\dot{m}_{tot} = \dot{m}_F + Z \dot{m}_\phi$$

$$\left\{ \sum_{i=1}^{8} X_i \left[\int_{T^0}^{T} C_{p_i}(T)\, dT + (H^0_{T^0})_i \right] - (H^0_{T^0})_F - (H^0_{T^0})_\phi \right\} +$$

$$+ \frac{\left[w_{o_F} Q_F + w_{o_\phi} Q_\phi \right] m_{em}}{\left[w_{o_F} - w_F + w_{o_\phi} - w_\phi \right] 4.186\, 10^{10}} + \left[w_{o_F} - w_F + w_{o_\phi} - w_\phi \right] \frac{R^2 T^2 y^2}{m_{em} p^2\, 4.186\, 10^{10}} = 0$$

$$y = \sum_{i=1}^{8} X_i$$

Equations 68 through 70 (chemical species conservation)

Equations 71 through 75 (chemical equilibrium equations)

where $Q_{F,\phi}$, represents the energies needed to warm up the liquids to their wet bulb temperatures, to vaporize them and to bring the vapors to the reference temperature $T^0 = 298^0$ (see Appendix A). The gas kinetic energy and $Q_{F,\phi}$ are small quantities within the energy equation where the balance between the change of latent enthalpy of the gases and the difference between the heats of formation of the products and those of the reactants dominates. If gas kinetic energy and $Q_{F,\phi}$ were neglected, the propellant fluxes would appear only in the variable z which specifies the local mixture ratio of the gases. Thus the solution of the above equations can be expected to depend mostly on z (or equivalently on EQR since EQR = $3/z$) and on the pressure, as in the "adiabatic flame temperature" problem. The pressure itself can be expected to have a minor influence. The above equations determine the values of m_{em}, h, T, X_i, y and p/ρ since $p/\rho = RTy/m_{em}$. Thus these quantities can be expected to depend primarily on EQR for all values of $w_{o_{F,\phi}}$, p_0, M_ℓ and $\bar{u}_e/u$ for which the complete set of equations (Equations 61 through 76) were solved. This is in-

deed the case as Figs. 18 and 19 show. T, m, p/ρ are functions of EQR only within $\pm$ 5% due primarily to the influence of the pressure. The ratio of specific heats (γ), $a = \gamma p/\rho$, the internal energy of the gases (e), and the heat released by the chemical reaction (φ^0) are also determined by the solution of the above equations and therefore are also, approximately, functions of EQR alone. In conclusion m_{e_m}, h, T, X_i, γ, p/ρ, γ, a, e and φ^0 can approximately be considered functions of EQR alone rather than of EQR, $w_{O_{F,\phi}}$, $w_{F,\phi}$ and p. For most conventional studies this approximation should be both useful and acceptable since most of the uncertainties are centered around the distribution, motion and vaporization of the drops and a 5% error in the above gas properties should be quite acceptable. Notice however that ρ, u and therefore M still depend on $w_{O_{F,\phi}}$, $w_{F,\phi}$, and p as well as on EQR. Thus, instead of studying the complete system of equations, one could have studied the following one which is considerably simpler

$$\rho u = w_{O_F} - w_F + w_{O_\phi} - w_\phi$$

$$\rho u^2 = p_0 - p + w_{b_F} u_{x_F} - w_F \bar{u}_e + w_{O_\phi} u_{x_\phi} - w_\phi \bar{u}_e$$

$$\frac{p}{\rho} = \frac{p}{\rho}\left(\frac{w_{O_\phi} - w_\phi}{w_{b_F} - w_F}\right)$$

where the last equation can be looked at as an equation of state characteristic of the propellants and valid within a reasonably wide range of pressures (given in Fig. 19 for the LOX/ethanol system). A similar approach was followed by Campbell and Chadwick[20]. They assumed chemical equilibrium of the reaction prod-

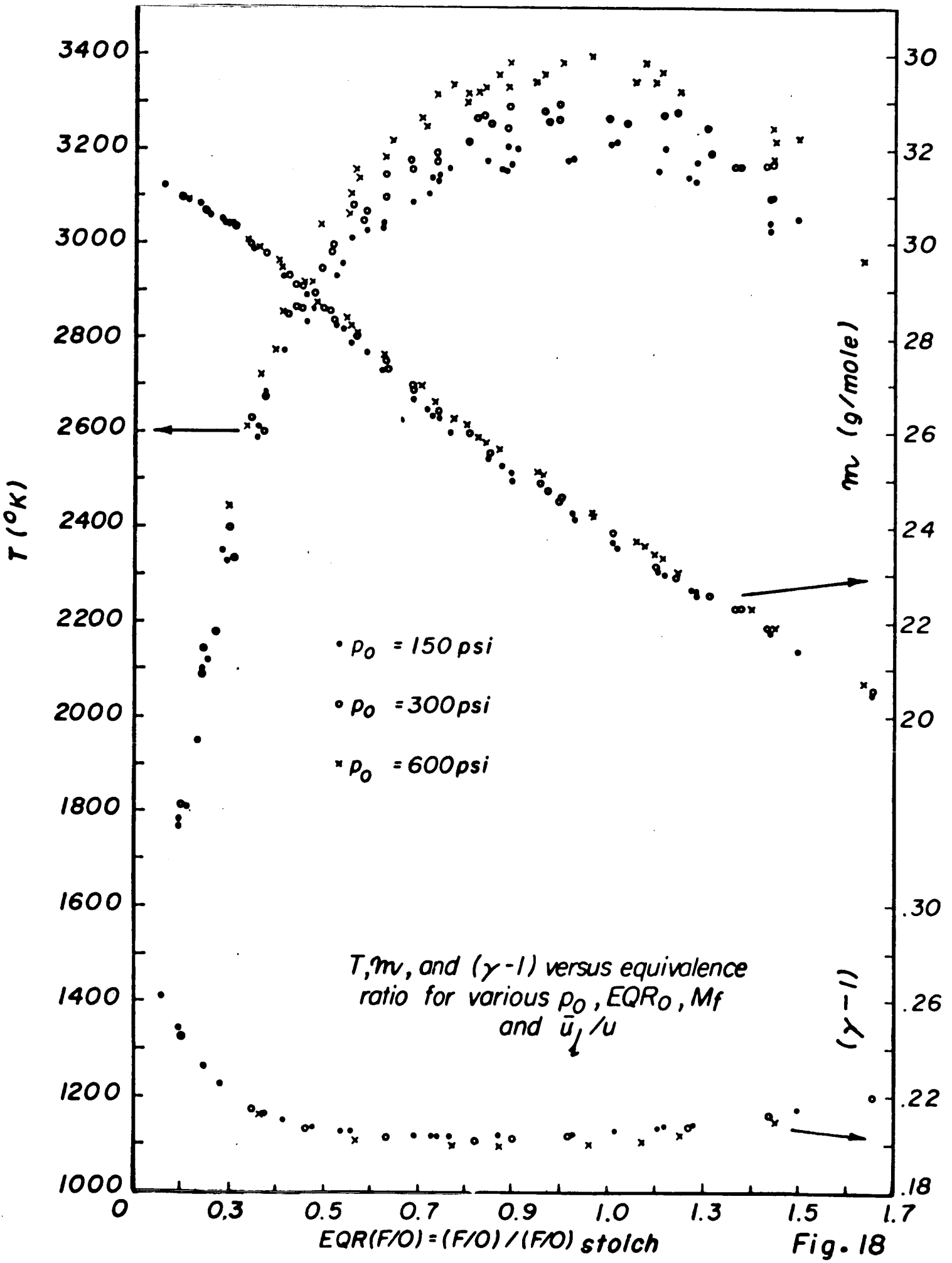
3400
3200
3000
2800
2600
2400
2200
2000
1800
1600
1400
1200
1000
T (°K)
30
32
30
28
26
24
22
20
.30
.26
.22
.18
$\bar{m}$ (g/mole)
$(\gamma - 1)$
• p_o = 150 psi
° p_o = 300 psi
× p_o = 600 psi
T, $\bar{m}$, and $(\gamma - 1)$ versus equivalence ratio for various p_o, EQR_o, Mf and $\bar{u}_1/u$
0
0.3
0.5
0.7
0.9
1.0
1.3
1.5
1.7
EQR(F/O) = (F/O) / (F/O) stoich

Fig. 18

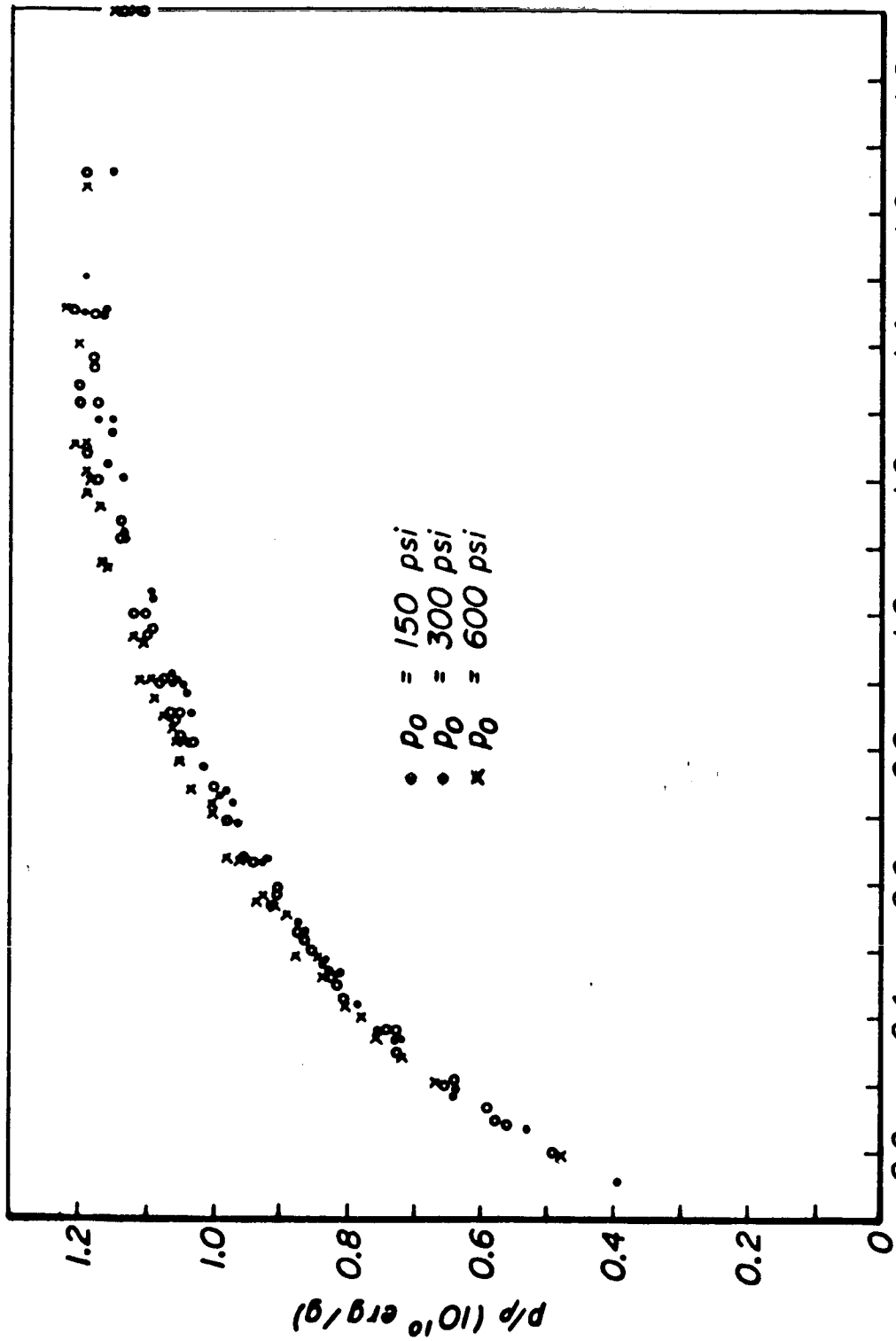

p/ρ versus equivalence ratio for varying p_o, EQR_o, M_f and $\bar{u}_f/u$

Fig. 19

ucts and read into their computer program tables of "adiabatic flame temperature" parameters versus pressure, temperature and mixture ratio. They could have gone one step further and expressed the above gas properties versus mixture ratio alone. The error would have been small and the computations considerably simplier. In summary, if the engine configuration is given its steady-state could be studied by the above three equations which contain six unknowns: ρ , u , W_F , W_ϕ, p , and $\bar{u}_e/u$. Three of them must be measured or specified (generally W_ϕ , $\bar{u}_e/u$, p) to obtain solutions for the other three. At this point it is important to notice that the bulk gas properties which depend primarily on EQR are very sensitive to it (see Figs. 18 and 19). In general, EQR will change along the engine axis and therefore those bulk gas properties which depend on it can be expected to exhibit axial non-uniformities. The problem of the axial uniformity of the gas properties will shortly be reconsidered. In conjunction with the energy equation the following observations are also of interest:

a) The fact that Q_f , Q_g have little influence on the solution of the equations used in the direct method, means that its results are not sensitive to the assumption made about the temperature of the liquids as previously stated.

b) The fact that the temperature drops below realistic values when EQR tends to zero implies that the assumption of chemical equilibrium of the products together with that of complete vapor-

ization of the oxidizer and of uniform one-dimensional flow with no recirculation lead to unrealistic results near the injector. For this reason most of the charts presented in this report originate at some distance from the injector. In Section 3.4 the region very close to the injector is studied for one specific engine configuration in an attempt to get some qualitative information about this region which could be important for instability. Parenthetically notice that with the direct approach the far region of the engine can be studied without either calculating the near region or postulating anything about it. If one had used the conventional approach, he would have had to start his calculations from the injector (or at some distance from it but only after having postulated the initial values of the parameters at that distance[20]).

c) In this study the following eight products have been assumed to be present: OH, CO, CO_2, O, O_2, H_2, H_2O, H. Computations show that none of these products is consistantly negligible for all cases of the parametric study. It is probably true that omission of some of the above products would not have large effects on the bulk gas properties while simplifying somewhat the compu-

tations. However, as previously explained, one could avoid using energy and chemical equilibrium equations altogether still introducing no more than a 5% error in the bulk gas properties. This is then the way to go if one wants to simplify the computations, rather than that of eliminating a few products.

d) In theoretical instability studies, where reasonable simplifications are necessary, one often sets $e = p/\rho(\gamma-1)$ where for γ one usually selects its complete combustion steady-state value. For the above expression to hold exactly, the gas should be thermally and calorically perfect. But the composition of the actual combustion gas changes axially and the specific heats change with temperature. Thus the above expression for e is not exact. It was previously explained that the actual local values of e, p/ρ and γ depend almost exclusively on the local mixture ratio of the gas. Comparing the actual, local value of e (calculated for the local composition and with varying heat capacities) with the actual, local value of $p/\rho(\gamma-1)$, one finds that the latter is some 10% to 20% larger than the former. If instead of using the local value of γ one used its complete combustion value the error in the colder part of the engine would be larger (closer to 25%).

Most of the difference can be explained by the variation of the specific heats with temperature. Using the values of the specific heats (or of γ) relative to the local chamber temperature leads to overestimating the internal energy since the specific heats increase as T goes from its reference value to its local chamber values. Thus, wanting to set $e = p/\rho(\gamma - 1)$, one should use for γ a value slightly higher (or for the specific heats slightly lower) than that corresponding to complete combustion. For the LOX/ethanol system $\gamma = 1.235$ (rather than $\gamma = 1.21$) is suggested.

e) The parametric study shows that only one parameter comes close to being axially uniform for all injection mixture ratios and chamber pressures but for small chamber Mach numbers. This is the energy released by the chemical reaction per unit volume of the combustion chamber ($\rho\varphi^0$). The energy equation can also be written as follows (see Appendix A)

$$\rho u\left(e+\frac{p}{\rho}+\frac{u^2}{2}\right) = \rho u \varphi^0 - \left[w_F\left(\lambda_F+\frac{u_F^2}{2}\right) - w_{oF}\left(\lambda_{oF}+\frac{u_{oF}^2}{2}\right) + w_\phi\left(\lambda_\phi+\frac{u_\phi^2}{2}\right) - w_{o\phi}\left(\lambda_{o\phi}+\frac{u_{o\phi}^2}{2}\right)\right]$$

where:

$$e + \frac{p}{\rho} = 4.186\ 10^{10} \sum_{i=1}^{8} x_i \int_{T0}^{T} C_{p_i}(T)\,dT / m_{em}$$

$$-u\rho\varphi^0 = \rho u h^0 + (w_F - w_{oF})\,h_F^0 + (w_\phi - w_{o\phi})\,h_\phi^0$$

In the above energy equation, the right hand side

represents the energy source for the gases. The quantity ($\rho\varphi^0$) was found to be proportional to the chamber pressure and roughly independent of equivalence ratio, particularly if the very high, unpractical values of EQR_0 are excluded (see Fig. 20). Thus for $M_t \leq .15$ one could set

$$\rho\varphi^0 \simeq \frac{5.25\ 10^7}{150\ \ 68.97\ 10^3}\ p = 5.08\ p$$

The exact reason for such a relationship is not clear. One could notice, however, that as the nozzle is approached the gas density always decreases while the chemical energy released tends to increase, reflecting more favorable gas mixture ratios in spite of higher dissociation. One may also notice that if kinetic energies and vaporization energies are neglected in the above steady-state energy equation, the chemical heat released goes into latent enthalpy of the gas

$$e + \frac{p}{\rho} = \varphi^0$$

One could then set $e = p/\rho\ (\gamma - 1)$, still being aware that this expression is itself an approximate one as explained above, thus finding

$$\frac{\gamma}{\gamma - 1}\ p = \rho\varphi^0$$

which shows that, whenever kinetic energies and vaporization energies are negligible and $e = p/\rho\ (\gamma - 1)$, then the volumetric energy released can be expected to be uniform. For $\gamma = 1.235$ the coefficient of p

		No.	EQR_o	M_f	u_f/u
● p_o = 150 psi		1	0.897	0.142	0.2 and 1.0
		2	0.897	0.511	"
○ p_o = 300 psi	and	3	1.44	0.151	"
		4	1.44	0.597	"
× p_o = 600 psi		5	1.90	0.145	"
		6	1.90	0.554	0.2 and 1.0

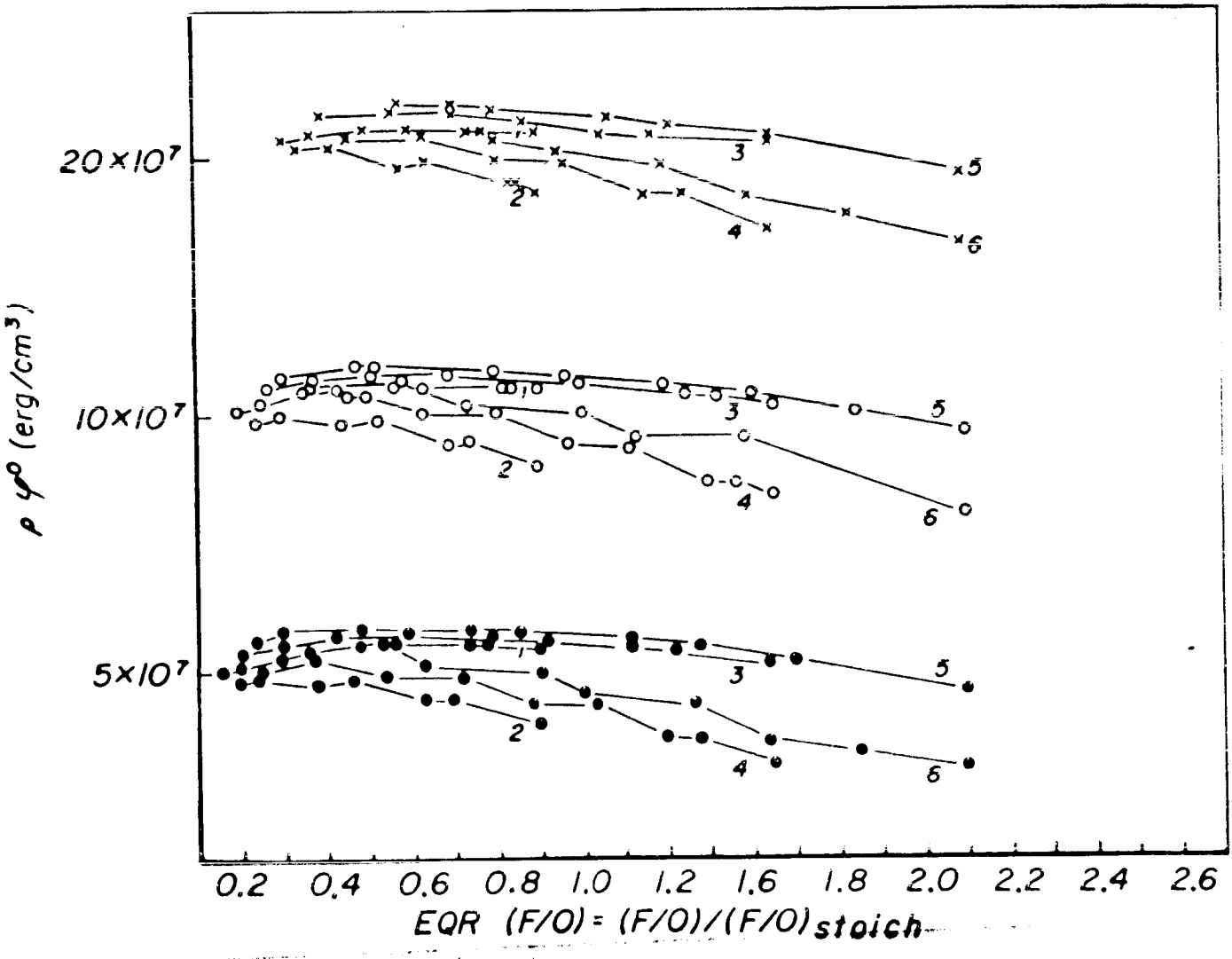

Volumetric energy released ($\rho\varphi^{99}$) versus equivalence ratio varying p_o, EQR_o, M_f and u_f/u

represents the energy source for the gases. The quantity ($\rho\varphi^0$) was found to be proportional to the chamber pressure and roughly independent of equivalence ratio, particularly if the very high

Fig. 20

would be 5.25. This dependence of the volumetric energy released on the chamber pressure, but not on mixture ratio, might be of some use in the problem of scaling of rocket engines.

f) The relationship between steady-state mass and energy sources is of some interest. The steady-state is often assumed to be uniform within terms of the order of the chamber Mach number. In this model[21], pressure, density and temperature are axially uniform, and mass source, energy source and gas velocity gradient are proportional. In Appendix A, it is shown that the latent stagnation enthalpy of the gas $(e + p/\rho + u^2/2)$ is axially uniform when the vaporization processes are such that, at any distance from the injector, equal fractions of the two propellants have vaporized. This is a practical example in which the above uniform steady-state model would be verified (within terms of the order of the chamber Mach number). In general, however, one of the two propellants vaporizes more quickly than the other and an axially non-uniform gas composition occurs. From this, non-uniformities in the temperature and in the other parameters of the gas can be expected to follow. Similarly the energy source can be expected not to be proportional to the mass source as a direct consequence of the vary-

ing mixture ratio of the gas. The non-uniformity of the gas parameters will be reconsidered in Section 3.3.5 (for the LOX/ethanol system). Here the relationship between mass and energy sources is briefly considered. Thus mass and energy conservation equation can be written as follows (Appendix A)

$$\frac{d}{dx}(\rho u) = -\frac{d}{dx}\left(\rho_F u_F + \rho_\phi u_\phi\right) = Q$$

$$\frac{d}{dx}\left(\rho u\left(e + \frac{p}{\rho} + \frac{u^2}{2}\right)\right) = -\frac{d}{dx}\left(\rho u h^0 + \rho_F u_F h_F^0 + \rho_\phi u_\phi h_\phi^0 + \right.$$

$$\left. + \rho_F u_F\left(\Lambda_F + \frac{u_F^2}{2}\right) + \rho_\phi u_\phi\left(\Lambda_\phi + \frac{u_\phi^2}{2}\right)\right) = \Phi$$

Recalling that the chemical energy released (Appendix A) is given by

$$-\rho u \varphi^0 = \rho u h^0 + (w_F - w_{0F}) h_F^0 + (w_\phi - w_{0\phi}) h_\phi^0$$

and substituting it into the expression for the energy source one gets

$$\Phi = -\frac{d}{dx}\left[-\rho u \varphi^0 + w_{0F} h_F^0 + w_{0\phi} h_\phi^0 + \rho_F u_F\left(\Lambda_F + \frac{u_F^2}{2}\right) + \right.$$

$$\left. + \rho_\phi u_\phi\left(\Lambda_\phi + \frac{u_\phi^2}{2}\right)\right] = \frac{d}{dx}\left[\rho u \varphi^0 - \rho_F u_F\left(\Lambda_F + \frac{u_F^2}{2}\right) - \rho_\phi u_\phi\left(\Lambda_\phi + \frac{u_\phi^2}{2}\right)\right]$$

Calculations show that in the above expression the leading term is that containing the chemical energy released ($\rho u \varphi^0$), whereas the vaporization energies ($(\rho u \Lambda)_{F,\phi}$) are smaller, even though not negligible (except in the vicinity of the injector where they are as large as u_p). Recalling also that the volumetric chemical energy re-

leased ($\rho\varphi^0$) was found to be nearly axially uniform, one concludes that the gas velocity gradient is roughly proportional to the energy sources

$$\Phi \simeq \rho\varphi^0 \frac{d}{dx} u$$

However energy and mass sources are not proportional

$$\Phi / Q \simeq \rho\varphi^0 \frac{d}{dx} u \Big/ \frac{d}{dx}(\rho u)$$

If the density were axially uniform one would find again the proportionality between mass and energy sources. Typical axial density profiles (for the LOX/ethanol system) are given in Figs. 5, 10, 15 and 24 and they are seen to be quite non-uniform. To evaluate a typical Φ/Q ratio, the engine configuration II of Table IV, whose ρ and u are given in (Figs. 9 and 10), is now considered. First the following dimensionless terms are introduced in the above equation

$$\rho^* = \rho/\rho_f \qquad u^* = u/u_f \qquad x^* = x/50^*$$

thus getting

$$(\Phi/Q)/(\rho\varphi^0/\rho_f) = \left(\frac{d}{dx^*} u^*\right)/\left(\frac{d}{dx^*}(\rho^* u^*)\right)$$

Toward the end of the combustion region, both numerator and denominator of the right hand side of the above equation tend to zero. For physical reasons they will have to be infinitesimal of the same order so that their ratio is finite.

Actually the ratio will tend to 1.0 since, for $\rho \to \rho_f$, $\Phi/Q \to \varphi^o$ (within the approximations made to obtain the above relationship). Thus the departure of the right hand side from 1.0 is the measure of the axial disuniformity of the ratio Φ/Q (see Figure 20b). It is difficult to relate the behavior of Φ/Q directly to the behavior of the various gas variables since the definitions of Φ and Q involve the derivatives of the gas variables rather than the gas variables themselves. Figure 20b says that the rate at which energy is added to the gas is, near the injector, lower than the rate at which mass is added. Soon, however, the situation is reversed and at some distance from the injector a situation is reached where the rate of energy released per unit rate of mass released has a maximum (probably related to a more favorable gas mixture ratio). Toward the end of the combustion both rates decrease and become proportional to each other (or the dimensionless rates ratio tend to 1.0). A similar trend was exhibited by the engine configuration I of Table IV. Before closing this section it might be worth noting that the complete combustion value of φ^o , as calculated by computer and including dissociation, was found to be $6.152\ 10^{10}$ erg/g while excluding

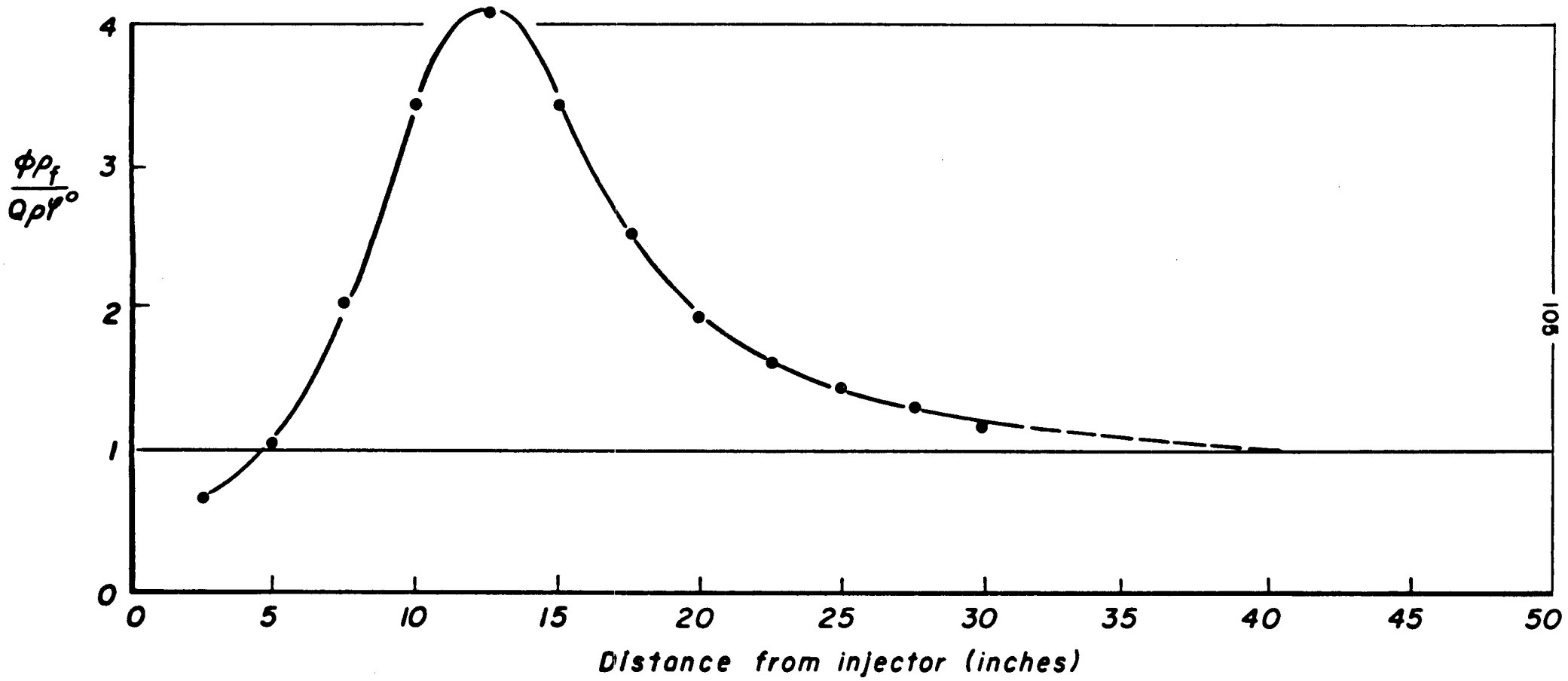

Fig. 20b

$\phi\rho_f / Q\rho\psi^\circ$ versus distance from injector

dissociation would have been 8.4 10^{10}erg/g indicating the extent of the role played by dissociation (Configuration II of Table IV).

3.3.4 The Momentum Equation

Two questions about the momentum equation will now be discussed. The first one is about the momentum exchanged between the gas and the liquids. The second one is about the importance of the initial momenta of the liquids. Again only that region of the engine where no more liquid oxidizer exists is now considered. The momentum equation then is

$$\rho u^2 + p - p_o + \left(w_F \bar{u}_\ell - w_{o_F} u_{x_F} \right) - w_{o_\beta} u_{x_\beta} = 0$$

The term within parenthesis can also be written as

$$w_F \bar{u}_\ell - w_{o_F} u_{x_F} = \int_0^x \frac{d}{dx}\left(w_F \bar{u}_\ell \right) dx = \int_0^x \frac{d}{dx}(w_F)\, \bar{u}_\ell \, dx + \int_0^x w_F \frac{d\bar{u}_\ell}{dx}\, dx$$

The first integral is always negative since the flux of liquid fuel (w_F) decreases continuously with x due to the vaporization. This term represents the momentum given by the liquid to the gas, due to the vaporization of the liquid. The second integral is always positive in the region where $\bar{u}_\ell < u$. This term represents the momentum taken by the liquid from the gas due to the drag on the liquid. A question of some interest is whether the two effects (vaporization and drag) are of the same order or one is negligible with respect to the other. If the effect of drag were smaller than that of vaporization, the term ($w_F \bar{u}_\ell - w_{o_F} u_{x_F}$) would be negative. The value of this term (divided by momentum of the gas) vs the loss of static pressure (divided by the complete combustion static pressure loss) is

given in Fig. 21 for all the cases of the parametric study. For each engine configuration, there are two curves corresponding to $\bar{u}_\ell/u = 0.2,\ 1.0$. The actual value of $(w_F \bar{u}_\ell - w_{0_F} u_{x_F})$ will fall between these two curves. At first glance one would conclude that drag and vaporization effects in the momentum equation of the gas are equally important since $(w_F \bar{u}_\ell - w_{0_F} u_{x_F})$ seems to take on both positive and negative values. However, if the injection velocity is limited to less than, say, 150 ft/sec (4572 cm/sec) as in practice is, then most of the engine configurations which gave neutral or negative values of $(w_F \bar{u}_\ell - w_{0_F} u_{x_F})$ would be ruled unrealistic. Further, the actual value of $\bar{u}_\ell / u$ is likely to be closer to 1.0 than .2 in most of the engine (as the calculations of Section 3.6 also show). Thus one should conclude that, in practical cases, the effect of drop drag on the momentum of the gas is larger than (or at least equal to) that of the drop vaporization. This is due to fact that the momentum that the liquid carries into the chamber ($w_{0_F} u_{x_F}$) is usually small, due to low injection velocities, and therefore the momentum that the vaporized liquid adds to the gas is small. On the other hand, the momentum taken by the drops from the gas through the drag is generally high as it is shown by the tendency of $\bar{u}_\ell \to u$ rather than staying constant. In Fig. 21 notice also that in the vicinity of the injector, where the loss of static pressure is still small, the ratio of $(w_F \bar{u}_\ell - w_{0_F} u_{x_F})$ to ρu^2 is very high. Thus in this region the proper handling of the momentum of the liquid becomes important to the accuracy of the solution, and this brings up the subject of the importance

		No.	EQR_0	M_f	$\bar{u}_\ell/u$
● p_0 = 150 psi		1	0.897	0.142	0.2 and 1.0
		2	0.897	0.511	"
○ p_0 = 300 psi	and	3	1.44	0.151	"
		4	1.44	0.597	"
× p_0 = 600 psi		5	1.90	0.145	"
		6	1.90	0.554	0.2 and 1.0

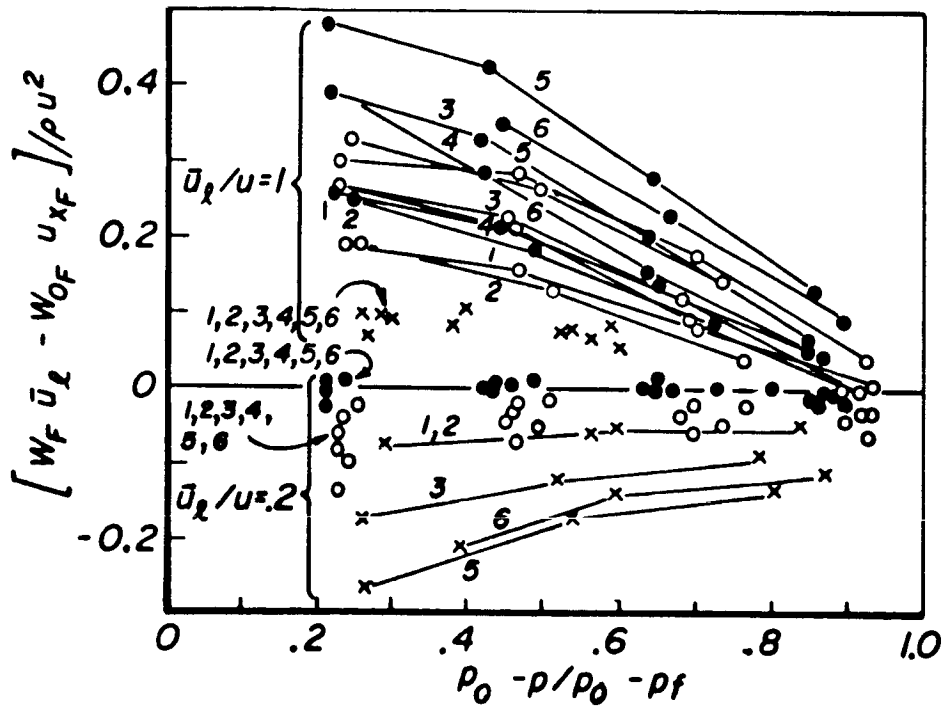

Liquid vaporization and drag effects on the momentum of the gas

Fig. 21

of the initial momenta of the liquid.

In the vicinity of the injector the initial momenta of the liquids are essential to the accurate determination of the steady-state for all chamber pressures, injection equivalence ratios and nozzle entrance Mach numbers. If one assumes that $\bar{u}_e/u = 1$, mass and momentum conservation give

$$\left[\frac{u}{u_f}\right]_{\bar{u}_e/u=1} \simeq \left[\frac{W_{oF}\,u_{xF} + W_{o\phi}\,u_{x\phi}}{p_o - p_f}\right] + \left[1 - \frac{W_{oF}\,u_{xF} + W_{o\phi}\,u_{x\phi}}{p_o - p_f}\right]\left[\frac{p_o - p}{p_o - p_f}\right]$$

Thus the ratio of the local gas velocity to the final gas velocity (u/u_f) is a linear function of the percent loss of static pressure and intersect and slope are functions of the initial momenta of the liquids. If the initial momenta of the liquids were neglected one would obtain

$$\left[\frac{u}{u_f}\right]_{\bar{u}_e/u=1} \simeq \frac{p_o - p}{p_o - p_f}$$

In Fig. 22 the results of the parametric study are given. The above linear dependence is evidenced. It can be seen that the departure from the 45° straight line (initial momenta neglected) is large, particularly near the injector and for high injection velocities, thus showing the importance of the initial momenta of the liquids. Notice that one could calculate the local gas velocity, from measured static pressure data, directly from the previous linear relationship by just knowing the basic parameters of the engine if he were to assume that $\bar{u}_e/u = 1$ (not even the assumption of chemical equilibrium of the products would be necessary). The influence of $\bar{u}_e/u \neq 1$ is shown in Fig. 22 by the results of the parametric study. The $\bar{u}_e/u \neq 1$ results come

	No.	EQR_0	M_f	$\bar{u}_2/u$
● p_0 = 150 psi	1	0.897	0.142	0.2 and 1.0
	2	0.897	0.511	"
○ p_0 = 300 psi and	3	1.44	0.151	"
	4	1.44	0.597	"
× p_0 = 600 psi	5	1.90	0.145	"
	6	1.90	0.554	0.2 and 1.0

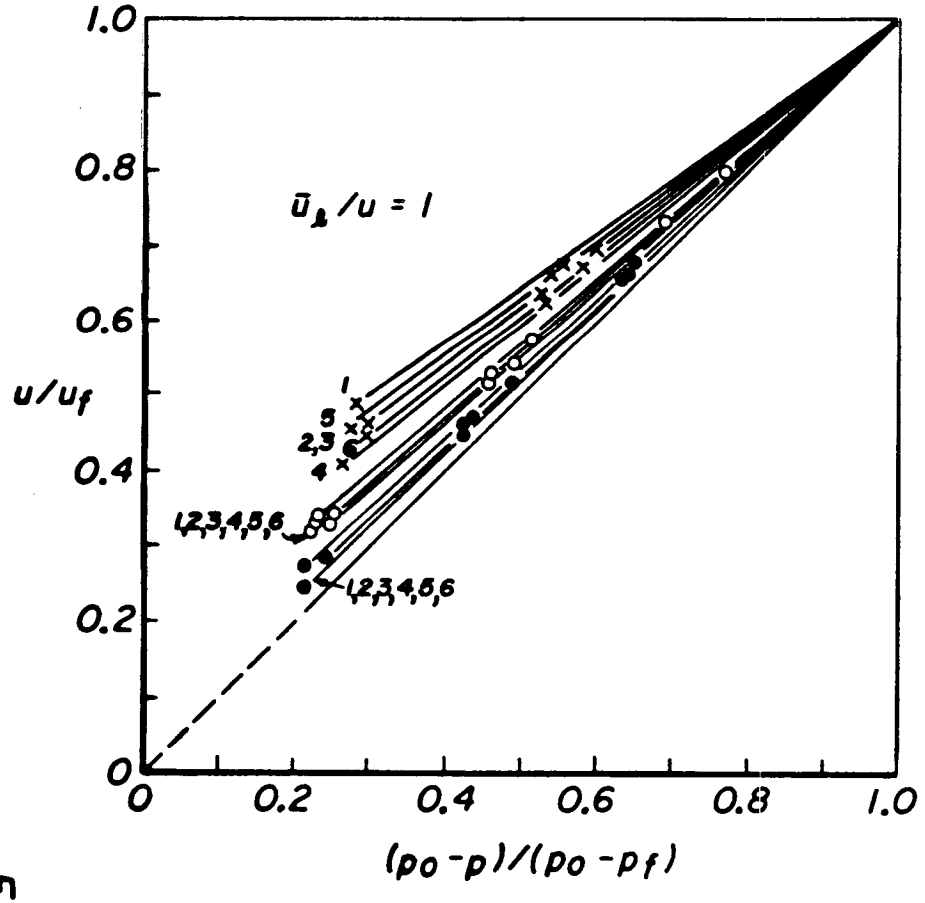

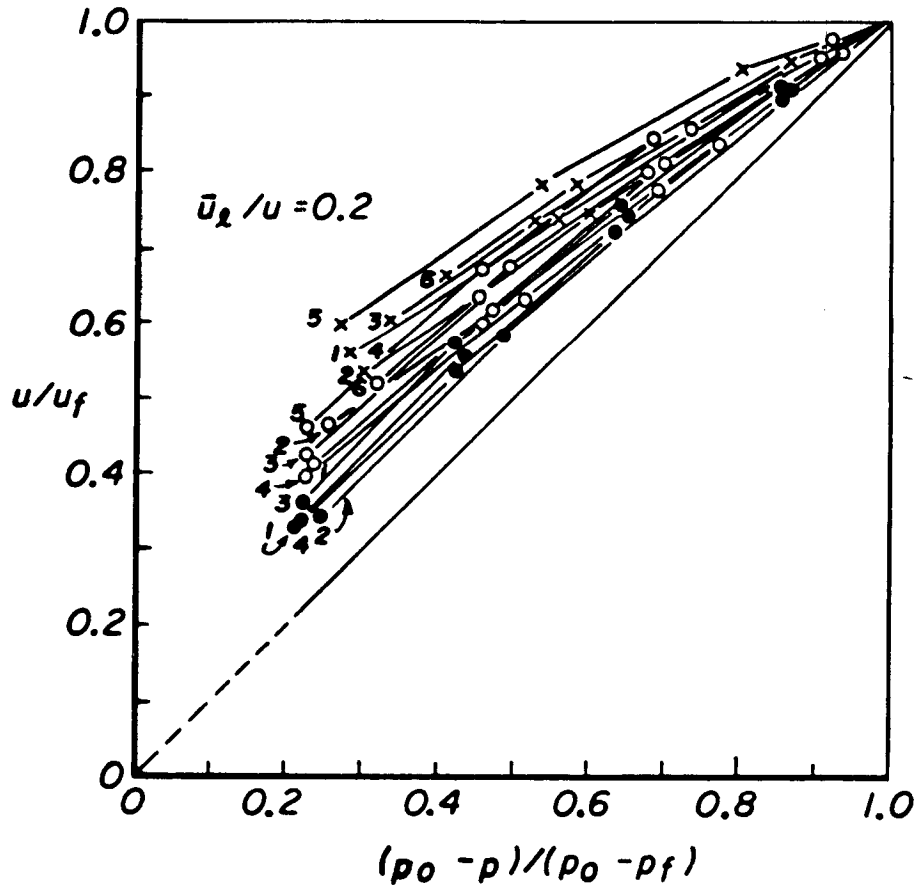

Effect of the initial momenta of the liquids

Fig. 22

now from the solution of the complete system of equations and therefore they are functions, in particular, of the assumption of chemical equilibrium of the reaction products. Indeed from mass and momentum conservation one now gets only the following relationship for $\bar{u}_e/u \neq 1$

$$\left[\frac{u}{u_f}\right]_{\bar{u}_e/u \neq 1} = \left[\frac{\rho u + \frac{\bar{u}_e}{u} W_F}{\rho u + W_F}\right]\left[\frac{u}{u_f}\right]_{\bar{u}_e/u = 1}$$

And the gas flux (ρu) is now to be determined using the complete set of equations.

3.3.5 Axial Uniformity

The question of steady-state axial uniformity is relevant to many important theoretical and practical problems such as the order of the terms in the conservation equations for theoretical instability studies (Section 3.5), the interactions between liquid and gas phases (see Section 3.6) and the heat transfer to the chamber walls. The results which are about to be discussed are valid for the LOX/ethanol system for subcritical engine conditions of practical interest. They are subject to the validity of the assumption of chemical equilibrium of the combustion gas and of no recirculation (except in the vicinity of the injector) which in turn have led to satisfactory results in the three engine configurations tested. They do not depend on any droplet drag, vaporization or distribution model. The result is that all gas parameters exhibit some degree of axial non-uniformity. The trends of the individual parameters are not evident a priori due to the nonlinear nature of the equations which interrelate them. Some of the most important parameters are now individually

considered.

p : The axial change of static pressure is of $O(M_f^2)$ or more specifically

$$\frac{p_0^* - p_f}{p_0^*} = \frac{\gamma_f M_f^2}{1 + \gamma_f M_f^2} \qquad p_0^* = p_0 + w_{0_F} u_{x_F} + w_{0_\phi} u_{x_\phi}$$

Thus for $M_f < .5$ the maximum change of p is 20% and it is independent of chamber pressure and mixture ratio.

T : The axial change of temperature depends strongly on the injection mixture ratio (Fig. 23). If the injection mixture is lean, $EQR_0 < 1$, the temperature increases uniformally along the engine starting from a value which could be as much as 50% lower than its final one. If the injection mixture is rich ($EQR_0 > 1$, say maximum c* mixture) a higher degree of temperature uniformity is expected. Near the injector it is still lower but it quickly reaches a value close to its final one as soon as enough fuel has vaporized as to make the mixture ratio of the gas close to stoichiometric. If the mixture were very rich, the temperature would be low quite close to the injector but would then rise quickly to decrease again before combustion of the liquid fuel is completed. Such rich mixtures, however, are not practically used. It is interesting to note that the maximum c* mixture, is also the one which exhibits the greatest temperature axial uniformity. Also higher chamber pressure and Mach number favor temperature uniformity.

m : The average molecular weight of the products changes by as much as 50% as the mixture ratio of the gas varies (Fig. 18). Notice that, for EQR_0's of practical interest (say $EQR_0 < 1.44$,

No.	EQR_0	M_f	u_l/u
1	0.897	0.142	0.2 and 1.0
2	0.897	0.511	"
3	1.44	0.151	"
4	1.44	0.597	"
5	1.90	0.145	"
6	1.90	0.554	0.2 and 1.0

• p_0 = 150 psi
○ p_0 = 300 psi and
× p_0 = 600 psi

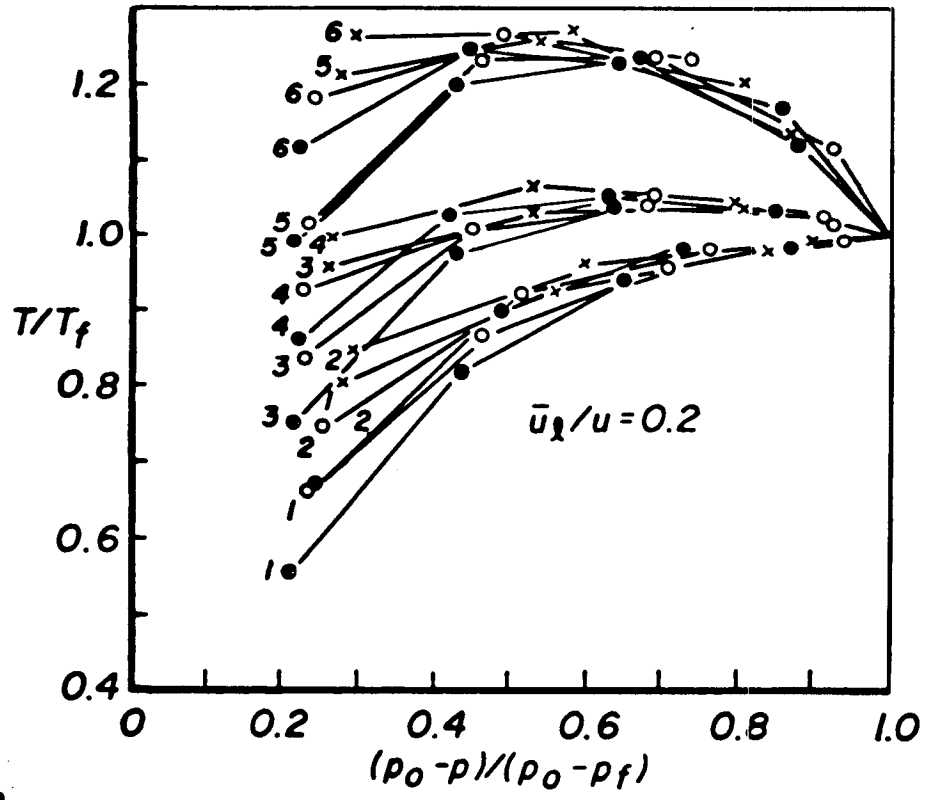

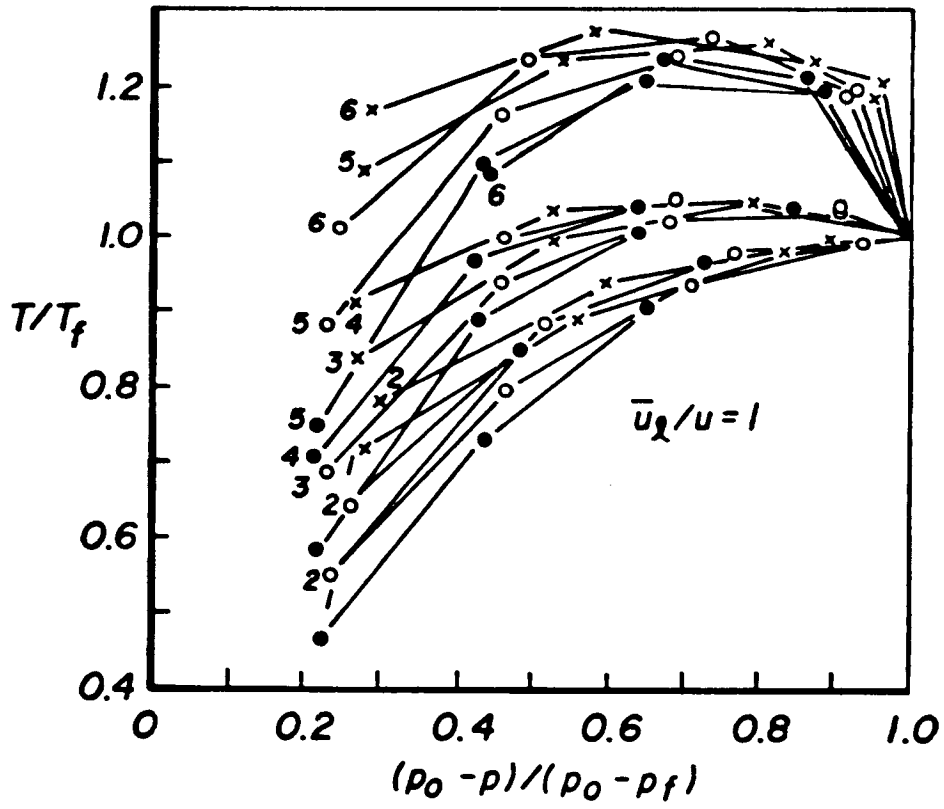

Fig. 23 Gas temperature axial variations

which corresponds to maximum c*) the temperature mostly increases along the engine while the average molecular weight decreases. This brings about a strong axial non-uniformity in the density since $\rho = p m/RT$ and p decreases as well along the engine. m is practically independent of chamber pressure and Mach number.

ρ : The density, as above indicated, is the quantity which undergoes the strongest axial disuniformity (Fig. 24). The density at the injector can be expected to be at least twice as large as the complete combustion density, for practical engine configurations. Density uniformity is strongly influenced by chamber pressure with higher pressures bringing about higher uniformity. Also rich mixtures and lower M_f favor density uniformity.

γ : The ratio of the specific heats is rather uniform ($1.26 < \gamma < 1.2$) but the factor $(\gamma - 1)$ can be expected to change by 30% along the combustion chamber.

a : The quantity $a = (\gamma p/\rho)^{1/2}$ varies roughly as $(1/\rho)^{1/2}$ (see Fig. 25) and the variations of ρ have already been considered. Notice that the variation of a is more closely related to that of ρ than to that of T due to the simutaneous variations of m ($\frac{\gamma p}{\rho} = \frac{\gamma RT}{m}$). Notice, for example, that a increases uniformly along the chamber length for mixture ratios of practical interest, while T could actually first increase and then decrease. The quantity $(\gamma p/\rho)^{1/2}$ is close to the speed at which an infinitesimal perturbation would move (speed of sound) but it does not necessarily coincide with it due to the reactive nature of the medium under consideration and to the presence in it of mass, momentum, and energy sources (see Section 3.5).

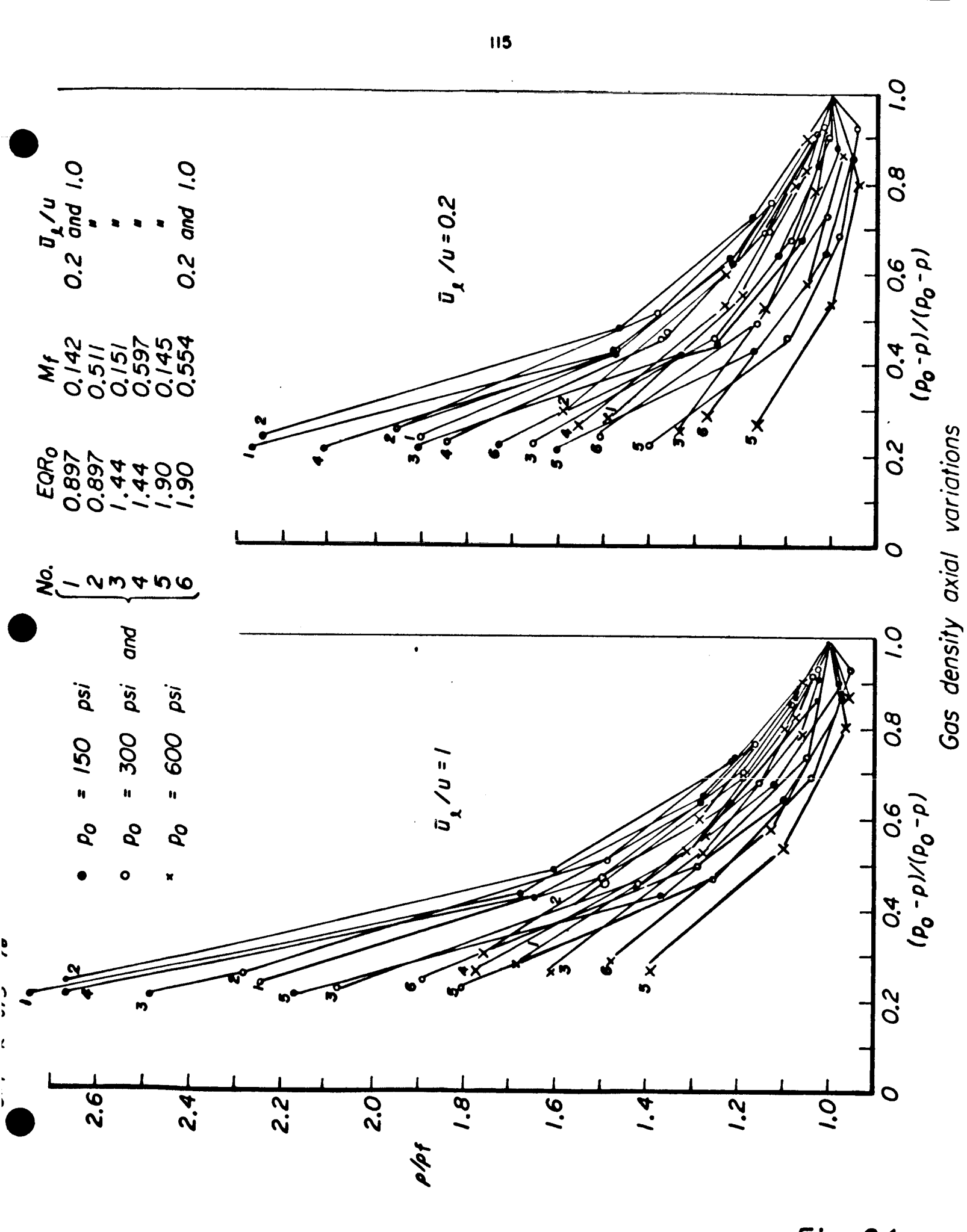
Gas density axial variations
ρ/ρf
(ρo - ρ)/(ρo - ρ)
ū_x/u = 1
ū_x/u = 0.2
• ρo = 150 psi
o ρo = 300 psi and
× ρo = 600 psi
No. EQRo Mf ū_x/u
1 0.897 0.142 0.2 and 1.0
2 0.897 0.511 "
3 1.44 0.151 "
4 1.44 0.597 "
5 1.90 0.145 "
6 1.90 0.554 0.2 and 1.0

Fig. 24

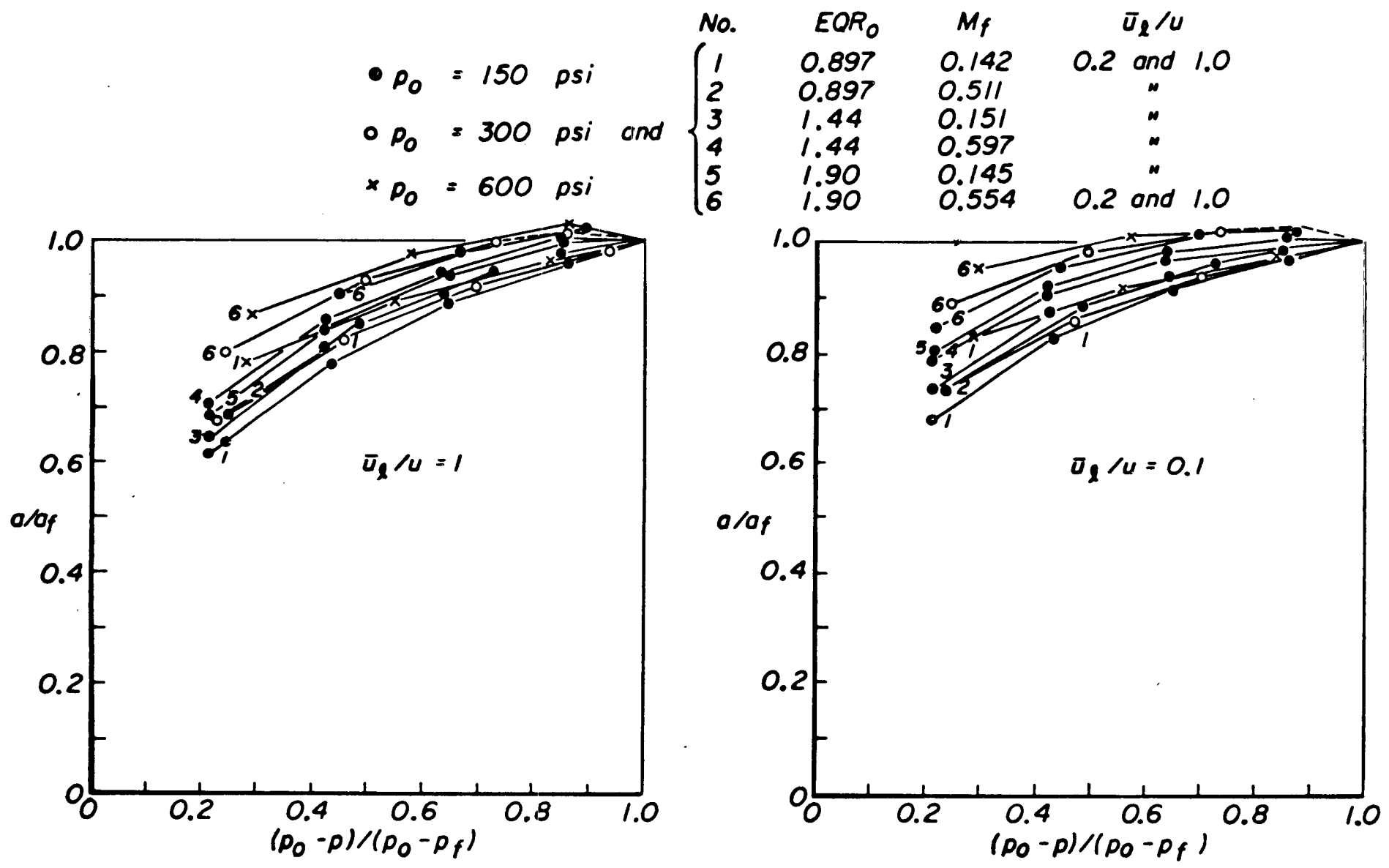

Gas speed of sound axial variations

Fig. 25

$\rho\varphi^{\circ}$: The volumetric energy released is close to uniform along the engine for mixture ratios of practical interest and for low chamber Mach numbers. Its value is proportional to the chamber pressure and roughly independent of the mixture ratio as already indicated (see Section 3.3.3).

e : The specific internal energy of the gas varies roughly as $p/\rho(\gamma-1)$ if p, ρ, and γ are given their local values as previously indicated. Since both p and $(\gamma-1)$ tend to decrease along the chamber, the changes of e resemble those of $1/\rho$.

3.4 Region With Liquid Oxidizer

The one-dimensional approach to the study of this region is hardly justifiable, as is the assumption of uniform chemical equilibrium of the gaseous species. Even accepting the above two limitations, this region could not be determined with any degree of accuracy since the experimental measurements in this region show great randomness. The determination of the non-measured variables by Equations 51 through 76 and by the use of the measured ones, then becomes a matter of interpretation of the experimental data. This is most unfortunate since this region is likely to be important as far as high frequency instability is concerned. Thus, this region will now be investigated qualitatively. A number of interesting results will be reached among which are the following ones:

a) The initial momentum of the liquid should not be neglected in steady-state calculations.

b) The increase of static pressure in the vicinity of the injector is produced by the initial mo-

mentum of the liquid.

c) The point at which the liquid velocity is equal to the gas velocity ($u_\ell = u$) is further from the injector than the point at which the static pressure tops off after increasing ($p_x = 0$).

d) The velocity of the liquid need not necessarily decrease before increasing.

e) Temperature and static pressure measurements near the injector help considerably in defining the local state.

The first engine Configuration of Table I is specifically studied in this section.

The momentum equation is considered first. If one assumes that both liquid fuel and liquid oxidizer move at the same velocity (u_ℓ) and sets $\rho_\ell = \rho_F + \rho_\phi$, then he can write the momentum equation in the following equivalent forms

$$(\rho u^2)_x + p_x + (\rho_\ell u_\ell^2)_x = 0$$

$$(\rho u)_x u + (\rho u) u_x + p_x + (\rho_\ell u_\ell) u_{\ell x} + (\rho_\ell u_\ell)_x u_\ell = 0$$

$$\rho u^2 + p - p_0 + \left[\rho_\ell u_\ell^2 - \left(w_{0_F} u_{x_F} + w_{0_\phi} u_{x_\phi} \right) \right] = 0$$

Static pressure measurements near the injector indicate that the static pressure first increases a bit before decreasing. In the first engine configuration, the static pressure reaches a maximum between 1 and 2 inches from the injector (see Fig. 3). The first of the above equations shows that as long as the static pressure increases the liquid must be losing momentum (the first two terms are positive, the third must be negative). The second

equation shows that the liquid can be losing momentum while its velocity is still increasing provided that the vaporization is sufficiently strong (the first three terms are positive, the fourth term could be positive or negative and the fifth one is negative). The third equation shows that as long as the static pressure is greater than the injector static pressure, the driving force is provided by the initial momentum of the liquids (in the first engine configuration, approximately the first 2 inches). In this region the largest terms are the liquid propellant terms while the gas momentum and the static pressure difference terms are small. Finally, it should be noted that the point where $u_\ell = u$ must occur further away from the injector than the point at which $p_x = 0$. When $u_\ell = u$ the drag term is zero ($u_{\ell_x} = 0$), and $(\rho u)_x u$ and $(\rho_\ell u_\ell)_x u_\ell$ cancel each other out because of mass conservation. Thus the second equation can be satisfied only if p_x is negative. Hence in the first engine configuration the condition $u_\ell = u$ must occur further away from the injector than say 1.5 or 2 inches. The fact that the velocity of the liquid fuel might actually be different from that of the liquid oxidizer produces more possibilities and, for instance, one propellant could slow down after injection while the other could accelerate. The fact still remains that as long as the static pressure is greater than the injector static pressure, the driving force is provided by the initial momenta of the liquids and that at least one of the two $u_f = u$, $u_g = u$ distances must be further than the $p_x = 0$ distance. Mass and energy equations are now considered under the assumption of uni-

form chemical properties of the gas. This region is characterized by low temperature (less than 2400°K). No dissociation phenomena need then be considered, and all the fuel can be assumed to give CO_2 and H_2O products. The energy released per mole of gaseous fuel is then constant. Equations 66 through 70 involving the chemical species in the gaseous products can now be greatly simplified

$$C_a H_\ell O_c + z O_2 \rightarrow X_1 CO_2 + X_2 O_2 + X_3 H_2O$$

$$m_{gm} = 12a + \ell + 16(c + 2z) \tag{66a}$$

$$y = z + \frac{c}{2} + \frac{\ell}{4} \tag{67a}$$

$$X_1 = a \tag{68a}$$

$$X_3 = \ell/2 \tag{69a}$$

$$X_2 = [\, c + 2z - (2a + \ell/2)]/2 \tag{70a}$$

$$\varphi^0 = -4.184\, 10^{10} \left\{ a(-94) + \frac{\ell}{2}(-57.8) - (H^0_{298})_F \right\} / m_{gm}$$

In the above equations z, which represents the local mixture ratio of the gaseous components, is the only unknown. z now depends on the vaporization of both fuel and oxidizer. If it is assumed again that both liquid fuel and liquid oxidizer move at the same average speed, then one can identify the fractions of liquid fuel and liquid oxidizer by the following parameters

$$\alpha_F = u_e \rho_F / w_{oF} \qquad \alpha_\beta = u_e \rho_\beta / w_{o\beta}$$

Then z can be written as

$$z = \frac{w_{o\beta}\, m_F}{w_{oF}\, m_\beta} \left[\frac{1 - \alpha_\beta}{1 - \alpha_F} \right] \tag{15a}$$

The mass conservation and state equations now give

$$\alpha_F = 1 - \rho u / [\, w_{oF} (1 + z\, m_o/m_F)\,] \tag{11a}$$

$$T = p\, m_{am} / \rho \gamma R \tag{14a}$$

It could be shown that after some algebra the energy equation reduces to

$$z = G_1 + G_2 \rho \qquad G_1 = -2.56 \qquad G_2 = 4.34\ 10^{3}\ m^3/g$$

The above equation includes the effects of the vaporization energy now as important as the mechanical work (p/ρ). The energy equation need not be simplified and could be handled by computer as it was done in the previous section for the region with no liquid oxidizer. Here, however, one is after more qualitative arguments and then it is useful to solve the approximate system of equations in closed form to discuss its behavior. Even so the results from the above equations match the results from the more accurate equations given in Section 3.2 if $\alpha_o = 0$ (no liquid oxidizer) and for temperatures less than 2400°K, and greater than 2000°K. Using Equations 61a, 63a and 65a the following relation between z, α_o, u is found

$$z^2 + \left[G_1 + \frac{\alpha_o - 1}{u^*} \frac{m_o}{m_F} \right] z + \frac{\alpha_o - 1}{u^*} = 0 \qquad u^* = \frac{u\, m_o}{G_2\, w_{oo}}$$

If one assumes that the gas velocity varies linearly from the injector to five inches (where it is known, see Fig. 4) and that the liquid oxidizer decreases linearly in the same interval (to

be zero at five inches) one finds the interesting result that ξ is constant in the interval. By virtue of Equations 63a, 64a, 66a, 67a and 70a, this implies constant gas composition, density and temperature while by virtue of Equation 65a the fuel would be vaporizing linearly within the interval (to its value at five inches). Move specifically one would get (see Fig. 26)

$x = 0 \longrightarrow 5''$
$u = 0 \longrightarrow 7000$ cm/sec
$d_\phi = 1 \longrightarrow 0$
} Assumptions

$\xi = 12.6$
$\rho = 3.5\ 10^{-3}$ g/cm^3
$T = 2140$ °K
$d_F = 1 \longrightarrow .735$
} Results

However, temperature measurements indicate that the temperature is not constant in the 0 to 5" region. So close to the injector at any given distance from it, the temperature is found to vary considerably according to whether it is measured in front of a fuel or an oxidizer orifice, or in between (this merely shows the inaccuracy of the simple one-dimensionality assumption in this region). At 1' the temperature measured in the first engine configuration was about 2000°F between oxygen and ethanol orificies and about 1200°F in front of the ethanol orifice. At 3" the measured temperatures are roughly 3800°F and 1800°F respectively. Wishing to carry the one-dimensional analysis further, the temperatures of 1200°K and 1700°K and 1" and 3" respectively were used. Further assuming that the fraction of liquid fuel decays linearly in the interval from 0" to 5" (from 1 at the injector to .735 at 5") one can then calculate the

other parameters, thus finding:

x =	1"	3"
$T(°k)$ =	1200	1700
Z =	25	17
$\rho\ (g/cm^3)$ =	$6.34\ 10^{-3}$	$4.5\ 10^{-3}$
α_F =	.947	.841
α_g =	.603	.190
$u\ (cm/sec)$ =	1420	4180
$u_\ell\ (cm/sec)$ =	2080	3000

Where the average velocity of the liquids, u_ℓ , was calculated by using the momentum equation and the measured static pressure (Fig. 26). The above results could be used as such although they lead to a linear variation of gas particle velocity in the region 0" to 5" and to a $u_\ell = u$ distance of 1.5" more or less coinciding with the $p_x = 0$ distance (see Fig. 3). Experiments show that the gas velocity is not quite linear in the region 0" to 5" and one would like the point $u_\ell = u$ to be a bit further away from the injector than the point $p_x = 0$. Both points can be taken into account by abolishing the assumption that the fraction of liquid fuel decays linearly in the interval 0" to 5". Thus assuming that at 1", $\alpha_F = .98$ one finds

At 1" $T = 1200°k$ $Z = 25$ $\rho = 6.34\ 10^{-3}\ \frac{g}{cm^3}$ $\alpha_F = .98$ $\alpha_g = .85$
$u = 536\ cm/sec$ $u_\ell = 2080\ cm/sec$

The above results lead to the third graph of Fig. 26 . As previously stated, these results are only qualitative. However, since they are derived by the direct use of experimental data (temperature, static pressure, particle velocity) and since they respect basic equations they can be recognized to have some indicative value.

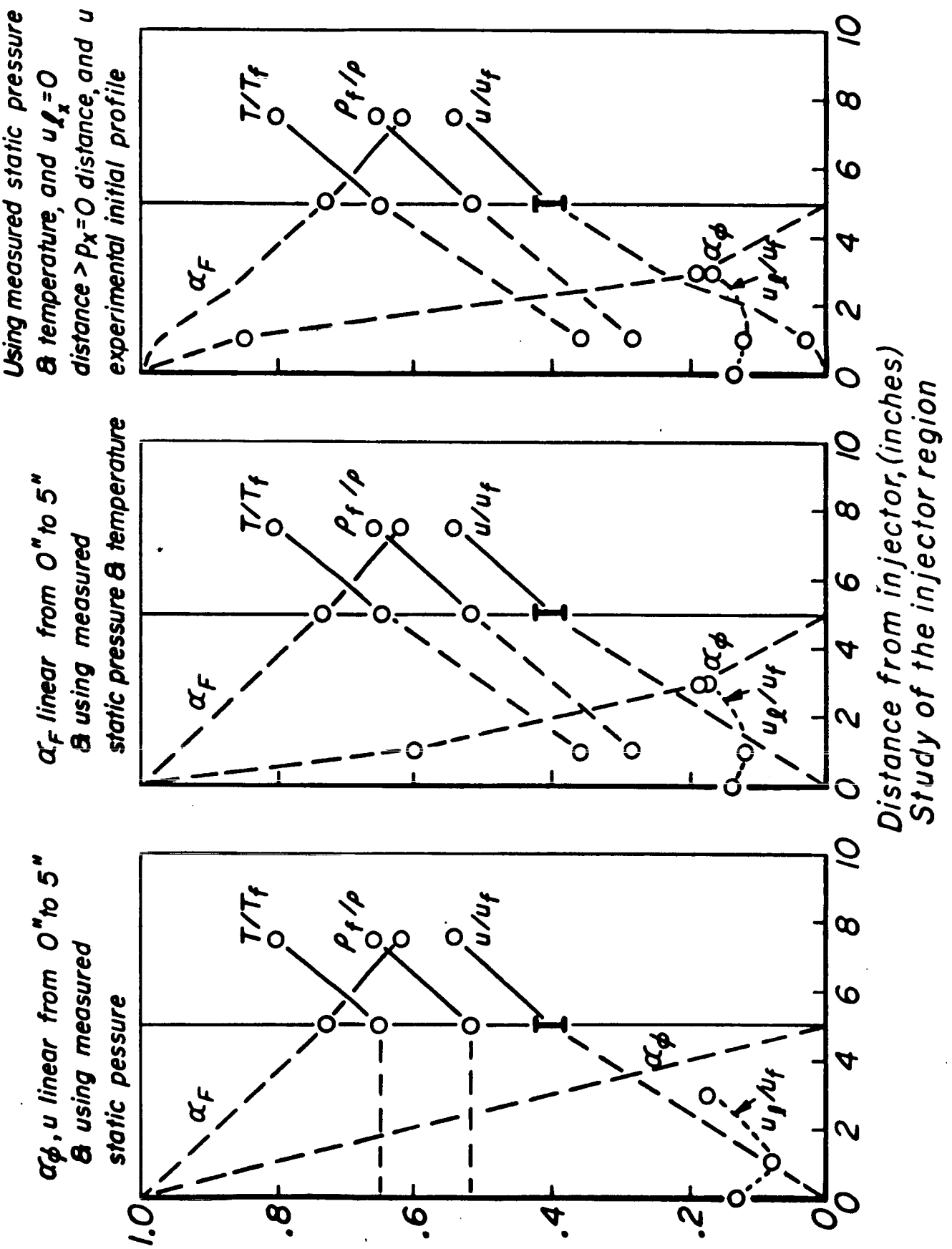
α_ϕ, u linear from 0" to 5"
& using measured
static pessure
α_F linear from 0" to 5"
& using measured
static pressure & temperature
Using measured static pressure
& temperature, and $u_{f_x}=0$
distance > $p_x=0$ distance, and u
experimental initial profile
α_F
T/T_f
ρ_f/ρ
u/u_f
α_ϕ
u_g/u_f
1.0
.8
.6
.4
.2
0
0
2
4
6
8
10
Distance from injector, (inches)
Study of the injector region

Figure 26

3.5 Perturbation of the Steady State

It is desired to find a perturbation scheme, for the conservation equations, consistent with the steady state axial nonuniformities discussed in previous sections and to evaluate the effect of the steady state axial disuniformity on the frequency of a small periodic perturbation. For simplicity, the internal energy is replaced by $p/\rho(\gamma-1)$ with γ = const. but its value is assumed to have been properly selected as to minimize the error involved in the substitution. The unsteady conservation equations given in Appendix A are then considered and the following dimensionless quantities are introduced

$$x^* = \frac{x}{L} \qquad t^* = \frac{t a_f}{L} \qquad \rho^* = \frac{\rho}{\rho_f} \qquad \rho^*_{F,\phi} = \frac{\rho_{F,\phi}}{\rho_f} \qquad u^* = \frac{u}{a_f}$$

$$u^*_{F,\phi} = \frac{u_{F,\phi}}{a_f} \qquad p^* = \frac{p}{p_f} \qquad h^{o*} = \frac{h^o}{p_f/\rho_f(\gamma-1)} \qquad h^{o*}_{F,\phi} = \frac{h^o_{F,\phi}}{p_f/\rho_f(\gamma-1)} \qquad \Lambda^*_{F,\phi} = \frac{\Lambda_{F,\phi}}{p_f/\rho_f(\gamma-1)}$$

with $a_f^2 = \gamma p_f/\rho_f$.

Omitting the stars, the dimensionless equations are

$$\frac{\partial}{\partial t}\left(\rho+\rho_F+\rho_\phi\right)+\frac{\partial}{\partial x}\left(\rho u+\rho_F u_F+\rho_\phi u_\phi\right)=0$$

$$\frac{\partial}{\partial t}\left(\rho u+\rho_F u_F+\rho_\phi u_\phi\right)+\frac{\partial}{\partial x}\left(\rho u^2+\rho_F u_F^2+\rho_\phi u_\phi^2+\frac{p}{\gamma}\right)=0$$

$$\frac{\partial}{\partial t}\left[\rho\left(\frac{p}{\rho\gamma}+\frac{\gamma-1}{2}u^2+\frac{h^o}{\gamma}\right)+\rho_F\left(\frac{\Lambda_F}{\gamma}+\frac{\gamma-1}{2}u_F^2+\frac{h^o_F}{\gamma}\right)+\rho_\phi\left(\frac{\Lambda_\phi}{\gamma}+\frac{\gamma-1}{2}u_\phi^2+\frac{h^o_\phi}{\gamma}\right)\right]+$$

$$\frac{\partial}{\partial x}\left[\rho u\left(\frac{p}{\rho}+\frac{\gamma-1}{2}u^2+\frac{h^o}{\gamma}\right)+\rho_F u_F\left(\frac{\Lambda_F}{\gamma}+\frac{\gamma-1}{2}u_\phi^2+h^o_F\right)+\rho_\phi u_\phi\left(\frac{\Lambda_\phi}{\gamma}+\frac{\gamma-1}{2}u_\phi^2+\frac{h^o_\phi}{\gamma}\right)\right]=0$$

If ϵ is a quantity of $\mathcal{O}(M_f)$, the following ordering for the steady state quantities follows from what has been learned about

the steady state of the LOX/ethanol system (Sec. 3.3)

$$\rho(x) = \rho_0^{(0)}(x)$$

$$\rho_{F,\phi}(x) = \rho_{F,\phi_0}^{(0)}(x)$$

$$u(x) = 0 + \epsilon u_0^{(1)}(x) + \cdots$$

$$u_{F,\phi}(x) = 0 + \epsilon u_{F,\phi_0}^{(1)}(x) + \cdots$$

$$p(x) = 1 + 0 + \epsilon^2 p_0^{(2)}(x) + \cdots$$

$$h^0(x) = h_0^{0(0)}(x)$$

$$h_{F,\phi}^0 = h_{F,\phi}^{0(0)}$$

$$\Lambda_{F,\phi}(x) = \Lambda_{F,\phi_0}^{(0)}(x)$$

where, for any given chamber pressure and injection mixture ratio, the axial variations of $\rho, \rho_{F,\phi}, h^0$ are of order 1. Also ρ_ϕ is different from zero only near the injector; $h_{F,\phi}^0$ are constants; $\Lambda_{F,\phi}$ are independent of M_f. In the above expressions, the subscript zero stands for "Steady State" and the superscript refers to the corresponding power of ϵ. The previous ordering simply eliminates the kinetic energies and introduces a constant static pressure in the energy equation. The resulting lowest order equations are consistent with the steady state previously calculated in the entire engine

$$\frac{d}{dx}\left[\rho_0^{(0)} u_0^{(1)} + \rho_{F_0}^{(0)} u_{F_0}^{(1)} + \rho_{\phi_0}^{(0)} u_{\phi_0}^{(1)}\right] = 0$$

$$\frac{d}{dx}\left[\rho_0^{(0)} u_0^{(1)2} + \rho_{F_0}^{(0)} u_{F_0}^{(1)2} + \rho_{\phi_0}^{(0)} u_{\phi_0}^{(1)} + p^{(2)}/\gamma\right] = 0$$

$$\frac{d}{dx}\left[u_0^{(1)} + \frac{\rho_0^{(0)} u_0^{(1)} h_0^{0(0)}}{\gamma} + \frac{\rho_{F_0}^{(0)} u_{F_0}^{(1)}}{\gamma}\left(\Lambda_{F_0}^{(0)} + h_F^{0(0)}\right) + \frac{\rho_{\phi_0}^{(0)} u_{\phi_0}^{(1)}}{\gamma}\left(\Lambda_{\phi_0}^{(0)} + h_\phi^{0(0)}\right)\right] = 0$$

If one assumes that one of the two propellants vaporized instantaneously at the injector, he can then eliminate the corresponding terms from the above equations and introduce its initial flux, momentum and energy through the boundary conditions at the injector end. In the case of the Lox/ethanol system, the vaporization length of the fuel is much longer than that of the oxidizer, thus the above assumption seems reasonable and can be used also to study the perturbation of the steady state. Thus, if the steady state is subject to an unsteady perturbation of amplitude ϵ , one could modify the previous steady state ordering as follows

$$\rho(x,t) = \rho_o^{(o)}(x) + \epsilon\left[\rho^{(1)}(x,t)\right] + \cdots$$

$$\rho_\ell(x,t) = \rho_{\ell_o}^{(o)}(x) + \epsilon\left[\rho_\ell^{(1)}(x,t)\right] + \cdots$$

$$u(x,t) = 0 + \epsilon\left[u_o^{(1)}(x) + u^{(1)}(x,t)\right] + \cdots$$

$$u_\ell(x,t) = 0 + \epsilon\left[u_{\ell_o}^{(1)}(x) + u_\ell^{(1)}(x,t)\right] + \cdots$$

$$p(x,t) = 1 + \epsilon\left[p^{(1)}(x,t)\right] + \cdots$$

$$h^o(x,t) = h_o^{o(o)}(x) + \epsilon\left[h^{o(1)}(x,t)\right] + \cdots$$

$$h_\ell^o(x,t) = h_\ell^{o(o)}$$

$$\Lambda_\ell(x,t) = \Lambda_{\ell_o}^{(o)}(x) + \epsilon\left[\Lambda_\ell^{(1)}(x,t)\right] + \cdots$$

Where the subscript ℓ refers to the slowly vaporizing propellant. If one further assumes that the derivatives of the quantities are of the same order as the quantities themselves and retains only the lowest order terms, one then finds

$$\frac{\partial}{\partial t}\left[\rho^{(1)} + \rho_\ell^{(1)}\right] + \frac{\partial}{\partial x}\left[\rho_0^{(0)} u^{(1)} + \rho_{\ell_0}^{(0)} u_\ell^{(1)}\right] = 0$$

$$\frac{\partial}{\partial t}\left[\rho_0^{(0)} u^{(1)} + \rho_{\ell_0}^{(0)} u_\ell^{(1)}\right] + \frac{\partial}{\partial x}\left[\frac{p^{(1)}}{\gamma}\right] = 0$$

$$\frac{\partial}{\partial t}\left[p^{(1)} + \rho_0^{(0)} h^{o(1)} + h_0^{o(0)} \rho^{(1)} + \rho_{\ell_0}^{(0)} \Lambda_\ell^{(1)} + \rho_\ell^{(1)}\left(\Lambda_{\ell_0}^{(0)} + h_\ell^{o(0)}\right)\right] +$$

$$+ \frac{\partial}{\partial x}\left[\gamma u^{(1)} + \rho_0^{(0)} h_0^{o(0)} u^{(1)} + \rho_{\ell_0}^{(0)}\left(\Lambda_{\ell_0}^{(0)} + h_\ell^{o(0)}\right) u_\ell^{(1)}\right] = 0$$

The orderings so far discussed are not unique and may even be inadequate if more equations, such as those coming from droplet drag and vaporization models, are added to the previous ones. They are, however, consistent with the steady-state results of this study. However, in the ordering for the steady-state perturbation it was assumed that the perturbation of the liquid quantities (ρ_ℓ , u_ℓ , Λ_ℓ) are of the same order as the perturbation of the gas quantities. This is simply an assumption unrelated to the steady-state study. In some engines, small perturbations are found to grow to full strength shocks in a few cycles (as in some of the LOX/ethanol engine configurations used in this study). This would indicate that the sources are strong and therefore equal orders for the perturbation quantities of both gas and liquid phases seem reasonable. In other engines the growth of small perturbations occurs over many cycles indicating weaker sources (or larger losses) and the assumption that liquid perturbation quantities are of higher order would seem reasonable. In this case one could visualize that the inertia of the drops

prevents them from changing their velocity as much as the velocity of the gas changes (perturbation of u_ℓ of higher order than perturbation of u). But one could conceive that the perturbation of the drop mass is still of the same order as the perturbation of the gas density (perturbation of ρ_ℓ of the same order as perturbation of ρ) since the vaporization rate is affected by both relative velocity and gas properties (pressure). In this case the lowest order perturbation equations would be

$$\frac{\partial}{\partial t}\left(\rho^{(1)}+\rho_\ell^{(1)}\right)+\frac{\partial}{\partial x}\left(\rho_0^{(0)}u^{(1)}\right)=0$$

$$\frac{\partial}{\partial t}\left(\rho_0^{(0)}u^{(1)}\right)+\frac{\partial}{\partial x}\left(\frac{p^{(1)}}{\gamma}\right)=0$$

$$\frac{\partial}{\partial t}\left[p^{(1)}+\rho_0^{(0)}h^{o(1)}+h_0^{o(0)}\rho^{(1)}+\rho_{\ell_0}^{(0)}\Lambda_\ell^{(1)}+\rho_\ell^{(1)}\left(\Lambda_{\ell_0}^{(0)}+h_\ell^{o(0)}\right)\right]+$$

$$+\frac{\partial}{\partial x}\left[\gamma u^{(1)}+\rho_0^{(0)}h_0^{o(0)}u^{(1)}\right]=0$$

Notice that, in this case, one has mass and energy sources in the lowest order equations but <u>there is no momentum source</u>. Finally one could go a step further and assume that also the perturbation of the drop mass is of higher order. Then with no perturbation of the liquid quantities, at lowest order, the perturbation of Λ_ℓ and of h^o should be put to higher order too, thus getting

$$\frac{\partial}{\partial t}\left(\rho^{(1)}\right)+\frac{\partial}{\partial x}\left(\rho_0^{(0)}u^{(1)}\right)=0 \tag{77}$$

$$\frac{\partial}{\partial t}\left(\gamma\rho_0^{(0)}u^{(1)}\right)+\frac{\partial}{\partial x}\left(p^{(1)}\right)=0 \tag{78}$$

$$\frac{\partial}{\partial t}\left(p^{(1)}+h_0^{o(0)}\rho^{(1)}\right)+\frac{\partial}{\partial x}\left(\gamma u^{(1)}+\rho_0^{(0)}h_0^{o(0)}u^{(1)}\right)=0 \tag{79}$$

Where the energy equation states that the time rate of increase of internal energy ($p^{(1)}$) and chemical heat addition ($h_o^{o(o)} \rho^{(1)}$) within the control volume due to the perturbation is balanced by the influx of internal energy ($u^{(1)}$) and of additional chemical heat ($\rho_o^{(o)} h_o^{o(o)} u^{(1)}$) and by the mechanical work done on the boundary ($(\gamma-1) u^{(1)}$). Thus both the steady state density nonuniformity and the steady state chemical heat released nonuniformity influence the propagation of the perturbation. From the previous system one gets the following P.D.E. for $u^{(1)}$

$$\rho_o^{(o)} u_{tt}^{(1)} - u_{xx}^{(1)} - \left(\frac{\rho_o^{(o)} h_{o\,x}^{o(o)}}{\gamma} u^{(1)} \right)_x = 0$$

Actually $h_o^{o(o)}$ is the heat of formation of the products from which the heats of formation of the reactants should be subtracted to obtain the chemical heat released. If, considering the approximations already made, one neglects the latter in comparison to the former, then ($\rho_o^{(o)} h_o^{o(o)}$) could be considered approximately equal to the steady state volumetric energy source which was found to be approximately axially uniform (Sec. 3.3.3). Due to the non-dimensionalization it then turns out* that $\rho_o^{(o)} h_o^{o(o)} = -\gamma$ and the above equation for $u^{(1)}$ becomes

$$\rho_o^{(o)} u_{tt}^{(1)} - u_{xx}^{(1)} - \left(\frac{\rho_{o\,x}^{(o)}}{\rho_o^{(o)}} u^{(1)} \right)_x = 0$$

while for $p^{(1)}$ one finds: $\rho_o^{(o)} p_{tt}^{(1)} - p_{xx}^{(1)} = 0$

*Putting back the stars on the dimensionless quantities one has

$$\rho_o^{(o)*} h_o^{o(o)*} = \frac{\rho_o^{(o)}}{\rho_f} \frac{h_o^{o(o)}}{h_f/\rho_f(\gamma-1)} = \frac{\rho_f h_f^o}{\rho_f h_f/\rho_f(\gamma-1)} = \frac{\rho_f}{\rho_f} \frac{\left(-\gamma \frac{h_f}{\rho_f(\gamma-1)}\right)}{h_f/\rho_f(\gamma-1)} = -\gamma$$

where the assumed constancy of ρh^o is used and it is further set that the heat of formation of the products goes into latent enthalpy of the gas. If one had used $\rho h^o \simeq 5.08 p$ (see Sec. 3.3.3) he would have found 1.2 instead of γ.

An earlier analysis led to an equation for $u^{(1)}$ which did not fully include the effects of the steady-state nonuniformities. One can write the unsteady conservation equations isolating the sources (neglecting kinetic energies) as follows

$$\rho_t + (\rho u)_x = Q$$
$$(\rho u)_t + (\rho u^2 + p/\gamma)_x = \psi$$
$$p_t + \gamma (p u)_x = \gamma \Phi$$

One then finds that the following steady state ordering is consistent with steady state results if $Q_0^{(1)}$, $\psi_0^{(2)}$, $\Phi_0^{(1)}$ are properly defined

$$\rho(x) = \rho_0^{(0)}(x)$$
$$u(x) = 0 + \epsilon u_0^{(1)}(x) + \cdots$$
$$p(x) = 1 + 0 + \epsilon^2 p_0^{(2)}(x) + \cdots$$
$$Q(x) = 0 + \epsilon Q_0^{(1)}(x) + \cdots$$
$$\psi(x) = 0 + 0 + \epsilon^2 \psi_0^{(2)}(x) + \cdots$$
$$\Phi(x) = 0 + \epsilon \Phi^{(1)}(x) + \cdots$$

where the energy source now contains also the heat of formation of the gas. Going then to the unsteady perturbation, for the case in which the perturbation of the liquid is assumed to be of higher order than that of the gas, one would set

$$\rho(x,t) = \rho_0^{(0)}(x) + \epsilon [\rho^{(1)}(x,t)] + \cdots$$
$$u(x,t) = 0 + \epsilon [u_0^{(1)}(x) + u^{(1)}(x,t)] + \cdots$$
$$p(x,t) = 1 + \epsilon [p^{(1)}(x,t)] + \cdots$$
$$Q(x,t) = 0 + \epsilon [Q_0^{(1)}(x)] + \epsilon^2 [Q^{(2)}(x,t)] + \cdots$$
$$\psi(x,t) = 0 + 0 + \epsilon^2 [\psi_0^{(2)}(x) + \psi^{(2)}(x,t)] + \cdots$$
$$\Phi(x,t) = 0 + \epsilon [\Phi_0^{(1)}(x)] + \epsilon^2 [\Phi^{(2)}(x,t)] + \cdots$$

and upon substitution and using the steady state equations one would find

$$\rho_0^{(0)} u_{tt}^{(1)} - u_{xx}^{(1)} = 0 \tag{80}$$

where the effect of nonuniform chemical heat released has disappeared. When one assumes that the perturbation of the motion and of the burning of the liquid is of higher order, one simply states that the motion and combustion of the liquid proceed as in the steady state, i.e., there is no additional contribution from the liquid due to the perturbation of the gas. However, in steady state the energy added to the gas is not axially uniform due to axially nonuniform gas phase mixture ratio. The perturbation of this axially nonuniform steady state source is then felt by the gas even though the liquid adds no extra mass or energy contribution. Thus, terms of the form $h_0^{*(0)} \rho^{(1)}$, $\rho_0^{(0)} h_0^{*(0)} u^{(1)}$ should appear even though perturbations of ρ_ℓ, u_ℓ are of higher order.

The above variable-speed-of-sound wave equation was solved for some typical $\rho_0^{(0)} = \rho_0^{(0)}(x)$ to get an idea of the influence of the steady-state uniformity on the frequency of a periodic perturbation.

Consider a combustion chamber of length approximately equal to that of the active combustion zone (L). Looking for periodic solutions, one sets

$$u^{(1)} = U(x)\, e^{i\omega t}$$

Then substituting in the variable coefficient wave equations, one

gets

$$U'' + \omega^2 \rho_0^0(x)\, U = 0$$

If $\rho_0^{(0)} \equiv 1$, using the homogeneous boundary conditions one would get

$$U = A \sin \omega x \qquad \omega = n\pi \qquad n = 1, 2, \cdots$$

Thus the fundamental frequency would be

$$\omega = \pi \qquad \text{[or in cycles per second } f = \omega \frac{a_f}{L} \frac{1}{2\pi} = \frac{a_f}{2L} \text{]}$$

Let $\rho_0^{(0)}(x)$ now vary linearly from the injector to the nozzle entrance and set the origin of the coordinates at the nozzle entrance

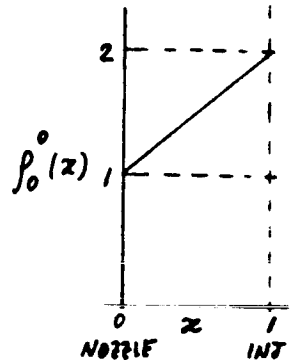

Then the equation to be solved is

$$U'' + \omega^2 (1+x)\, U = 0 \qquad U(0) = U(1) = 0$$

By setting

$$W = \frac{2}{3}\omega (1+x)^{3/2} \qquad U = u(W)\left(\frac{3}{2}W\right)^{1/3}$$

the above equation is transformed into Bessel's equation

$$W^2 u'' + W u' - \left(\frac{1}{9} - \omega^2\right) u = 0 \qquad u\left(\tfrac{2}{3}\omega\right) = u\left(\tfrac{2}{3}\omega\, 2^{3/2}\right) = 0$$

Hence the desired solution is given by

$$U(x) = \left[A\, J_{+1/3}\left(\tfrac{2}{3}\omega(1+x)^{3/2}\right) + B\, J_{-1/3}\left(\tfrac{2}{3}\omega(1+x)^{3/2}\right)\right] \omega^{1/3} (1+x)^{1/2}$$

Where A, B, ω are still to be determined. Applying the boundary conditions

$$A\, J_{+1/3}\left(\tfrac{2}{3}\omega\right) + B\, J_{1/3}\left(\tfrac{2}{3}\omega\right) = 0$$

$$A\, J_{+1/3}\left(\tfrac{2}{3}\omega 2^{3/2}\right) + B\, J_{-1/3}\left(\tfrac{2}{3}\omega 2^{3/2}\right) = 0$$

The above system has no trivial solution for A, B only if the determinant of the coefficients is zero. Expressing Bessel's functions in forms of Airy's functions (A_i , B_i) the above condition, after some algebra, leads to the following relationship

$$A_i(-z)\, B_i(-2z) = B_i(-z) A_i(-2z) \qquad z = \omega^{2/3}$$

Both sides of the above equation are plotted in Fig. 27 and it is seen that the first eigenvalue of ω is 1.88 hence the fundamental dimensionless frequency would be

$$\omega = z^{3/2} = 2.54$$

In contrast, for the uniform steady-state case ($\rho_o^{(o)} = 1$), it was found to be π . This represents a 20% difference in the fundamental frequency.

Having the eigenvalue of $\omega = 2.54$ one can express A as a function of B

$$A = -B\, \frac{J_{-1/3}\left(\tfrac{2}{3}\,2.54\right)}{J_{+1/3}\left(\tfrac{2}{3}\,2.54\right)} = -.1527\, B$$

and now the solution becomes ($\omega = 2.54$)

$$U(x) = B\left\{\omega^{1/3}(1+x)^{1/2}\left[J_{-1/3}\left(\tfrac{2}{3}\omega(1+x)^{3/2}\right) - .1527\, J_{+1/3}\left(\tfrac{2}{3}\omega(1+x)^{3/2}\right)\right]\right\}$$

where the amplitude B is undetermined. The above function is plotted in Fig. 28. The constant B was so chosen as to give a maximum amplitude of $U(x)$ equal to 1.0. For comparison, Fig. 28

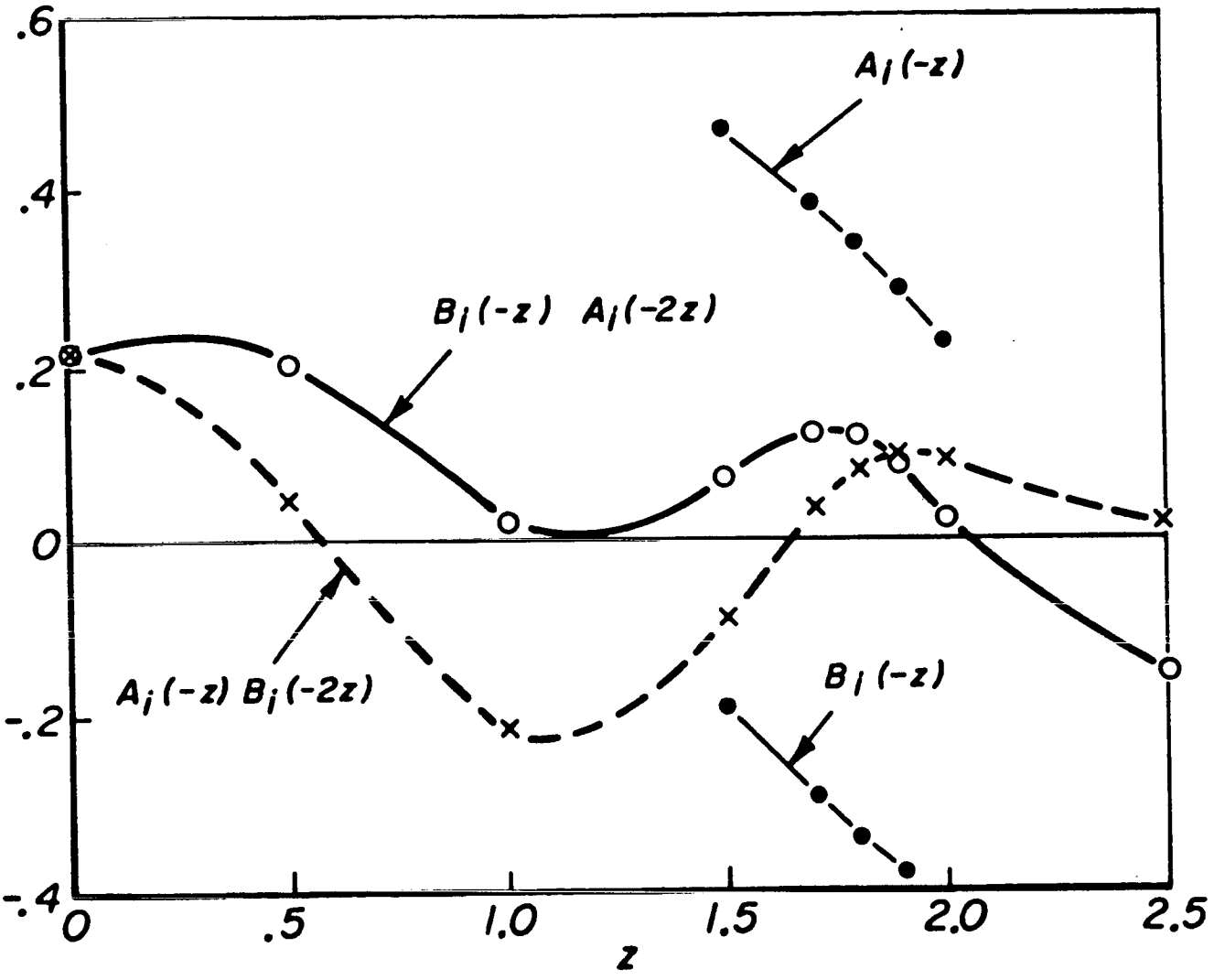

Fundamental frequency of
$U''+\omega^2(1+x)U=0$

Figure 27

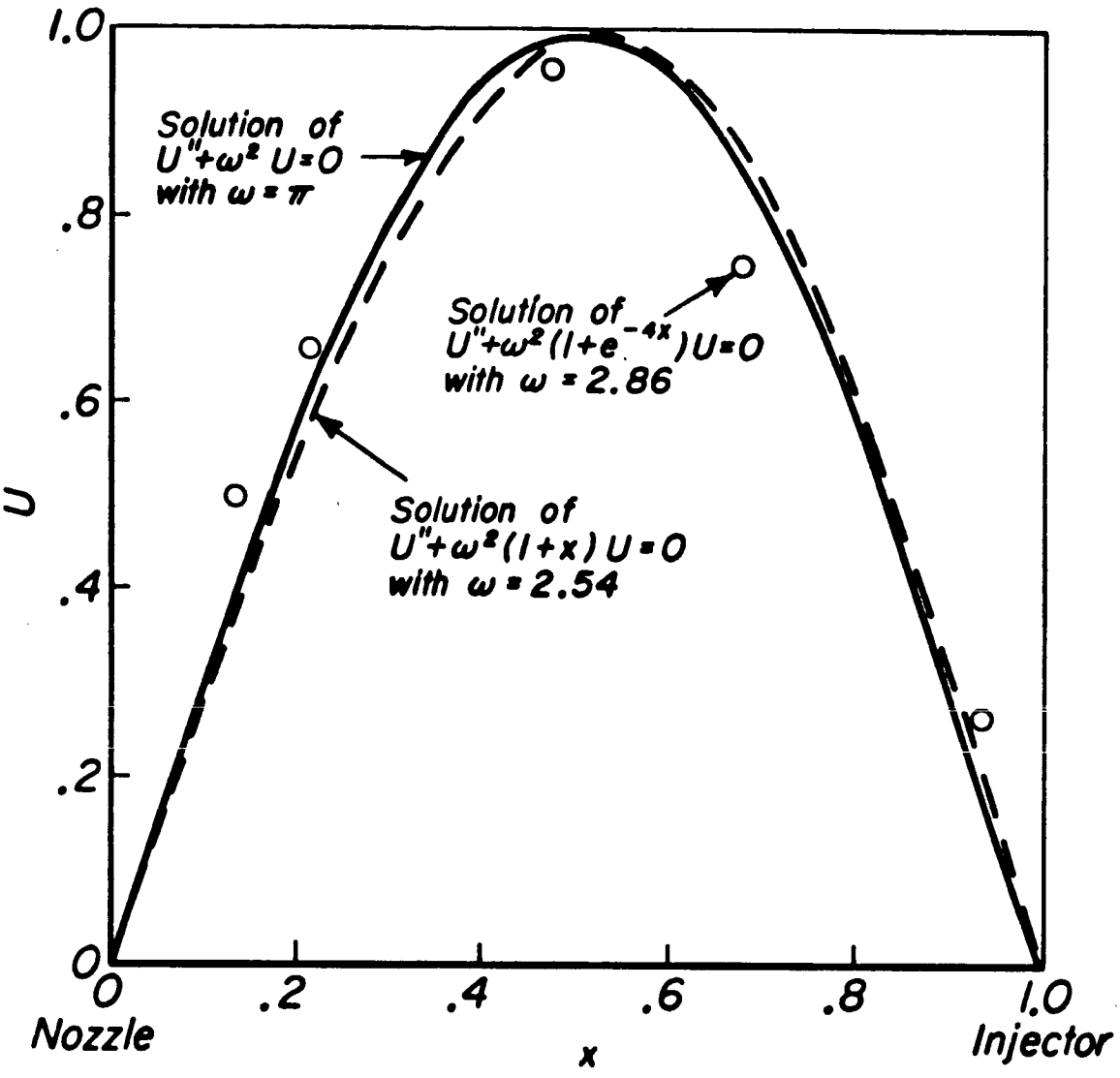

Various particle velocity perturbation profiles

Figure 28

gives also the function $\sin \pi x$ which would be the solution of the $\rho_0^{(0)} = 1$ case. It is seen that the shape of the perturbation velocity is similar in the two cases (for the fundamental frequency). The two frequencies, however, were shown to be different and nothing can be said about the two amplitudes.

The linear variation of $\rho_0^{(0)}$ is not a good approximation of the real steady-state density variation. Indeed the density varies more strongly near the injector as Fig. 24 shows. An exponential function is then a more realistic choice for $\rho_0^{(0)}(x)$. With the origin of the coordinates at the injector, the proper form for $\rho_0^{(0)}$ is

$$\rho_0^{(0)} = a^2 + b^2 e^{cx}$$

Then the equation to be solved now is

$$U'' + \omega^2 (a^2 + b^2 e^{cx}) U = 0 \qquad U(0) = U(1) = 0$$

By setting

$$z = 2 b \omega e^{cx/2} \qquad \& \qquad p^2 = 4\omega^2 a^2$$

it is found that

$$z^2 U'' + z U' + \left(\frac{p^2}{c^2} + \frac{z^2}{c^2} \right) U = 0$$

Two solutions are sought of the form

$$U(z) = \sum_{n=0}^{\infty} B_n z^{2n+s}$$

The indicial equation gives $s = \pm i \left| \frac{p}{c} \right|$ and the two solutions are

$$U_+(z) = B_0 \left[z^{i\left|\frac{p}{c}\right|} + \sum_{n=1}^{\infty} \frac{(-1)^n c^{-2n} z^{2n + i\left|\frac{p}{c}\right|}}{2^{2n} n! \left(1 + i\left|\frac{p}{c}\right|\right)\left(2 + i\left|\frac{p}{c}\right|\right) \cdots \left(n + i\left|\frac{p}{c}\right|\right)} \right]$$

$$U_-(z) = B_0 \left[z^{-i\left|\frac{p}{c}\right|} + \sum_{n=1}^{\infty} \frac{(-1)^n c^{-2n} z^{2n - i\left|\frac{p}{c}\right|}}{2^{2n} n! \left(1 - i\left|\frac{p}{c}\right|\right)\left(2 - i\left|\frac{p}{c}\right|\right) \cdots \left(n - i\left|\frac{p}{c}\right|\right)} \right]$$

The above two solutions are complex and conjugate. The general solution would be

$$U = c_1 U_+ + c_2 U_-$$

By choosing the two arbitrary constants C_1, C_2 to be complex and conjugate, the general solution takes the form:

$$U = A U_R + B U_I$$

where U_R and U_I are the real and imaginary parts of U_+. Retaining only the first terms of the two infinite series (for the range of interest this approximation can be shown to be acceptable) one gets

$$U(z) = A\left\{\cos\left[\left|\frac{b}{c}\right| \ln z\right]\cdot\left[1-\frac{z^2}{4c^2\left(1+\frac{b^2}{c^2}\right)}\right]-\sin\left[\left|\frac{b}{c}\right| \ln z\right]\cdot\left[\frac{z^2\left|\frac{b}{c}\right|}{4c^2\left(1+\frac{b^2}{c^2}\right)}\right]\right\}+$$

$$+B\left\{\cos\left[\left|\frac{b}{c}\right| \ln z\right]\cdot\left[\frac{z^2\left|\frac{b}{c}\right|}{4c^2\left(1+\frac{b^2}{c^2}\right)}\right]+\sin\left[\left|\frac{b}{c}\right| \ln z\right]\cdot\left[1-\frac{z^2}{4c^2\left(1+\frac{b^2}{c^2}\right)}\right]\right\}$$

To have non-trivial solutions for A, B, the determinant of their coefficients must vanish since we have homogeneous boundary conditions on U at $z_1 = 2\ell\omega$ and $z_2 = 2\ell\omega e^{c/2}$. From this condition the relationship is found

$$\tan\left[-\left|\frac{b}{c}\right|\frac{c}{2}\right] = \frac{\left|\frac{b}{c}\right|(2\ell\omega)^2(e^c-1)}{4c^2\left(1+\frac{b^2}{c^2}\right)+\frac{(2\ell\omega)^4 e^c}{4c^2}-(2\ell\omega)^2(e^c+1)}$$

The above relationship determines the eigenvalues of ω since a, b, c are known and $b = 2\omega a$. Specializing now to the two exponential behaviors of $f_0^{(0)}$ given in Fig. 29 and looking only for the fundamental frequency (which is expected to be approximately π), the above relationship simplifies to the following one

$$\tan\omega \simeq -\frac{\omega^3\ell^2}{32+\omega^2(8-2\ell^2)}$$

For the lowest of the two exponential curves of Fig. 29 ($\ell^2 = 1$) one finds for the first eigenvalue $\omega = 2.86$.

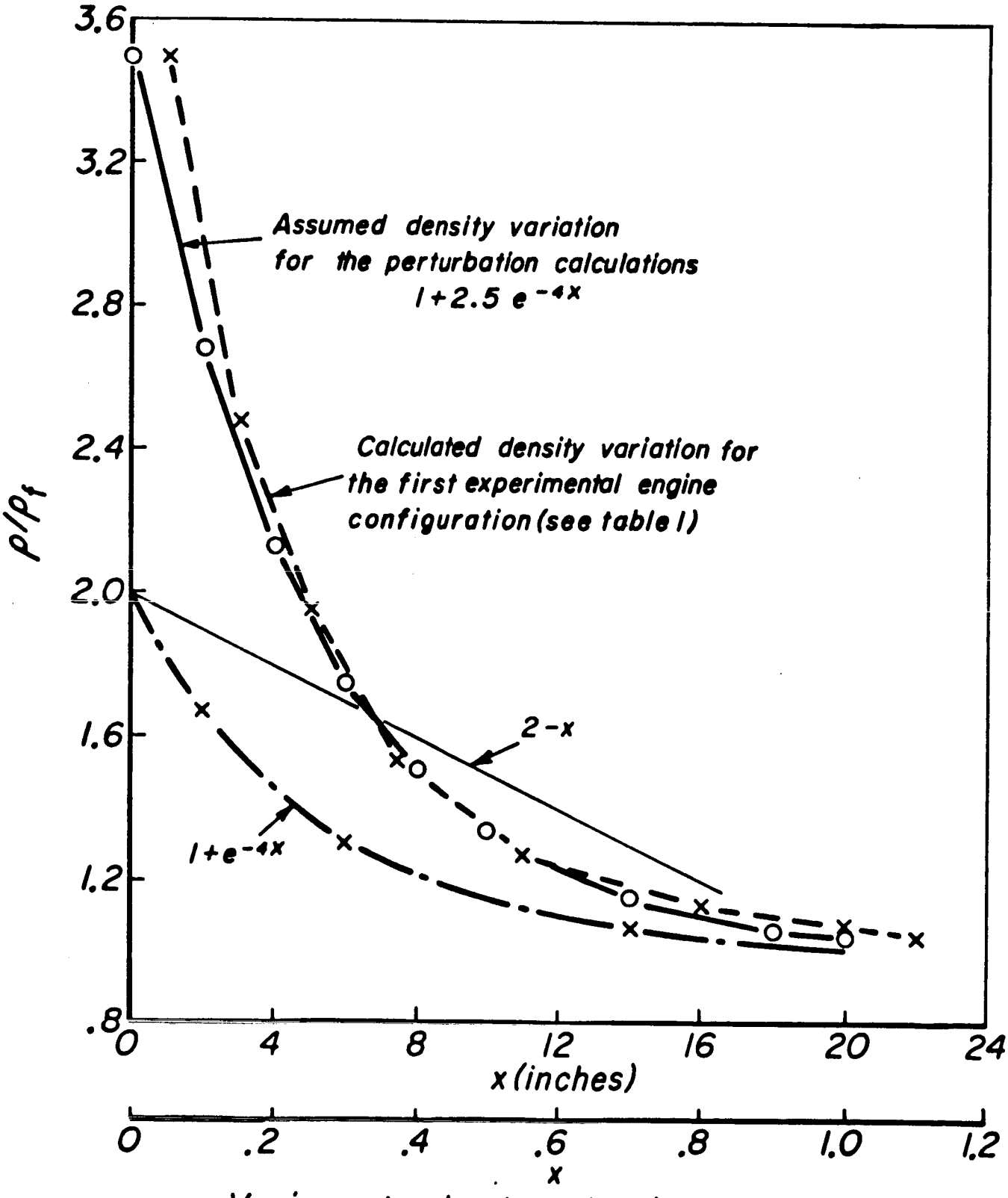

Various steady state density profiles

Figure 29

For the highest of the two exponential curves of Fig. 29 ($b^2 = 2.5$) one finds $\omega = 2.49$.

These values of ω are down 10% and 20% respectively from that calculated without taking into account the nonuniformity of the steady state. Having ω one could proceed to determine B as a function of A. However A remains undertimined. The solution for $b^2 = 1$, $\omega = 2.86$ is sketched in Fig. 28. The constant A was so chosen as to give a maximum amplitude of $v(x)$ approximately equal to 1.0.

From the three examples of this section it could be concluded that the nonuniformity of the steady state could lower the fundamental frequency of a small perturbation by as much as 20%. The shape of the perturbation velocity is not changed significantly (in the fundamental frequency).

An alternative, intuitive and simple way of calculating the frequency of the periodic perturbation has been suggested (Crocco, as an application of the WKBJ method, personal correspondence, and Tsuji[34]). Having the following wave equation ($\rho_0^{(0)}$ = const)

$$u^{(1)}_{tt} - \frac{1}{\rho_0^{(0)}} u^{(1)}_{xx} = 0$$

Its general solution is known to be $u^{(1)}(x,t) = f(x + \rho_0^{(0)\,-1/2} t) + g(x - \rho_0^{(0)\,-1/2} t)$ and $\rho_0^{(0)\,-1/2}$ is the actual constant speed at which the perturbation propagates. However, if $\rho_0^{(0)}$ is not constant the general solution of the above equation is not of the form

$$u^{(1)}(x,t) = f(x + \rho_0^{(0)\,-1/2} t) + g(x - \rho_0^{(0)\,-1/2} t)$$

Nevertheless, intuitively, one could think that the wave is travelling locally with the speed $\rho_0^{(0)\,-1/2}$ and could calculate

its dimensionless period by

$$\int_0^1 \rho_0^{(0)\,1/2}\, dx$$

This way one finds the following dimensionless periods (τ) and corresponding values of ω (in parenthesis the ω's previously calculated)

$$\rho_0^{(0)} = 2 - x \qquad \tau = 1.22 \qquad \omega = 2.57 \quad (2.54)$$

$$\rho_0^{(0)} = 1 + e^{-4x} \qquad \tau = 1.11 \qquad \omega = 2.83 \quad (2.86)$$

$$\rho_0 = 1 + 2.5\, e^{-4x} \qquad \tau = 1.25 \qquad \omega = 2.51 \quad (2.49)$$

One can see that this simple way of calculating ω gives excellent results.

The result of this section is of interest in relation to the frequency of shock-type longitudinal instability. Under the assumption of uniform chamber temperature, one would expect the frequency of the oscillating shock to be higher than the acoustic frequency since a shock wave moves faster than the speed of sound (e.g., for p_2/p_1 = 1.5 the shock velocity would be about 1.20 times the speed of sound) and gas velocity effects cancel out over a cycle. However, hot firings show that the frequency of the oscillating shock is close to the acoustic frequency. This contradiction disappears if the assumption of uniform chamber properties is removed. The acoustic frequency calculated in this section with typical axially nonuniform density profiles is indeed some 20% smaller than that calculated with the assumption of axial uniformity. In other words, the longitudinal shock instability frequency as calculated with the

speed of sound based upon the temperature for completed combustion is probably accurate because of the cancelling of the errors from two inaccurate assumptions.

3.6 Review of Some Droplet Distribution, Drag and Vaporization Models

In Section 3.2 the variables of the gas and the dimensionless liquid fuel flux (W_F/W_{OF}) were determined for three specific Lox/ethanol engine configurations without assuming anything about the distribution, the drag and the vaporization of the drops. Static pressure measurements were used instead. Thus, after having measured some unknowns (first step in the direct approach) and having calculated most of the others by basic conservation equation (second step in the direct approach), one should now investigate some possible models with the purpose of selecting the model which best fits the already computed solution (third step in the direct approach). Such an investigation is undertaken in this section.

The selected main goal of this section must be clearly spelled out from the very beginning. The main goal was not that of considering the most complete (and complex) of the possible models. The main goal was, on the contrary, that of finding the simplest schematization which would contain the main physical elements and lead to reasonably accurate steady-state calculations. The reason for this choice is that this study was conceived to aid analytical instability studies where simple, yet reasonably complete, steady-state models are needed. Thus a specific engine configuration was selected (configuration II

of Table IV whose $u = u(x)$, $\rho = \rho(x)$, $T = T(x)$ and W_p/W_{0_2} versus x are given in Figures 9 through 12 and were curve fitted as indicated in those figures). Quasi-steady droplet drag and vaporization were assumed. The droplet surface temperature was taken to be equal to the boiling temperature. The following vaporization rate equations were studied

$$\frac{dr}{dt} = -\frac{K_1}{8r} \tag{81}$$

$$\frac{dr}{dt} = -\frac{K_2}{8r}\left[1 + .3\, P_r^{1/3}\, Re^{1/2}\right] \quad * \tag{82}$$

$$\frac{dr}{dt} = -\frac{K_3}{8r}\, Re^{1/2} \tag{83}$$

$$\frac{dr}{dt} = -\frac{K_4}{8r}\, Re \tag{84}$$

$$\frac{dr}{dt} = -\frac{K_1^*}{8\rho r} \tag{85}$$

$$\frac{dr}{dt} = -\frac{K_2^*}{8\rho r}\left[1 + .3\, P_r^{1/3}\, Re^{1/2}\right] \quad * \tag{86}$$

$$\frac{dr}{dt} = -\frac{K_3^*}{8\rho r}\, Re^{1/2} \tag{87}$$

$$\frac{dr}{dt} = -\frac{K_4^*}{8\rho r}\, Re \tag{88}$$

---

* In some of the computations the factor .276 instead of .3 was used following Williams[9] (then $.276\, P_r^{1/3} = .258$). The difference between the results obtained in the two cases is small and no special effort is made to discuss them separately.

where

$$Re = 2r\rho|u-u_e|/\mu$$

$$P_2 = 4\gamma/(9\gamma-5) \quad ; \quad \gamma = 1.22 \Rightarrow .3P_2^{1/3} = .28$$

The effect of forced convection is absent in the first equation and progressively more important in the following three equations. The fourth equation is herein investigated both to assess the effect of a forced convection dominated vaporization rate equation and because it would simplify steady and unsteady combustion studies. Most of the study was done with the drag coefficient either equal to zero (no drag) or with Stokes's drag equation ($C_D = 24/Re$). But the case of higher drag was also examined. Droplet breakup was not included. Both the uniform and the distributed drop radius cases were studied. In both cases, however, the initial velocity of all drops was taken to be equal (u_{ℓ_0}). Some of these assumption might be questionable, particularly if carried over into instability studies, but it will presently be seen that, in spite of the above simplifying assumptions, there are still enough uncertain points which need investigation. Theories exist to evaluate the K's appearing in some of the above vaporization rate equations as functions of the local chamber conditions (see Appendix B). However, these theories are based on relatively arbitrary schematization of what actually happens in a combustion chamber and how the local chamber conditions should be used in those theories also involves some arbitrariness. Furthermore, these K's set the scale for the combustion length. Thus a factor of 2

error in estimating K brings about a similar error in the estimate of the combustion length. For these reasons the above K's were taken to be constant along the combustion chamber and their values were so selected as to give the best agreement with the already determined W_F/W_{0_F}. Thus the above vaporization rate equations have been treated more as probable functional forms than self-consistent applicable vaporization models. Comparison between the K's which gave the best results and those possibly predicted by the corresponding theories were made a posteriori (see Appendix B). The initial radius of the drops (r_{J_0} when distributed initial drop radii were used) has an effect on the computation of the combustion length similar to that of the K's. However, it can more accurately be estimated (at least for the engine configuration presently under consideration) using the equations and experiments of Ingebo (see Appendix C). Accordingly, its value was changed but only within the relatively narrow, predicted limits. A listing of the models which were reviewed is given in Table V. But before discussing them it might be helpful to anticipate the conclusions which have been reached.

The conclusion of this study has been somewhat of a surprise to the author. The author had hoped he would find a more or less unique model which agreed and explained the variables calculated by the direct method and given in Figures 9 through 12. He actually found either no satisfactory model or a multitude of them. If the parameters K_1, K_2, K_3 and K_4, appearing in the vaporization rate equations, 81 through 84, are given the values recommended in the literature (Appendix B), none of the models examined even gets

	u_{ℓ_0}	τ_0	C_D	1 $\kappa_1 \delta^2$	2 $\kappa_2 [1+.20\, Re^{1/2}]/Re$	3 $\kappa_3 Re^{1/2}/\rho u$	4 $\kappa_4 A/\tau u$	5 $\kappa_1^*/\delta\rho u$	6 $\kappa_2^* [1+.28\, Re^{1/2}]/\delta\rho u$	7 $\kappa_3^* Re^{1/2}/\delta\rho u$	8 $\kappa_4^* Re/\delta\rho u$
A	Uniform	Uniform	0	N	N	N	N	N	N	N	N
B	Uniform	Uniform	$< 24/Re$	-	Y*	Y*	-	N*	N*	N*	N*
C	Uniform	Uniform	$24/Re$	N	N	N	N	N	Y	Y	N
D	Uniform	Uniform	$> 24/Re$	N*	N*	N*	N*	-	-	-	-
E	Uniform	Distributed	0	N	Y	Y	N	-	N	-	-
F	Uniform	Distributed	$< 24/Re$	-	M*	M*	-	-	-	-	-
G	Uniform	Distributed	$24/Re$	M	M	M	M	Y	Y	Y	Y
H	Uniform	Distributed	$> 24/Re$	-	N	N*	-	-	M	M	-

N = Not Acceptable

Y = Acceptable

M = Marginally Acceptable

* = Conclusion Deduced from the Study of the Other Cases

TABLE V. SUMMARY OF THE MODELS EXAMINED AND THEIR DEGREES OF ACCEPTABILITY

close to representing accurately the engine under consideration. If, on the contrary, one reserves the freedom of choosing proper values for the parameters K_1, K_2, K_3 and K_4 (to which he is somewhat entitled, see Appendix B) and perhaps for r_{30} and the drag coefficient, then he can make many of the examined models give seemingly satisfactory results. This is so simply because he generates enough degrees of freedom to meet his requirements. In spite of this lack of uniqueness, it was possible to reach some interesting conclusions. The models examined could be classified according to the following criterion. At one extreme there are those models which are controlled by the effect of the relative velocity between gas and liquid drops and the dimensionless liquid fuel flux yielded by them behaves like the dashed line in the following sketch (Model A8 represents such an extreme, the drag is zero so that $u_\ell = u_{\ell_0}$ = constant and the relative velocity is large, the vaporization rate equation is strongly dependent on the relative velocity and the vaporization rate, far from the injection, is further enhanced by the presence of the $1/\rho$ term)

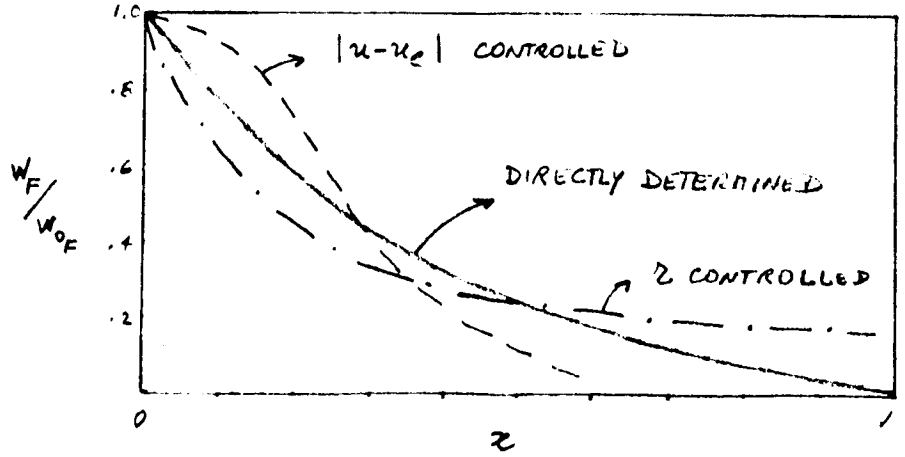

At the opposite extreme there are those models which are controlled by the effect of the drop radius and their W_F/W_{0_F} behaves as the dotted-dashed lines (Model D1 represents such an extreme the drag is high so that the relagive velocity quickly tends to zero, the vaporization rate is independent of the relative velocity and far from the injector the vaporization rate is not even enhanced by the presence of the $1/\rho$ term). In fact it is found that it takes a relatively fine balance between the two effects for a model to reproduce accurately the trend of the already known W_F/W_{0_F}. One then concludes that vaporization rate equations 86 and 87 with experimentally determined K_2^* and K_3^* (almost one order of magnitude smaller than those possibly predicted by the theory) and a Stokes' drag equation are necessary to reproduce satisfactorily the already known W_F/W_{0_F} in magnitude and trend. The use of the distribution function is not necessary, although it does tend to improve the agreement. The proper initial drop radius to use when a distribution function is not used is $r_0 = 5\, r_{30}/3.915$. In this study the typical drop Reynolds number is of the order of 100 so that Stokes' drag equation might be difficult to accept. In the trade, much stronger drag equations are used[20] following Rabin[28] who suggested accounting for the droplet flattening at high Re. However, Eisenklan[29] et al noticed no flattening for Re up to 400 and actually suggested lower drag for burning drops than for solid spheres. This work finds the high drag results hard to accept and suggests agreement with Eisenklan results.

Another result is that steady state calculations are very

sensitive to the values of the key parameters such as r_{30} and the K's . Stability results might be just as sensitive to to those parameters. It would then follow that a model should first be checked for its accuracy in predicting the steady state in some specific engine configuration before it is used in stability studies. This work should be seen as one such check.

3.6.1 Summary of Models

MODELS: A1, A2, A3, A4 of Table V. All drops have initially the same radius and velocity and vaporize according to vaporization rate equations, 81 through 84. The drag is zero, the K's are constant and they are selected as to give the best agreement between the calculated and the directly determined W_F/W_{0_F}. The initial drop radius is 95 μ corresponding to the radius of that group of drops whose collective volume (mass) is greater than the collective volume of any other group of drops ($r_{3_{MAX}} = 5\ r_{30}/3.915$). The r_{30} was selected using Ingebo data ($55\mu \leq r_{30} \leq 75\mu$). The initial drop radius of 75 μ was also used but the trends of the $r_0 = 95\mu$ case can be obtained again by properly adjusting the values of the K's. In Appendix D it is shown that for these models

$$W_F / W_{0_F} = (r/r_0)^3$$

and r is determined by the step-by-step integration of the various vaporization rate equations with $u_\ell = u_{\ell_0}$ = constant. The results of Models A1 and A4 are given in Figure 30. A2 and A3 gave intermediate trends.

Notice:

a) The overall burning rate is too low near the injector and too high far from it. In these models the effect of the

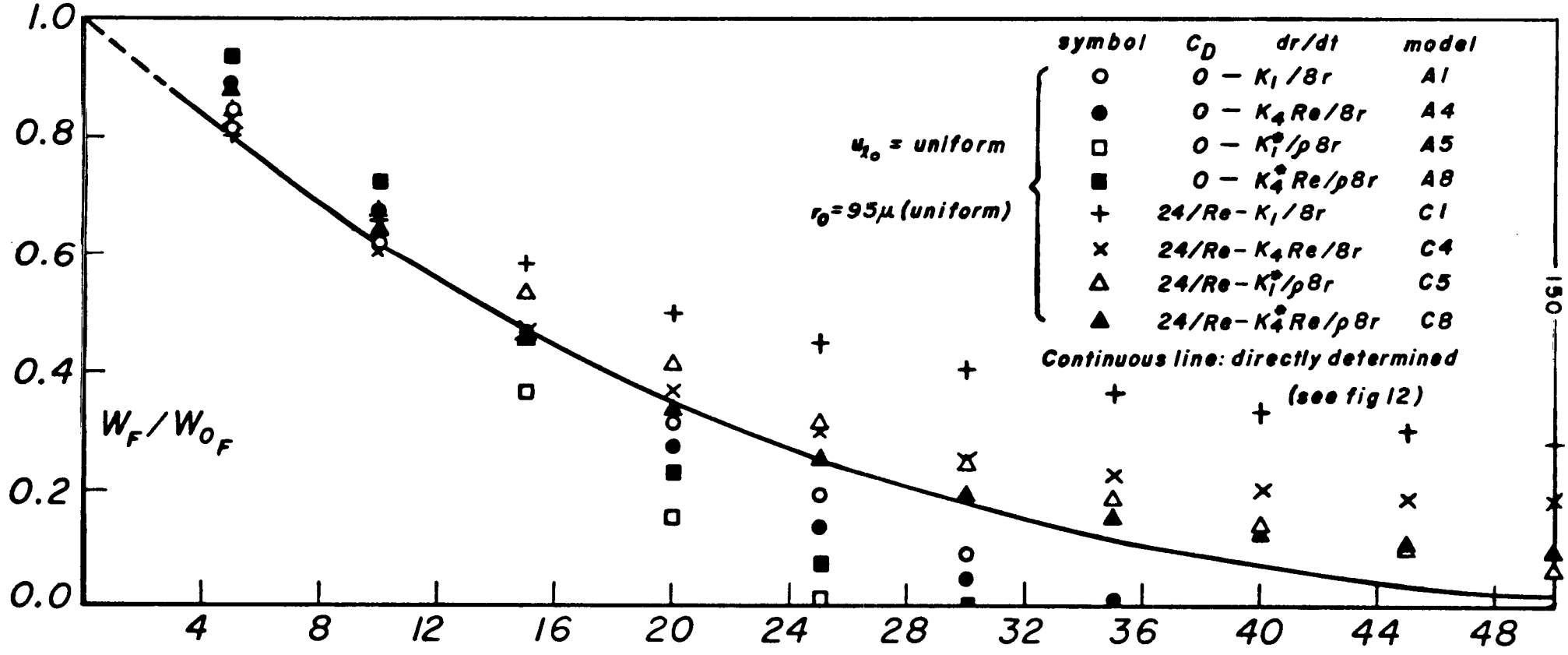

Figure 30

W_F / W_{0_F} as calculated by models, A1, A4, A5, A8, C1, C4, C5, C8

relative velocity is dominant. As long as the relative velocity is low the combustion rate is also low, but it increases quickly after a proper relative velocity has been reached.

b) All the four vaporization rate equations gave essentially the same trend even though their functional forms are quite different.

These models were judged unsatisfactory.

MODELS: C1, C2, C3, C4 of Table V. As previous models except that now the drag is different from zero. Stokes' drag equation is now used: $C_D = 24/Re$. Since the typical Re in these calculations is of the order of 100, Stokes' drag is still smaller than that most authors would agree should be experienced by the drops. In Appendix D it is shown that for these models

$$W_F / W_{0_F} = (r/r_0)^3$$

and r is determined by the step-by-step integration of the various vaporization rate equations together with the drag equation

$$\frac{du_e}{dt} = \frac{4.5\mu}{\rho_l r^2} \frac{u-u_e}{u_e} \qquad \text{for} \quad C_D = 24/Re$$

The results of Models C1 and C4 are given in Figure 30. C2 and C3 gave intermediate trends. Notice

a) The overall burning rate trend is now opposite to that of the previous models. The burning rate is too high near the injector and too low far from it. By adjusting the values of the K's one can obtain good agreement either near the injector (proper local overall burning rate) or far from

it (proper overall combustion length) but cannot obtain both at the same time. In this model the effect of the drop radius is dominant. The relative velocity tends to become small and the effect of the radius becomes dominant.

b) All the four vaporization rate equations gave again similar trends.

These models were judged unsatisfactory.

MODELS: B1, B2, B3, B4 of Table V. As previous models except $0 < C_D < 24/Re$. No calculations were made for these models but from the study of the previous ones one can conclude that they could conceivably have yielded satisfactory agreement for some proper selection of C_D. This is because the previous two sets of models gave opposite overall burning rate trends and differed only for their C_D. Thus some intermediate C_D function should give the proper overall burning rate trend.

MODELS: D1, D2, D3, D4 of Table V. As previous models except $C_D > 24/Re$. No calculations were made for these models but they should worsen the already unacceptable trends of the models for which $C_D = 24/Re$. Increasing the drag, further decreases the relative velocity and the overall burning rate tends to get even higher near the injector and even lower far from it.

MODELS: C5, C6, C7, C8 of Table V. The models in which $C_D = 24/Re$ were judged unsatisfactory because of their high overall burning rate near the injector. One way of reducing the burning rate near the injector is that of making the K's temperature dependent. In previous sections it has been shown that the steady-state gas temperature is lower near the injector. It was thus

assumed that the vaporization rate is lower where the temperature is lower. The K's were then taken to be proportional to the local gas temperature (but the inverse of the density was actually used) and were replaced by K^*/ρ's where the K^*'s are new constants. This change achieved the goal of reducing the overall burning rate near the injector and increasing it far from it (see Figure 30). Models C6 and C7 (based on the modified versions of the Priem and Heidman, and of Spalding vaporization rate equations) were judged satisfactory and the dimensionless liquid fuel fluxes yielded by them are given in Figure 31. In conclusion a model using a uniform initial drop radius and velocity, a Stokes' drag and a modified Priem and Heidman or Spalding vaporization rate equation has been found to represent properly the combustion in the engine under configuration. However, the values of the K^*/ρ's are as much as one order of magnitude different from those predicted by the theories (see Appendix B). In Figure 31 the results from the models which include the droplet distribution function are also given although they will be reconsidered later. It can be seen that the distribution function improves the agreement but not in an essential manner.

MODELS: A5, A6, A7, A8, B5, B6, B7, B8 of Table V. It has been seen that in order to get acceptable agreement when a uniform initial drop radius is used, one should either use a $C_D < 24/Re$ and one of the first four vaporization rate equations, or $C_D = 24/Re$ and some of the second four vaporization rate equations. Both lower drag and lower vaporization rate near the injector serve the purpose of reducing the overall burning rate near the injector and

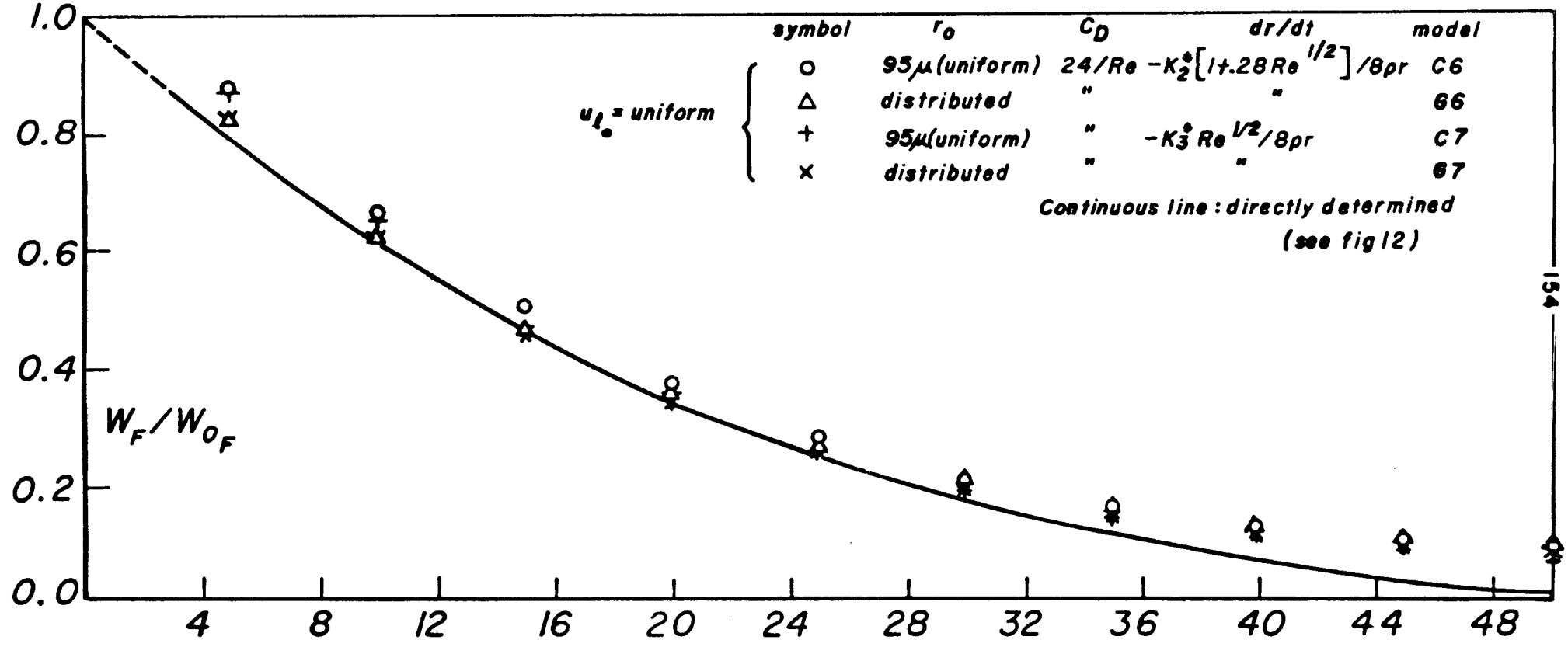

154

Figure 31

W_F/W_{O_F} as calculated by models, C6, G6, C7, G7

increasing it far from it. When both effects are combined, the correction is too strong so that Models A5, A6, A7, A8, B5, B6, B8 are not acceptable (see Figure 30).

MODELS: D5, D6, D7, D8 of Table V. These models were not explored, but on the basis of the above reasoning they could possibly yield acceptable results.

In the other models of Table V, a Nukiyama-Tanasawa initial distribution function for the drop radius was used. The introduction of the distribution function did not change the nature of the trends. It just smoothed out the differences making more models acceptable or marginally so. However, a stretching of the combustion length due to the slow burning of the largest drops was noticed. Thus, in general, those models which with a single initial drop radius tended to give too high an overall burning rate far from the injector, i.e., the low drag, relative velocity sensitive models, give now better results, the opposite being true for the high drag radius sensitive models. Some representative trends are shown in Figure 32. Discussions of the models involving the drop distribution function starts below.

MODELS: G1, G2, G3, G4 of Table V . In these models it was assumed that all drops have initially the same velocity but their radii are distributed according to some specified distribution function (soon to be identified as a Tanasawa-Nukiyama type). It was also assumed that there is no nucleation or drop break-up so that drops which initially have the same radius will always have the same velocity (distribution function $f = f(x,r)$). Under these assumptions the spray equation[19] reduces to (see Appendix D)

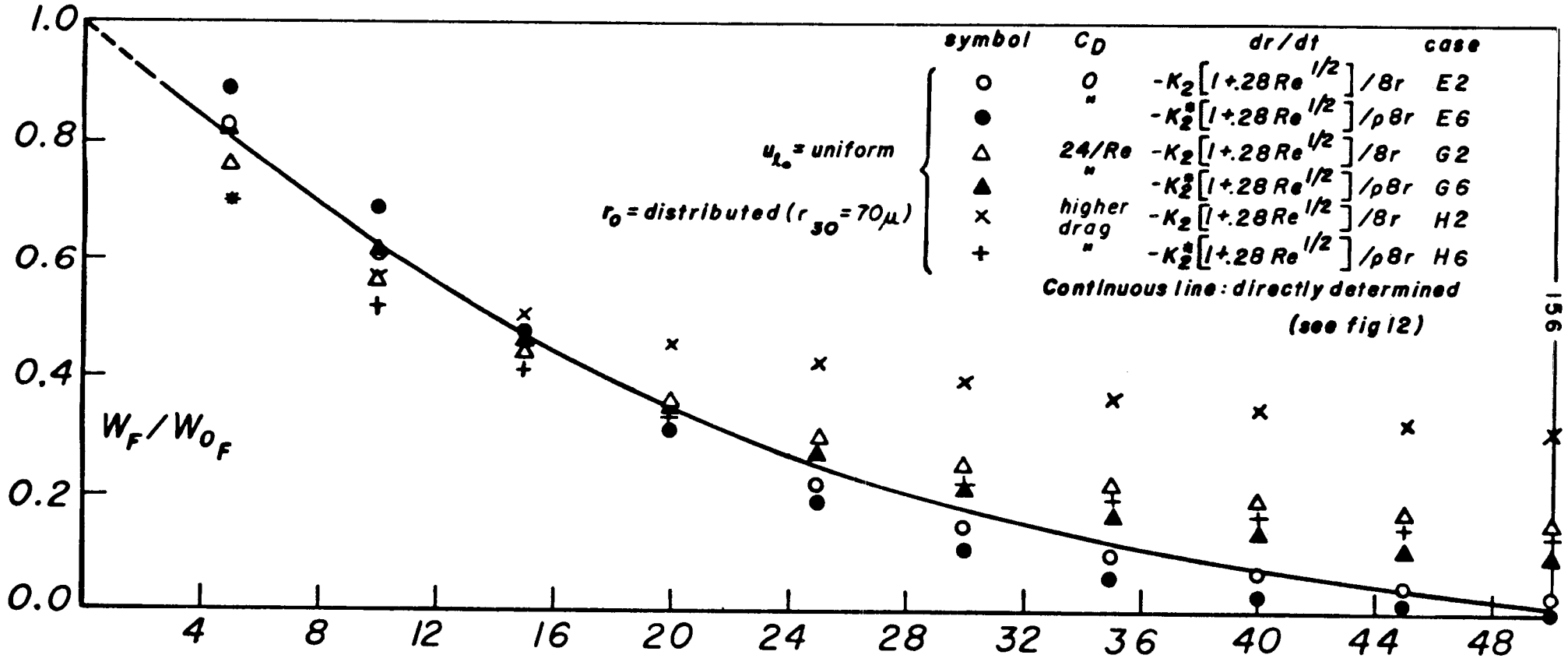

W_F/W_{O_F} as calculated by models, E2, E6, G2, G6, H2, H6

Figure 32

$$\frac{\partial}{\partial x}(u_e f) + \frac{\partial}{\partial r}(R f) = 0 \tag{90}$$

which is equivalent to

$$\frac{dr}{dx} = \frac{R}{u_e} \qquad \& \qquad R \equiv \frac{dr}{dt} \tag{91}$$

$$\frac{d\, h_m f}{dx} = -\frac{1}{u_e}\left[\frac{\partial R}{\partial r} + \frac{\partial u_e}{\partial x}\right] \tag{92}$$

where the second equation specifies the change of f along lines defined by the first one. In these equations u_e, R and f are seen as functions of x, r. In these models, the drag on a drop follows Stokes' equation

$$\frac{du_e}{dx} = \frac{3}{8}\frac{C_D}{r}\frac{\rho}{\rho_L}\frac{|u-u_e|}{u_e}(u-u_e) = \frac{4.5\,\mu}{\rho_L r^2}\frac{(u-u_e)}{u_e} \tag{93}$$

and the coefficients K_1, K_2, K_3 and K_4 of the vaporization rate equations are constant. Equations 91 and 93 determine $u_e = u_e(x, r_0, u_{e_0})$ and $r = r(x, r_0, u_{e_0})$ if $u = u(x)$ and $\rho = \rho(x)$ are known. Fortunately, $u = u(x)$ and $\rho = \rho(x)$ are known (Figures 9 and 10) through the application of the direct method. While integrating equations 91 and 93, one can also evaluate the changes of f by equation 92, but some care must be used since in this equation R and u_e must be seen as functions of x and r. However, u_e is not explicitly known as a function of x and r but it is implicitly defined as such by equations 91 and 92. Equations 91, 92 and 93 were numerically solved for the various burning rate equations (see Appendix E). A number of observations can be made before answering the question of whether these models are satisfactory or not.

a) Equation 92 can be written as follows

$$\frac{f(r,t)}{f_0(0,r_0)} = \exp\left\{-\int_0^x \frac{1}{u_e}\left[\frac{\partial R}{\partial t} + \frac{\partial u_e}{\partial x}\right] dx\right\} \qquad (94)$$

It can then be seen that while integrating equations 91 and 93 one can evaluate the ratio f/f_0 without having to specify $f_0(0,r_0)$. This means that one can appreciate the influence of the selected burning rate equation (91) and of the selected drag equation (93) on the distribution function without specifying the actual drop distribution function at $x=0$ and valid for any drop distribution function he may later specify at $x=0$. Thus, in Figure 33 through 36, the f/f_0's for the various cases are given. It can be seen that when equation 81 is used (Figure 33), small drops burn much faster (inverse dependence on r). Thus, at 5" from the injector all drops with radius $< 35\,\mu$ have practically already been burned. On the contrary, large drops burn very slowly. Thus at 40" the radius of the largest drops was reduced only from $155\,\mu$ to $134\,\mu$. Or, to put it another way, at 40" the number of drops having $134\,\mu$ radius is still 30% of the original number. The slope of the vertical lines indicates the rate of decrease of the number of drops of a specified initial radius: a small slope line means fast rate of decrease. It can be seen that the slope gets smaller as the radius gets smaller. Quite a different picture is offered by Figure 36. Here large drops burn much faster and very small drops hardly burn

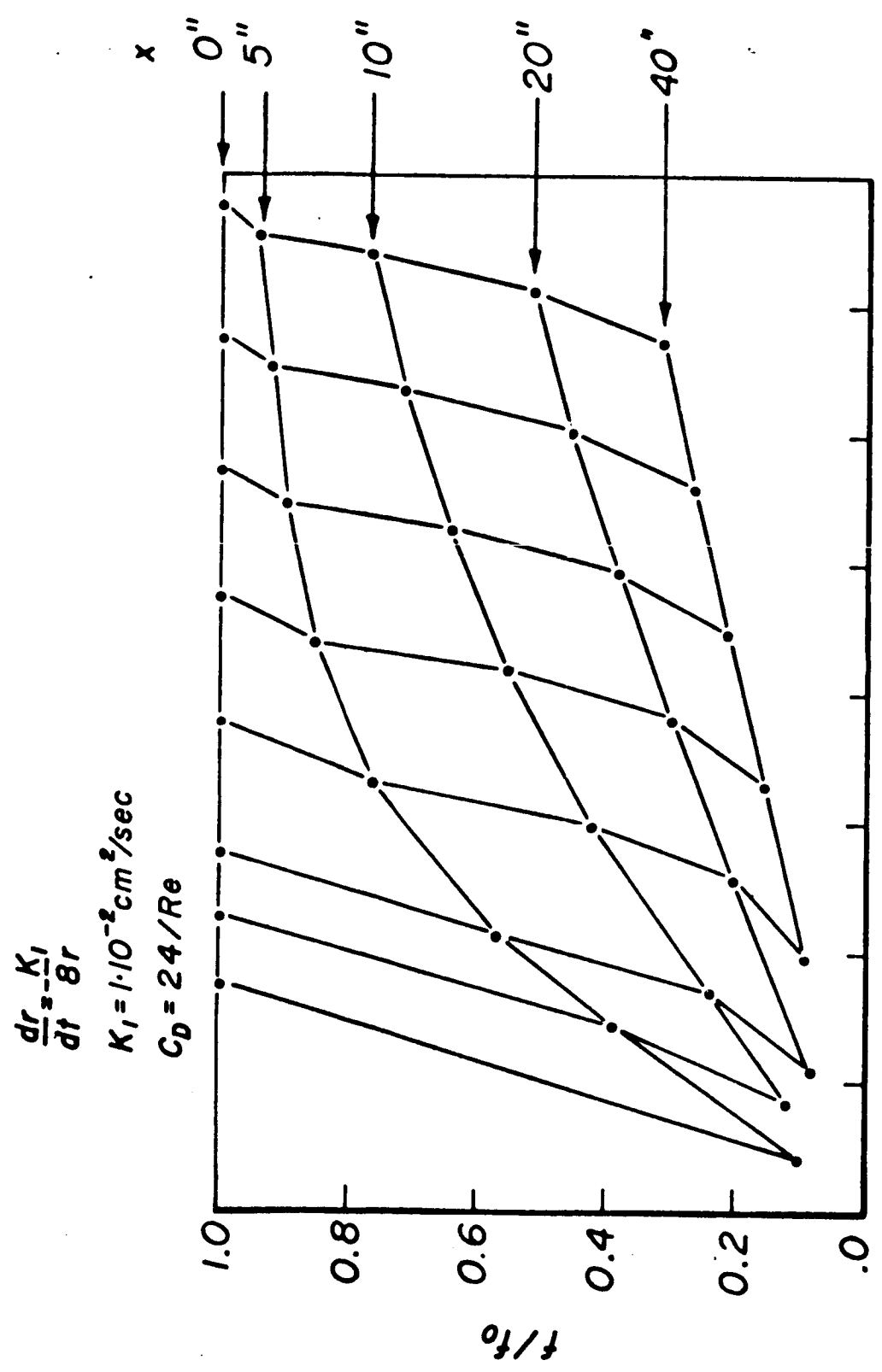

Distribution function change vs r and x for model GI

JP 21 R 4430 69

Figure 33

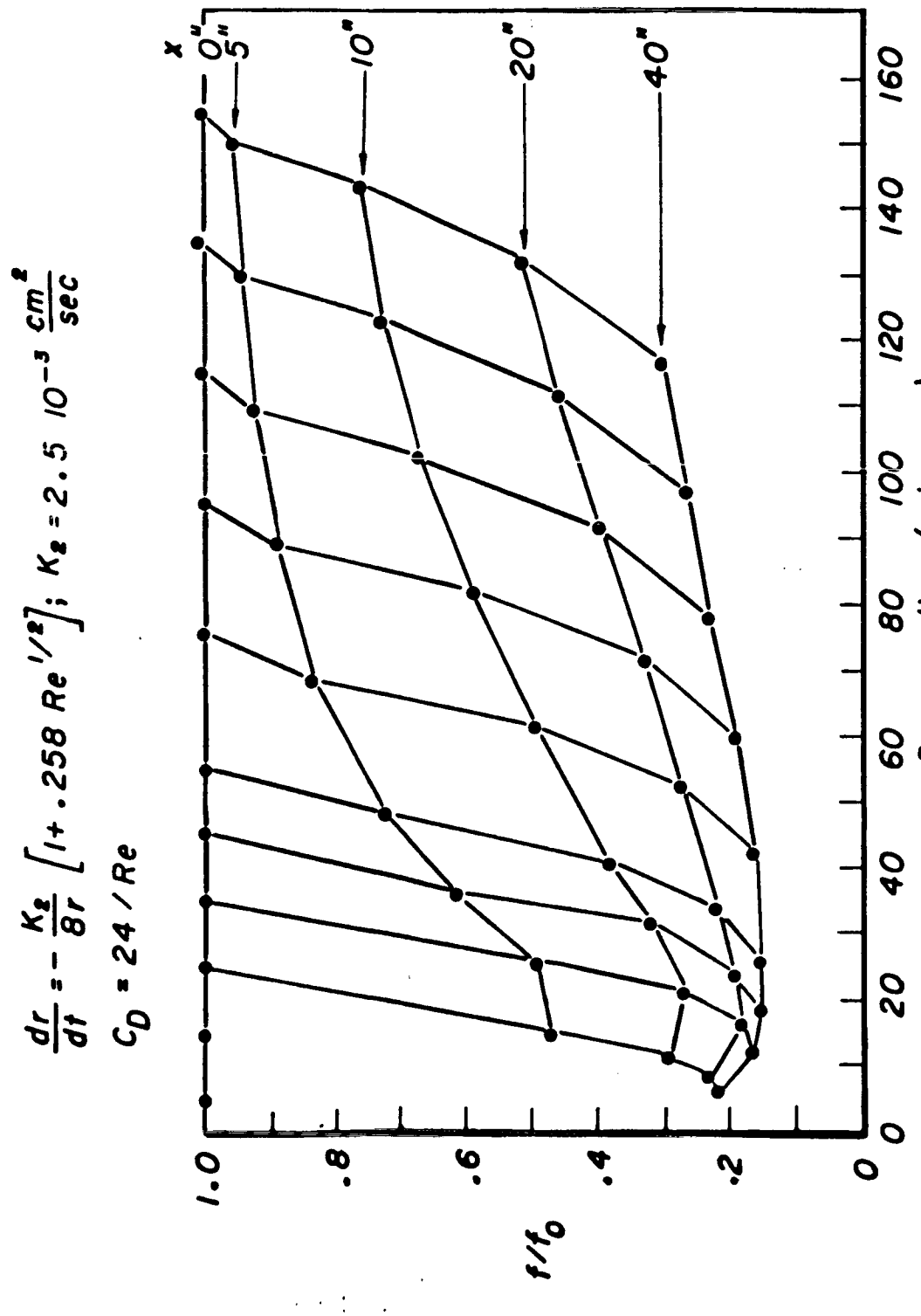

Distribution function change versus r and x for model G2

Fig. 34

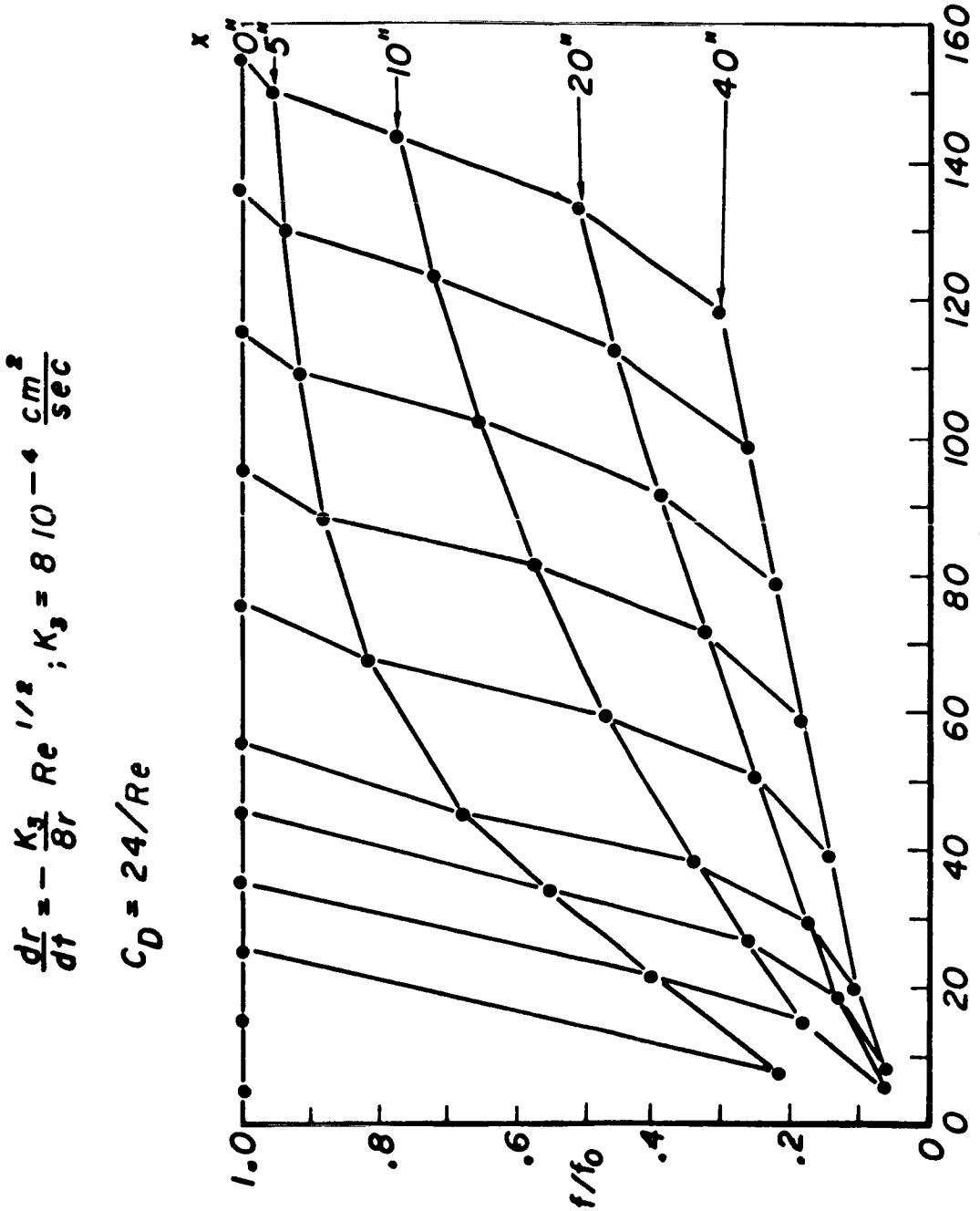

Distribution function change versus r and x for model G3

Fig. 35

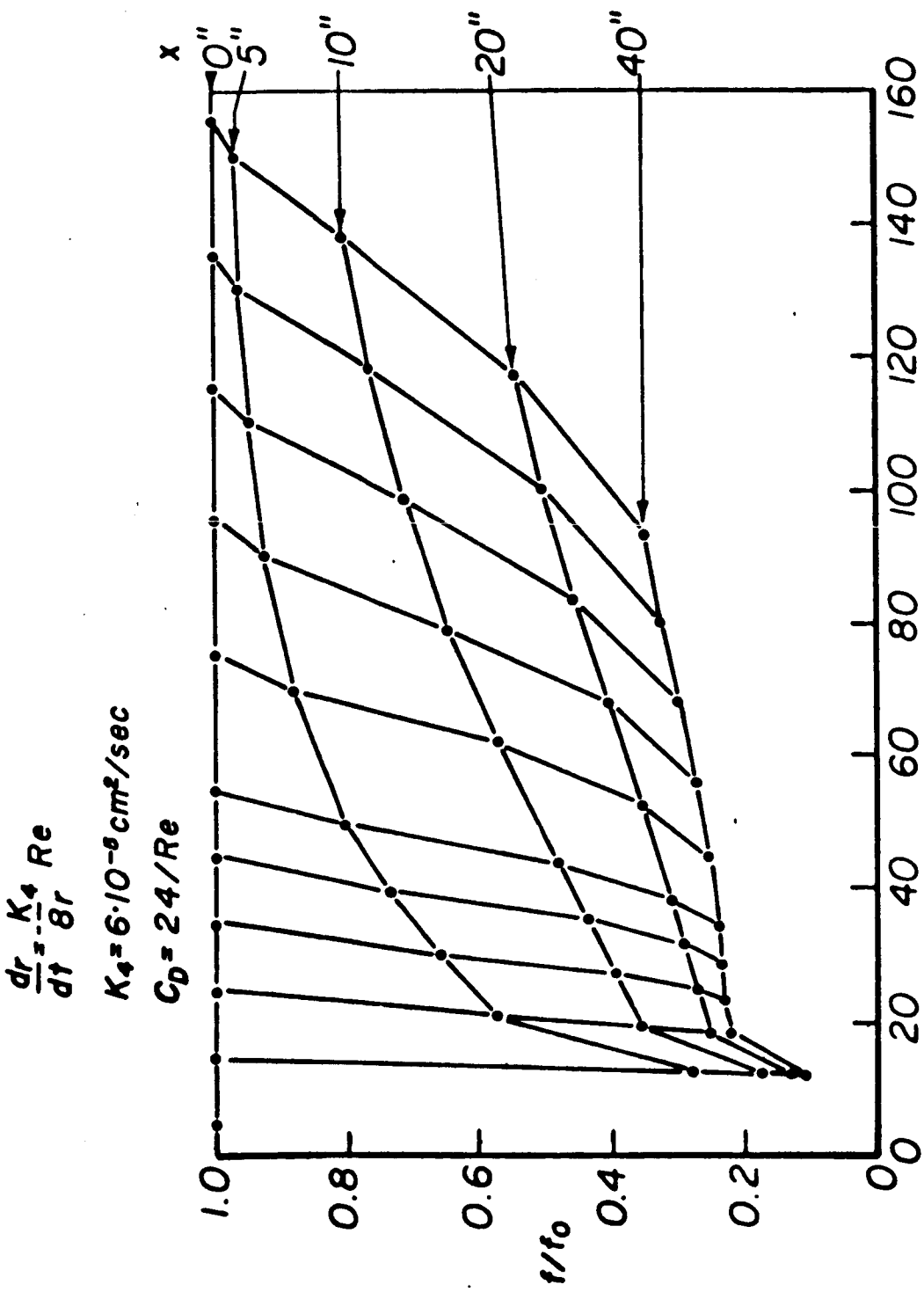

Distribution function change vs r and x for model G4

Figure 36

at all. Here the burning rate equation is independent of the drop radius and depends mostly on the relative velocity; small drops tend to move at the local gas speed whereas large drops tend to maintain their original speed. In Figure 36 one sees that 12 μ drops are still present at 40" while the largest drop radius at 40" is only 93 μ . In this case, the horizontal lines indicate that at 40" the number of drops in all radii groups have been reduced roughly by the same percentage. The number of small drops is reduced mostly near the injector, due to the high initial relative velocity, whereas the number of large drops is reduced mostly far from the injector. In summary, fuel consumption that is high near the injector and low far from it is calculated with vaporization rate equation 81. The opposite is true for vaporization rate equation 84.

b) The actual local distribution function ($f = f(x,r)$) can be evaluated if the initial distribution function ($f_0 = f_0(0,r_0)$) is specified. Ingebo (Appendix C) measured the drop distribution function near the injector under LOX/ethanol firing conditions. He also correlated the volume-mean drop size (r_{30}) to orifice diameter and relative jet gas velocity. An unusual amount of specific information is then available to select the initial distribution function for the engine under consideration. A Nukiyama-Tanasawa distribution function with r_{max}=155μ and r_{30} between 50μ and 70μ was then selected

$$f_0(0, r_0) = 4\,B\,r_0^2\,e^{-3.915\,r_0/r_{30}} \tag{95}$$

The local distribution function is then given in Figures 37 and 38 for the case of Stokes' drag, vaporization rate equation 82, and $r_{30} = 70\,\mu$ and $50\,\mu$. The quantity F, defined by

$$F = 10^{-1}\,\frac{f(x,r)}{\int_0^{r_{MAX}} f_0\,dr_0} \tag{96}$$

is the local (at x) percentage of the initial (at $x=0$) number of drops with radius between r and $r + 10\mu$ (see Appendix C).

c) An interesting question can now be answered, will an initially Nukiyama-Tanasawa distribution function remain the same throughout the engine? In general there is no reason to expect it. If this were the case one could set

$$f(x,r) = 4\,B(x)\,r^2\,e^{-3.915\,r/r_{30}(x)}$$

and one should get straight lines (of varying slope and intersect) from the following function when evaluated at several x's

$$\ln\left[\frac{f(x,r)}{r^2}\right] = \ln\left[4B(x)\right] - \frac{3.915\,r}{r_{30}(x)}$$

Figure 42 shows that one does get straight lines when the vaporization rate equation is equation 84 (if very small drops are not considered). The other three burning rate equations did not quite give straight lines (see Figures 39, 40 and 41).

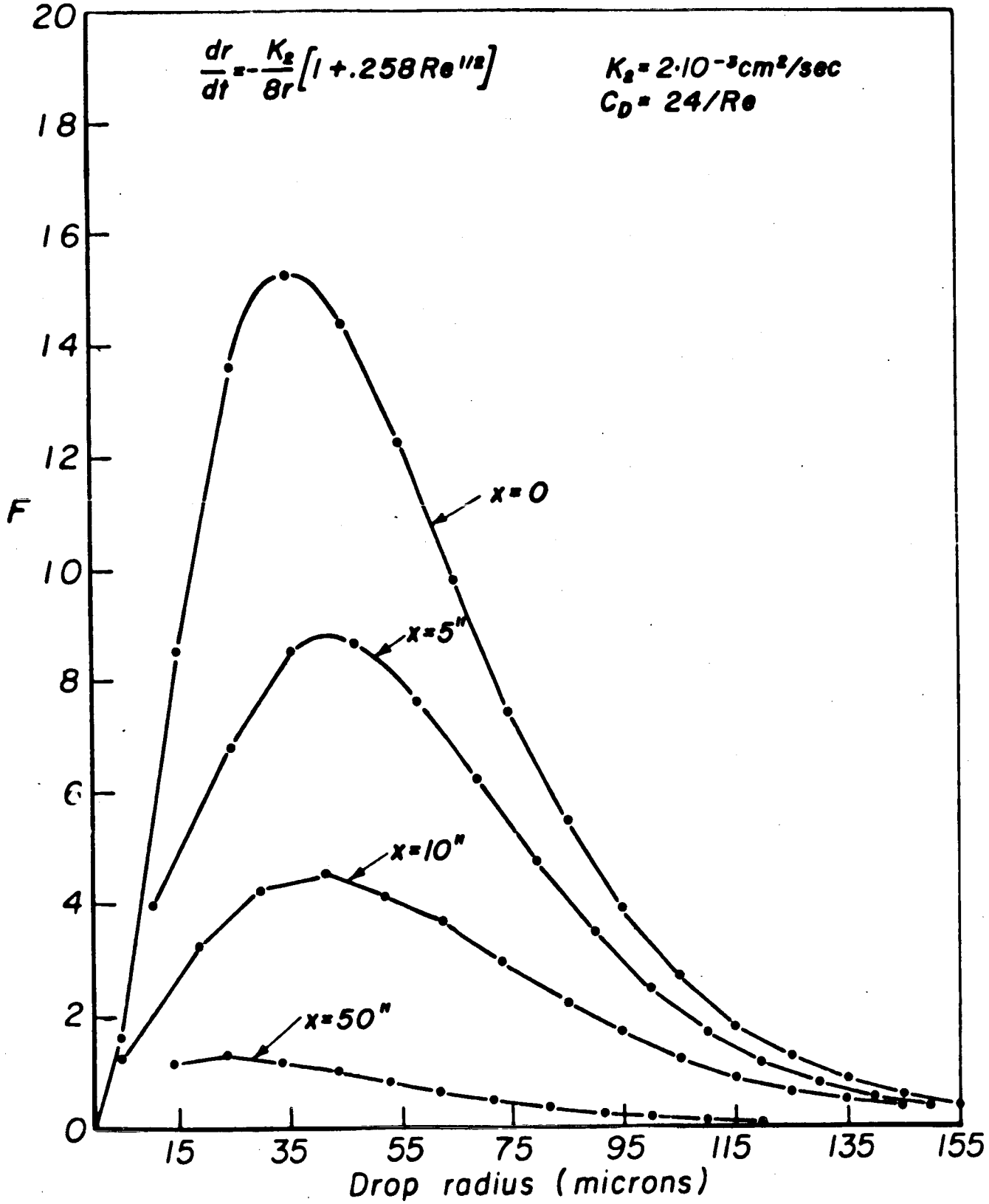

Distribution function change vs r and x for model G2, $r_{so} = 70\mu$

Figure 37

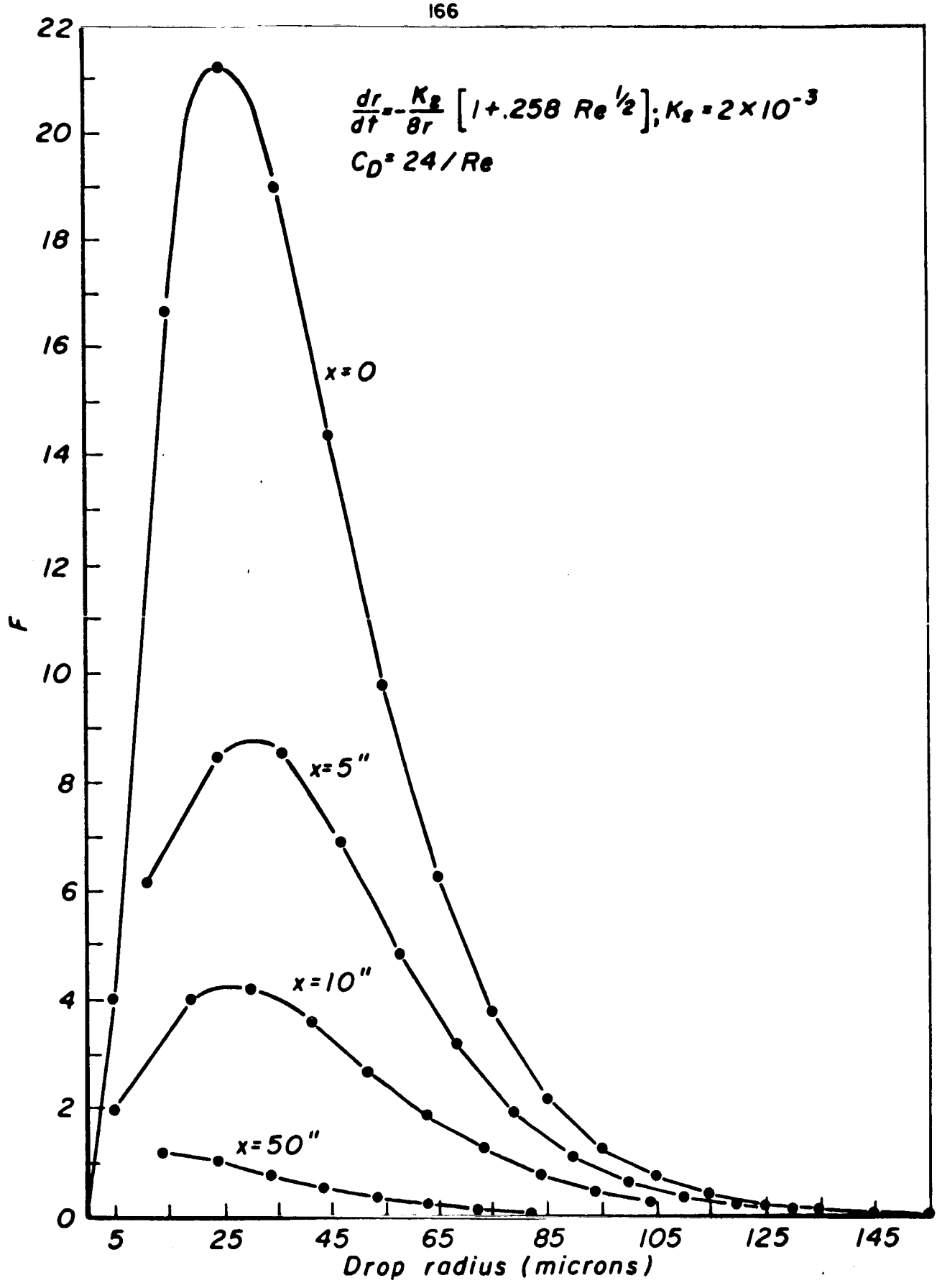

Distribution function change vs r and x for model G2 and $r_{30} = 50\mu$

Fig. 38

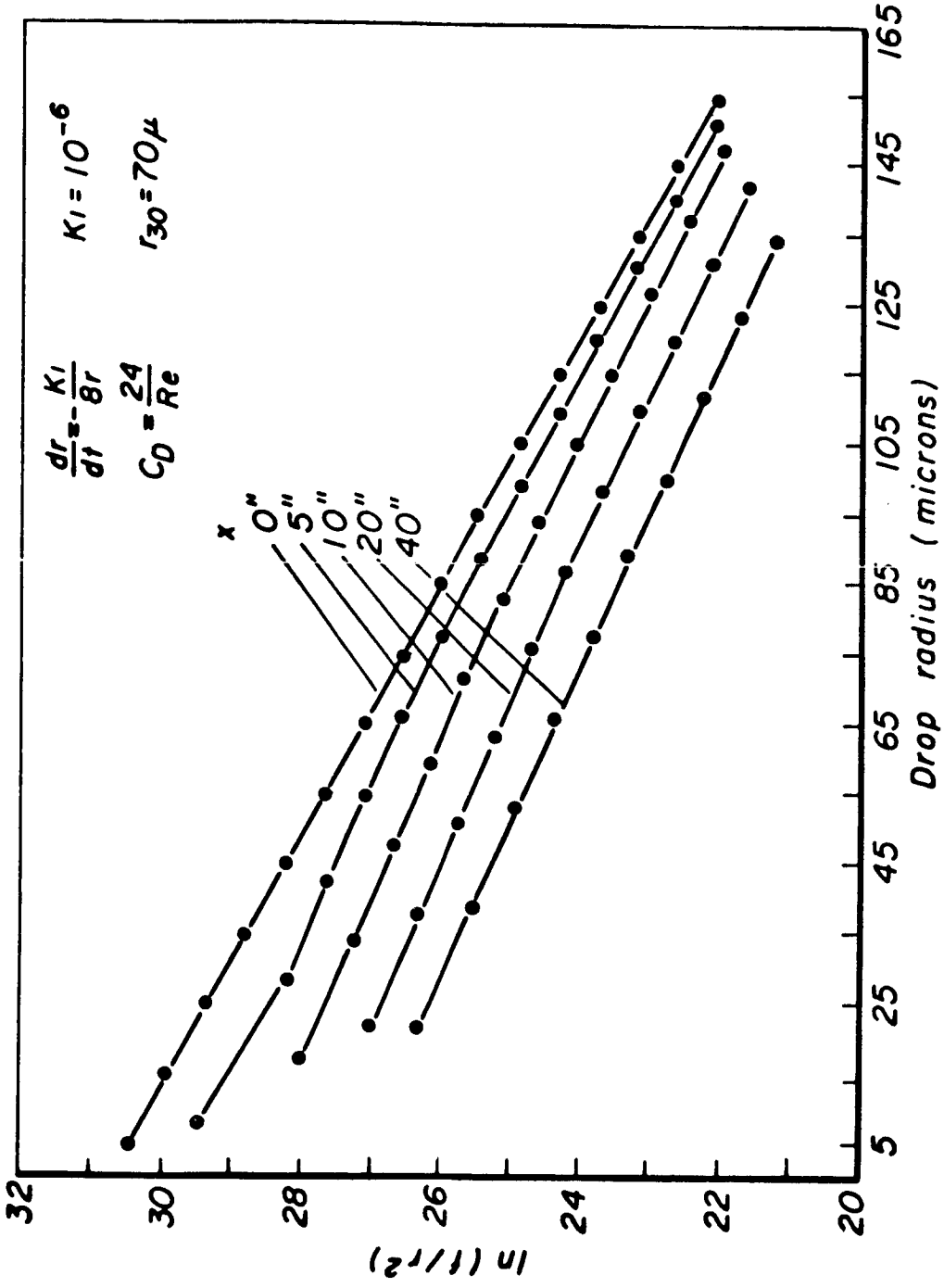

ln (f/r²) versus r and x for model GI

Fig. 39

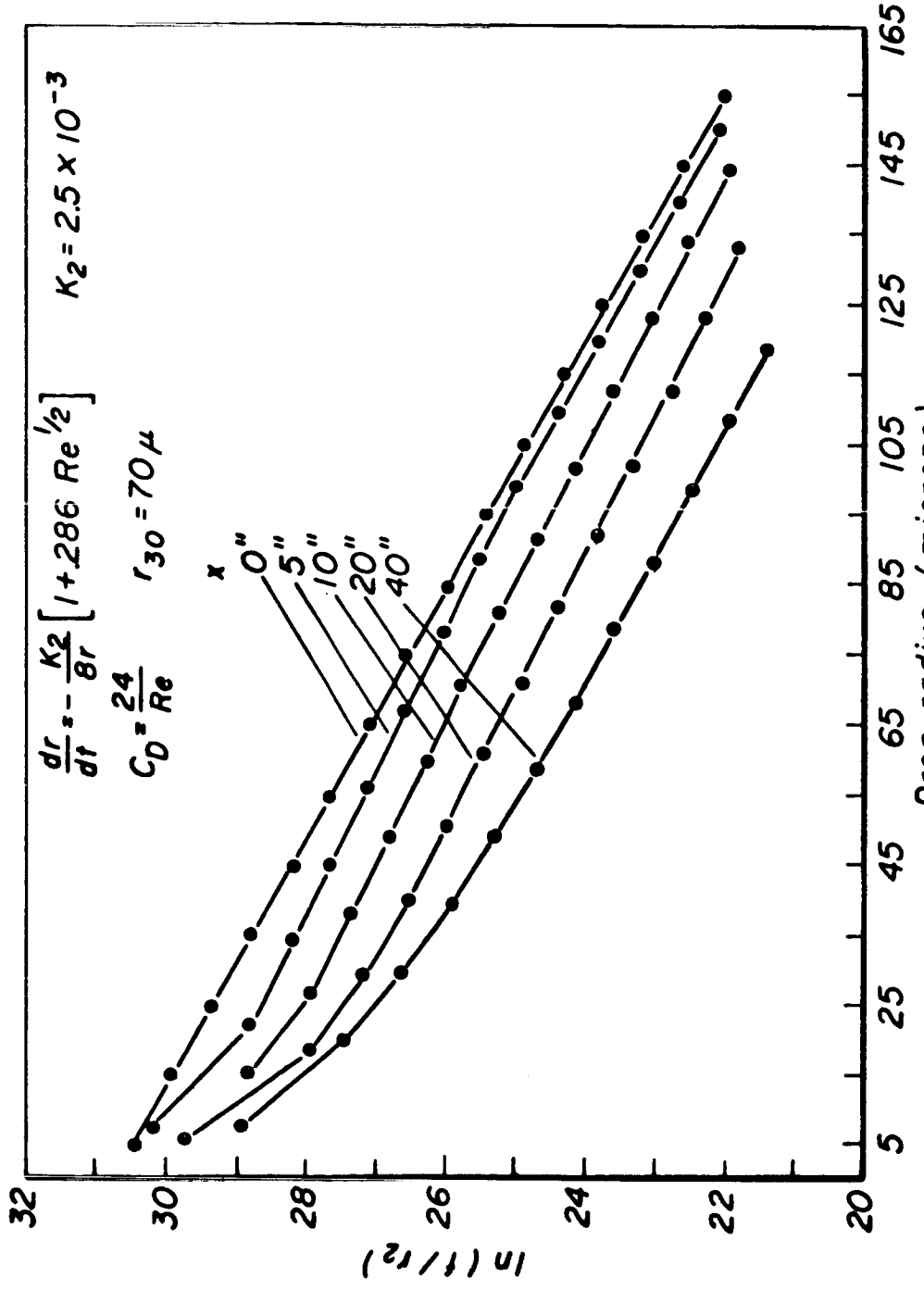

ln (f/r²) versus r and x for model G2

Fig. 40

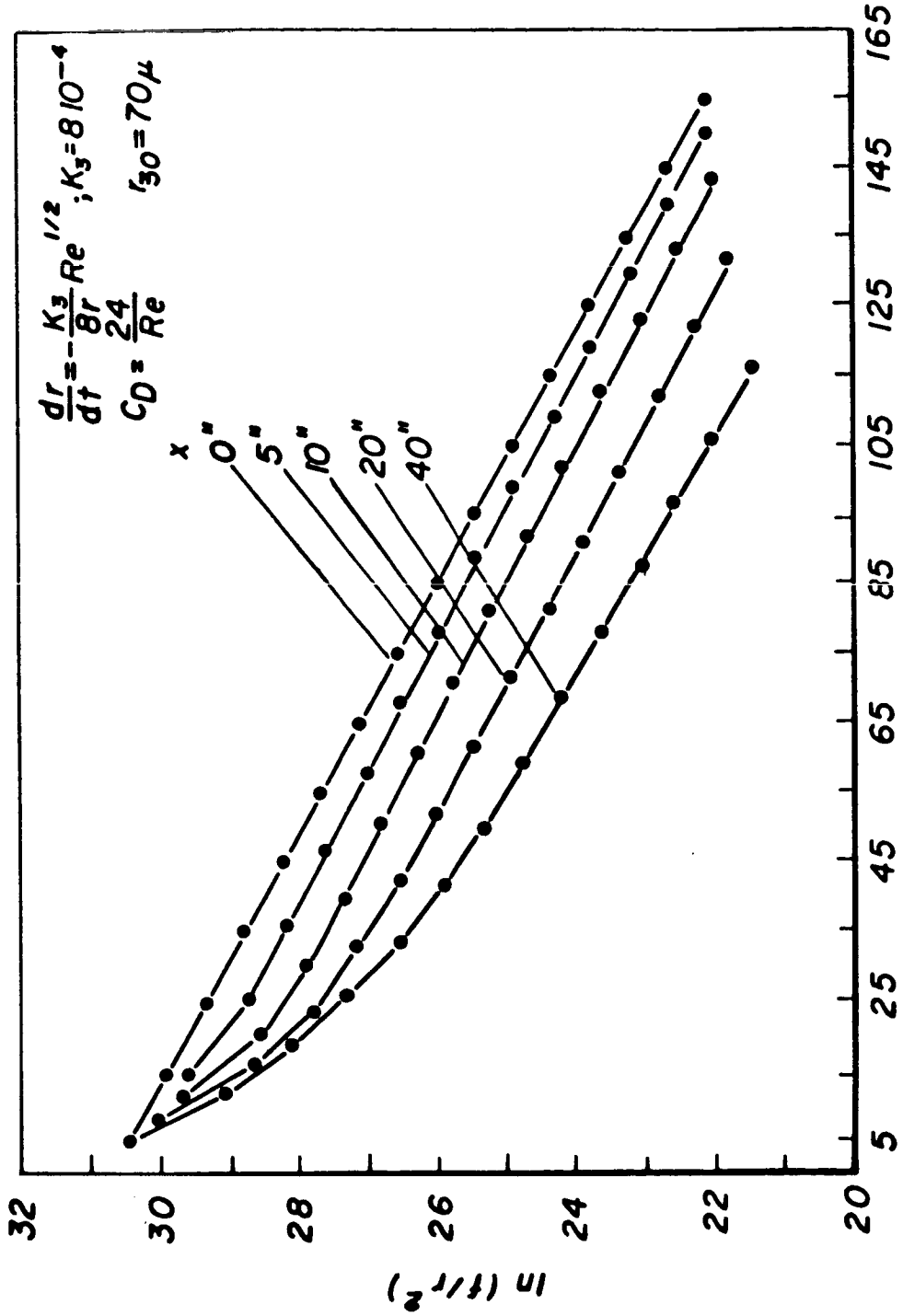

ln (f/r²) versus r and x for model G3

Fig. 41

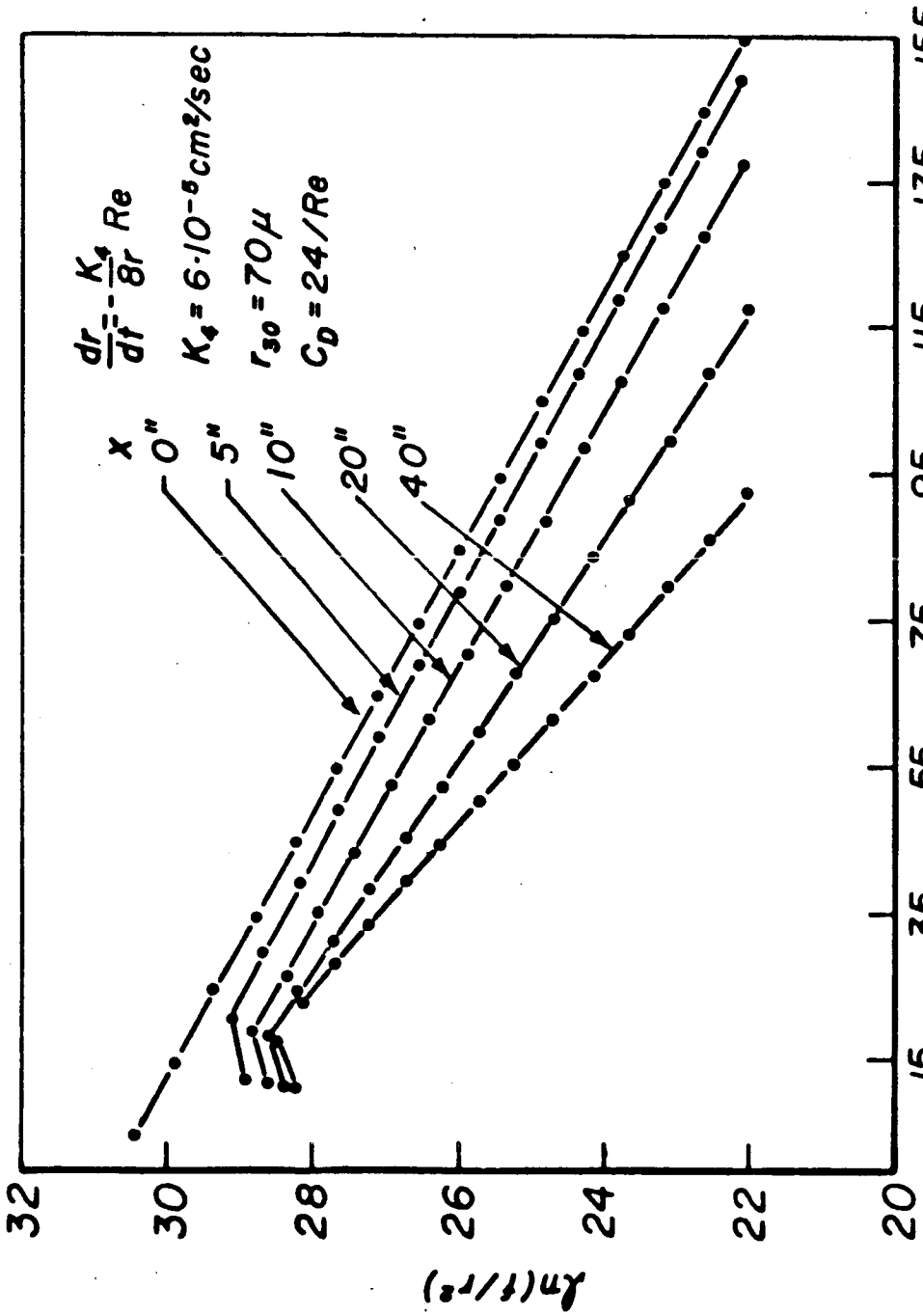
$\frac{dr}{dt} = -\frac{K_4}{8r} Re$
$K_4 = 6 \cdot 10^{-5} cm^2/sec$
$r_{50} = 70\mu$
$C_D = 24/Re$
X
0"
5"
10"
20"
40"
32
30
28
26
24
22
20
15
35
55
75
95
115
135
155
$\ln(f/r^2)$
Drop radius (microns)
$\ln(f/r^2)$ vs r and x for model G4

Figure 42

d) A model which involves the distribution function is adequate if the local dimensionless fuel flux as calculated by it agrees with that calculated by the direct method and given in Figure 12. Having the distribution function $f = f(x, r)$ satisfying the spray equation 90, it can be shown that the dimensionless fuel flux can be evaluated by either one of the following two expressions (see Appendix E)

$$\frac{d}{dx}\left(\frac{W_F}{W_{0_F}}\right) = \frac{1}{A\, W_{0_F}} \int_0^{r_{max}(x)} 4\pi r^2 \rho_L R f \, dr \tag{97}$$

$$\frac{W_F}{W_{0_F}} = \frac{1}{A\, W_{0_F}} \int_0^{r_{max}(x)} \frac{4}{3}\pi r^3 \rho_L u_r f \, dr \tag{98}$$

An excellent check is then available on the overall validity and accuracy of any given solution. The above two expressions must yield the same (W_F / W_{0_F}) for all x's. Calculations show that when u_r is constant the above check is met exactly whereas in the more complicated cases in which u_r is a function of both r and x the above check is met with decreasing accuracy as x increases, but is still more than adequate for the purpose of these computations (one can hardly distinguish W_F/W_{0_F} calculated by equation 97 from that calculated by equation 98 in figures like Figure 30).

The basic question of whether these models are adequate or not can now be answered with the help of Figure 44. As this figure shows, all the four vaporization rate equations are satisfactory for the first part of the engine, but tend to give too long a combustion length. Alternatively, by properly selecting the values of K_1, K_2, K_3 and K_4, one could have had good agreement on the combustion length but then the combustion as calculated by these vaporization rate equations would have been much too active near the injector. In conclusion, these models are not completely satisfactory. Before going to other models, it might be pointed out that the values of the constants K_1, K_2, K_3 and K_4 and of t_{30} have a strong influence on the overall solution. This is adequately demonstrated in Figure 43.

MODELS: G5, G6, G7, G8 of Table V. The previous models are not quite acceptable because they give an overall combustion rate which tends to be too high near the injector and too slow far from it. Thus, if instead of using the K's one uses the K^*/ρ's, as in Models C5, C6, C7, C8, one can expect a better agreement since the substitution achieves the goal of reducing the vaporization rate near the injector and of increasing it far from the injector. Accordingly, the vaporization rate equations given by equations 85 through 88 were used again, together with a Nukiyama-Tanasawa initial drop distribution function and Stokes' drag. Figure 45 shows that now all four vaporization rate equations give satisfactory results. Vaporization rate equations 86 and 87 could possibly be selected as those giving better results while vaporization rate equation 88 might still be considered acceptable and

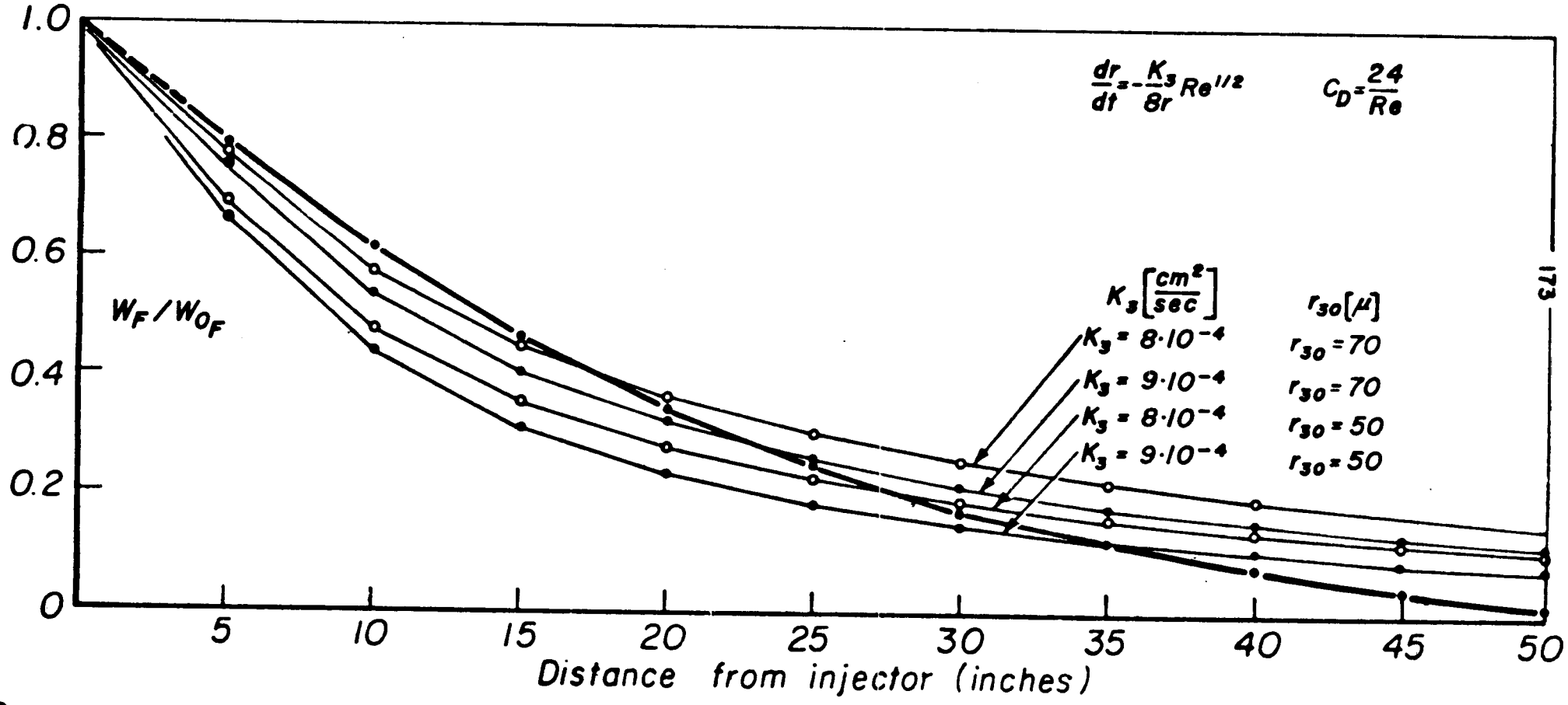

Figure 43

Influence of K_3 and r_{30} on W_F / W_{0_F} (model G3)

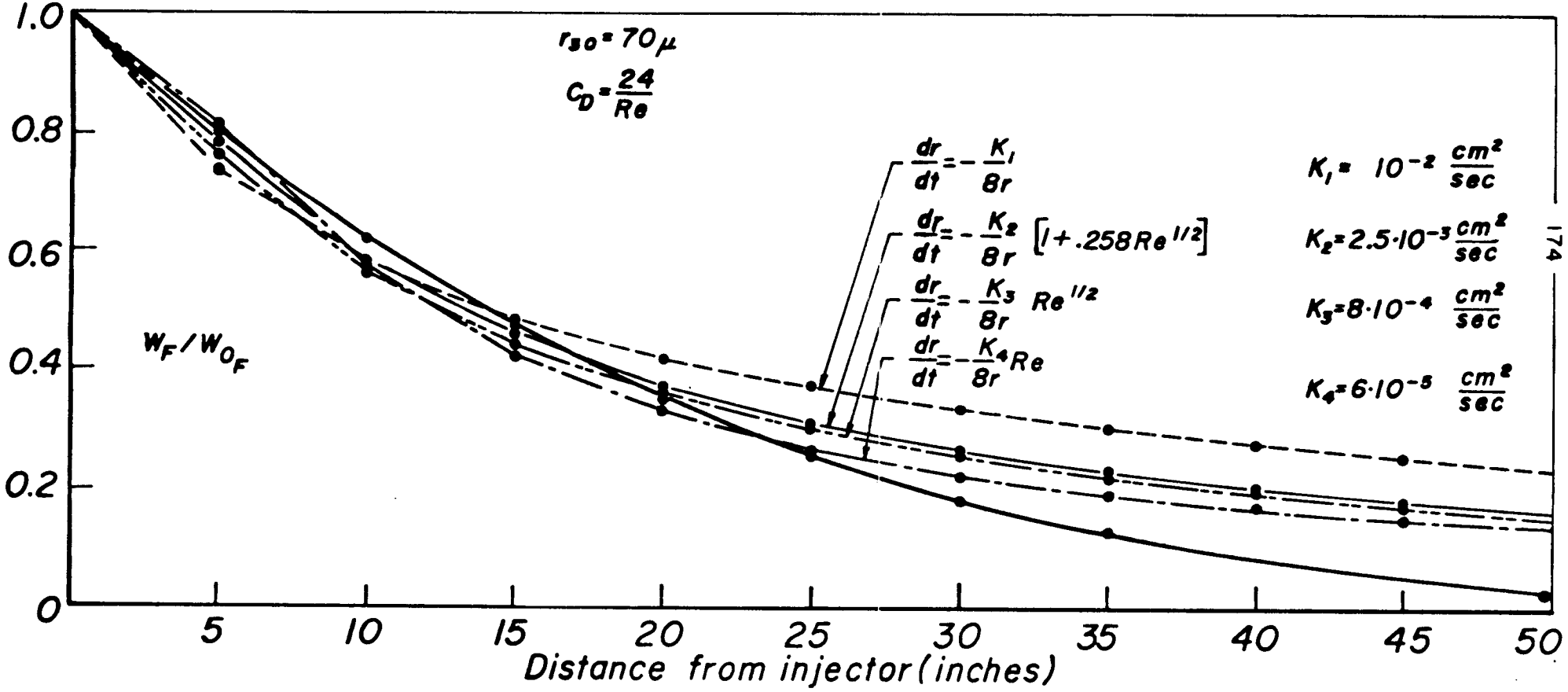

Figure 44

W_F / W_{O_F} as calculated by models, G1, G2, G3, G4

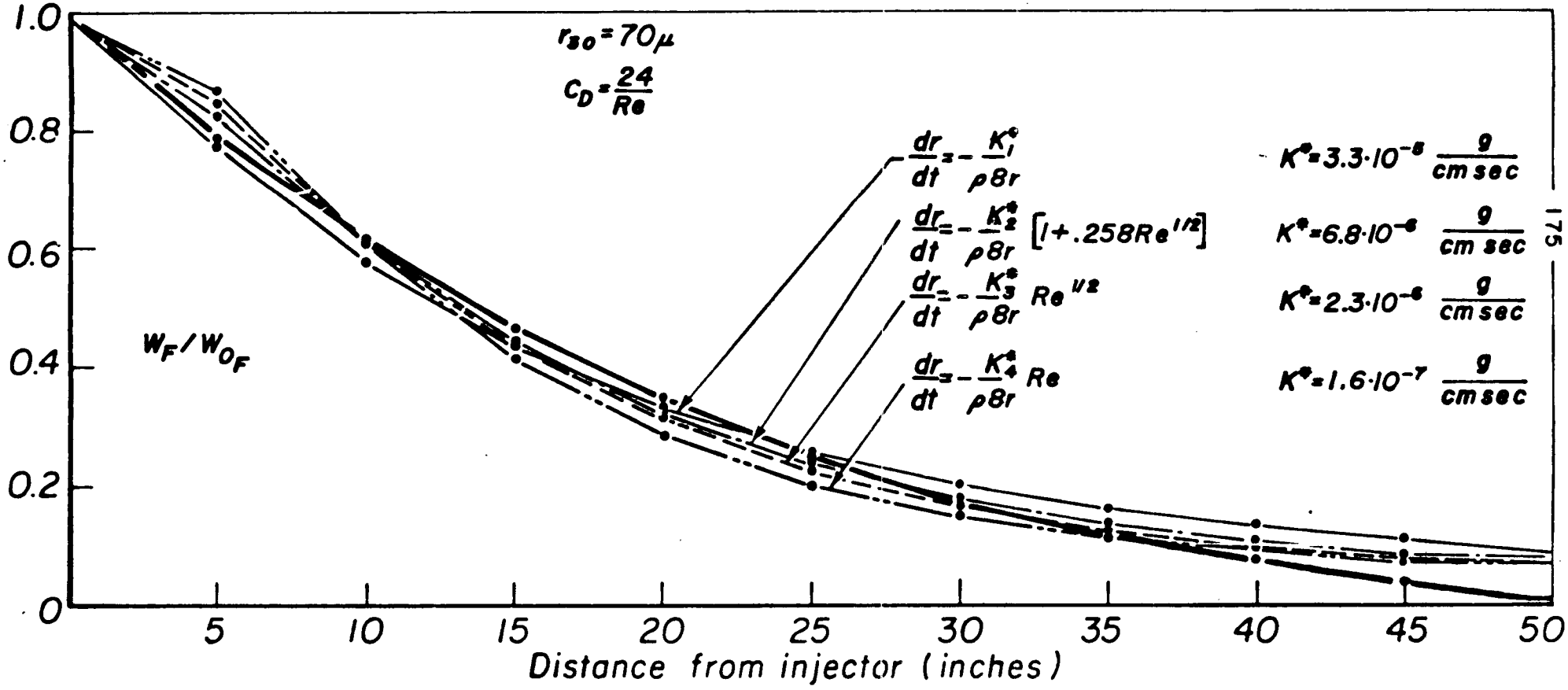

W_F / W_{O_F} as calculated by models, G5, G6, G7, G8

Figure 45

it is attractive for its mathematical simplicity

$$\frac{dr}{dt} = -\frac{K_4^*}{4\mu}\left|u-u_\ell\right| \tag{99}$$

It can be shown that with this vaporization rate equation and with $c_D = 24/Re$ closed form solutions of the spray equation can be obtained for some specific $u = u(x)$ functions.

MODELS: E1, E2, E3, E4 of Table V. In these models, a Nukiyama-Tanasawa initial drop distribution function was again selected and the spray equation was solved but with the further assumption of no drag (all drops move at constant speed) and with the vaporization rate equations 81 through 84. Figure 46 shows that vaporization rate equations 82 and 83 would give again reasonably good results. Indeed in these models one has again decreased the overall burning rate near the injector and increased it far from it. This was achieved not through a modification of the burning rate equations, but through a modification of the drag equation. The setting of $u_\ell = u_{\ell_0}$ = constant is the limiting case of an extremely weak drag. Parenthetically, notice that the assumption of constant drop velocity also improved the result obtained with the vaporization rate equation 81 in which the relative velocity does not appear at all. This is because the space rate of change of η still depends on u_ℓ (Equation 91) and so do the distribution function (Equation 92) and the dimensionless fuel flux (Equations 97 or 98). Also notice that the vaporization rate Equation 84, which depends heavily on the relative velocity, now gives too high a rate of overall combustion far from the injector.

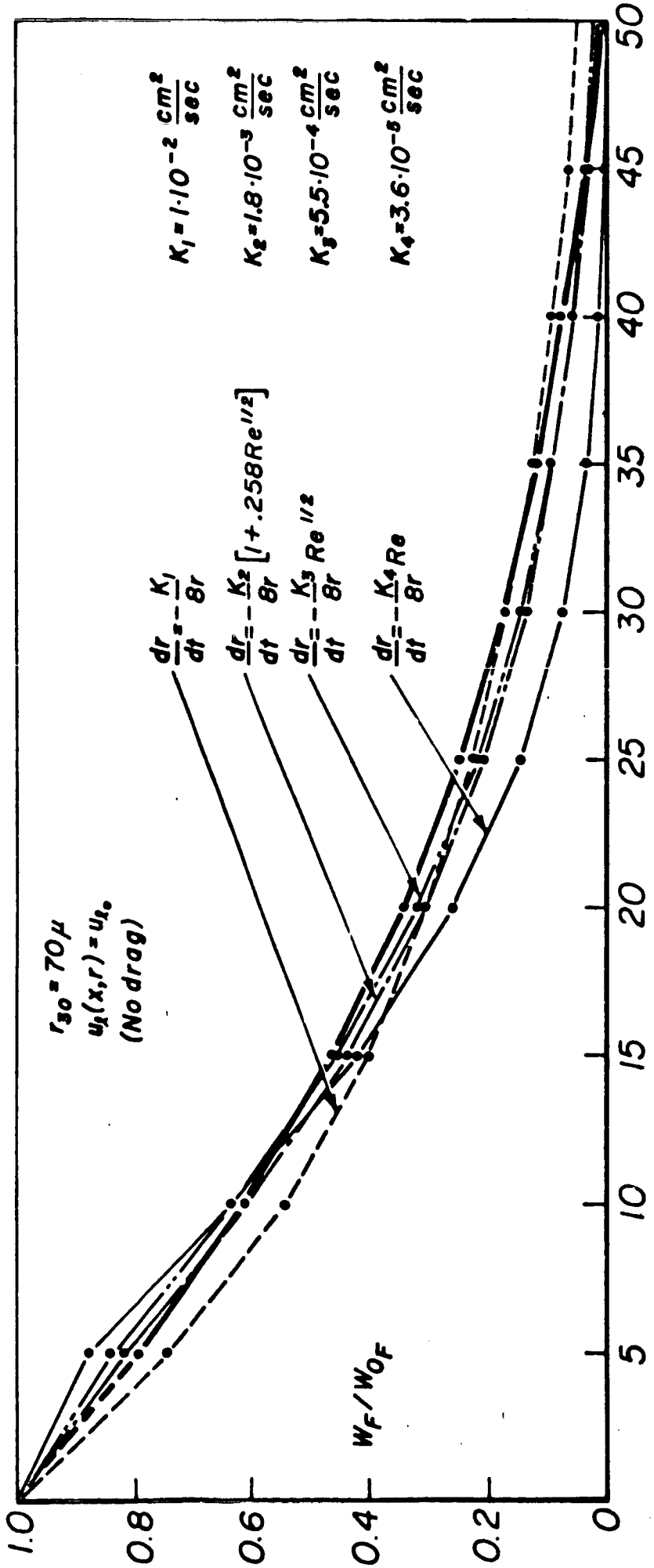

W_F / W_{O_F} as calculated by models, E1, E2, E3, E4

Figure 46

MODELS: H2 and H6 of Table V. In these models a Nukiyama-Tanasawa initial drop distribution function was used, and the steady state euqation was solved for the case in which the drag of the drops is higher than that given by Stokes's equation. The following drag equations suggested by Rabin[28] were used

$$C_D = 27 / Re^{.84} \qquad Re \leq 80$$

$$C_D = .271\ Re^{.217} \qquad Re > 80$$

Vaporization rate quations 82 and 86 were used. The dimensionless fuel fluxes thus calculated are given in Figure 32 and they are seen to exhibit the behavior characteristic of the high drag model high burning rate near the injector and low far from it due to the low relative velocity which is quickly established thanks to the high drag. There is no way of matching the directly determined W_P/W_{o_F} by varying K or K* or r_{30}. Model H6 (and Model H7 which was also calculated) gave marginally acceptable results due to the factor $1/\rho$ which increased the vaporization rate far from the injector, thus partially offsetting the effect of the high drag.

3.7 Conclusions for the LOX/ethanol System

The following conclusions about the steady combustion of the LOX/ethanol system have been reached through the experimental and analytical work presented in the previous section. Extension of these conclusions to other propellant systems must be made with care. The main conclusions are:

1) The problem of steady rocket combustion is particularly suited for the application of the direct method. Droplet

drag and vaporization processes are anything but completely understood. By the application of the direct method, most of the gas variables can be determined using only static pressure measurements and without any droplet drag, vaporization and distribution models. In the process the main assumption becomes that of instantaneous chemical equilibrium of the reaction products. This assumption can hardly be avoided whether one uses the "direct" or the "conventional" approach (3.0).

2) The assumption of instantaneous chemical equilibrium of the reaction products has been found to lead to good results (for the LOX/ethanol system) (Section 3.3.2).

3) For chamber pressures between 150 and 600 psi, injection equivalence ratios between .9 and 1.9 (O/F by weight between 2.32 and 1.1), and nozzle entrance Mach numbers up to .55 the steady state of the LOX/ethanol system can be determined by solving three algebraic equations containing six unknowns (ρ, u, p, W_F, W_ϕ, $\bar{u}_e/u$). One of the unknowns is the flux of liquid oxygen (W_ϕ) and can be set equal to zero for most of the engine. A second unknown is the ratio between liquid drop velocity and gas velocity ($\bar{u}_e/u$) and can be estimated at various distances from the injector. The influence of $\bar{u}_e/u$, although not negligible, is not very large so that estimates for it are sufficient. One is then left with three equations in four unknowns (ρ, u, p, W_F) and

the measurements of one of them (usually the static pressure, p) is sufficient to determine the other three. Among the variables thus determined is the flux of liquid fuel (W_F) which is of great interest for the study of combustion efficiency, of the relation between mass and energy sources, of droplet drag and vaporization models and, possibly, of combustion stability (Section 3.3.2). Similar equations could be obtained for other propellant combinations and should be of practical use.

4) One of the most important findings is that the steady state of the LOX/ethanol system can be expected to be anything but axially uniform in engine designs of practical use. This finding probably holds true for most LOX hydrocarbon systems as well. Gas pressure, temperature, density, average molecular weight, speed of sound, composition and ratio of specific heats, all exhibit axial non-uniformities of different magnitudes depending on injection mixture ratio, chamber pressure and nozzle entrance Mach number (Section 3.3.5). The only variable which shows axial uniformity (at low nozzle entrance Mach number) has been found to be the volumetric energy release, i.e., the energy added to the gas per unit volume of the combustion chamber (Section 3.3.3).

5) When the axially nonuniform steady state was subjected to a small amplitude periodic perturbation, it was found that its frequency is about 20% smaller than it would

have been had one assumed a axially uniform steady state (Section 3.5). This explains why the frequency of the shock-type longitudinal instability has been measured to be close to the "acoustic" frequency (based on the axially uniform steady-state assumption). A shock-type wave should exhibit a higher frequency than the acoustic one. Indeed it does, it is the acoustic frequency which has been overestimated by assuming steady-state axial uniformity.

6) Relevant to theoretical studies of instability is the finding that, in steady state, the effect of droplet drag on the momentum equation of the gas is probably higher than (or at least equal to) the effect of vaporization (Section 3.3.4). Then there seems to be no reason for neglecting drag terms and keeping vaporization terms in theoretical instability studies. If anything, it would seem more consistent (and mathematically simpler) to neglect both (Section 3.5).

7) Also relevant to theoretical studies of instability is the finding that the quantity $p/\rho(\gamma-1)$ overestimates the actual internal energy of the gases by as much as 25% (if the complete combustion value of γ is used throughout the engine). Wanting to express the internal energy by $p/\rho(\gamma-1)$, a γ somewhat higher than that corresponding to complete combustion is suggested (to account roughly for the fact that the specific heats of the products change as the temperature goes from its reference value

to its local chamber value). For LOX/ethanol $\gamma = 1.235$ rather than $\gamma = 1.21$ is suggested (a 12% difference in $(\gamma-1)$) (Section 3.3.3). Perhaps more important is the finding that the energy source is not proportional to the mass source due to an axially varying gas mixture ratio (Section 3.3.3). The ratio of the two sources can be expected to exhibit the same degree of axial disuniformity that the gas variables exhibit since they are both related to the axially varying gas mixture ratio (Section 3.3.3).

8) The one-dimensional approach to the study of the processes occurring in the first few inches near the injector is hardly justifiable. However, some conclusions were reached which are believed to be correct and of practical interest. The static pressure has been found to increase in the vicinity of the injector before decreasing below its injector value. The initial momenta of the liquids are responsible for the increase. The point at which the liquid velocity is equal to the gas velocity ($u_\ell = u$) is further from the injector than the point at which the static pressure tops off after increasing (Section 3.4)

9) The initial momenta of the liquids should not be neglected in steady-state computations. Their contribution to the accurate calculation of the gas velocity is important throughout the engine (Section 3.3.4).

10) The previous conclusions have been reached without specifying anything about the distribution, drag and vaporization of the droplets. Some possible models for the distribution drag and vaporization of the drops were then studied. It was concluded that a Nukiyama-Tanasawa initial drop distribution function, a Stokes' drag and either of the following two vaporization rate equations

$$\frac{dr}{dt} = -\frac{K_2^*}{8\rho r}\left[1+.3\,P_r^{1/3}\,Re^{1/2}\right]$$ Modified Priem-Heidmann

$$\frac{dr}{dt} = -\frac{K_3^*}{8\rho r}\,Re^{1/2}$$ Modified Spalding

Reproduced accurately the steady state of one specific LOX/ethanol engine configuration (Configuration II of Table IV) but no droplet breakup effect was included. It must also be noted that the coefficients K^*_2/ρ and K^*_3/ρ represent somewhat arbitrary modifications to the vaporization rate equations suggested by Priem-Heidmann and Spalding respectively. Had one used those vaporization rate equations in their original forms, he would have reporduced very poorly the actual steady state. He would have overestimated the overall burning rate near the injector and underestimated it far from it. He would have concluded that most of the propellants are burned in the first few inches and the remaining linger on at length while the direct method revealed a combustion axially more distributed. It was also found that the use of the distribution function is not really necessary,

although it does tend to improve the results. The proper initial drop radius to be used when a distribution function is not used is $r_0 = 5 r_{30}/3.915$. In this study the typical drop Reynolds number was of the order of 100. Nevertheless Stokes' drag equation was found to give better results than higher drag equations. Indeed higher, drag equations could have hardly been judged acceptable without substantial modifications to the vaporization rate equations. Introduction of very specific droplet break-up processes could have possibly made the higher drag models acceptable (Section 3.6).

4.0 UNSTEADY SOLID PROPELLANT BURNING

This author has recently[30] become aware of a procedure, introduced by Ya. B. Zel'dovich[31] in 1942, to study unsteady solid propellant combustion. This procedure has since become widely used in the Russian literature. It actually represents an application of the "direct" method although it is generally viewed as an intelligent trick to solve a particular problem rather than a specific application of a general way of solving physical problems. Both the "conventional" and the "direct" (Zel'dovich) approaches to the study of unsteady solid propellant burning are here briefly reviewed. The emphasis is on the comparison between the two approaches rather than on the discussion of the problem of unsteady solid propellant burning. The work of C. L. Merkle, S. L. Turk and M. Summerfield[32] will be closely followed in presenting the "conventional" approach to this problem.

Consider a one-dimensional, semi-infinite, homogeneous solid propellant which is burning steadily. At $t=0$, the pressure becomes a specified function of t, $p=p(t)$, due, for example, to depressurization. The problem is that of determining the resulting unsteady burning rate $r=r(t)$. The physical system is made up of a solid phase, a gaseous phase and the common interface. The characteristic times for heat transfer, chemical reaction, and mass diffusion in the gaseous phase are found to be two to three orders of magnitude smaller than the characteristic time for heat transfer in the solid so that the gas phase can be treated in a quasi-steady manner.

Fixing the coordinate on the regressing surface of the solid one can then derive the following equations

$$\lambda_p \frac{\partial^2 T}{\partial x^2} + \rho_p c_p r(t) \frac{\partial T}{\partial x} = \rho_p c_p \frac{\partial T}{\partial t} \qquad \text{Energy conservation in solid}$$

$$-\lambda_p \left(\frac{\partial T}{\partial x}\right)_{s,p} = r(t) \rho_p Q_s - \lambda_g \left(\frac{\partial T}{\partial x}\right)_{s,g} \qquad \text{Energy balance at solid-gas interface}$$

$$\lambda_g \frac{d^2 T}{d x^2} + \rho_p r c_g \frac{dT}{dx} + Q_f \dot{\epsilon} \rho_g = 0 \qquad \text{Energy conservation in gas}$$

where T = temperature

$\lambda_{p,g}$ = thermal conductivity of solid propellant, gas

$\rho_{p,g}$ = density of solid propellant, gas

$c_{p,g}$ = specific heat of solid propellant, gas (at constant pressure)

$( )_{s,p}$ = evaluated at the solid propellant side of the solid-gas interface

$( )_{s,g}$ = evaluated at the gas phase side of the solid-gas interface

$Q_{s,f}$ = heat released at surface, in the flame

$\dot{\epsilon}$ = rate of product generation

$r(t)$ = burning rate

in the third of the above equations use has already been made of the quasi-steady gas phase assumption, which also implies that, in this equation, the burning rate r should be considered constant. In both the conventional and the direct methods, the third equation is then a steady-state gas phase energy balance. In the conventional method one then formulates a model for the steady-state gas flame and solves the third equation for dT/dx on the gas phase side of the solid-gas interface. This derivative

will be a function of r and p which appear both explicitly and through $\dot{\epsilon}$

$$\left(\frac{dT}{dx}\right)_{s,q} = \varphi(r,p)$$

Having this derivative and substituting it into the second equation one finds

$$\left(\frac{\partial T}{\partial x}\right)_{s,p} = \phi(r,p)$$

The first equation can now be solved for $r(t)$. Indeed the problem is now reduced to the solution of the heat equation given the boundary conditions at the solid-gas interface ($\phi = \phi(r,p)$) and at infinity on the solid side (T_∞). For any given value of t there will be a value of r which satisfies both the first equation and its boundary conditions and the desired $r = r(t)$, given $p = p(t)$, is thus determined. Notice that in the actual application of the conventional method experimental results connecting the steady-state burning rate to the pressure for a given propellant temperature (T_∞) are actually used to supplement the lack of information about the actual steady-state flame structure[32]. Thus, even in the conventional approach an experimental function of the type $r = r(p, T_\infty)$ is used. Zel'dovich proposed to do away completely with the problem of the steady-state flame structure and to determine the steady-state ϕ-function by an additional set of steady state measurements. In steady state ϕ can be expressed as

$$\phi = \frac{r}{\lambda_p / \rho_p c_p}\,(T_s - T_\infty)$$

where T_s is the burning surface temperature and T_s and T_∞ can be eliminated in favor of p, r if, besides measuring $r = r(p, T_\infty)$ one also measures $r = r(T_s, p)$.

Thus, the "direct" use of measured quantities splits the problem of unsteady solid propellant burning and its quasi-steady gas flame into two problems which can be analysed separately (Splitting Property). On one hand there is the problem of the unsteady burning of the solid propellant which can be studied independently of any gas flame model and on the other hand there is the problem of the structure of the gas flame which could also be studied using the experimentally determined $\phi = \phi(x,t)$ (but this part of the study does not seem to have been performed). However, in this particular case the equations are split also in the conventional approach due to the quasi-steady gas phase assumption. Most important, in the direct approach, the assumptions have been split. This solution of the problem of unsteady solid propellant burning is not subject to the validity of the flame model but only to the assumption of quasi-steady gas phase (Assumption Splitting). If the results obtained with the direct approach of Zel'dovich were found to be in disagreement with further experimental data (say, of stability of the solid propellant combustion) one would have either to declare the quasi-steady gas phase assumption incorrect, or check into the accuracy of the measured $\phi = \phi(x,t)$ since only basic equations were used (Experimental Data Check). This particular application of the direct method is one in which the maximum information property of the direct approach is well exemplified. The complete problem consists of both solid and gas phases and a complete model would require not only the solution of the heat equation in the solid, but also the determination of the flame structure in the gas. Thus, after having gone through the

first two steps of the direct approach (namely i) collection of experimental data ii) solution of basic equations using directly experimental data) one should go to the third and last step of determining a complete model. But even before going through the third step (i.e., while the structure of the flame is still unknown) a wealth of information of practical use on stability, ignition, reignition, etc. of solid propellants has become accessible simply through the study of the restricted solution (as in the case of the steady-state combustion of the LOX/ethanol system). Some of these studies have recently been collected into a single publication[33] which should become available in 1970.

REFERENCES

1. Edwards, D. H., "A Survey of Recent Work on the Structure of Detonation Waves; 12th Symposium on Combustion," The Combustion Institute, Pittsburgh, Penna., 1969.

2. Zel'dovich, I. G. and Kompaneets, A. S., "Theory of Detonation," Academic Press, New York, 1960.

3. Lewis, B. and Von Elbe, G., "Combustion, Flames and Explosions of Gases," Academic Press, New York, 1961.

4. Gordon, W. E., "Pressure Measurements in Gaseous Detonation by Means of Piexoelectric Gauges," 3rd Symposium on Combustion, Williams and Wilkins, Baltimore, Md., 1949.

5. Campbell, Littler and Whitworth: Proc. Roy. Soc. (London) 137, 380, 1932.

6. Dremin, A. N., Zaitzev, V. M., Ilyukhin, V. S. and Pokhil, P. F., "Detonation Parameters," 8th Symposium on Combustion, Williams and Wilkins, Baltimore, Md., 1962.

7. Mac Dougall, D. P., Messerley, C. H., Hurwitz, M. D., et al, "The Rate of Detonation of Various Explosive Compounds and Mixtures," OSRD-564; see also Urizar, M. J., et al, Physics of Fluids, 4, 2, 262, 1961.

8. Taylor, G. I., Tankin, R. S., "Gas Dynamical Aspects of Detonation: CP 3 of High Speed Aerodynamics and Jet Propulsion," Emmons, H. W., Editor, Princeton University Press, 1955.

9. Williams, F. A., "Combustion Theory," Addison-Wesley, Rading, Mass., 1965.

10. Von Neumann, J., "Theory of Detonation Waves," O.S.R.D. Report 549, 1942.

11. Brinkley, S. R. and Richardson, J. M., "On the Structure of Plane Detonation Waves with Finite Reaction Velocity," 4th Symposium on Combustion, Williams and Wilkins, Baltimore, Md., 1953.

12. Kirkwood, J. G. and Wood, W. W., "Structure of a Stead-State Plane Detonation Wave with Finite Reaction," Rade, J. of Chem. Physics, 22, 11, 1915, 1954.

13. Wood, W. W. and Salsburg, Z. W., "Analysis of Steady-State Supported One Dimensional Detonations and Shocks," The Physics of Fluids, 3, 4, 549, 1960.

14. Jones, H. and Miller, A. R., "The Detonation of Solid Explosives," Proc. Roy, Soc. London A194 (480-507) 1948.

15. Taylor, J., "Detonation in Condensed Explosives," Oxford University Press, 1952.

16. Cook, M. A., J. Chem. Physics 15, 518, 1947; 16, 1081, 1948.

17. Lutzky, M., "The Flow Field Behind a Spherical Detonation in TNT using LSZK Equation of State; NOL TR 64-40, 1964.

18. Bracco, F. V., "Chemical and Dynamic Aspects of Propellant Explosions," Wyle Laboratories Report WR 66-42, 1966.

19. Williams, F. A., "Combustion Theory," Addison-Wesley, 1965.

20. Campbell, D. T. and Chadwich, W. D., "Combustion Instability Analysis at High Chamber Pressure," Technical Report AFRPL-TR-68-179, 1968.

21. Crocco, L. and Cheng, S., "Theory of Combustion Instability in Liquid Propellant Rocket Motors," AGARDograph No. 8, Butterworths SC Pub., 1956.

22. Ranz, W. E. and Marshall, W. R., "Evaporization from Drops," Part One: Chem. Eng. Prog., Vol. 48, No. 3, 1952, Part Two: Chem. Eng. Prog., Vol. 48, No. 4, 1952.

23. Priem, R. J. and Heidmann, M. F., "Propellant Vaporization as a Design Criterion for Rocket-Engine Combustion Chambers," NASA TR R-67, 1960.

24. Spalding, D. B., "The Combustion of Liquid Fuels," 4th Symposium on Combustion, Williams and Wilkins, 1953.

25. Bevans, R. S., "Mathematical Expressions for Drop Size Distributions in Sprays," Conference of Fuel Sprays, University of Michigan, Ann Arbor, Mich., 1949.

26. Ingebo, R. D., "Drop Size Distributions for Impinging-Jet Break-up in Air Streams Simulating Velocity Conditions in Rocket Combustors," NACA TN-4222, 1958.

27. Ingebo, R. D., "Photomicrographic Tracking of Ethanol Drops in a Rocket Chamber Burning Ethanol and Liquid Oxygen, NASA TN D-290, 1960.

28. Rabin, E. A., et al, "The Motion and Shattering of Propellants Droplets," AFOSR TN-60-59, 1960.

29. Eisenklam, S. A., et al, "Evaporation Rates and Drag Resistance on Burning Drops," 11th Combustion Symposium, 1966.

30. Summerfield, M., et al, "Relation Between Temperature Sensitivity and Dynamic Burning Rate of a Solid Propellant," Post-Session Paper prepared for Aerospace Sci. Meeting, AIAA, New York, January 1970.

31. Zel'Dovich, Va. B., "The Theory of Burning of Powders and Explosives," Journal of Exper. and Theor. Physics, Vol. 12, issues 11-12, 1942.

32. Merkle, C. L., Turk, S. L. and Summerfield, M., "Extinguishment of Solid Propellants by Rapid Depressurization," Princeton University, AMS Report No. 880, July 1969.

33. Librovich, V. B., Lectures presented at Princeton University (Dec. 1969-Jan. 1970) on the "Theory of Unsteady Flames," to be published by Academic Press.

34. Tsuji, H. and Takeno, T., "Propagation of Pressure Waves in High-Frequency Combustion Oscillations," AIAA Journal, Vol. 6, No. 4, April 1968.

APPENDIX A: ONE DIMENSIONAL CONSERVATION EQUATIONS

Consider a fluid made up of gaseous reaction products and drops of liquid fuel and oxidizer. If one assumes that:

1) It is sufficient to consider some average velocities for the two liquids
2) Negligible friction and heat transfer effects
3) The volume of the liquids is negligible

Then the following conservation equations can be written

$$\frac{\partial}{\partial t}\left(\rho+\rho_F+\rho_\phi\right)+\frac{\partial}{\partial x}\left(\rho u+\rho_F u_F+\rho_\phi u_\phi\right)=0$$

$$\frac{\partial}{\partial t}\left(\rho u+\rho_F u_F+\rho_\phi u_\phi\right)+\frac{\partial}{\partial x}\left(\rho u^2+\rho_F u_F^2+\rho_\phi u_\phi^2+p\right)=0$$

$$\frac{\partial}{\partial t}\left[\rho\left(e+\frac{u^2}{2}+h^\circ\right)+\rho_F\left(\Lambda_F+\frac{u_F^2}{2}+h_F^\circ\right)+\rho_\phi\left(\Lambda_\phi+\frac{u_\phi^2}{2}+h_\phi^\circ\right)\right]+$$

$$+\frac{\partial}{\partial x}\left[\rho u\left(e+\frac{u^2}{2}+h^\circ\right)+\rho_F u_F\left(\Lambda_F+\frac{u_F^2}{2}+h_F^\circ\right)+\rho_\phi u_\phi\left(\Lambda_\phi+\frac{u_\phi^2}{2}+h_\phi^\circ\right)+pu\right]=0$$

The steady-state equations of Section 3.2 are obtained from the previous ones after integrating them from the injector to any station

$$\rho u=-\left[w_F-w_{oF}+w_\phi-w_{o\phi}\right]$$

$$\rho u^2=-\left[p-p_0+w_F u_F-w_{oF}u_{xF}+w_\phi u_\phi-w_{o\phi}u_{x\phi}\right]$$

$$\rho u\left(h+\frac{u^2}{2}\right)=-\left[w_F\left(\Lambda_F+\frac{u_F^2}{2}+h_F^\circ\right)-w_{oF}\left(\Lambda_{oF}+\frac{u_{oF}^2}{2}+h_F^\circ\right)\right.$$
$$\left.+w_\phi\left(\Lambda_\phi+\frac{u_\phi^2}{2}+h_\phi^\circ\right)-w_{o\phi}\left(\Lambda_{o\phi}+\frac{u_{o\phi}^2}{2}+h_\phi^\circ\right)\right]$$

If one assumes that the temperature of the liquids go instantaneously from their injection temperatures ($T_{o_{F,\phi}}$) to their wet bulb temperatures relative to some average chamber pressure ($T_{v_{F,\phi}}$), he would then get for $\Lambda_{o_{F,\phi}}$, $\Lambda_{F,\phi}$ the following expressions

$$\Lambda_{o_{F,\phi}} = -\left[c\,(T_v - T_o) + \lambda + c_b\,(T^\circ - T_v)\right]_{F,\phi} = -\left[\lambda^\circ + c\,(T^\circ - T_o)\right]_{F,\phi}$$

$$\Lambda_{F,\phi} = -\left[\qquad\qquad \lambda + c_b\,(T^\circ - T_v)\right]_{F,\phi} = -\left[\lambda^\circ + c\,(T^\circ - T_v)\right]_{F,\phi}$$

thus recovering the equations of Section 3.2.

Some considerations on the constancy of the steady-state latent stagnation enthalpy of the gas can be made rewriting the previous energy equation as follows[21]

$$e + \frac{p}{\rho} + \frac{u^2}{2} = -\left[h^\circ + \frac{\dot{w}_F}{\rho u}\left(\Lambda_F + \frac{u_F^2}{2} + h_F^\circ\right) - \frac{\dot{w}_{oF}}{\rho u}\left(\Lambda_{o_F} + \frac{u_{oF}^2}{2} + h_F^\circ\right) + \right.$$

$$\left. + \frac{\dot{w}_\phi}{\rho u}\left(\Lambda_\phi + \frac{u_\phi^2}{2} + h_\phi^\circ\right) - \frac{\dot{w}_{o\phi}}{\rho u}\left(\Lambda_{o_\phi} + \frac{u_{o\phi}^2}{2} + h_\phi^\circ\right)\right]$$

Where the left hand side is the latent stagnation enthalpy of the gas and the right hand side can be called the energy source for the gas. This source would be the energy actually made available to the gas, i.e., the chemical energy released minus the energy taken up by the vaporization processes and the kinetic energy of the liquids. Setting $\left(\Lambda_F + \frac{u_F^2}{2}\right) = \left(\Lambda_{o_F} + \frac{u_{oF}^2}{2}\right)$ and $\left(\Lambda_\phi + \frac{u_\phi^2}{2}\right) = \left(\Lambda_{o_\phi} + \frac{u_{o\phi}^2}{2}\right)$ (which means that the energy taken up by the unit weight of liquid, to warm up and vaporize and move, is constant with x) the previous equation gives

$$e + \frac{p}{\rho} + \frac{u^2}{2} = -\left[h^\circ + \frac{(\dot{w}_F - \dot{w}_{oF})}{\rho u}\left(\Lambda_{o_F} + \frac{u_{oF}^2}{2} + h_F^\circ\right) + \frac{(\dot{w}_\phi - \dot{w}_{o\phi})}{\rho u}\left(\Lambda_{o_\phi} + \frac{u_{o\phi}^2}{2} + h_\phi^\circ\right)\right]$$

which shows that the latent stagnation enthalpy of the gas is

constant with x when the vaporization process is such that at any distance from the injector, equal fractions of the two propellants have vaporized. In this case one could set

$$\frac{w_F - w_{oF}}{w_{oF}} = \frac{w_\phi - w_{o\phi}}{w_{o\phi}} = \alpha(x) \quad \Rightarrow \quad \rho u = -(w_{oF} + w_{o\phi})\,\alpha(x)$$

and the previous equation becomes

$$e + \frac{p}{\rho} + \frac{u^2}{2} = -\left[h^\circ - \frac{w_{oF}}{w_{oF} + w_{o\phi}}\left(\Lambda_{oF} + \frac{u_{oF}^2}{2} + h_F^\circ\right) - \frac{w_{o\phi}}{w_{oF} + w_{o\phi}}\left(\Lambda_{o\phi} + \frac{u_{o\phi}^2}{2} + h_\phi^\circ\right)\right]$$

and h° would be constant, since the composition of the gases is constant, $h_{F,\phi}^\circ$ are constant by definition and $\left(\Lambda + \frac{u_{o\phi}^2}{2}\right)_{F,\phi}$ are constant by assumption. Another case in which the latent stagnation enthalpy of the gas would be constant is when both h° = const. and $\left(\Lambda_F + \frac{u_F^2}{2} + h_F^\circ\right) = \left(\Lambda_{oF} + \frac{u_{oF}^2}{2} + h_F^\circ\right) = \left(\Lambda_\phi + \frac{u_\phi^2}{2} + h_\phi^\circ\right) = \left(\Lambda_{o\phi} + \frac{u_{o\phi}^2}{2} + h_{o\phi}^\circ\right)$ = const. in general, however, the latent stagnation enthalpy of the gas can be expected to change with the distance from the injector even in steady state.

The steady state energy equation as used in the actual numerical computations, was written in a slightly different form. This alternative way isolates the chemical energy released rather than the net energy source for the gas

$$\rho u\left(e + \frac{p}{\rho} + \frac{u^2}{2}\right) = -\left\{\left[\rho u h^\circ + (w_F - w_{oF})h_F^\circ + (w_o - w_{o\phi})h_\phi^\circ\right] + \right.$$

$$\left. + w_F\left(\Lambda_F + \frac{u_F^2}{2}\right) - w_{oF}\left(\Lambda_{oF} + \frac{u_{oF}^2}{2}\right) + w_\phi\left(\Lambda_\phi + \frac{u_\phi^2}{2}\right) - w_{o\phi}\left(\Lambda_{o\phi} + \frac{u_{o\phi}^2}{2}\right)\right\}$$

where the term in brackets is the chemical energy released (difference between the enthalpy of formation of the products and that of the reactants) part of which goes to warm up, vaporize and move the liquids but most of which acts as energy source for the gas.

This term was replaced by $-\rho u \varphi^0$ where φ^0 is given by

$$\varphi^0 = -\frac{4.186\ 10^{10}}{m_{em}}\left[\sum_{i=1}^{8} X_i (H^0_{298})_i - (H^0_{298})_F - z(H^0_{298})_\phi\right]$$

To verify the equivalency between the two expressions for the term in brackets, one recalls the definitions of m_{em} and z

$$\left.\begin{aligned} m_{em} &= m_F + z m_\phi \\ z &= \frac{m_F (w_{0\phi} - w_\phi)}{m_\phi (w_{0F} - w_F)} \end{aligned}\right\} \Rightarrow m_{em} = m_F \frac{(w_{0F} - w_F) + (w_{0\phi} - w_\phi)}{(w_{0F} - w_F)} = \frac{\rho u}{(w_{0F} - w_F)/m_F}$$

and substitutes them in the definition of φ^0

$$-\rho u \varphi^0 = \rho u \frac{4.186\ 10^{10}}{m_{em}} \sum_{i=1}^{8} X_i (H^0_{298})_i - \rho u \frac{4.186\ 10^{10}}{m_{em}} (H^0_{298})_F - \rho u \frac{4.186\ 10^{10}}{m_{em}} z (H^0_{298})_\phi$$

$$= \rho u h^0 - \rho u \frac{4.186\ 10^{10}}{\rho u m_F} (w_{0F} - w_F) \sum_i (H^0_{298})_i - \rho u \frac{4.186\ 10^{10}}{\rho u m_F} (w_{0\phi} - w_\phi) \frac{m_F}{m_\phi} \frac{(w_{0\phi} - w_\phi)}{(w_{0F} - w_F)} (H^0_{298})_\phi$$

$$= \rho u h^0 + (w_F - w_{0F}) h^0_F + (w_\phi - w_{0\phi}) h^0_\phi$$

Thus the steady state energy equation can now be written as

$$\rho u \left(e + \frac{p}{\rho} - \varphi^0 + \frac{u^2}{2}\right) = -\left[w_p \left(\Lambda_p + \frac{u_p^2}{2}\right) - w_{0F} \left(\Lambda_{0F} + \frac{u_{0F}^2}{2}\right) + w_\phi \left(\Lambda_\phi + \frac{u_\phi^2}{2}\right) - w_{0\phi} \left(\Lambda_{0\phi} + \frac{u_{0\phi}^2}{2}\right)\right]$$

for the numerical computations the following definitions were further introduced

$$e + \frac{p}{\rho} = \frac{4.186\ 10^{10}}{m_{em}} \left\{\sum_{i=1}^{8} X_i \int_{T_0}^{T} C_{p_i}(T)\, dT\right\}$$

$$Q_{F,\phi} = \left[\left(\lambda^0 + C(T^0 - T_0) - \frac{w}{w_0}\left(\lambda^0 + C(T^0 - T_V)\right)\right]_{F,\phi}\right.$$

$$H_{\phi T} = -w_{0F} \frac{u_{0F}^2}{2} - w_{0\phi} \frac{u_{0\phi}^2}{2} + w_F \frac{u_F^2}{2} + w_\phi \frac{u_\phi^2}{2}$$

By which the energy equation, as used in the numerical computations, is obtained

$$\rho u \frac{4.186\ 10^{10}}{m_{cm}} \left[\sum_{i=1}^{8} X_i \left(\int_{T^o}^{T} C_{p_i}(T)\,dT + \left(H^o_{298}\right)_i \right) - \right.$$

$$\left. - \left(H^o_{298}\right)_F - 2\left(H^o_{298}\right)_{\phi} \right] + W_{o_F} Q_F + W_{o_\phi} Q_\phi + H\phi T + \frac{\rho u^3}{2} = 0$$

APPENDIX B: COMMENTS ON THE DROP VAPORIZATION RATE EQUATIONS

In the first section of this appendix, the origin of the vaporization rate equations used in this study is briefly summarized and the theoretical values of their coefficients are compared with the values which gave satisfactory results for the engine under consideration. In the second section, some conclusions are offered.

1.0 The following vaporization rate equation was studied

$$R = \frac{dr}{dt} = -\frac{\dot{m}}{4\pi\rho_L r^2} = -\frac{K}{8r}\left[1 + g\,Re^{q}\right] \qquad 1, g, q = \text{constants}.$$

$$Re = 2\rho r |u - u_d| / \mu$$

Actually only several particular cases of the above equation were studied. The following four cases were then selected as sufficiently representative and studied in more detail

$$R = -K_1 / 8r \tag{1a}$$

$$R = -K_2\left[1 + .276\, Pr^{1/3} Re^{1/2}\right] / 8r \tag{1b}$$

$$R = -K_3\, Re^{1/2} / 8r \tag{1c}$$

$$R = -K_4\, Re / 8r \tag{1d}$$

Equation 1a. This equation in the form

$$\dot{m} = \frac{4\pi\lambda r}{c_p} \ln\left\{1 + \frac{1}{L}\left[c_p (T_\infty - T_L) + \frac{q}{i} Y_{0,\infty}\right]\right\} \tag{2}$$

in which case

$$K_1 = \frac{8\lambda}{\rho_L c_p} \ln\left\{1 + \frac{1}{L}\left[c_p (T_\infty - T_L) + \frac{q}{i} Y_{0,\infty}\right]\right\} \tag{3}$$

can analytically be derived under the following assumptions[9]:

One dimensional, spherically symmetric system, no forced convection.

Steady state.

No oxidizer on the surface of drop.

Constant and uniform drop temperature (equal to the boiling temperature).

No fuel in the ambient atmosphere.

$\rho D = \lambda/c_p$ = constant (L_e = Const and ρD independent of drop distance).

The burning rate given by this equation was found to agree well (within a factor of 2 for K_1) with measured burning rates, in controlled experiments (mostly in ambient air). The parameter K_1 was found[9] to be of the order of 10^{-2} cm^2/sec. K_1 , for the engine under consideration, near the injector (say at 4") where there is plenty of hot gaseous oxygen (say $Y_{O_2 \infty} = .9$; $T_\infty = 2000^\circ K$) and the relative velocity is small, is now evaluated. It is set

$\bar{q}$ = 6630 cal/g (Heat of reaction per unit mass of fuel vapor)

[The reaction under consideration is:

$$C_2H_5OH + 3O_2 \rightarrow 3H_2O + 2CO_2$$

Then the heat of reaction per mole of C_2H_5OH is:
3(57.798) +2(94.04) - 56.24 = 305 Kcal/mole
Hence $\bar{q}$ = (305 000 cal/mole)/46 g/mole = 6630 cal/g]

i = 2.09 $g_{oxidizer}/g_{fuel}$ (stoichiometric mixture ratio)

[$i = m_{ox} X_{ox_{STOICH}} / m_F X_{F_{STOICH}} =$ 32x3/46x1 = 2.09]

c_p = .34 cal/g $^\circ K$ (Specific heat)

[Computer Calculated for the engine under consideration at 4"]

T_∞ = 2000 °K

[Computer calculated for the engine under consideration at 4"]

λ = $1.2\ 10^{-4}$ cal/cm sec °K (Thermal conductivity)

[Evaluated at 1500°K (see Lorell, J., Wise, H., Carr, R. E., J. Chem. Phys. 25, 325 (1956)]

ρ_L = .8 g/cm^3 (fuel density)

L = 136 cal/g (Latent heat of vaporization per unit mass of fuel @ p = 300 psi)

T_L = 454°K (Liquid temperature = boiling temperature @ p = 300 psi)

$Y_{O,\infty}$ = .9

from which one can evaluate K_1 to find: $K_1 = 1.15\ 10^{-2}$ cm^2/sec. The comparison with the K's and K^*/ρ's (evaluated at 4" where $\rho = 3.4810^{-3}$ g/cm^3) which gave the best agreement between the calculated and the directly determined W_F / W_{OF}, for the various drag coefficients, is given in Table VI. The agreement is seen to be satisfactory. Notice, however, that a vaporization rate equation of the form $d_s/dt = -K/8_s$, which does not include any forced convection effect, is not very realistic for the engine under consideration where R_e is of the order of 100 even in the case of high drag (low relative velocity).

Equation 1b. This equation was proposed by Ranz and Marshall[22] who found it to correlate well with vaporization rates in conduction and forced convection experiments ($0 \leq R_e \leq 200$) but without combustion. They used drops of various liquids in air at temperatures up to 220°C

	u_{e_0}	r_0	C_D	1 K_1/δ^2	2 $K_2[1+.28\,k_c^{1/2}]/\delta^2$	3 $K_3 k_c^{1/2}/\delta^2$	4 $K_4 k_c/\delta^2$	5 $K_1^*/\rho\delta^2$	6 $K_2^*[1+.28\,k_c^{1/2}]/\rho\delta^2$	7 $K_3^* k_c^{1/2}/\rho\delta^2$	8 $K_4^* k_c/\rho\delta^2$
A	Uniform	Uniform	0.0	$1.0\ 10^{-2}$	$1.8\ 10^{-3}$	$5.5\ 10^{-4}$	$3.6\ 10^{-5}$	$.95\ 10^{-2}$	$1.15\ 10^{-3}$	$4.6\ 10^{-4}$	$2.59\ 10^{-5}$
B	Uniform	Uniform	$< 24/k_c$	-	-	-	-	-	-	-	-
C	Uniform	Uniform	$24/k_c$	$1.0\ 10^{-2}$	$2.5\ 10^{-3}$	$8\ 10^{-4}$	$6\ 10^{-5}$	$.95\ 10^{-2}$	$1.96\ 10^{-3}$	$6.6\ 10^{-4}$	$4.6\ 10^{-5}$
D	Uniform	Uniform	$> 24/k_c$	-	-	-	-	-	-	-	-
E	Uniform	Distributed	0.0	$1.0\ 10^{-2}$	$1.8\ 10^{-3}$	$5.5\ 10^{-4}$	$3.6\ 10^{-5}$	-	$1.15\ 10^{-3}$	-	-
F	Uniform	Distributed	$< 24/k_c$	-	-	-	-	-	-	-	-
G	Uniform	Distributed	$24/k_c$	$1.0\ 10^{-2}$	$2.5\ 10^{-3}$	$8\ 10^{-4}$	$6\ 10^{-5}$	$.95\ 10^{-2}$	$1.96\ 10^{-3}$	$6.6\ 10^{-4}$	$4.6\ 10^{-5}$
H	Uniform	Distributed	$> 24/k_c$	-	$3\ 10^{-3}$	-	-	-	$2.87\ 10^{-3}$	$1.15\ 10^{-3}$	-
Theoretical Values of K or K^*/ρ				$1.15\ 10^{-2}$	$1.15\ 10^{-2}$	$1.45\ 10^{-2}$	-	$1.15\ 10^{-2}$	$1.15\ 10^{-2}$	$1.45\ 10^{-2}$	-

TABLE VI COMPARISON BETWEEN THE K'S AND K^*/ρ'S (EVALUATED AT 4"), AND THEIR CORRESPONDING THEORETICAL VALUES. THE UNITS OF K AND K^*/ρ ARE: cm^2/sec.

with $300\mu \leq r \leq 555\mu$ and the temperature of the drops was close to the wet bulb temperature. The term $.276\ P_r^{1/3} Re^{1/2}$ (actually $.3\ Sc^{1/3} Re^{1/2}$)[9,22] was intended to be a correction factor due to the forced convection to be added to the pure conduction vaporization coefficient. Thus, according to this theory $K_2 = K_1 = 1.15\ 10^{-2}$ cm^2/sec. From the results of Table VI one concludes that the theoretical vaporization rate coefficient is roughly five times higher than the experimental one (the combustion chamber length calculated with the theoretical vaporization rate coefficient would have been roughly five times shorter than the actual one). This vaporization rate equation is herein referred to as the Priem and Heidmann[23] equation since they introduced it in the liquid propellant engine problem after having modified it to account for the difference between the chamber pressure and the liquid drop vapor pressure.

Equation 1c. Spalding[24], using stationary porous spheres (mostly of 1" diameter) and moving air at room temperature found that the following vaporization rate equation fitted satisfactorily his measurements ($800 \leq Re \leq 4000$)

$$\frac{\dot{m}'}{\mu} = .53\left[\frac{c_p (T_\infty - T_s)}{L} + \frac{\bar{q}}{i_L} Y_{o,\infty}\right]^{3/5} Re^{1/2} \qquad (4)$$

In this equation $\dot{m}'$ is "taken to be the mean rate of mass transfer per unit area times the diameter" thus

$$\dot{m}' = \frac{1}{4\pi r^2}\, \dot{m}\, 2r$$

and

$$K_3 = \frac{.53\,\mu\, 4}{\rho_L}\left[\frac{c_p (T_\infty - T_s)}{L} + \frac{\bar{q}}{i_L} Y_{o,\infty}\right]^{3/5} \qquad (5)$$

And using the coefficients previously given (and $\mu = 8\ 10^{-4}$ g/cm sec)*, one finds $K_3 = 1.45\ 10^{-2} cm^2/sec$ which is more than one order of magnitude larger than that giving the best agreement between the computed and the directly determined W_F / W_{0F} .

Equation 1d. This equation could be visualized as representing a vaporization rate even more strongly affected by forced convection than the previous ones.

It might be worth noting that the same K's and K''/ρ's gave the best results in both the uniform and the distributed drop radii cases (see Table VI and recall that in the uniform drop case $t_0 = 5\ t_{30}/3.915$, i.e., the drop group in which most of the mass is concentrated was used), thus indicating again that the use of the distribution function does not change substantially the nature of the results. Also one should notice that the calculations show that in order to obtain good agreement with the directly determined W_F / W_{0F}, the factor multiplying, for example, $[\ 1 + .3\ P_2^{1/3}\ \rho_2^{1/2}\ ]$ shouldn't be constant but actually should increase with x starting, say, with a value of $2.5\ 10^{-3}$ cm^2/sec at 4".

---

*A constant viscosity coefficient of $8\ 10^{-4}$ g/cm sec for the combustion products was used throughout the computations. The range of temperature of greatest interest is $2000^{\circ}K \leq T \leq 3200^{\circ}K$ so that the viscosity coefficient can be expected to vary by $(3.2/2)^{1/2} = 1.264$ or approximately 11.5% from its average value. Moreover, if the varying composition of the combustion gas is taken into account (as $T=2027^{\circ}K$ the calculated main gas products are (mole fractions): O_2(65%), CO_2(13.9%), H_2O(20.9%); while at $T=3174^{\circ}K$: CO (25.7%), CO_2(12.7%), H_2O(44%)) one finds that the viscosity coefficient is $7.10 \leq \mu \leq 8.40\ 10^{-4}$ g/cm sec with a slightly smaller variation than that predicted by the square root temperature dependence. A value $\mu = 8\ 10^{-4}$ g/cm sec was then selected because the higher temperature region is of higher interest. It was not judged necessary to consider a varying μ due to the presence of more far reaching uncertainties about the drag and vaporization models. Similarly the specific gravity (ρ_L) of the liquid fuel was kept constant and equal to .7 g/cm^3.

The theoretical value of this factor on the contrary would start from a higher value of 1.15 10^{-2} cm^2/sec and probably decrease with x . This is because, in equation 3, the factor $q\, Y_{o,\infty}/i$ probably decreases more rapidly than the factor $c_p (T_\infty - T_L)$ increases (but the value to be assigned to $Y_{o,\infty}$ becomes quite arbitrary). Thus the overall burning rate, calculated with the theoretical K , would be much too high near the injector and much too low far from it.

2.0 The main reason for briefly reviewing the origin of the vaporization rate equations which were used, is to emphasize that both the theoretical conditions under which they were derived, and the experimental conditions under which they were verified, are indeed quite different from those occurring in rocket engines. Composition, temperature, density, etc. of the gases within which a drop burns in an engine change considerably within the life time of the drop and so do the relative velocity and the Reynold's number. Even after accepting the assumption of quasi-steady droplet burning one still does not have enough experimental data to check the validity of the burning rate equations corresponding to the entire range of situations to which a drop is exposed in an actual engine.

It is then reasonable to conclude that the vaporization rate Equations 1a, 1b, 1c and 1d are to be interpreted more as possible functional forms to be tried out in an engine, than as exact, or even approximate, relationships. This is to justify the freedom which was used in these calculations in the definition of the k's and $k/_f$'s. This also helps emphazing the need for stability studies

to be based on vaporization rate equations whose capability of giving correct steady state results have been checked. Thus, while the theoretical coefficient of burning rate Equation 1a was found to be of the correct order of magnitude for the engine under consideration, that of burning rate Equation 1c was more like one order of magnitude off.

It should also be pointed out that these calculations show that the "right order of magnitude" of the vaporization rate coefficient will roughly lead to the estimate of the "right order of magnitude of the combustion length" and this, in general, can hardly be considered sufficient.

APPENDIX C: INITIAL DROP DISTRIBUTION FUNCTION

In the first section of this appendix the terminology of the distribution function is reviewed. In the second section the selection of the particular distribution function used in this study is justified.

1.0 In this section the paper of Bevans[25] is closely followed. Having a group of drops of different sizes (photo of a spray) one may consider

Total Number (N_T),
Total Volume (R_{v_T}),
Total Mass (R_{m_T}) = ρ_L (R_{v_T}).

Then one may be interested in:

(N) = total number of drops which have diameters larger than D,

(R_v) = total volume of the drops which have diameters larger than D,

(R_m) = total mass of the drops which have diameters larger than D,

where N, R_v, R_m are cumulative forms to express a districution.

[Notice that if one were interested in:

Number of drops which have diameters larger than D,

Volume of drops which have volumes larger than $\pi D^3/6$,

Mass of drops which have masses larger than $\rho_L \pi D^3/6$

he would come up with the same distribution function in all 3 cases since the number of drops with volume $> \pi D^3/6$ is equal to the number of drops with mass $> \rho_L \pi D^3/6$ and also equal to the number of drops with diameter > D]. Or one may be interested in:

$f_n dD = dN$ = number of drops with diameter between D and D + dD (out of the total number)

$f_v dD = dR_v$ = volume of drops with diameter between D and D + dD (out of the total number)

$f_M \, dD = dR_M$ = mass of the drops with diameter between D and D + dD (out of the total number)

where f_N, f_V, f_M are differential forms to express a distribution (equal to the derivatives of the corresponding cumulative forms).

Experimentally it has been found that the measured values of the f's (distribution functions) versus D are well correlated by a function of the form $a D^p e^{-\ell D^q}$

Thus, if one sets

$$f_N = \frac{dN}{dD} = a D^p e^{-\ell D^q} \tag{1}$$

then

$$f_V = \frac{dR_V}{dD} = a' D^{p+3} e^{-\ell D^q} \tag{2}$$

Since $f_N \, dD$ is the number of drops having diameter between D and D + dD and their volume f_V is $\frac{\pi}{6}\left(\frac{D+(D+dD)}{2}\right)^3 f_N \simeq \frac{\pi}{6} D^3 f_N$.

Finally

$$f_M = \rho_L f_V \tag{3}$$

Of the constants appearing in Equation 1, one can say that

- a depends on the size of the sample (since the number of drops with radius between D and D + dD will be dependent on the total number of drops)
- ℓ is related to the average drop size
- q is related to the spread around the average (high q → low spread)
- p is, in principle, arbitrary
- ℓ, q, p are interrelated.

Experimentally it is found that with $p=2$, $q=1$ (Nukiyama-Tanasawa) liquid sprays are often well correlated. If f_N, f_V, f_M, are

defined on the basis of a unit mass of liquid in the spray, then a is defined in terms of ℓ, q, p .

Averages: in general one can define averages by setting

$$\left(D_{JK}\right)^{J-K} = \frac{\int D^J \, dN}{\int D^K \, dN} = \frac{\int D^{J-3} \, dR_v}{\int D^{K-3} \, dR_v} \qquad \text{since } dR_v \propto D^3 dN$$

Two common averages are

$$D_{10} = \frac{\int D \, dN}{\int dN} = \frac{\text{sum of all diameters}}{\text{total no. of drops}} = \text{diameter - number mean}$$

$$D_{30} = \left(\frac{\int D^3 \, dN}{\int dN}\right)^{1/3} = \left(\frac{\text{sum of all volumes}}{\text{total no. of drops}}\right)^{1/3} = \text{volume - number mean}$$

D_{30}, equal to the diameter of the average drop volume, is usually used although the diameter of the average drop projected area (D_{20}) should be the one more easily measurable.

Expressing b in terms of D_{10}, D_{30}

Having

$$f_N = \frac{dN}{dD} = a D^2 e^{-\ell D}$$

$$\text{then } D_{10} = \frac{\int_0^\infty a D^3 e^{-\ell D} dD}{\int_0^\infty a D^2 e^{-\ell D} dD} = \frac{\int_0^\infty y^3 e^{-y} dy}{\ell \int_0^\infty y^2 e^{-y} dy} = \frac{3}{\ell} \Rightarrow \ell = \frac{3}{D_{10}} \qquad (4)$$

$$\text{also } D_{30} = \left[\frac{\int_0^\infty a D^5 e^{-\ell D} dD}{\int_0^\infty a D^2 e^{-\ell D} dD}\right]^{1/3} = \left[\frac{\int_0^\infty y^5 e^{-y} dy}{\ell^3 \int_0^\infty y^2 e^{-y} dy}\right]^{1/3} = \left(\frac{60}{\ell^3}\right)^{1/3} \Rightarrow \ell = \frac{3.915}{D_{30}} \qquad (5)$$

having recalled that $\int_0^\infty y^n e^{-y} dy = \Gamma(n+1) = n!$

and having set $y = \ell D$.

The same results are obtained from $f_v = \frac{dR_v}{dD} = a' D^5 e^{-\ell D}$

$$\text{since } D_{10} = \frac{\int_0^\infty a' D^3 e^{-\ell D} dD}{\int_0^\infty a' D^2 e^{-\ell D} dD} \Rightarrow \ell = \frac{3}{D_{10}}$$

$$\text{and } D_{30} = \left[\frac{\int_0^\infty a' D^5 e^{-\ell D} dD}{\int_0^\infty a' D^2 e^{-\ell D} dD}\right]^{1/3} \Rightarrow \ell = \frac{3.915}{D_{30}}$$

substitutions D_{10} and D_{30} in Equations 1, 2, and 3 (with $b=2$, $q=1$) one gets

$$f_N = a D^2 e^{-3\frac{D}{D_{10}}} = a D^2 e^{-3.915\frac{D}{D_{30}}} \tag{1b}$$

$$f_V = a' D^5 e^{-3\frac{D}{D_{10}}} = a' D^5 e^{-3.915\frac{D}{D_{30}}} \tag{2b}$$

$$f_M = \rho_L f_V \tag{3b}$$

The distribution functions $\begin{Bmatrix} f_N \\ f_V \\ f_M \end{Bmatrix}$ have so far been defined as fractions of $\begin{Bmatrix} \text{total number} \\ \text{total volume} \\ \text{total mass} \end{Bmatrix}$.

If one divides them by the $\begin{Bmatrix} \text{total number} \\ \text{total volume} \\ \text{total mass} \end{Bmatrix}$ he gets new distribution functions giving fractions of $\begin{Bmatrix} \text{unit number} \\ \text{unit volume} \\ \text{unit mass} \end{Bmatrix}$.

The total number is given by $\int_0^\infty dN = \int_0^\infty \frac{a}{\ell^3} y^2 e^{-y} dy = \frac{2a}{\ell^3}$ (7)

The total volume is given by $\int_0^\infty dR_V = \int_0^\infty \frac{a'}{\ell^6} y^5 e^{-y} dy = \frac{120 a'}{\ell^6}$ (8)

The total mass is ρ_L times the total volume, hence

$$\int_0^\infty dR_M = \frac{\rho_L 120 a'}{\ell^6} \tag{9}$$

finally dividing $\begin{Bmatrix} f_N \\ f_V \\ f_M \end{Bmatrix}$, from Equations $\begin{Bmatrix} 1b \\ 2b \\ 3b \end{Bmatrix}$, by Equations $\begin{Bmatrix} 7 \\ 8 \\ 9 \end{Bmatrix}$ and taking into account Equations 4 and 5, one gets:

$$f_N^* \begin{pmatrix} \text{fraction of} \\ \text{unit number} \end{pmatrix} = \frac{1}{2}\left(\frac{3.915}{D_{30}}\right)^3 D^2 e^{-3.915\frac{D}{D_{30}}} \tag{10}$$

$$f_v^* \left(\begin{matrix}\text{fraction of}\\ \text{unit volume}\end{matrix}\right) = \frac{1}{120}\left(\frac{3.915}{D_{30}}\right)^6 D^5 e^{-3.915\frac{D}{D_{30}}} \qquad (11)$$

$$f_n^* \left(\begin{matrix}\text{fraction of}\\ \text{unit mass}\end{matrix}\right) = \frac{1}{120\rho_L}\left(\frac{3.915}{D_{30}}\right)^6 D^5 e^{-3.915\frac{D}{D_{30}}} \qquad (12)$$

Equation 11 is the equation used by Ingebo[26,27]. This equation gives the volume of the drops with diameter between D and D+1 per unit drop volume (in other words, the volume of the drops with diameter between D and D+1 has been divided by the volume of all drops included in the sample see Table I of Reference 26).

2.0 The measurements of fuel drop distribution function made by Ingebo on a Lox/ethanol engine[26] (under firing conditions) and on sprays from impinging n-Heptane Jets in air streams[27], give us an unusually pertinent amount of information for the selection of the initial drop distribution function for the engine under consideration. In 1958, Ingebo, using n-Heptane impinging jets (90°) in air-streams, measured the drop distribution function at 8" from the impingement point over a specific range of orifice diameters (D_J), liquid jet velocity (V_J) and velocity difference (ΔV) (see Table I of Ingebo[26]). He found that the distribution function 11 correlated well his measurements, i.e.

$$f_v^* = \frac{dR_v^*}{dD} = \frac{1}{120}\left(\frac{3.915}{D_{30}}\right)^6 D^5 e^{-3.915\frac{D}{D_{30}}} \qquad \text{(Nukiyama-Tanasawa)} \quad (13)$$

Furthermore, he found the following correlation between D_{30}, D_J, V_J, and ΔV

$$\frac{D_J}{D_{30}} = 2.64\left(D_J V_J\right)^{1/2} + .97\, D_J\, \Delta V \qquad \begin{matrix}\text{Diameters in Inches}\\ \text{Velocities in}\\ \text{Feet/sec}\end{matrix} \qquad (14)$$

In the engine under consideration D_J = .059", V_J = 2540 cm/sec = 86.7 ft/sec, ΔV(@ 5") $\simeq$ 4000cm/sec = 130 ft/sec and Ingebo's correlation yields D_{30} = 111 μ . Directly from his table[26] for D_J = .06, V_J = 65 ft/sec and ΔV = 115 ft/sec, one reads D_{30} = 131 μ and D_{max} = 325 μ .

In 1960 in a Lox/ethanol firing engine, Ingebo[27] again found that the above distribution function correlated well the drop size measurements at 4" from the injector. The ethanol jets however were not impinging. He had V_J = 25 ft/sec, D_J = .032", $\Delta V \geq$ 80 ft/sec (estimated from the velocity of his smaller drops) which, applying his earlier correlation, would have given D_{30} = 167 μ . He measured D_{30} = 155 μ and D_{max} = 344 μ , which indicates that his cold flow correlation gives a reasonable estimate of D_{30} also under firing conditions and different impingement angle (provided the relative velocity is high enough).

Thus, it was concluded that, for the engine under consideration:

1) A Nukiyama-Tanasawa distribution function is likely to give a good description of the drop sizes near the injector (it will actually be used at the injector).

2) The maximum drop diameter is likely to be between 300 μ and 340 μ .

3) D_{30} is likely to be between 110 μ and 150 μ although this estimate might not be as accurate as the previous two.

Although a Nukiyama-Tanasawa distribution function was used, it was not used in the form given by Ingebo (Equation 13, i.e., volume of drops with diameter between D and D+1 divided by the

volume of all drops) but rather in the form 1b (number of drop with diameter between D and D+1 out of the total number of drops)

$$f_N = a D^2 e^{-3.915 \frac{D}{D_{30}}}$$

which was actually written as

$$f_0(0, r_0) = 4 B r_0^2 e^{-3.915 \frac{r}{r_{30}}} \qquad \begin{matrix} 55\mu \leq r_{30} \leq 75\mu \\ 150\mu \leq r_{max} \leq 170\mu \end{matrix} \qquad (15)$$

and f_0 is then the "total number of drops per unit length of the combustion chamber with radius between r and r+1" its dimensions are $1/cm^2$. The following expression will also be used

$$F(x, r) = \frac{f^2(x, r) \quad 10^{-3} \, 10^2}{\int_0^{r_{max}} f_0 \, dr}$$ = local (at x) percentage

of the initial (at x = 0) number of drops with radius between r and r + 10μ.

Finally the coefficient B, which is related to the total number of drops per unit length of combustion chamber at the injector, will have to be determined by proper conditions (see Appendix F).

APPENDIX D: SPRAY EQUATION

In the first section of this appendix, the spray equation is systematically simplified. In the second section, the vaporization rate is related to W_p/W_{b_F} for the case in which $f = f(x)$. In the third section, it is shown that $f = f(x)$ if $d(W_p/W_{b_F})/dx$ = constant.

1.0 The spray equation (see Williams[9]) can be written as follows

$$\frac{\partial f}{\partial t} = -\frac{\partial}{\partial r}(Rf) - \frac{\partial}{\partial x}(u_\ell f) - \frac{\partial}{\partial u_\ell}(Ff) + Q + \Gamma \tag{1}$$

where

a) only liquid fuel drops are considered

b) $f(r, x, u_\ell, t)\, dr\, dx\, du_\ell =$ total number of drops with radius between r and $r + dr$, with velocity between u_ℓ and $u_\ell + du_\ell$ in the engine length dx between x and $x + dx$, at time t. Hence the dimensions of f here are $(1/cm^3 \times cm/sec \times 1/cm)$.

c) $R = R(r, x, u_\ell, t) \equiv dr/dt =$ rate of change of r following a liquid drop.

d) $F = F(r, x, u_\ell, t) \equiv du_\ell/dt =$ force per unit mass acting on a liquid drop

e) $Q = Q(r, x, u_\ell, t) =$ the rate of increase of f due to drops formation (nucleation) or destruction (break up).

f) $\Gamma = \Gamma(r, x, u_\ell, t) =$ the rate of increase of f due to collisions.

Considering only steady state and neglecting nucleations, breakups, and collisions one gets

$$\frac{\partial}{\partial r}(Rf) + \frac{\partial}{\partial x}(u_\ell f) + \frac{\partial}{\partial u_\ell}(Ff) = 0 \tag{2}$$

where R = R (r, x, u_ℓ); F = F (r, x, u_ℓ); f = f (r, x, u_ℓ) and the dimensions of f are ($1/cm \times cm^2/cm \times 1/cm$).

If one assumes that, at any given x , all drops having a given r have the same velocity, he practically assumes that $u_\ell = u_\ell(x, r)$. He can then conceptually substitute this new $u_\ell = u_\ell(x, r)$ in the above expressions for R, F, f , thus getting

$$R(r, x, u_\ell(r, x)) = R(r, x)$$
$$F(r, x, u_\ell(r, x)) = F(r, x)$$
$$f(r, x, u_\ell(r, x)) = f(r, x)$$

and Equation 2 simplifies to

$$\frac{\partial}{\partial r}(Rf) + \frac{\partial}{\partial x}(u_\ell f) = 0 \qquad (3)$$

where R = R(r, x), f = f (r, x), and the dimensions of f are ($1/cm \times 1/cm$), $f\,dr\,dx =$ total number of drops with radius between r and $r + dr$ in the engine length dx between x and $x + dx$.

If one further assumes that, at any given x , all drops have a specific r and a specific u_ℓ , he practically assumes that $r = r(x)$ and $u_\ell = u_\ell(x)$. He can then conceptually substitute these new $r = r(x)$, $u_\ell = u_\ell(x)$ in the previous expressions for R and f and get

$$R(r(x), x) = R(x)$$
$$f(r(x), x) = f(x)$$

and Equation 3 simplifies to

$$\frac{d}{dx}(u_\ell f) = 0 \qquad (4)$$

where $f = f(x)$ and $u_\ell = u_\ell(x)$

and the dimension of f is (V_{cm}) and $f\,dx$ = total number of drops in the engine length dx between x and $x+dx$.

If one further assumes that u_ℓ is constant for all x's, i.e., $u_\ell = u_{\ell_0}$, the above equation then implies that f = const, i.e., the total number of drops in the unit engine length is constant.

2.0 The case in which $f = f(x)$, and $u_\ell = u_\ell(x)$ is now further considered. Equation 4 is then the spray equation. The proper way of calculating the local liquid fuel flow rate is to relate its local change to the local change of drop radius and to the local number of drops

$$\frac{d}{dx}\left(\frac{W_F}{W_{o_F}}\right) = \frac{1}{A\,W_{o_F}}\,4\pi r^2 \frac{dr}{dt}\,\rho_L\,f \tag{5}$$

However, consider the following function

$$\frac{W_F}{W_{o_F}} = \frac{1}{A\,W_{o_F}}\,\frac{4}{3}\pi r^3 \rho_L\,f\,u_\ell \tag{6}$$

and take its x-derivative

$$\frac{d}{dx}\left(\frac{W_F}{W_{o_F}}\right) = \frac{1}{A\,W_{o_F}}\,4\pi r^2 \frac{dr}{dx}\,\rho_L\,u_\ell\,f + \frac{1}{A\,W_{o_F}}\,\frac{4}{3}\pi r^3 \rho_L \frac{d}{dx}(u_\ell f)$$

then the derivative of Equation 6 is equal to Equation 5 since $u_\ell\,dr/dx \equiv dr/dt$ and $d(u_\ell f)/dx = 0$ because of Equation 4. Thus, the local liquid fuel flow rate calculated by Equation 6 is identical to that calculated by Equation 5 provided in both equations the same initial value is used. Thus, in this case Equation 6 can be used to evaluate the local liquid fuel flow.

Then using Equation 6 and applying it at any x and at $x = 0$,

one gets

$$\frac{\frac{W_F}{W_{OF}}}{1} = \frac{\frac{1}{A\,W_{OF}}\,\frac{4}{3}\pi r^3 \rho_L u_\ell f}{\frac{1}{A\,W_{OF}}\,\frac{4}{3}\pi r_0^3 \rho_L u_{\ell_0} f_0} = \frac{V u_\ell f}{V_0 u_{\ell_0} f_0}$$

but $u_\ell f = u_{\ell_0} f_0$ (Equation 4) thus

$$V = V_0 W_F / W_{OF}$$

and

$$r^3 = r_0^3 W_F / W_{OF}$$

and the drop vaporization rate is given by

$$R = \frac{dr}{dt} = u_\ell \frac{dr}{dx} = u_\ell \frac{r_0}{3}\left(\frac{W_F}{W_{OF}}\right)^{-2/3} \frac{d}{dx}\left(\frac{W_F}{W_{OF}}\right) \tag{7}$$

The above equation is valid for both the constant u_ℓ (no drag) and the varying u_ℓ cases, and directly gives the drop vaporization rate when the local liquid fuel flux is known as in the present case (Fig. 12).

3.0 A particular case of some interest is that in which

$$\frac{d}{dx}\left(\frac{W_F}{W_{OF}}\right) = \text{CONSTANT} \tag{8}$$

Fig. 12 shows that for the first 16" of the engine under consideration, the above relationship could justifiably be accepted (a similar trend was found in other engine configurations). One could then get from Equation 7

$$R = \frac{dr}{dt} \propto u_\ell \frac{r_0}{3}\left(\frac{r}{r_0}\right)^{-2} \propto \frac{u_\ell}{r^2} \Rightarrow \dot{m} = 4\pi r^2 \rho_L \frac{dr}{dt} \propto u_\ell$$

When Equation 8 applies, the distribution function must be a function of x only, and the above vaporization rate proportionalities must hold. In general one has

$$\frac{d}{dx}\left(\frac{W_F}{W_{OF}}\right) = \frac{1}{A\,W_{OF}} \iint 4\pi r^2 \rho_L R f \, dr \, du_\ell \qquad f = f(x, r, u_\ell)$$

For this integral to be constant for all x's, either the integrand is zero or

$$f(x, u_e, r) = f^{**}(x, u_e, r)\, \delta(t - r^*)\, \delta(u_e - u_e^*)$$

in which case the above integral is equal to

$$4\pi r^{*2}(x)\, R(x, u_e^*(x), r^*(x))\, f^{**}(x, u_e^*(x), r^*(x)) \qquad (9)$$

since the integrand is zero for all values of r and u_e except for r^* and u_e^* which can still be different at different x's. It then follows that $f = f(x)$. Furthermore, for Expression 9 to be constant one must have

$$R = \frac{dr}{dt} \propto \frac{1}{r^2 f}$$

But in the case in which $f = f(x)$, as in this case, it has already been shown that $u_e f = u_{e_0} f_0$. Thus, substituting one gets

$$R = \frac{dr}{dt} \propto \frac{u_e}{r^2} \Rightarrow \dot{m} \propto u_e$$

APPENDIX E: NUMERICAL SOLUTION OF THE SPRAY EQUATION

In the first section of this appendix, the scheme which was used to integrate the spray equation is explained. In the second section it is shown that there are two identical and independent ways of computing w_F/w_{oF} so that the accuracy of the integration can be tested. In the third section it is shown how a parameter appearing in the initial distribution function is determined.

1.0 The solution of

$$\frac{\partial}{\partial x}(u_e f) + \frac{\partial}{\partial r}(R f) = 0 \tag{1}$$

where $u_e = u_e(x,r)$, $R = R(x,r)$, $f = f(x,r)$ is equivalent to the solution of

$$\frac{d\, \ln f}{dx} = -\frac{1}{u_e}\left[\frac{\partial R}{\partial r} + \frac{\partial u_e}{\partial x}\right] \tag{2}$$

along r, x lines defined by

$$\frac{dr}{dx} = \frac{R}{u_e}$$

where R is the vaporization rate equation, taken to be of the following general form

$$R = -\frac{K}{Br}\left[1 + g\,Re^{g}\right] \text{ where } Re = 2rg|u-u_e|/\mu \text{ and } K, 1, g, g = \text{constants.}$$

Then the above equation becomes

$$\frac{dr}{dx} = -\frac{K}{Br\,u_e}\left[1 + g\,Re^{g}\right] \tag{3}$$

In general this equation contains $u_e = u_e(x,r)$ which in turn is unknown and therefore cannot be solved directly to give $r = r(x)$.

One more equation for u_e is needed; the drag equation can be used

$$\frac{4}{3}\pi r^3 \rho_L v_e \frac{du_e}{dx} = \frac{1}{2} C_D \pi r^2 \rho |u-u_e|(u-u_e) \Rightarrow \frac{du_e}{dx} = \frac{3}{8} \frac{C_D}{r} \frac{\rho}{\rho_L} \frac{|u-u_e|}{u_e}(u-u_e) \quad (4)$$

[In particular for $C_D = 24/Re$ one has $\frac{du_e}{dx} = \frac{45\mu}{\rho_L r^2}\frac{(u-u_e)}{u_e}$]

Thus one first solves the system of Equations 3 and 4 to get $r = r(x, r_o, u_{e_o})$, $u_e = u_e(x, r_o, u_{e_o})$ and then evaluates f by Equation 2

$$\frac{f(x,r)}{f_0(0,r_0)} = \exp\left[-\int_0^x \frac{1}{u_e}\left(\frac{\partial R}{\partial r} + \frac{\partial u_e}{\partial x}\right) dx\right] \quad (5)$$

This is a possible approach to solve Equation 1 for both numerical and analytical methods.

In both cases one must evaluate $\partial R/\partial r$ and $\partial u_e/\partial x$ where $R = R(x,r)$ and $u_e = u_e(x,r)$. R in general contains x, r, u_e and u_e is not known explicitly but is defined implicitly by the drag equation (Eq. 4). Thus one can write

$$\frac{f(x,r)}{f_0(0,r_0)} = \exp\left\{-\int_0^x \frac{1}{u_e}\left[\left(\frac{\partial R}{\partial r}\Big|_{\substack{\text{EXPLICIT}\\ \text{DEPENDENCE}}} + \frac{\partial R}{\partial u_e}\frac{\partial u_e}{\partial r}\right) + \frac{\partial u_e}{\partial x}\right] dx\right\} \quad (6)$$

The terms $(\partial R/\partial r)_{\text{EXPLICIT DEPEN.}}$ and $\partial R/\partial u_e$ do not present any problem and are given below:

$$\frac{\partial R}{\partial r}\Big|_{\substack{\text{Explicit}\\ \text{Dependence}}} = -\frac{K}{8}\left[g_1 g_2 Re^{g_2-1}\frac{1}{r}\frac{\partial Re}{\partial r}\Big|_{\substack{\text{Explicit}\\ \text{Dependence}}} - (1+g_1 Re^{g_2})\frac{1}{r^2}\right]$$

$$= -\frac{K}{8}\frac{1}{r^2}\left[g_1 Re^{g_2}(g_2-1) - 1\right] \quad (7)$$

Since

$$\frac{\partial Re}{\partial r}\Big|_{\substack{\text{EXPLICIT}\\ \text{DEPENDENCE}}} = \frac{Re}{r}$$

also:

$$\frac{\partial R}{\partial u_\ell} = -\frac{\kappa q}{8r} q Re^{q-1} \frac{\partial Re}{\partial u_\ell} = \frac{\kappa q \rho}{8r} \frac{Re^{q}}{(u-u_\ell)}$$

$$\text{since } \frac{\partial Re}{\partial u_\ell} = \frac{2\rho r}{\mu} \frac{\partial |u-u_\ell|}{\partial (u-u_\ell)} \frac{\partial (u-u_\ell)}{\partial u_\ell} = -\frac{Re}{(u-u_\ell)} \qquad (8)$$

The terms $\partial u_\ell / \partial r$ and $\partial u_\ell / \partial x$ were evaluated by finite differences since $u_\ell = u_\ell(x,r)$ is not explicitly known. For each r_o and u_{ℓ_o} (the same for all r_o's) the vaporization and the trajectory of the drop were computed, using the vaporization rate equation (3) and the drag equation (4) and numerically integrating them with respect to x . The gas variables appearing in those equations (x, ρ) are known from Figures 9 and 10. Thus, at each x , u_ℓ and r are now known for each and all the r_o's . To illustrate how these quantities are used to determine $\partial u_\ell / \partial r$ and $\partial u_\ell / \partial x$ use is made of Figure 47. In the upper portion of this figure, u_ℓ is plotted versus x for various r_o's. A similar set of curves could have been plotted for x for various r_o's . Thus at points A and B (at a constant x) both u_ℓ and r are known and $\Delta u_\ell / \Delta r$ at constant x can be evaluated. In the lower portion of this figure, u_ℓ is plotted versus r for various r_o's . By the x-integration of Equations 3 and 4 one moves from point C to point E (and from G to F) by changing both u_ℓ and r . Thus to evaluate $\Delta u_\ell / \Delta x$ at constant r , it is necessary to extrapolate the value of u_ℓ at point D from its values at points E and F. A linear extrapolation was used and $\Delta u_\ell / \Delta x$ at constant r was thus determined.

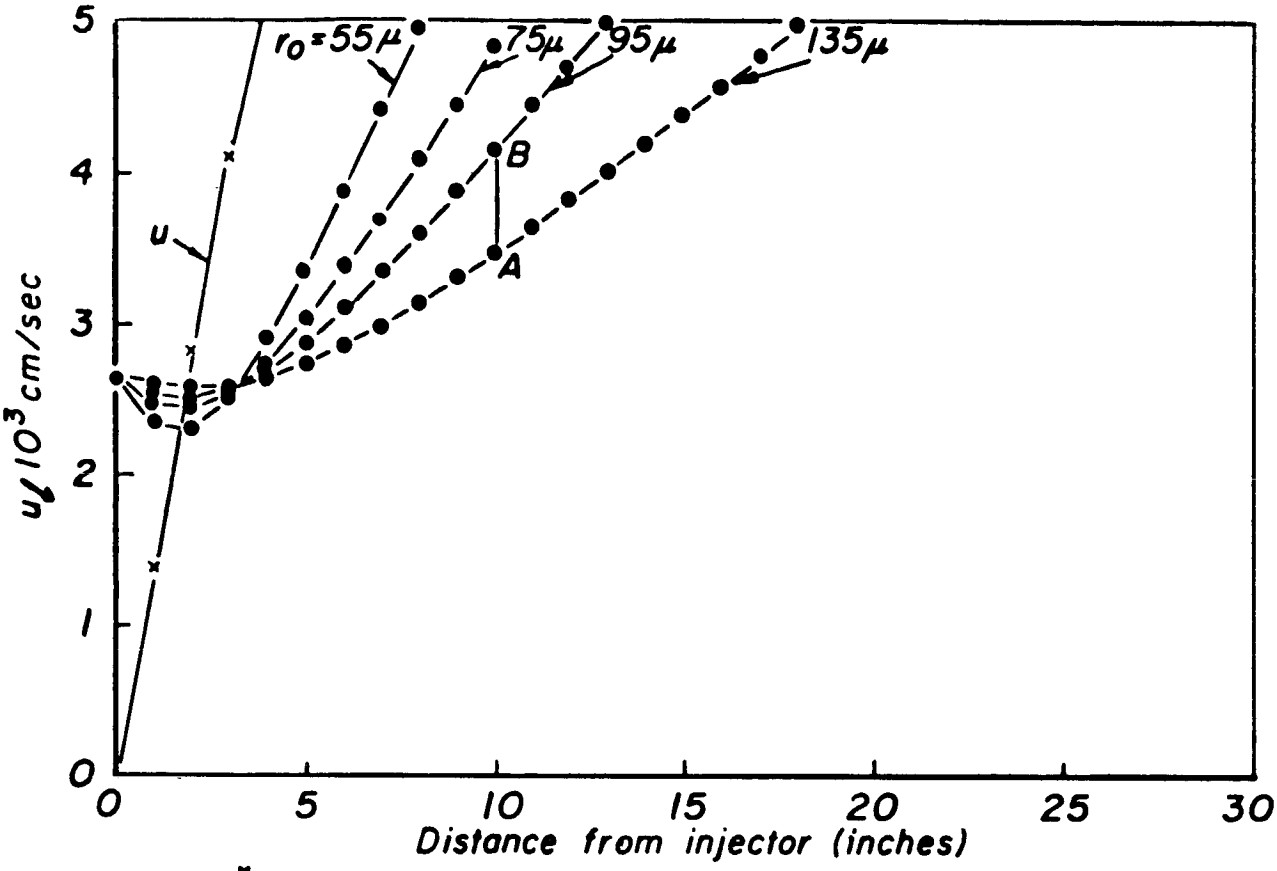

$$R = -\frac{K_3^*}{8\rho r} Re^{1/2} \qquad C_D = \frac{24}{Re} \qquad K_3^* = 2.5 \times 10^{-6} \qquad r_{30} = 70\mu \qquad (G7)$$

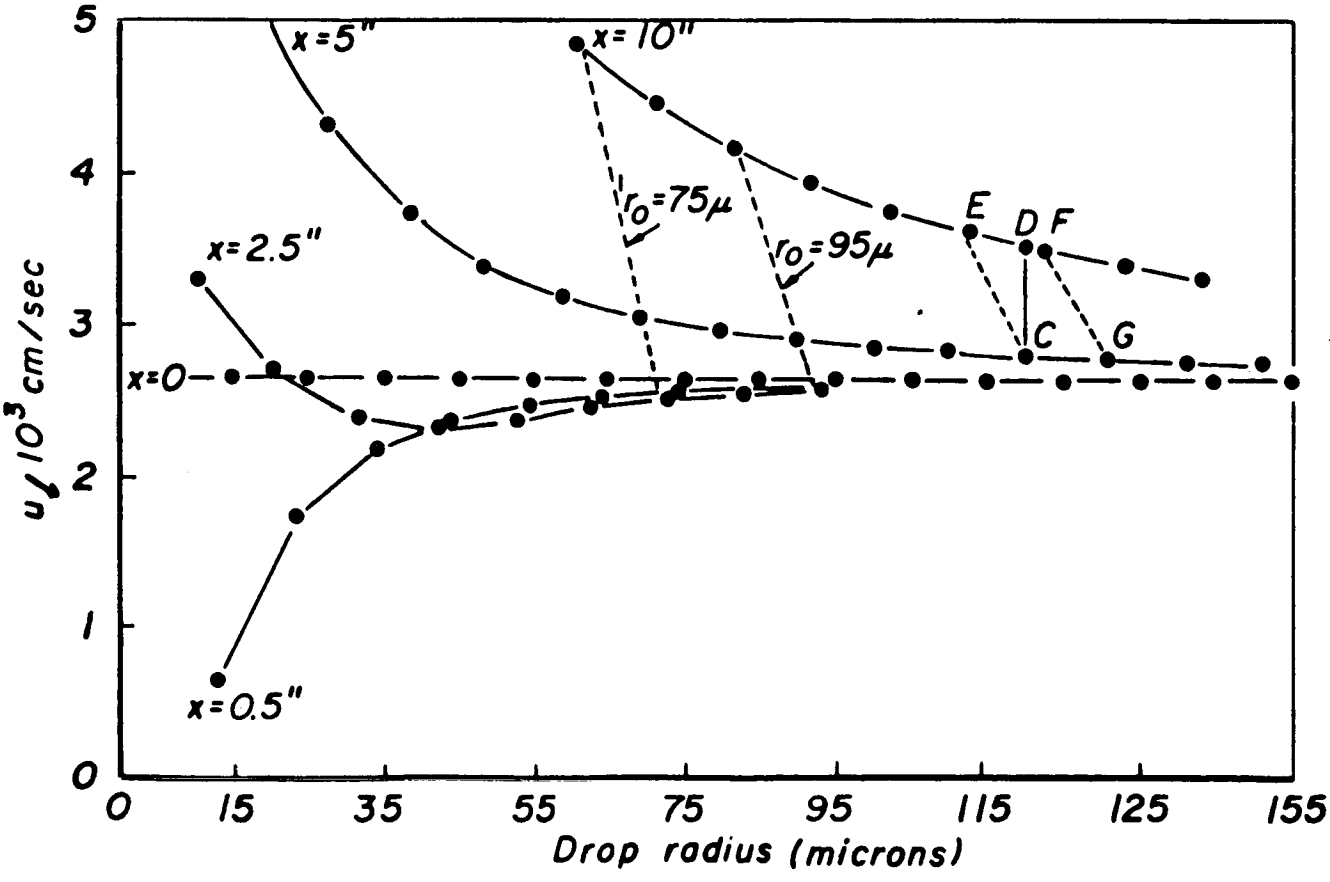

Example of evaluation of the derivatives of $u_l(x,r)$

Fig. 47

2.0 It is shown that, if $f(x,r)$ satisfies the following equation

$$\frac{\partial}{\partial r}(Rf) + \frac{\partial}{\partial x}(u_\ell f) = 0 \tag{9}$$

Then the local liquid fuel flow rate can be calculated by either of the following two expressions

$$\frac{d}{dx}\left(\frac{W_F}{W_{OF}}\right) = \frac{1}{A\,W_{OF}} \int_0^{R_{MAX}(x)} 4\pi r^2 \rho_L R f \, dr \tag{10}$$

$$\frac{W_F}{W_{OF}} = \frac{1}{A\,W_{OF}} \int_0^{R_{MAX}(x)} \frac{4}{3}\pi r^3 \rho_L u_\ell f \, dr \tag{11}$$

Equation 10 relates local changes of liquid fuel flow rate to the local changes of drop radius (R) and drop number (f). Equation 11 simply counts all the drops going through a specific cross-section in the unit time. The fact that there are two different ways to calculate the same parameter, for a given solution of Equation 9, affords an excellent check on the validity of the solution itself. This check was systematically included in the calculations, and was satisfactorily met in all cases. To apply Equations 10 and 11, one must first determine $f(x,r)$ through Equation 6. Equations 7 and 8 and the finite difference evaluations of $\partial u_\ell/\partial r$ and $\partial u_\ell/\partial x$ are in the process used. Thus, there are quite a few numerical computations involved in getting W_F/W_{OF} and errors can be expected to accumulate. Nevertheless, the W_F/W_{OF} calculated by the two methods agree quite closely in all cases. The best agreement was found when the drag is zero so that two of the three terms appearing in Equation 6 are identically zero. The largest difference was found when all the

terms of Equation 6 are different from zero. Even in such cases the difference is so small that it can hardly be noticed in figures such as Figure 30. The difference was found to be a function of Δx (not so much of Δr) particularly for the high drag cases where the velocity of the drops undergoes drastic changes if Δx is too large. In most of the calculations $\Delta r = 10\mu$ and $\Delta x \simeq .5$ cm were used to keep the computation time down but in the high drag cases it was necessary to use $\Delta x \simeq .25$ cm, thus doubling the computation time.

To prove our statement that Equations 10 and 11 are equivalent, take the x-derivative of Equation 11

$$\frac{d}{dx}\left(\frac{W_F}{W_{0F}}\right) = \frac{1}{A W_{0F}} \frac{4}{3}\pi r_{MAX}^3(x) \rho_L u_e\left(x, r_{MAX}(x)\right) f\left(x, r_{MAX}(x)\right) \frac{d}{dx} r_{MAX}(x) +$$

$$+ \frac{1}{A W_{0F}} \int_0^{r_{MAX}(x)} \frac{4}{3}\pi r^3 \rho_L \frac{\partial}{\partial x}(u_e f)\, dr$$

If Equation 9 is satisfied then one can sutstitute

$$\frac{\partial}{\partial x}(u_e f) = -\frac{\partial}{\partial r}(Rf)$$

Substituting and integrating by parts, one gets

$$\frac{d}{dx}\left(\frac{W_F}{W_{0F}}\right) = \frac{1}{A W_{0F}} \frac{4}{3}\pi r_{MAX}^3(x) \rho_L u_e\left(x, r_{MAX}(x)\right) f\left(x, r_{MAX}(x)\right) \frac{d}{dx} r_{MAX}(x) -$$

$$- \frac{1}{A W_{0F}} \frac{4}{3}\pi r^3 \rho_L R f \Big|_0^{r_{MAX}(x)} + \frac{1}{A W_{0F}} \int_0^{r_{MAX}(x)} 4\pi r^2 \rho_L R f\, dr =$$

$$= \frac{1}{A W_{0F}} \left\{ \frac{4}{3}\pi r_{MAX}^3(x) \rho_L f\left(x, r_{MAX}(x)\right) \left[u_e\left(x, r_{MAX}(x)\right) \frac{d}{dx} r_{MAX}(x) - R\left(x, r_{MAX}(x)\right) \right] \right\} +$$

$$+ \frac{1}{A W_{0F}} \int_0^{r_{MAX}(x)} 4\pi r^2 \rho_L R f\, dr$$

But the term in the above brackets is zero since by definition $R = u_\ell \frac{dr}{dx}$ for any r including r_{MAX} . Thus the derivative of Equation 11 is equal to Equation 10 for any x . Thus, the local liquid fuel flow rate calculated by Equation 11 is identical to that calculated by Equation 10 provided, in both equations, the same initial value is used.

3.0 In Appendix C, the following initial distribution function was selected

$$f_0(0, r_0) = 4B r_0^2 e^{-3.915 \frac{r}{r_{30}}}$$

where the factor B was not specified since it is related to the flow rate into the specific engine under consideration. Equation 11 can now be used to determine B

$$1 = \frac{1}{A W_{0F}} \int_0^{r_{MAX}^{(0)}} \frac{4}{3} \pi r_0^3 \rho_L u_{\ell_0} 4 B r_0^2 e^{-3.915 \frac{r}{r_{30}}} dr_0$$

from which it follows that

$$B = \frac{3 A W_{0F} b^6}{16 \pi \rho_L u_{\ell_0}} \Big/ \int_0^{y_{MAX}} y^5 e^{-y} dy$$

where

$$b = 3.915 / r_{30}$$

$$y_{MAX} = b r_{MAX}^{(0)}$$